Vaal University of Technology
Your world to a better future

VUT

ADSORPTION STUDIES OF TOXIC METAL IONS (Co(II), Ni(II), Cu(II), Cr(VI) and Pb(II)) AND METHYLENE BLUE USING BLACK CUMIN (*Nigella sativa* L.) SEEDS

This thesis was submitted to Vaal University of Technology in partial fulfilment of the requirements for the award of the degree of

DOCTOR OF PHILOSOPHY

IN

CHEMISTRY

Title

By

P.M. Thabede (214026582)

PROMOTER: Dr N. D. Shooto

CO-PROMOTER: Dr T. Xaba

CO-PROMOTER: Prof. E. B. Naidoo

Year: 2021

ACKNOWLEDGEMENT

I would like to thank the Lord for making it possible to complete this journey. None of these could be possible without His mercy and protection.

I would like to express sincerity to my husband (Muzuthini Nicholas Thabede) who supported my dream to further my studies. I appreciate the love, support, patience and understanding he has given me during PhD duration.

I would like to thank my promoter, Dr. N.D. Shooto for believing in me when no one else did. For taking a risk to work with me, teaching me, guiding me, showing support at all times and encouragement during the course of this work. He gave me a lot of suggestions and moral support. I am very grateful to him for his patience and availing himself in order to help me during my roughest time during research.

I would also like to thank my co-promoter Prof. E. B. Naidoo for his support, for having faith in me, encouragement and motivation. I am grateful to Dr. T. Xaba for being my co-promoter.

I wish to thank my siblings; Florence Bahupileng Masike and Marcia Refilwe Nkwane for inspiring me and giving me support all the way during my studies. A special thank you to my mother who always highlighted the importance of obtaining a qualification.

I thank the Vaal University of Technology and Department of Chemistry for accepting me in their institution. Special acknowledgements to NRF for funding this research.

DECLARATION

I Patience Mapule Thabede declare that this work is my own, unaided work. I also declare that the thesis has been written by myself and any help that I have received in preparing this document and all sources used have been acknowledged in this thesis. It is submitted for the degree of Doctor of Philosophy in Faculty of Applied Computers and Sciences at the Vaal University of Technology, Vanderbijlpark campus. It has not been submitted before for any degree or examination in any other University.

THESIS FORMAT

This thesis is submitted in an article format.

SUMMARY

High levels of pollutants in water are found to have poisonous effects on human health. Due to increasing awareness about the environment and strict environmental regulations, wastewater treatment has become a very important aspect of research. Thus, this makes the adsorption of pollutants an urgent matter. The aim of this research was to investigate the adsorption capacity of black cumin seeds in the removal of cobalt-Co(II), nickel-Ni(II), copper-(II), chromium-Cr(VI), lead-Pb(II), and methylene blue (MB) dye from aqueous solution. In this research work the black cumin seeds were reacted with sodium hydroxide (NaOH), hydrochloric acid (HCl), phosphoric acid (H_3PO_4), potassium permanganate ($KMnO_4$) and sulfuric acid (H_2SO_4). Thereafter it was carbonized at 200 and 300 °C and functionalized with magnetite-sucrose nanoparticles and further carbonized at 600 °C to improve the adsorption capacity of the materials towards different pollutants.

The seeds were characterized by scanning electron microscopy (SEM), thermogravimetric analyser (TGA), X-ray diffractometer (XRD), Brunauer, Emmett and Teller (BET) and Fourier transformed infrared (FTIR) spectroscopy. The SEM images showed that the surface morphology of the treated adsorbents was more porous and had cavities more than the starting material. The TGA profile showed a major weight loss between 198-487 °C which was due to disintegration of cellulose, lignin and hemicellulose. The XRD spectra of adsorbents showed broad peaks at 2θ value of 21° associated crystalline lignocellulose content. FTIR results showed that the adsorbents had functional groups such as hydroxyl (-OH), carboxyl (-COOH), amide (-NH) and carbonyl (-C=O). The BET surface area of pristine black cumin seeds was 2.7 m^2/g and increased after treatment with $KMnO_4$ and H_3PO_4 to 10.1 and 9.3 m^2/g respectively. The surface area of the carbon black cumin seeds was 11.67 m^2/g whilst the activation of carbon from black cumin seeds with 10 and 20% H_2SO_4 gave the surface area of

20.14 and 21.54 m^2/g respectively. The seeds activated with 20% H_2SO_4 showed larger pore width of 7.13 nm compared to 6.81 and 3.78 nm after treatment with 10% H_2SO_4 and carbon black cumin seeds respectively. The results show that there is an increase in surface area and pore size for both 10 and 20% H_2SO_4 in comparison with carbon black cumin seeds.

The adsorption of Co(II), Ni(II), Cu(II), Cr(VI) and Pb(II) and MB in the solution was investigated by studying the effect of initial concentration, contact time, temperature and pH. The batch adsorption experiments were conducted using different ion solution concentrations of 20, 40, 60, 80 and 100 mg/L, contact time was determined at intervals of 1, 5, 10, 15, 20, 30, 60, 90 and 120 min, while temperature was studied at 298, 303, 313, 333 and 353 K. On the other hand, the effect of pH on all solutions was studied at pH 1, 3,5,7 and 9. The results showed that the acid treated black cumin seeds (AT-BCS) and base treated black cumin seeds (BT-BCS) were successfully used for quaternary adsorption study of Cu(II), Co(II), Pb(II) and Ni(II) ions from aqueous solution. The results for the adsorbents indicated that the BT-BCS adsorbed more metals than AT-BCS and the UT-BCS. The maximum capacity for BT-BCS was 190.7 mg/g for Cu(II) whilst AT-BCS and UT-BCS showed capacities of 180.1 and 135 mg/g respectively for Pb(II).

The uptake of Cr(VI) and Cd(II) ions onto pristine black seeds (PBS), $KMnO_4$ black seeds (KMBS) and H_3PO_4 black seeds (H_3BS) treated adsorbents showed that the trend for Cr(VI) ions was KMBS>H_3BS>PBS with capacities of 16.12, 15.98 and 10.15 mg/g respectively. Meanwhile the adsorption of Cd(II) ions showed maximum capacities of 19.15, 19.09 and 16.80 mg/g for KMBS, H_3BS and PBS respectively. Carbon from black cumin (CBC) seeds was modified with 10 % and 20 % sulfuric acid (H_2SO_4) then carbonized at 200 °C to obtain the activated adsorbents of ACBC-10 and ACBC-20. The new adsorbents were used for the

adsorption of Cd(II) and methylene blue (MB). The adsorbents maximum trend for Cd(II) was ACBC-10>ACBC-20>CBC meanwhile the trend for methylene blue (MB) dye was ACBC-20>ACBC-10>CBC. The overall capacities showed that the prepared materials adsorbed more MB dye (16.42 mg/g) than Cd(II) ions (13.65 mg/g). The preparation of carbon from black cumin seeds (BCC) and activation with 10 and 20 % sulfuric acid (H_2SO_4) at 300 °C to obtain new adsorbents namely (BCAC-10) and (BCAC-20) respectively was used for the adsorption of Pb(II) ions and MB dye from aqueous solution. The maximum adsorption of Pb(II) ions was 17.19, 17.71 and 17.98 mg/g onto BCC, BCAC-10 and BCAC-20 respectively. Whilst for MB dye it was 11.63, 12.71 and 16.85 mg/g onto BCC, BCAC-10 and BCAC-20 respectively. The utilization of pristine *Nigella Sativa* (PNS) and magnetite-sucrose functionalized *Nigella Sativa* (FNS) seeds as the adsorbents for the uptake of Cr(VI) and Pb(II) ions from synthetic wastewater revealed that the maximum adsorption capacities for Cr(VI) were 15.6 and 13.0 mg/g onto PNS and FNS composites respectively at pH 1. On the hand, the maximum sorption capacities for Pb(II) ions were 39.7 and 37.9 mg/g onto PNS and FNS respectively at pH 5.

The sorption study of Cr(VI), Cd(II) ions and MB dye by pristine *Nigella Sativa* (PNS) seeds, defatted and carbonized *Nigella Sativa* seeds from aqueous solution was investigated. The PNS seeds were treated using acetone (then named ANS) and N,N dimethylformamide (named DNS). The defatted ANS and DNS adsorbents were carbonized at 600 °C and named CANS and CDNS. The results of pristine, defatted and carbonized seeds maximum capacities were compared with each other and found that CANS had highest adsorption capacity of 99.82 mg/g for MB, 96.89 mg/g for Cd(II) and 87.44 mg/g for Cr(VI) followed by CDNS with 93.90, 73.91 and 65.38 mg/g for MB, Cd(II) and Cr(VI) respectively. ANS capacities were 58.44, 45.28 and 48.96 mg/g whilst DNS capacities were 48.19, 32.69 and 34.65 mg/g for MB, Cd and Cr(VI) respectively. PNS had the lowest sorption capacities at 43.88, 36.01 and 19.84 mg/g for

MB, Cd and Cr(VI) respectively. Therefore, this makes black cumin seeds a promising material for use in wastewater treatment to mitigate metal ions and dye pollution.

Keywords: adsorption, composite, kinetics, isotherms, equilibrium, ANS, DNS, CANS, BCC, BCAC-10 and BCAC-20

TABLE OF CONTENTS

LIST OF PUBLICATIONS

1. Ntaote David Shooto, **Patience Mapule Thabede,** Eliazer Bobby Naidoo. 2019. Simultaneous adsorptive study of toxic metal ions in quaternary system from aqueous solution using low-cost black cumin seeds *(Nigella Sativa*) adsorbents. South African Journal of Chemical Engineering 30, 15-27.

2. **Patience Mapule Thabede**, Ntaote David Shooto, Thokozani Xaba, Eliazer Bobby Naidoo. 2020. Adsorption studies of toxic cadmium(II) and chromium(VI) ions from aqueous solution by activated black cumin (*Nigella Sativa*) seeds. Journal of Environmental Chemical Engineering 8, 104045.

3. **Patience Mapule Thabede**, Ntaote David Shooto, Thokozani Xaba, Eliazer bobby Naidoo. 2020. Sulfuric activated carbon of black cumin (*Nigella sativa* L.) seeds for the removal of cadmium(II) and methylene blue dye. Asian Journal of Chemistry 32(6), 1361-1369.

4. **Patience Mapule Thabede**, Ntaote David Shooto, Eliazer Bobby Naidoo. 2020. Removal of methylene blue dye and lead ions from aqueous solution using activated carbon from black cumin seeds. South African Journal of Chemical Engineering 33, 39-50.

5. **Patience Mapule Thabede,** Ntaote David Shooto, Thokozani Xaba, Eliazer Bobby Naidoo. 2021. Magnetite functionalized *Nigella Sativa* seeds for the uptake of chromium(VI) and lead(II) ions from synthetic wastewater. Adsorption Science and Technology 2021.6655227.

6. **Patience Mapule Thabede**, Ntaote David Shooto, Eliazer Bobby Naidoo. 2021. Sorption of chromium(VI), cadmium(II) ions and methylene blue dye by pristine, defatted and carbonized *Nigella sativa* L. seeds from aqueous solution**.** Asian Journal of Chemistry 33(2), 471-483.

CONFERENCE ATTENDANCE

Green Chemistry New Zealand

3-6 December 2019, University of Auckland, New Zealand

Title: Simultaneous adsorptive study of toxic metal ions in quaternary system from aqueous solution using low-cost black cumin seeds *(Nigella Sativa*) adsorbents.

LIST OF FIGURES

LIST OF SCHEMES

LIST OF TABLES

LIST OF ABBREVIATIONS

AAS-Atomic Absorption Spectroscopy

ACBC-Activated carbon black cumin

ANS-Acetone *Nigella Sativa*

AT-BCS-Acid treated black cumin seeds

BCAC-Black cumin activated carbon

BCC-Black cumin carbon

BCS-Black cumin seeds

BET-Brunauer-Emmett-Teller

BT-BCS-Base treated black cumin seeds

C_2H_6CO-Acetone

C_3H_7NO-N,N dimethylformamide (DMF)

$C_{12}H_{22}O_{11}$-Sucrose

$C_{16}H_{18}ClN_3S$-Methylene blue

CANS-Carbonized acetone *Nigella Sativa*

CBC-Carbonized black cumin

$Cd(CH_3COO)_2$-Cadmium acetate salt

CDNS-Carbonized DMF *Nigella Sativa*

$Co(NO_3)_2$-Cobalt(II)nitrate

$CuSO_4.5H_2O$-Copper sulfate pentahydrate

CVD-Catalytic vapour deposition

DNS-DMF *Nigella Sativa*

EAP- Estimated pore adsorption

ESA - Estimated surface adsorption

EPA-Environmental Protection Agency

$FeCl_2 \cdot 4H_2O$-Iron(II) chloride

$FeCl_3 \cdot 6H_2O$-Iron(III) chloride

FNS-Functionalized *Nigella Sativa*

FTIR-Fourier Transform Infrared

H_2SO_4-Sulphuric acid

H_3BS-Phosphoric black seeds

H_3PO_4-Phosphoric acid

HCl-Hydrochloric acid

HNO_3-Nitric acid

IPD-Intraparticle diffusion

$K_2Cr_2O_7$-Potassium dichromate

KMBS-Potassium permanganate black seeds

$KMnO_4$-Potassium permanganate

MB-Methylene Blue dye

$Na_2S_2O_3$-Sodium thiosulfate

$NaNO_3$-Sodium nitrate

NaOH-Sodium hydroxide

NH_4OH-Ammonium hydroxide

$Ni(NO_3)_2$-Nickel(II)nitrate

NP- Nanoparticles

$Pb(NO_3)$-Lead nitrate

PNS-Pristine *Nigella Sativa*

PFO-Pseudo first order

PSO- Pseudo second order

PZC-Point zero charge

SEM-Scanning Electron microscopy

TGA-Thermogravimetric analysis

UT-BCS-Untreated black cumin seeds

UV-Vis-Ultraviolet-visible

WHO-World Health Organization

XRD-X-ray diffraction

CHAPTER 1: INTRODUCTION

1.1 Background

Clean water is important in order for life to be continued on earth, however, the world is facing a challenge due to less availability of fresh water (Dargahi et al. 2016b; Rajasulochana & Preethy, 2016). The development of industries such as metal plating, leather tanning, surface finishing, mining, paper producing, smelting, dyeing and others, have shown an increased number of effluents containing chemical substances particularly metal ions being directly or indirectly released into the environment and also into freshwater (Song et al. 2016; Ali et al. 2019). An increase in such activities has caused the discharge of enormous amounts of hazardous pollutants into aqueous systems. Therefore, these accumulated pollutants or toxins in water has become a potential hazard to ecological environments and health (Zhang et al. 2019; Ketsel et al. 2020).

There are different conventional methods of treatments for wastewater and contaminated water. Adsorption is a non-conventional method that has proven to be the best compared to the conventional methods (Tripathi & Ranjani, 2015). Conventional methods are expensive, processing cost is high, they do not have the ability completely remove metal toxic ions, uses high energy and has the ability to generate toxic sludge (Essomba et al. 2014). Of these, adsorption technique is effective for removing contaminants at low levels because it uses inexpensive materials as adsorbents, less requirement of control systems, easy design, versatile and simple (Matos et al. 2017; Ouma et al. 2018). This makes adsorption an economical and favourable technology for the removal of toxic ions from wastewater.

Adsorption is a process of mass transfer method which involves the accumulation of substance at the interface of two phases, namely; gas-solid or liquid-solid interface, liquid-liquid and gas-liquid (Babalola 2018). There are certain processes involved in the adsorption process and Fig. 1 shows the main process involved. The properties of both the adsorbent and adsorbate are specific and depend upon their individual constituents (De Gisi et al. 2016). The adsorbate is the substance that is being adsorbed and is transferred from one phase to another whilst the adsorbent is the material on which accumulation occurs. Adsorption is categorised into two types namely: (1) physical adsorption, where there is attraction between the adsorbate and adsorbent through the Van der Waals interactions in which case the resulting process is reversible and (2) chemical adsorption is as a result of chemical reactions between the adsorbate and the adsorbent which leads to the formation of covalent or ionic bonds (Tyagi et al. 2017; Moon & Palaniandy, 2019).

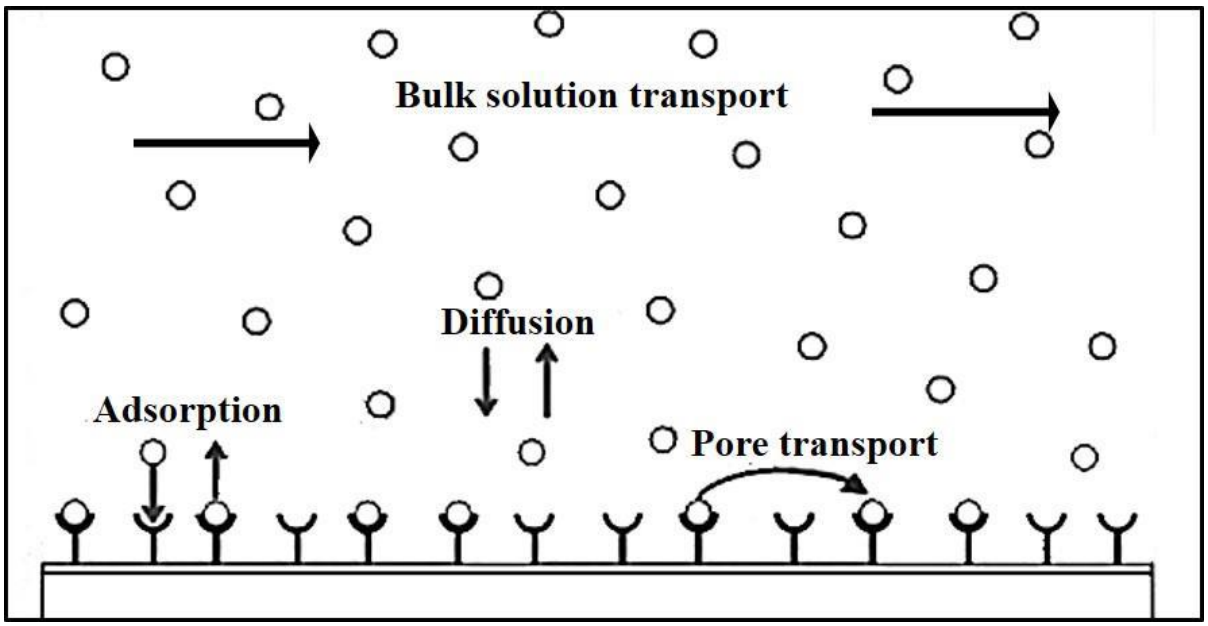

Figure 1: Schematic presentation of the adsorption process (Moon & Palaniandy, 2019)

The importance of adsorption in water treatment for pollution control has been well emphasized in literature. Adie et al. (2012); Carolin et al. (2017), stated that the use of adsorption for separation of pollutants from mixtures has been endlessly increasing and that the main advantages of adsorption are high capacity of the adsorbent for pollutants even at low concentration and high selectivity compared with other separation techniques. Carolin et al. (2017), further mentioned that adsorption does not produce toxic pollutants. Many toxic metals have poisonous effects at high concentration (Kumarasinghe et al. 2009). The presence of toxic metals in effluents and industrial wastewater has become a great concern due to their high toxicity and adverse accumulation characteristics (Bargat et al. 2014).

In the same context, the dyes are also regarded as harmful pollutants due to their different use in several industries such as printing, textile, food processing, leather tanning, cosmetics, plastics, rubber and dye manufacturing industries (Yazidi et al. 2020). The existence of dyes in textile wastes and effluents can also cause serious environmental effects and human health risks when they are released without proper treatment (Qiu et al. 2017; Siyal et al. 2018). Literature have shown that dyes such as methylene blue (MB), heavy metal ions such as nickel [Ni(II)], cadmium [Cd(II)], lead [Pb(II)] and cobalt [Co(II)] are priority water pollutants (Shajahan et al. 2017). Other metals ions include copper [Cu(II)] and chromium [Cr(VI)]. Hence, in the present study the adsorption of toxic metal ions namely; cobalt [Co(II)], nickel [Ni(II)], copper [Cu(II), chromium [Cr(VI)], cadmium [Cd(II)] and lead [Pb(II)] as well as methylene blue dye (MB) were investigated and their health effects are discussed in the following section.

Cobalt

Cobalt (Co) is a very toxic metal ion contained in compounds that are widely used in many industrial applications such as electroplating, mining, paints, metallurgical, pigments and electronic (Prabakaran & Arivoli, 2013; Tizro & Baseri, 2017). Additionally, Co may also be used for food irradiation, radiation source for medical radiotherapy (Liu et al. 2019) and dyes (Hu et al. 2018). The derivative of cobalt is also used to fabricate high-strength alloys, industrial catalysts and new energy batteries (Liu et al. 2019). The presence of cobalt ions in the environment leads to several health troubles such as low blood pressure, vomiting, nausea, heart failure, vision problems, sterility, thyroid and liver damage, hair loss, bleeding, diarrhoea, bone defects and may also cause mutations (genetic changes) in living cells (Nadaroglu & Ekrem Kalkan, 2012). The permissible limits of cobalt in the livestock wastewater and irrigation water are 1.0 and 0.05 mg/L, respectively (Sayadi et al. 2014). So, the effective removal of Co(II) from the aqueous solution is necessary for human and the environmental protection.

Nickel

Nickel with atomic number 28 is an element of environmental concern (Hummel & Curti, 2003). Ni(II) belongs to the group of most toxic metal ions such as Cd(II), Co(II), Zn(II), Hg(II), Cu(II) and Pb(II) which are subjected to concentration restrictions in drinking water (Islam et al., 2018; (Dehghani et al. 2019). Nickel is referred to as one of the most significant toxic metals used in various industries namely; chemical fertilizers, as cars exhaust, food products, super phosphates, industrial waste hydrogenated oils, nuclear tests, stainless steel industry and so forth (Carolin et al. 2017). Ni(II) is a non-biodegradable and is prone to accumulate in living creatures and can cause several health events such as dizziness, headache,

chest pain, nausea, cyanosis, rapid respiration, cancer, cardiovascular and kidney diseases (Mahmoud et al. 2017; Islam et al. 2019). Environmental Protection Agency (EPA) recommended limit for Ni(II) concentration should not exceed 0.015 mg/L in drinking water (Hannachi et al. 2010). Therefore, it is very important to remove and treat wastewater with Ni(II) before the release to the environment.

Copper

In order for our bodies to function properly copper ions Cu(II) have to support certain enzyme systems (Festa & Thiele 2011) and does crucial work in animal metabolism (Nassef et al. 2017). But excess of Cu(II) is hazardous to human health and the environment because it has a tendency to accumulate in the brain, eyes, liver and leads to Wilson disease (Ganey et al. 2000). Cu(II) ion is listed in the eleven hazardous priority substances of pollutants (Rozada et al. 2008). Cu and its compounds if released into the water, the copper that dissolves can be carried in surface water as free copper or in the form of copper compounds or most likely, copper can bind to suspended particles in the water (Torres-Caban et al. 2019). Excessive intake of Cu can cause problems to the liver, kidney, gastrointestinal; central nervous system damage; severe headaches, nausea and alopecia (Rozada et al. 2008; Brewer 2010). Environmental guidelines require surface water to contain less than 0.1 ppm Cu (Kettum et al. 2018). Therefore, the control and the removal of Cu(II) ion from wastewater before it is discharged it imperative.

Chromium

Chromium has three forms common oxidation states in its compounds namely; (II), (III), and (VI) (Dehghani et al. 2016a). Cr(VI) in the environment has a 100 times higher toxicity compared to Cr(III) (Miretzky & Cirelli, 2010; Barsainya et al. 2016). Chromium is used in industries such as leather industries, fungicides, tanning, crafts, glass, manufacturing

industries, pigments, ceramics, photography, catalyst and electroplating industry (Yeu et al. 2009; Dehghani et al. 2016b). With Cr(VI) being the most toxic amongst other chromium oxidation states it can cause genomic dysregulation, cancer, skin and stomach tumors, lung cancer and osteoblasts functions. (Cerveira et al. 2014; Haney et al. 2014). World Health Organisation (WHO) has set its regulations of total chromium at 0.05 mg/ L (USEPA, 2012) meanwhile the United States Environmental Protection Agency (USEPA) has established the maximum contaminant limit of total chromium in drinking water as 0.1 mg/L. Thus, the removal of chromium(VI) from wastewater is tremendously important before its discharge into the aquatic system.

Cadmium

Cadmium [Cd(II)] is regarded as an element of high toxicity and can cause serious damage to the bones and kidneys (Carolin et al. 2017; Uddin 2017). When cadmium accumulates in the body it can have additional effects such as; renal dysfunction, hypertension, lung damage, cancer, liver disease and abnormal physiological development (Kim et al. 2015; Noh et al. 2017). The addition of cadmium to the environment is introduced by human activities, such as electroplating, electrolyzing, alloy preparation, metal mining, cement preparation, synthesis of pigments, petrochemical industries, battery production and many others (Awual et al. 2018). The maximum allowable concentration by WHO of cadmium in drinking water is 0.003 mg/ L.

Lead

Lead [Pb(II)] is the most significant toxin of the trace metal ions and human contact to the inorganic forms is through inhalation, water and food ingestion (Moyo et al. 2013). The above-mentioned form affects the peripheral nervous system and haematopoietic, renal, cardiovascular, reproductive systems and gastrointestinal (Beltrame et al. 2018; Nkutha et al. 2020). Also, accumulation of lead in the human body may cause certain damage to the brain (leading to a decline in learning and memory), causing genetic mutations and affecting bone metabolism (Googerdchian et al. 2018; Kenawy et al. 2018). Lead gets released into the environment through melting, mining, paints, galvanizing and industrial metallurgical processes, from batteries, lead piping, ceramics and munitions (Wongrod et al. 2018; Seema et al. 2018). Lead precipitates in the form of Pb phosphates and Pb sulphates because of their low solubility and availability (Akhtar et al. 2013). The maximum contaminant level of lead in drinking water allowed by the Environmental Protection Agency (EPA) and the World Health Organization (WHO) is 0.05 mg/dm^{-3} (Mahmud et al. 2016). Therefore, it is essential to remove lead from wastewaters before releasing into the natural water streams.

Methylene Blue (MB)

Ramabrahmam (2016) indicated that dyes are aromatic molecular structures which are estimated to be firm, steady and as a result, are difficult to degrade. Synthetic dyes have been extensively useful in many technological areas which include the textile industry, photo electrochemical cells, leather tanning, food technology, hair colouring products and paper production (Luo et al. 2017; Hoong & Ismail, 2018). Based on research studies, it is projected that 280,000 tons of textile dyes are discharged every year from the textile industry as effluent worldwide, making it the first place in the usage of dyes among various industries (Frindt et al.

2017). So, discharging of effluent from the above-mentioned industries into receiving water bodies becomes a major environmental problem since most of dyes have toxic effects on the aquatic life, as well as carcinogenicity and mutagenicity for human beings (Duman et al. 2016). Dyes are generally classified as cationic, anionic and non-ionic depending on the ionic charge on the dye molecules with cationic dyes being more toxic than anionic dyes (El-Sayed 2011). Methylene blue (MB) is one of the cationic dyes that has shown to have harmful effects on living organisms on short periods of exposure (El-Sayed 2011). MB is used in food industries, pharmaceutical industry, medicine, pulp and paper industries as well as textile industries (Edokpayi et al. 2019). Extended period exposure to MB can cause anaemia, high fever, headache, chest pain, confusion, nausea and vomiting, hypertension and blue skin (Foo et al. 2012). Therefore, for these reasons it is important to treat industrial effluents containing dyes prior to their discharges into the environment.

1.2 Problem statement

The challenge facing industries is to find ways of disposing effluent safely. Industry effluents contain toxic metal ions and dyes that are disposed in the environment posing serious threat to humans and other organisms (Ahmad & Haseeb, 2014). Toxic metal contaminants are not susceptible to biological degradation (Saleem et al. 2016). It is therefore important to use a method that can remove toxic ions from effluent water. Adsorption, a non-conventional method is the most promising technique because it is sustainable, affordable and effective method. Various adsorbents such as activated carbon, zeolites and many others have been used for the removal of toxic metals ions from aqueous solutions. In this work, black cumin seeds (BCS), a non-conventional, highly abundant, inexpensive, biologically favourable, and eco-friendly adsorbent has been chosen for the removal toxic pollutants in aqueous solutions. BCS have a

number of oxygenous groups (carboxyl, hydroxyl and amines) at the surface which makes them advantageous for adsorption applications.

1.3 Aim

To investigate the adsorption capacity of BCS by removing cobalt [Co(II)], nickel [Ni(II)], copper [Cu(II)], chromium [Cr(VI)], lead [Pb(II)], cadmium [Cd(II)] and methylene blue (MB) dye from aqueous solution.

1.4 Objectives

(a) To determine the phsysico-chemical properties of the untreated black cumin seeds (UT-BCS), acid treated (AT-BCS) and base treated (BT-BCS) using SEM, TGA, XRD and FTIR spectroscopy.

(b) To conduct simultaneous (quaternary) adsorption of cobalt [Co(II)], nickel [Ni(II)], copper [Cu(II)] and lead [Pb(II)] using UT-BCS, AT-BCS and BT-BCS while varying time, pH, temperature and concentration.

(c) To activate black cumin seeds by potassium permanganate ($KMnO_4$) and phosphoric acid (H_3PO_4) for the removal of chromium Cr(VI) and cadmium Cd(II) ions from aqueous solution by varying time, pH, temperature and concentration.

(d) To activate BCS using sulfuric acid and carbonize the activated seeds at different temperatures (200 and 300° C) and conduct single adsorption of MB, Pb(II) and Cd(II) under different parameters (temperature, concentration, time and pH).

(e) To functionalized black cumin seeds using sucrose and iron oxide to form composites for the removal of Cr(VI) and Pb(II) ions in aqueous solution. Thereafter, conduct adsorption studies under different parameters (temperature, concentration, time and pH).

(f) To modify black cumin seeds using different solvents such as acetone and N,N dimethylformamide (DMF) and carbonize the seeds at 600° C for the sorption MB, Cd(II) and Cr(VI) while varying parameters such as temperature, concentration, time and pH.

(g) To determine the point of zero charge (pH_{PZC}) of the UT-BCS, AT-BCS, BT-BCS, functionalized and activated adsorbents.

(h) To determine the reusability of the UT-BCS, AT-BCS, BT-BCS, modified and the carbonized seeds.

(i) To conduct adsorption kinetics, isotherms and thermodynamics of Co(II), Ni(II), Cu(II), Cr(VI) and Pb(II) ions and methylene blue.

1.5 Purpose of the research

Different researchers have used black cumin (*Nigella Sativa* L.) seeds for uptake of different toxic metal ions and dyes. However, there is no study of quaternary ions of Co(II), Ni(II), Cu(II), and Pb(II) using UT-BCS, AT-BCS and BT-BCS on the adsorptive capacity of these seeds. In addition, there has been no work on defatted black cumin seeds using acetone and DMF for the adsorption MB, Cd(II) and Cr(VI). Also there has been limited research on single metal ions adsorption using black cumin seeds. Hence this research will explore the efficiency of black cumin adsorbents. The focus of this research is to modify black cumin seeds via chemical methods and to assess their adsorption capacity. The adsorption capacity of the seeds will also be investigated using different chemical conditions. The modified black cumin seeds together with activated carbons will also be used to remove pollutants (toxic metal ions) and methylene blue dye from aqueous solution.

1.6 Outline of the thesis

This thesis is made up of a number of chapters and they are explained below:

Chapter 1

This chapter give a brief background of waste water problems in general and toxic metals pollution. This is followed by problem statement, aim, objectives and purpose of the study is also discussed in this chapter. The chapter closes with the dissertation outline.

Chapter 2

Chapter 2 review the literature of different wastewater technologies and methods used globally for removal of toxic metals. Then an outline of different available adsorbents and their treatment is also discussed. The effects, health hazards and acceptable specifications on the studied metals toxic ions are discussed in this section.

Chapter 3

This chapter discusses the experimental materials, the preparations of adsorbents and the method used for the adsorption of toxic metals ions and dye from aqueous solution. The experiments were conducted using the most generally used batch system. The last section concludes by showing different instruments used during characterization.

Chapter 4

This chapter investigates the adsorption of quaternary metal ions Co(II), Pb(II), Cu(II) and Ni(II) using the acid treated AT-BCS, alkaline treated (BT-BCS) and untreated treated (UT-BCS) black cumin seeds.

Chapter 5

This chapter studies the effect of potassium permanganate ($KMnO_4$) and phosphoric acid (H_3PO_4) as activating agents for the removal of Cd(II) ions and Cr(VI) ions from aqueous solution. Kinetic studies and isotherms were investigated in order to understand the behaviour of adsorbents and the removal mechanisms involved in the adsorption process.

Chapter 6

This chapter discusses the results obtained from activating the black cumin seeds with 10 % and 20 % of sulfuric acid (H_2SO_4) and carbonizing them at 200 °C. The results of the carbonized black cumin seeds were compared with the chemical activated seeds. The different adsorbents were used for adsorptive studies of Cd(II) ions and MB dye.

Chapter 7

The specific aim of this chapter is to prepare carbon at 300 °C from black cumin seeds thereafter, activate them with 10 % and 20 % (H_2SO_4) and then use them for the adsorption of Pb(II) ions and MB dye. The carbon-based and the two activated adsorbents are compared with each other using different parameters.

Chapter 8

The purpose of this chapter is to make a composite by functionalizing black cumin seeds with sucrose and iron oxide. The results of the iron oxide-sucrose functionalized black cumin seeds are compared with raw black cumin seeds. The raw and the modified black cumin seeds are used for the removal uptake of Cr(VI) and Pb(II) ions.

Chapter 9

In this chapter the sorption study of Cr(VI), Cd(II) ions and MB dye is conducted using acetone and DMF to treat the black cumin seeds. The defatted seeds are further carbonized at 600 °C.

The results of raw, defatted and carbonized seeds are compared with each other using pH, contact time, initial concentration and temperature.

Chapter 10

This chapter provides the main conclusions from the dissertation, the contribution of the work and some recommendations for further study.

References

ADIE D. B., OKUOFU C.A. & OSAKWE C., 2012. Comparative analysis of the adsorption of heavy metals in wastewater using borrassus aethiopium and cocos nucifera. *International Journal of Applied Science and Technology,* 2(7), 314-322.

AHMAD, R. & HASEEB, S., 2014. Black cumin seeds (BCS): a non-conventional adsorbent for the removal of Cu(II) from aqueous solution. *Desalination Water Treatment*, 1-10.

AKHTAR, M.S., CHALI, B. & AZAM, T., 2013. Bioremediation of arsenic and lead by plants and microbes from contaminated soil. *Research Plant Science,* 1, 68-73.

ALI, I.H., AL MESFER, M.K., KHAN, M.I., DANISH, M. & ALGHAMDI, M.M., 2019. Exploring adsorption process of lead(II) and chromium(VI) ions from aqueous solutions on acid activated carbon prepared from Juniperus procera leaves. *Processes*, 7(217), 1-14.

AWUAL, M. R., KHRAISHEH, M., ALHARTHI, N.H., LUQMAN, M., ISLAM, A., KARIM, M.R., RAHMAN, M.M. & KHALEQUE, M. A., 2018. Efficient detection and adsorption of cadmium(II) ions using innovative nano-composite materials, *Chemical Engineering Journal* 343, 118-127.

BABALOLA, B., M., 2018. Investigating adsorption characteristics of *delonix regia* for heavy metals removal in wastewater and its potential for remediating contaminated soils. PhD Thesis. Lancaster University.

BARGAT, M., CHEGROUCHE, S., MELLAH, A., BENSMAIN, B., NIBOU, D. & BOUFATIT, M., 2014. Application of algerian bentonite in the removal of Cadmium (II) and Chromium (VI) from aqueous solutions. *Journal of Surface Engineered Materials and Advanced Technology*, 4, 210-226.

BARSAINYA, M., CHANDRA, P. & SINGH, D. P., 2016. Investigation of Cr(VI) uptake in saline condition using psychrophilic and mesophilic penicillium sp. *International Journal of Current Microbiology Applied Sciences*, 5(1), 274-288.

BELTRAME, K.K., CAZETTA, A.L., DE SOUZA, P.S.C., SPESSATO, L., SILVA, T.L. & ALMEIDA, V.C., 2018. Adsorption of caffeine on mesoporous activated carbon fibers prepared from pineapple plant leaves. *Ecotoxicology and Environmental Safety*, 147, 64-71.

BREWER, G.J. 2010. Copper toxicity in the general population. *Clinical Neurophysiology*, 121, 459-460.

CAROLIN, C. F., KUMAR, P. S., SARAVANAN, A., JOSHIBA, G. J. & NAUSHAD, M., 2017. Efficient techniques for the removal of toxic heavy metals from aquatic environment: A review. *Journal of Environmental Chemical Engineering*, 5, 2782-2799.

CERVEIRA, J.F., SANCHEZ-ARAGO, M., URBANO, A.M. & CUEZVA, J.M., 2014. Short-term exposure of nontumorigenic human bronchial epithelial cells to carcinogenic chromium(VI) compromises their respiratory capacity and alters their bioenergetic signature. *FEBS Open Bio* 4, 594-601.

DARGAHI A., GOLESTANIFAR, H., DARVISHI, P., KARAMI, A., HASAN, S.H., POORMOHAMMADI, A. & BEHZADNIA, A., 2016. An investigation and comparison of removing heavy metals (Lead and Chromium) from aqueous solutions using magnesium oxide nanoparticles. *Polish Journal Environmental Studies*, 25(2), 557-562.

DE GISI, S., LOFRANO, G., GRASSI, M. & NOTARNICOLA, M., 2016. Characteristics and adsorption capacities of low-cost sorbents for wastewater treatment: a review. *Sustainable Materials and Technologies*, 9, 10-40.

DEHGHANI, M. H., SANAEI, D., ALI, I. & BHATNAGAR, A., 2016a. Removal of chromium(VI) from aqueous solution using treated waste newspaper as a low-cost adsorbent: Kinetic modeling and isotherm studies. *Journal of Molecular Liquids,* 215, 671-679.

DEHGHANI, M.H., MOHAMMADTAHER, M., BAJPAI, A.K, HEIBATI, B., TYAGI, I., ASIF, M., AGARWAL, S. & GUPTA, V.K., 2016b. Removal of noxious Cr(VI) ions using

single-walled carbon nanotubes and multi-walled carbon nanotubes, *Chemical Engineering Journal*, 279, 344-352.

DEHGHANI, M.H., SARMADI, M., ALIPOUR, M.R., SANAEI, D., ABDOLMALEKI, H., AGARWAL, S. & GUPTA, V.K., 2019. Investigating the equilibrium and adsorption kinetics for the removal of Ni(II) ions from aqueous solutions using adsorbents prepared from the modified waste newspapers: A low-cost and available adsorbent. *Microchemical Journal*, 146,1043-1053.

DUMAN, O., TUNÇ, S., POLAT, T.G. & BOZOGLAN, B.K., 2016. Synthesis of magnetic oxidized multiwalled carbon nanotube-K-carrageenan-Fe_3O_4 nanocomposite adsorbent and its application in cationic Methylene Blue dye adsorption, *Carbohydrate polymers*,147.

EDOKPAYI, J. N., NDLOVU S. S. & ODIYO. J. O., 2019. Characterization of pulverized Marula seed husk and its potential for the sequestration of methylene blue from aqueous solution. *BMC Chemistry*, 13(10), 1-14.

EL-SAYED, G. O., 2011. Removal of methylene blue and crystal violet from aqueous solutions by palm kernel fiber. Desalination 272, 225-232.

ESSOMBA, J.S., NDI NSAMI, J., BELIBI BELIBI, P.D., TAGNE, G.M. & KETCHA MBADCAM. J., 2014. Adsorption of cadmium(II) ions from aqueous solution onto kaolinite and Metakaolinite. *Pure and Applied Chemical Sciences,* 2(1), 11-30.

FESTA, R.A. & THIELE, D.J., 2011. Copper: An Essential Metal in Biology. *Current Biology*, 21(21), 877.

FOO, K.Y. & HAMEED, B.H., 2012. Microwave-assisted preparation and adsorption performance of activated carbon from biodiesel industry solid reside: influence of operational parameters. *Bioresource technology*, 103, 398-404.

FRINDT, B., MATTUSCH, J., REEMTSMA, T., GRIESBECK, A. G. & REHOREK, A., 2017. Multidimensional monitoring of anaerobic/aerobic azo dye-based wastewater treatments by hyphenated UPLC-ICP-MS/ESI-Q-TOF-MS techniques. *Environmental Science and Pollution Research*., 24(12), 10929-10938.

GAVNEY, D. FELL, G.S. & O'REILLY, D.J., 2000. Wilson's disease: acute and presymptomatic laboratory diagnosis and monitoring. *Journal of Clinical Pathology*. 53(11), 807-812.

GOOGERDCHIAN, F., MOHEB, A., EMADI, R. & ASGARI, M., 2018. Optimization of Pb(II) ions adsorption on nanohydroxyapatite adsorbents by applying Taguchi method, *Journal of hazardous materials*, 349, 186-194.

HANEY JR., J.T., ERRAGUNTLA JR., N., SIELKEN, R.L. & VALDEZ-FLORES, C., 2014. Development of an inhalation unit risk factor for hexavalent chromium. *Regulatory Toxicology and Pharmacology* 68, 201-211.

HANNACHI, Y., SHAPOVALOV, N.A. & HANNACHI, A., 2010. Adsorption of nickel from aqueous solution by the use of low-cost adsorbents, *Korean Journal of Chemical Engineering*. 27(1), 152-158.

HOONG, N.J., ISMAIL, N., 2018. Removal of dye in wastewater by adsorption-coagulation combined system with Hibiscus sabdariffa as the coagulant. MATEC Web of Conferences 152, 01008.

HU, W., LU, S.H., SONG, W.C., CHEN, T.H., HAYAT, T., ALSAEDI, N.S., CHEN, C.L & LIU, H.B., 2018. Competitive adsorption of U(VI) and Co(II) on montmorillonite: a batch and spectroscopic approach, *Applied Clay Science*, 157, 121-129.

HUMMEL, W. & CURTI, E., 2003. Nickel aqueous speciation and solubility at ambient conditions: a thermodynamic elegy, *Monatshefte für Chemie/Chemical Monthly*, 134, 941-973.

ISLAM, M.A., AWUAL, M. R. & ANGOVE, M.J., 2019. A review on nickel(II) adsorption in single and binary component systems and future path, *Journal of Environmental Chemical Engineering*, 7(5).

KENAWY, I., HAFEZ, M., ISMAIL, M. & HASHEM, M., 2018. Adsorption of Cu(II), Cd(II), Hg(II), Pb(II) and Zn(II) from aqueous single metal solutions by guanyl-modified cellulose, *International Journal of Biological Macromolecules*. 107, 1538-1549.

KETSEL, G., ANIMEN, Z. & TALEMA, A., 2020. Adsorption of lead(II), cobalt(II) and iron(II) from aqueous solution by activated carbon prepared from white lupine (GIBITO) husk. *Journal Thermodynamics and Catalysis,* 11(1), 1-8.

KETTUM, W., TRAN, T. T. V., KONGPARAKUL, S., REUBROYCHAROEN, P., GUAN, G., CHANLEK, N., & SAMART, C., 2018. Heavy metal sequestration with a boronic acid-functionalized carbon-based adsorbent. *Journal of Environmental Chemical Engineering* 6,1147-1154.

KIM, S.Y., JIN, M.R., CHUNG, C.H., YUN, Y.S., JAHNG, K.Y. & YUL, K.Y., 2015. Biosorption of cationic basic dye and cadmium by the novel biosorbent Bacillus catenulatus JB-022 strain. *Journal Bioscience Bioengineering,* 119, 433-439.

KUMARASINGHE, D., PETTIGREW, L. & NGHIEM, L.D., 2009. Removal of heavy metals from mining impacted water by an electrocoagulation-ultrafiltration hybrid process. *Desalination and Water Treatment*, 11, 66-72.

LIU, C., ZHAO, D., ZHANG, K., XUAN, H., ALSAEDI, A., HAYAT, T. & CHEN, C., 2019. Fabrication of Si/Ti-based amino-functionalized hybrids and their adsorption towards cobalt(II). *Journal of Molecular Liquids,* 289, 111051.

LUO, X.-P., FU, S.-Y., DU, Y.-M., GUO, J.-Z & LI, B., 2017. Adsorption of methylene blue and malachite green from aqueous solution by sulfonic acid group modified MIL-101, *Microporous Mesoporous Materials,* 237, 268-274.

MAHMOUD, M.E., AMIRA, M.F., SELEIM, S.M. & MOHAMED, A.K., 2017. Adsorption isotherm models, kinetics study, and thermodynamic parameters of Ni (II) and Zn (II) removal from water using the LbL technique, *Journal of Chemical & Engineering Data*, 62, 839-850.

MAHMUD, H.N.M.E., HUQ, A.O. & YAHYA, R., 2016. The removal of heavy metal ions from wastewater/aqueous/solution using polypyrrole-based adsorbents: A review. *RSC Advances*, 6, 14778-14791.

MATOS, T.T.S., SCHULTZ, J., KHAN, M.Y., ZANOELO, E.F., MANGRICH, A.S., ARAUJO, B.R., NAVICKIENE, S. & ROMAO, L.P.C., 2017. Using Magnetized (Fe_3O_4/biochar nanocomposites) and activated biochar as adsorbents to remove two neuro-active pesticides from waters. *Journal of Brazilian Chemical Society*, 28(10), 1975-1987.

MIRETZKY, P. & CIRELLI, A.F., 2010. Cr(VI) and Cr(III) removal from aqueous solution by raw and modified lignocellulosic materials: a review, *Journal of hazardous materials*, 180, 1-19.

MOON, W. C. & PALANIANDY, P., 2019. A Review on Interesting Properties of Chicken Feather as Low-Cost Adsorbent. *The International Journal of Integrated Engineering*, 11(2), 136-146.

MOYO, M., CHIKAZAZA, L., NYAMUNDA, B.C. & GUYO, U., 2013. Adsorption batch studies on the removal of Pb(II) using maize tassel based activated carbon. *Journal of Chemistry*, 2013, 1-8.

NADAROGLU, H. & KALKAN, E., 2012. Removal of cobalt (II) ions from aqueous solution by using alternative adsorbent industrial red mud waste material. *International Journal of Physical Sciences*, 7(9), 1386-1394.

NASSEF, E., MAHMOUD, A. SALAH; H. & EL-TAWEEL, Y., 2017. Removal of copper ions from liquid wastes using adsorption technique. *International Journal of Research in Industrial Engineering*, 6(3), 522-562.

NKUTHA, C.S., SHOOTO, N.D. & NAIDOO, E.B., 2020. Adsorption studies of methylene blue and lead ions from aqueous solution by using mesoporous coral limestones. *South African Journal of Chemical Engineering*, 34, 151-157.

NOH, Y., JO, E.J., MUN, H., AHN, Y.D. & KIM, M.G., 2017. Homogeneous and selective detection of cadmium ions by forming fluorescent cadmium-protein nanoclusters, *Chemosphere*, 174, 524-530.

OUMA, I.L.A., NAIDOO, E.B. & OFOMAJA, A.E., 2018. Thermodynamic, kinetic and spectroscopic investigation of arsenite adsorption mechanism on pine cone-magnetite composite. *Journal of Environmental Chemical Eng*ineering, 6, 5409-5419.

PRABAKARAN, R. & ARIVOLI, S., 2013. Removal of cobalt (II) from aqueous solutions by adsorption on low cost activated carbon. *International Journal of Science, Engineering and Technology Research*, 2(2), 271-283.

QIU, J., FENG, Y., ZHANG, X., JIA, M. & YAO, J., 2017. Acid-promoted synthesis of UiO-66 for highly selective adsorption of anionic dyes: adsorption performance and mechanisms, *Journal of Colloid Interface and Science*, 499,151-158.

RAJASULOCHANA, P. & PREETHY, V., 2016. Comparison on efficiency of various techniques in treatment of waste and sewage water-A comprehensive review. *Resource Efficient Technologies,* 2, 175-184.

RAMABRAHMAM, V., 2016. Environmental effects of India due to water pollution. *International Journal of Engineering research* 4, 145-148.

ROZADA, F., OTERO, M., MORAN, A. & GARCIA, A.I., 2008. Adsorption of heavy metals onto sewage sludge-derived materials. *Bioresource Technology*, 99, 6332-6338.

SALEEM, H., RAFIQUE, U. & DAVIES, R., 2016. Investigation on post-synthetically modified UiO-66-NH_2 for the adsorptive removal of heavy metal ions from aqueous solution. *Microporous Mesoporous Materials,* 221, 238-244.

SAYADI, M.H., REZAEI, M.R. & REZAEI, A., 2014. Fraction distribution and bioavailability of sediment heavy metals in the environment surrounding MSW landfill: a case study. *Environmental Monitoring and Assessment*; 187(1), 4110.

SEEMA, K.M., MAMBA, B.B., NJUGUNA, J., BAKHTIZIN, R.Z. & MISHRA, A.K., 2018. Removal of lead (II) from aqueous waste using (CD-PCL-TiO_2) bio-nanocomposites. *International Journal of Biological Macromolecules,* 109, 136-142.

SHAJAHAN, A., SHANKAR, S., SATHIYASEELAN, A., NARAYAN, S.K., NARAYANAN, V., KAVIYARASAN, V. & IGNACIMUTHU, S., 2017. Comparative studies of chitosan and its nanoparticles for the adsorption efficiency of various dyes. 2017. *International Journal of Biological Macromolecules*, 104, 1449-1458.

SIYAL, A.A., SHAMSUDDIN, M.R., KHAN, M.I., RABAT, N.E., ZULFIQAR, M., MAN, Z., SIAME, J. & AZIZLI, K.A., 2018. A review of geopolymers as emerging materials for the adsorption of heavy metals and dyes, *Journal of Environmental Management*, 224, 327-339.

SONG, D., PAN, K., TARIQ, A., AZIZULLAH, A., SUN, F., LI, Z. & XIONG, Q., 2016. Adsorptive removal of toxic chromium from waste-water using wheat straw and eupatorium adenophorum. *PLOS ONE*, 11(12), 1-15.

TIZRO, S. & BASERI, H., 2017. Removal of cobalt ions from contaminated water using magnetite-based nanocomposites: Effects of various parameters on the removal efficiency. *Journal of Water and Environmental Nanotechnology*, 2(3), 174-185.

TORRES-CABAN, R., VEGA-OLIVENCIA, C.A., ALAMO-NOLE, L., MORALES-IRIZARRY, D., ROMAN-VELAZQUEZ F. & MINA-CAMILDE, N., 2019. Removal of copper from water by adsorption with calcium-alginate/spent-coffee-grounds composite beads. *Materials*, 12(395), 1-21.

TRIPATHI, A. & RANJAN, M.R., 2015. Heavy metal removal from wastewater using low cost adsorbents. *Journal of Bioremediation and Biodegradation*. 6(6), 1-5.

TYAGI, I., GUPTA, V., SADEGH, H., GHOSHEKANDI, R. & MAKHLOUF, A. S. H., 2017. Nanoparticles as adsorbent; a positive approach for removal of noxious metal ions: a review. *Science Technology and Development*, 34, 195-214.

UDDIN, M.K., 2017. A review on the adsorption of heavy metals by clay minerals, with special focus on the past decade, *Chemical Engineering Journal*, 308, 438-462.

USEPA and OAR, 2012. Chromium Compounds, Technology Transfer Networks Air Toxics.

WHO Guidelines for Drinking-water Quality (Cadmium in Drinking-water), World Health Organization, 2011.

WONGROD, S., SIMON, S., GUIBAUD, G., LENS, P.N.L., PECHAUD, Y., HUGUENOT, D. & VAN HULLEBUSCH, E.D., 2018. Lead sorption by biochar produced from digestates: Consequences of chemical modification and washing. *Journal of Environmental Management*, 219, 277-284.

YAZIDI, A., SELLAOUI, L., BADAWI, M., DOTTO G.L., BONILLA-PETRICIOLET, A., LAMINE, A.B. & ERTO, A., 2020. Ternary adsorption of cobalt, nickel and methylene blue on a modified chitin: Phenomenological modeling and physical interpretation of the adsorption mechanism. *International Journal of Biological Macromolecules*, 158,595-604.

YEU, Z., BENDER, S., WANGER, J. & ECONOMY, J., 2009. Removal of chromium(VI) by low-cost chemically activated carbon materials from water. *Journal of hazardous materials*, 166 (1), 74-78.

ZHANG, R., WANG, Z., ZHOU, Z., LI, D., WANG T., SU, P. & YANG, Y., 2019. Highly effective removal of pharmaceutical compounds from aqueous solution by magnetic Zr-based MOFs composites. *Industrial & Engineering Chemistry Research*, 58, 3876-3884.

CHAPTER 2: LITERATURE REVIEW

2.1 Environmental Pollution

A common feature of industrial effluents is that they almost always contain harmful toxic metals (Aba-aaki et al. 2013). According to Ketsela et al. (2020), water used in industries creates a wastewater that has a probable hazard for the environment because of introducing various pollutants such as metal toxic ions into soil and water resources. Therefore, to protect the environment, the maximum level of toxic metals must be restricted. Toxic metals ions can accumulate in the environment and spread to organisms through chain elements such as food chain and thus may pose a substantial health danger to organisms (Oljira 2016).

2.1.1 Water pollution

Water is one of the most important materials on earth (Sharma & Tyagi, 2013). All human beings, animals and plants need water to survive. If there is no water there would be no life on earth. It covers about 71% of the Earth's surface and is important for all known forms of life (Rajasulochana & Preethy, 2016). But only 2.5% of the Earth's water is fresh water. Due to fast growing industrialization, enormous volumes of wastewater contaminated with toxic ions, get released into environment and this valuable resource is used for irrigation (Khamis et al. 2009). Therefore, the risk of this polluted water consumption and its sanitation problem is increasing day to day (Rajasulochana & Preethy, 2016). As it is known that water scarcity is a problem, as such water pollution has significant negative influence on human livelihoods, economic development and environmental quality throughout the world. Hence, it has become a crucial to protect the water from getting polluted.

2.1.2 Metal and dye pollution

The disposal of effluent with toxic metal-rich ions from industries without treatment to the natural aquatic bodies and to the environment are a matter of great scientific concern (Dargahi et al. 2016). Most of the metals ions are known to be toxic and those include copper-Cu(II), chromium-Cr(VI), cadmium-Cd(II), lead-Pb(II), nickel-Ni(II), mercury-Hg(III), silver-Ag(I) and zinc-Zn(II) (Essomba et al. 2014) and they get released into the environment in amounts that pose a risk to human health. Toxic metal ions are non-biodegradable and tend to accumulate in living organisms causing various diseases and disorders (Ali et al. 2019). Therefore, the reduction of the pollution to an acceptable level is necessary especially when toxic metals ions are present in solution.

The textile industry is also a major pollutant producer due to the usage of dyestuff (Aichour et al. 2019). and they are generally employed in the dyeing of products (Regti et al. 2017; Deniz & Kepekci, 2017). An excessive wastewater amount containing dyes discharged without any decontamination can lead to serious health and environment issues (Husain et al. 2014). Methylene blue dye (MB) is used in different industries and it was stated that methylene blue dye has no dangerous effect when it is used as a medicinal product (Rafatullah et al. 2010). Methylene blue is not strongly hazardous, but it still has a harmful effect on living organisms when occurring at high concentration in water (Aichour et al. 2019). It is further mentioned that it dissociates into a cation and a chloride anion in aqueous solution.

2.2 Water Remediation Techniques

Conventional treatment procedures are commonly used for the elimination of metal ions from industrial wastewater. These methods include; chemical precipitation, membrane filtration technology, ion exchange**,** electrodialysis, coagulation and many others. These conventional

methods are expensive because the materials used are not cost effective and generation of toxic sludge as by-product is often ineffective for the sequestration of toxic metal ions from industrial wastewater (Ketsela et al. 2020). These technologies for toxic metal's removal from wastewater are ineffective (Bardestani et al. 2019). Due to the problems mentioned above adsorption has been regarded as a cheaper method because it uses low-cost materials, efficient at low concentration of cations and easy operation with no environmental side effects (Richards et al. 2019). The details of the all techniques are discussed in the following sections.

2.2.1 Chemical precipitation

Chemical precipitation involves the addition of chemical reagents followed by the separation of the precipitated solids from the treated water (Lakherwal 2014). Coagulants such as alum, lime, iron salts and other organic polymers are added in order to precipitate the heavy metals. These coagulants react with heavy metals and thereafter form insoluble precipitates (Agrwal & Singh, 2017). These precipitates are removed using sedimentation and then the clear water is decanted. The disadvantage of this method is that it produces a lot of sludge. It is useful in cases when the concentration of heavy metals is high and less effective for low heavy metal concentration (Agrwal & Singh, 2017).

2.2.2 Membrane filtration technology

This method uses filtration processes with different types of membranes such ultrafiltration, reverse osmosis, microfiltration, nanofiltration and electrodialysis (Fu & Wang, 2011). The aim of this method is to separate the heavy metal ions salts from water using selective membranes (Algureire & Abdulmajeed, 2016). The main disadvantage of this technique is the high cost of the membrane (Agrwal & Singh, 2017).

2.2.3 Ion exchange

Ion exchange involves the attraction of soluble ions from liquid phase to solid phase (Gunatilate 2015). This is the main method used for water treatment. Ion exchange resins are organic materials which are used as ion exchangers in this process. They are insoluble in water and absorb positively or negatively charged ions from an electrolyte solution and then release other ions of the same charges into the solution in an equal amount (Gunatilate 2015). The positively charged ions (hydrogen and sodium ions) in resins are exchanged with positively charged ions such as nickel, copper and zinc ions in water. Then negative ions (hydroxyl and chloride ions) in the resins are replaced by the negatively charged ions, the chromate, sulphate, nitrate, cyanide and dissolved organic carbon. It is said that this process is used only for low concentrated metal solutions and is sensitive to the pH of the solution. Other disadvantages include resin fouling and resin regeneration cost (Agrwal & Singh, 2017).

2.2.4 Electrodialysis

Electrodialysis is an electro-membrane procedure which involves the transport of ions from one solution to another through membrane under the influence of a potential gradient (Ciafalo et al. 2019). The applied voltage across the two electrodes create the potential field necessary for electrodialysis to operate, charged ions are driven through the membranes made from ion exchange materials (Babalola 2018). The membranes are selective and hence they can transport ions with negative or positive charge and reject oppositely charged ions (Babalola 2018). As a result, dialysis can be used for determined concentration and separation or elimination of ions (Akpor & Muchie, 2010). Electrodialysis still remains cost intensive stand-alone operation mode (Roman et al. 2019). Its development has been stagnated for some time due to poor performance of the membrane (Tian et al. 2020).

2.2.5 Coagulation

Coagulation is the water treatment process which is generally used in drinking water treatment process (Tang et al. 2014). It is also the most studied process to remove heavy metals ions in water for pollution control. In the flocculation process or coagulation process, the chemicals (coagulants or flocculants) are added into water for removal of heavy metals. Several factors have been found to affect the removal of heavy metals by coagulation. These include the type of coagulant used, pH, dosages, and concentration of metal ions (Tang et al. 2014). Aluminium sulfate (alum), polyaluminium chloride (PACl), ferric chloride and hydrated lime are used extensively as coagulants in water and wastewater treatment (Pang et al. 2011). The disadvantages of this method are the high cost and large consumption of a large amount of chemicals (Agrwal & Singh, 2017).

2.2.6 Adsorption

Adsorption is a physicochemical process that occurs at the solid-liquid interface and can remove toxic metal ions and dyes from industrial effluent effectively and efficiently (Bellir et al. 2013). Adsorption is a promising method of separating and purifying heavy metals because it has significant advantages such high efficiency in removing very low levels of toxic metals from dilute solutions, easy handling, lower operating cost, high selectivity, it does not produce harmful chemicals or sludge and adsorbents can be regenerated (Yarkandi 2014; Agrwal & Singh, 2017). The performance of previously mentioned conventional methods (section 2.2.1 to 2.2.6) are generally acceptable but they have several drawbacks; they cannot work very well in treating toxic metal ions and dyes at elevated concentrations (Rajasulochana & Preethy, 2016).

Adsorption is one of the best water treatment technologies that have been used extensively for the uptake of toxic metal ions from wastewater (Daci-Ajvazi et al. 2016). Therefore, continuously increasing demand for raw materials and the limited availability of natural resources has created a demand to investigate possible affordable materials that can be used as adsorbents for toxic metal ions. Adsorption may have disadvantage such as high investment and cost of materials however this is only applicable when commercial activated carbon is used. Therefore, in this study Black Cumin Seeds (BCS)-*Nigella sativa* L. have been selected as the material that was used for adsorption of toxic ions in aqueous solution.

2.2.6.1 Adsorption processes

Adsorption can be carried out as a semi batch, batch and continuous processes (Mathew et al. 2016). When small quantities are to be treated, batch processes are usually carried out and the equilibrium distribution depends on the contact time in batch process (Mishra & Tripathi, 2008). Adsorbates (pollutant/toxic metal ions) and adsorbents (materials) experience certain attractive forces which bind them and these forces are due to Van der Waals forces which are weak in nature or they may bind due to chemical bonds which are strong in nature (Mathew et al. 2016). Adsorption is categorized into two catogaries based on attraction and the strength of force predominant between adsorbate and adsorbent namely: physical adsorption and chemical adsorption.

Physical adsorption is also known as physisorption, it happens when the attractive forces present between adsorbate and adsorbent are due to Van der Waals forces (Esfandiari & Monajjemi, 2013). Physisorption has also low enthalpy ($\Delta H°$) values of adsorption which are between 2.1 to 20.9 KJ/mol (Aichour & Zaghouane-Boudiaf, 2019). This usually occurs with development of multilayer of adsorbate on adsorbent and this phenomenon decreases with an

increase in temperature and usually takes place at a lower temperature (Mathew et al. 2016). Chemical adsorption is also known as chemisorption, it takes place when the attractive forces between the adsorbate and adsorbent are chemical forces of attraction or via chemical bonding (Mathew et al. 2016). Here only a monolayer (single) formation of the adsorbate onto the adsorbent takes place and there is usually high enthalpy of adsorption with (ΔH°) adsorption values between 20.9 to 418.4 KJ/mol (Aichour & Zaghouane-Boudiaf, 2019). In this mechanism, the adsorption first increases and then decreases with a rise in temperature (Mathew et al. 2016).

2.3 Various types of adsorbents

Selecting the most capable type of biomass from a numerous huge pool of readily accessible and cheap biomaterials is the first most important challenge for the biosorption field and full-scale sorption process requires materials which have high metal binding capabilities (Mathew et al. 2016). It is further indicated that these biosorbent materials have been established, tested and reported to bind a variation of toxic metals to different extents.

2.3.1 Adsorption using activated carbon

Activated carbon (AC) is the most effective sorbent material for removing toxic metal ions from an industrial effluent and wastewater from municipal, landfill leachate and contaminated groundwater (Babalola 2018). Activated carbon is used in applications primarily related to toxic species removal through adsorption in liquid phase (Danish et al. 2018). The adsorption helps not only in the removal of unwanted toxic species from gas or liquid but also capable of recovering the adsorbate molecules (Danish et al. 2018). The adsorption of toxic metal ions

onto activated carbon is greatly influenced by the physical and chemical properties such as pore space volume, ash content, specific surface area and surface functionalities (Carolin et al. 2017). In order to increase the capacity of adsorbents for toxic ions adsorption, different researches have altered the properties of the activated carbon by incorporating nanoparticles, as well as addition of functional groups such as phosphates, nitrogen and many others.

Adsorption properties of NH_4Cl-modified activated carbon (NAC) and commercial standard activated carbon (SAC) were compared to one another in the research study of Alahabadi et al. (2017). The adsorption mechanism and performance of NAC and SAC were obtained by evaluating the effects of various physicochemical factors such as; agitation speed, pH, contact time, sorbent dose, temperature, equilibrium, kinetics and thermodynamic. Both activated carbons were used for the removal of an antibiotic namely; chlortetracycline (CTCN). The kinetic studies showed that the adsorption of CTCN onto the NAC was more rapid than SAC. Thermodynamic studies indicated that, the adsorption of CTCN onto the NAC surface was more spontaneous, feasible and favourable compared to SAC. Their result showed that, NAC had better performances and was best suitable choice for the removal of CTCN antibiotic from aqueous solutions compared to SAC.

Danmaliki & Saleh (2017) loaded activated carbon (AC) with two different metals (cerium-Ce and iron-Fe) to form composites. The three composites prepared were AC/Ce, AC/Fe, and AC/Ce/Fe. The composites were investigated for the simultaneous adsorption of desulfurization of thiophene, benzothiophene (BT) and dibenzothiophene (DBT). The loaded activated carbon was compared with the unloaded activated carbon. The unloaded AC had the highest surface area of 460.27 m^2/g and pore volume of 0.71 cm^3/g. Additionally, the unloaded AC showed the highest surface oxygen-containing groups but performed the least in

desulfurization. The AC/Ce/Fe performed the best in the adsorption of thiophene (31%), BT (30%), and DBT (75%) despite having the least surface area of 430.44 m^2/g and pore volume of 0.64 cm^3/g. The adsorptive desulfurization efficiency followed the order: AC < AC/Fe < AC/Ce < AC/Ce/Fe. The use of AC/Ce/Fe had high absorptive capacity of 16 mg/g and breakthrough for DBT.

Zhang et al. (2018) studied the adsorption behaviour of five volatile organic compounds (VOCs). The five VOCs were acetone, ethyl acetate, propyl acetate, butyl acetate, and isopropanol, which were chosen as pollutants. Commercial activated carbon (CAC) with surface area of 1099.74 m^2/g was used as an adsorbent. The adsorption capacities of the above VOCs were 289.8, 389.4, 443.7, 467.4, and 474.3 mg/g respectively. Their results showed that the higher molecular weights VOCs had high adsorption uptakes by CAC. Their findings would be helpful for the optimization of the adsorption system for the removal of VOCs.

Five commercial activated carbons granular (WG-12, ROW 08 Supra, Picabiol, Filtrasorb 300-[F-300] and Filtrasorb 100-[F-100]) were used for the adsorption of chloramphenicol (Lach 2019). The commercial activated carbons were modified at 400 and 800 °C in water vapour, atmosphere of air and carbon dioxide to remove chloramphenicol. The highest adsorption capacity was obtained for the use of Picabiol with 214 mg/g, characterized by the highest pore volume and specific surface area. Commercial activated carbon-Picabiol showed that it can be used to remove chloramphenicol from water because it was characterized by high adsorption capacity. Activated carbons were ranked according to their adsorption capacity in the following order: Picabiol> ROW 08>F-300>WG-12>F-100. The order of activated carbons according to the adsorption capacity was consistent with the order of total volume of pores and the total

volume of micro and mesopores. This indicated the importance of the phenomenon of volumetric pore filling.

2.3.2 Adsorption using zeolite

Zeolites have been generally used for toxic metal ions removal due to their high cation exchange capacity and surface sorption properties (Hong et al. 2019). Hong et al. (2019) prepared a sequence of amino-acid zeolite samples using alanine (A), glutamic acid (E), histidine (H), proline (P), arginine (R), serine (S) and threonine (T) as adsorbents for toxic metal ions removal of Pb(II), Cu(II) and Ni(II). The prepared amino-acid zeolite adsorbents were represented as MLTA-X, where X is the single letter code of an amino acid. The adsorption of Pb(II) and Cu(II) was dominated by cation exchange whilst the adsorption of Ni(II) was controlled by a surface reaction which showed dependence on the zeolite pore geometry and adsorption conditions. The adsorption capacities for Cu(II) and Pb(II) were around 170 and 510 mg/g. The adsorption of Ni(II) by zeolites was significantly influenced by hierarchical pore geometry, while the adsorption of Pb(II) or Cu(II) was dependent on cation exchange determined by the framework composition. The proline-mediated MLTA-P displayed enhanced adsorption of approximately 100 mg/g for Ni(II) at 301 K under neutral pH. Zeolite P was prepared through fly ash using hydrothermal method for the adsorption of copper-Cu(II) and nickel-Ni(II) ions in aqueous solution (Liu et al. 2019). The removal capacities for Cu(II) and Ni(II) can reach up to 138.1 and 77.0 mg/g respectively. The synthesized zeolite products can effectively remove Cu(II) and Ni(II), ions at higher temperatures.

Magnetically modified zeolite (MMZ) composite was used for the adsorption of lead-Pb(II). The adsorption capacity of Na-zeolite and modified zeolite were determined for the lead ions removal (Yuan et al. 2018). The modified adsorbent was obtained reacting iron oxide-Fe_3O_4 with zeolite and compared to Na-zeolite. The results showed that the adsorption capacity of the modified zeolite decreased with an increase in the pH of the solution and the maximum adsorption capacity reached equilibrium at pH 4.0 whilst the BET surface area increased from 25.15 to 28.12 m^2/g. Additionally, their results revealed that the equilibrium sorption capacity on each adsorbent increased with the increase of initial concentration and the Pb(II) maximum amount of sorption adsorbed on MMZ and Na-zeolite was 84.00 and 66.96 mg/g respectively. Adsorption of Pb(II) onto MMZ from aqueous solutions was related to porous microstructure containing a large number of channels and ion exchange characteristics.

2.3.3 Adsorption using low-cost adsorbents

The adsorption of toxic metals ions and dyes by using low-cost adsorbents seems to be more inspiring because there are several materials existing locally and abundantly such as agricultural wastes, natural materials and industrial by-products which can be utilized as low-cost adsorbents (Siti Nur et al., 2013). In order for the adsorbent to be commercially worthwhile, it should have high selectivity, enable fast separations, kinetic characteristics, chemical and thermal stability, resistance to fouling, low solubility in the liquid and regeneration capacity (Tripathi & Ranjan, 2015). Many low-cost adsorbents derived from several natural materials have been applied for treatment of wastewater polluted with toxic ions (Tripathi & Ranjan, 2015). Some of the low-cost adsorbents include wheat straw (Song et al. 2016), fruit hulls (Islam et al., 2017), waste carpets (Hassan & Elhadidy, 2017), banana peels (Ajmi et al., 2018), coffee waste (Suganya & Kumar, 2018), chaenomeles sinensis seeds (Hu

et al. 2019), *Delonix regia* seed pods (Akinola et al. 2019), white lupine husk (Ketsela et al. 2020) and many more.

The work of Suganya & Kumar (2018) showed that the removal of Cr(VI) is influenced by adsorbent dosage, temperature, initial ion concentration, and contact time. Their study explored the feasibility of using coffee waste (CW) based carbons treated with sulfuric acid (H_2SO_4) for the uptake of Cr(VI) ions from aqueous solution under different experimental conditions. The activation of CW enhanced the physiochemical and surface morphological properties after treatment with H_2SO_4. The removal efficiency was found to be increasing with increase in temperature and decreased with increase in metal ion concentration. The uptake capacity of the carbon-based activated CW was found to have optimum dosage of 3 g/L with initial concentration of 50 mg/l, temperature at 30 °C and contact time of 30 minutes.

Bhomick et al. (2018) prepared activated carbon from *Pinus kesiya* cone by $ZnCl_2$ for the removal of Alizarin Red S (ARS) dye. The efficiency of the prepared adsorbent was evaluated using various batch analysis such as the influence of initial concentration, adsorbent dosage, contact time and pH. ARS anionic dye adsorption onto activated carbon prepared from *Pinus kesiya* cones had maximum uptake of 118.06 mg/g. Textural and surface characterization of pine cone activated carbon showed that the surface area was 878.07m^2/g with total pore volume of 0.412 cm^3/g. It was concluded that the activated carbon prepared from *Pinus kesiya* cones are promising cost-effective adsorbent because of their high surface and adsorption capacity towards ARS dye.

Evaluation of different parameters such as contact time, concentration of pollutants, temperature, pH of the solution, mass of adsorbent and stirring speed was investigated by

Aichour et al. (2019) for the elimination of methylene blue (MB) dye from wastewater using unmodified citrus peels encapsulated with calcium alginate (UCP/A) and unmodified citrus peels (UCP). The batch studies indicated that the adsorption of MB was affected by the solution pH. The maximum uptake was found to be 185.83 mg/g for UCP and 964.54 mg/g for UCP/A. The high uptake of MB onto UCP/A was found to be 93% at pH 7. Their results proved to be effective in the removal of the cationic MB dye in batch studies. The sorption of copper-Cu(II) and lead-Pb(II) ions by pine cone shell (PCS) was investigated in batch experiments by Martin-Lara et al. (2016). The obtained maximum capacities were 6.52 and 17.41 mg/g for Cu(II) and Pb(II) respectively. Pine cone shell showed high uptake metal ions in the affinity order of Pb(II)>Cu(II).

Ethylenediaminetetraacetic acid (EDTA), sodium dodecylsulfate (SDS), sodium hydroxide (NaOH) and nitric acid (HNO_3) were used as surface modifying agents for jackfruit peels (JFP) in order to enhance the affinity of the unmodified JFP towards the adsorption of nickel metal Ni(II) ions (Ranasinghe et al. 2018). The adsorption capacities were determined by comparing the unmodified and modified forms of JFP. The efficiency of Ni(II) ion removal was obtained by optimising parameters such pH, contact time, adsorbent dosage and initial concentration. The maximum adsorption capacity of the unmodified JFP was lower than modified. The maximum adsorption capacity onto JFP for Ni(II) modified by EDTA, SDS, NaOH and HNO_3 were 52.08, 20.88, 27.17 and 21.88 mg/g respectively. The high adsorption ability was due to disruption of the lignocellulosic structure, promoting more negative surface charges. The adsorption capacity of JFP was enhanced by surface modification owing to their characteristics, such as ion-exchange, complexation and hydrolysis of surface functional groups.

The benefits of using low cost adsorbents or agricultural wastes for wastewater treatment include superior adsorption ability, economic benefit, easy technique, modest processing, availability and easy regeneration (Tripathi & Ranjan, 2015). The recent worldwide trend to achieve higher environmental standards favours the usage of low-cost adsorbents for treatment of effluent. The literature showed that chemical treatment or thermal modifications, extent of surface modification, concentration of adsorbate, and adsorbent characteristics are some the factors responsible for metal adsorption capability (Parmar & Singh, 2013). Other factors include pH, contact period, temperature, agitation rate and dosage of adsorbent. Cost effectiveness and technical applicability are the two vital key factors for selecting effective low-cost adsorbent for toxic metal ions removal (Tripathi & Ranjan, 2015).

2.4 Factors influencing the adsorption process

The adsorbent removal capacity from aqueous solution depends on numerous physicochemical factors related to both the sorbent and the liquid phase characteristics plus concentration in the solution, initial metal ion, solution pH, temperature, presence of other competitive ions, agitation speed and speciation of the pollutant (Ibrahimi & Sayyadi, 2015). It is further mentioned that the first five factors are solution dependent and the other factors are pollutants dependent parameters. The investigation of parameter factors affecting adsorption process is very important in order to understand the sorption mechanisms, the optimum conditions for the adsorption process and potential applications (Fan 2013). The mechanism and/or importance of each parameter on removal process is discussed as follows.

2.4.1 pH

The pH of the solution is the most important parameter in the adsorption process because it affects the surface functional groups of the biomass, surface properties of sorbents, the solubility of ions in aqueous solution and ionic state of metal species (Li et al. 2010; Babalola 2018). At low pH values hydrogen ions tend to occupy the binding sites, this increases the repulsive forces needed to be overcome by the metal ions before binding can take place and subsequently make it more difficult for the metal ions to access binding sites (Saeed et al. 2002). As pH of the solution increases the retention capacity of the adsorbing surface increases significantly, however, in lower pH the adsorption process gets affected (Mathew et al. 2016).

2.4.2 Contact time

The time of interaction between the adsorbent material and the pollutants in adsorption is very important for industrial application because a superior adsorbent should quickly adsorb the metal ions in the first few minutes of interaction with the solutions (Babalola 2018). To establish an appropriate contact time between the adsorbents and metal ions in the solution, adsorption capacities of metal ion need to be measured as a function of time (Hossain 2013). Normally the removal is higher and fast in the beginning between 5-30 minutes relative to equilibrium and it is called the fast adsorption (Hossain 2013; Kuang 2020). This may be due to the larger surface area of the adsorbents being available at the beginning for the adsorption of metals ions. As the adsorption surface sites become exhausted, the rate of removal is controlled by the rate at which the adsorbate is transported from the exterior to the interior sites of the adsorbent particles (Yang et al. 2009). After 30 minutes of contact time, the relative increase in the removal extent of adsorbate is usually not significant and with the increase of

time, the adsorption rate decreases gradually and this is called the slow adsorption process (Kuang 2020).

2.4.3 Initial concentration

The initial metal ion concentration in the aqueous solution significantly affects the adsorption process. Several studies have shown the effect of initial metal concentration on metal uptake by different adsorbents. At low metal concentrations, the adsorbent surface coverage is low and the formation of surface complexes is the main mechanism (Ibrahimi & Sayyadi, 2015). In most cases the increase of initial concentration results in an increase of the adsorption capacity and a decrease of the overall removal efficiency (Coruh, & Ergun, 2009). A further increase in metal ion concentration will result in saturation of adsorption sites and surface precipitation may be the main uptake mechanism (Doula & Dimirkou, 2008). Also, the saturated active sites are usually faster in the cases where the adsorbents exhibit low selectivity for a metal ion.

2.4.4 Temperature

Most studies in literature of toxic metal ion adsorption show that an increase in temperature improves the adsorption process. Typically, at higher temperatures the adsorption of toxic ions is higher due to higher affinity of the adsorbent for the metal and/or an increase in the active sites of the solid (Arief 2008). At higher temperature the energy of the system enables the attachment of metals on the adsorbent's surface. Inglezakis & Loizidou (2004) added that at elevated temperatures ions become smaller due to their reduced hydration and their movement becomes quicker resulting in higher removal efficiencies.

2.4.5 pH of point zero charge (pH_{PZC})

The pH at which the adsorbent surface charge is equal to zero value is defined as point of zero charge (pHpzc) (Aichour & Zaghouane-boudiaf, 2019). Thus, the net charge of adsorbent surface plays an important role in sorption processes and the characterization of protonation-deprotonation behaviour of adsorbent in aqueous solution is useful to explain sorption mechanism (Fiol &Villaescusa, 2009). At this pH, the charge of the positive surface sites is equal to that of the negative ones. At solution pHs higher than pHpzc, the adsorbent surface is negatively charged and may interact with metal positive species while at pHs lower than pHpzc, solid surface is positively charged and could interact with negative species (Aichour & Zaghouane-boudiaf, 2019).

References

ABA-AAKI, R., EZ-ZAHERY, M., ET-TALEB, S., EL HAOUTI, R., HAMMA M.S. & EL ALEM, N., 2013. Retention of heavy metals (Pb, Cd, Cr and Zn) by a sand area of Agadir: Equilibrium and kinetic. MATEC Web of Conferences, 5, 04020.

AGRWAL, R. M. & SINGH, K., 2017. Methodologies for removal of heavy metal ions from wastewater: an overview. *Interdisciplinary Environmental Review*, 18(2), 124-141.

AICHOUR, A. & ZAGHOUANE-BOUDIAF, H., 2019. Highly brilliant green removal from wastewater by mesoporous adsorbents: Kinetics, thermodynamics and equilibrium isotherm studies. *Microchemical Journal*, 146, 1255-1262.

AICHOUR, A., ZAGHOUANE-BOUDIAFA, H., ZUKI, F.B.M., AROUA, M.K. & IBBORA, C.V., 2019. Low-cost, biodegradable and highly effective adsorbents for batch and column fixed bed adsorption processes of methylene blue. *Journal of Environmental Chemical Engineering*, 7, 103409.

AJMI, R.N., MAITHAIM SULTAN, M. & HANNO, S.H., 2018. Bioabsorbent of chromium, cadmium and lead from industrial waste water by waste plant. *Journal of Pharmaceutical Sciences and Research* 10(3), 672-674.

AKINOLA, L.K., IBRAHIM, A. & MOHAMMED MOHAMMED, M., 2019. Adsorption of methylene blue on adsorbents derived from delonix regia seed pods and vigna subterranea fruit hulls: a kinetic study. *Science World Journal*,14(1), 23-27.

AKPOR, O. B. & MUCHIE, M., 2010. Remediation of heavy metals in drinking water and wastewater treatment systems: Processes and applications. *International Journal of Physical Sciences,* 5**,** 1807-1817.

ALAHABADI, A., HOSSEINI-BANDEGHARAEI, A., MOUSSAVI, G., AMIN, B., RASTEGAR, A., KARIMI-SANI, H., FATTAHI, M. & MOHAMMAD MIRI, M., 2017.

Comparing adsorption properties of NH_4Cl-modified activated carbon towards chlortetracycline antibiotic with those of commercial activated carbon. *Journal of Molecular Liquids,* 232, 367-381.

ALGUREIRE, A. H. & ABDULMAJEED, Y. R., 2016. Removal of heavy metals from industrial wastewater by using RO membrane. *Iraqi Journal of Chemical and Petroleum Engineering*, 17(4), 125-136.

ALGUREIRE, A. H. & ABDULMAJEED, Y. R., 2016. Removal of heavy metals from industrial wastewater by using RO membrane. *Iraqi Journal of Chemical and Petroleum Engineering*, 17(4),125-136.

ALI, I. H., AL MESFER, M.K., KHAN, M.I., DANISH, M., MAJED M. & ALGHAMDI, M.M., 2019. Exploring adsorption process of lead(II) and chromium(VI) ions from aqueous solutions on acid activated carbon prepared from Juniperus procera leaves. *Processes*, 7, 217.

ARIEF, V.O., TRILESTARI, K., SUNARSO, J., INDRASWATI, N. & ISMADJI, S., 2008. Recent progress on biosorption of heavy metals from liquids using low cost biosorbents:

characterization, biosorption parameters and mechanism studies, *Clean Soil Air Water*, 36, 937-962.

BABALOLA, B.M., 2018. Investigating adsorption characteristics of delonix regia for heavy metals removal in wastewater and its potential for remediating contaminated soils. PhD Thesis. Lancaster University.

BARDESTANI, R., ROY, C. & KALIAGUINE, S., 2019. The effect of biochar mild air oxidation on the optimization of lead(II) adsorption from wastewater. *Journal of Environmental Management*, 240, 404-420.

BELLIR, K., LEHOCINE, M. B. & MENIAI, A-H., 2013. Zinc removal from aqueous solutions by adsorption onto bentonite. *Desalination and Water Treatment,*1-13.

BHOMICK, P.C., SUPONG, A., BARUAH, M., PONGENER, C. & SINHA, D., 2018. Pine Cone biomass as an efficient precursor for the synthesis of activated biocarbon for adsorption of anionic dye from aqueous solution: Isotherm, kinetic, thermodynamic and regeneration studies. *Sustainable Chemistry and Pharmacy*, 10, 41-49.

CAROLIN, C. F., KUMAR, P. S., SARAVANAN, A., JOSHIBA, G. J. & NAUSHAD, M., 2017. Efficient techniques for the removal of toxic heavy metals from aquatic environment: A review. *Journal of Environmental Chemical Engineering*, 5, 2782-2799.

CIOFALO, M., LA CERVA, M., DI LIBERTO, M., LUIGI GURRERI, CIPOLLINA, A. & MICALE, G., 2019. Optimization of net power density in reverse electrodialysis. *Energy,* 181 576-588.

CORUH, S. & ERGUN, O.N., 2009. Ni^{2+} removal from aqueous solutions using conditioned clinoptilolites: kinetic and isotherm studies. *Environmental Progress and Sustainable Energy*, 28, 162-172.

DACI-AJVAZI, M., THACI, B., DACI, N. & GASHI, S., 2016. Membrane and adsorption processes for removing of organics and inorganics from urban wastewater. *Oriental Journal of Chemistry*, 32(5), 2391-2400.

DANMALIKI, G.I. & SALEH, T.A., 2017. Effects of bimetallic Ce/Fe nanoparticles on the desulfurization of thiophenes using activated carbon. *Chemical Engineering Journal*, 307, 914-927.

DARGAHI, A., GOLESTANIFAR, H., DARVISHI, P., KARAMI, A., HASAN, S.H., POORMOHAMMADI, A. & BEHZADNIA, A., 2016. An Investigation and comparison of removing heavy metals (lead and chromium) from aqueous solutions using magnesium oxide nanoparticles. *Polish journal of environmental studies*, 25(2), 557-562.

DENIZ, F. & KEPEKCI, R.A., 2017. Bioremoval of Malachite green from water sample by forestry waste mixture as potential biosorbent. *Microchemical Journal*,132, 172-178.

DOULA, M.K. & DIMIRKOU, A., 2008. Use of an iron-overexchanged clinoptilolite for the removal of Cu^{2+} ions from heavily contaminated drinking water samples, *Journal of Hazardous Materials*, 151, 738-745.

ESFANDIARI, B. & MONAJJEMI, M., 2013. Physical adsorption between mono and diatomic gases inside of carbon nanotube with respect to potential energy, *Journal of Physical and Theoretical Chemistry*, 10, 31-42.

ESSOMBA, J.S., NSAMI, J.N., BELIBI BELIBI, P.D., TAGNE, G.M. & KETCHA MBADCAM, J., 2014. Adsorption of cadmium(II) ions from aqueous solution onto kaolinite and metakaolinite. *Pure and Applied Chemical Sciences*, 2(1), 11-30.

FAN, J., 2013. Application of cupriavidus metallidurans and ochrobactrum intermedium for copper and chromium biosorption. Master's Thesis. University of Houston.

FIOL N. & VILLAESCUSA I., 2009. Determination of sorbent point zero charge: usefulness in sorption studies. *Environmental Chemistry Letters*, 7, 79-84.

FU, F. & WANG, Q., 2011. Removal of heavy metal ions from wastewater; A review. *Journal of Environmental Management*,92, 407-418.

GUNATILATE, S. K., 2015. Methods of removing heavy metals from idustrial wastewater. *Journal of Multidisciplinary Engineering Science Studies*, 1(1), 12-18.

HASSANA, A.F. & ELHADIDY, H., 2017. Production of activated carbons from waste carpets and its application in methylene blue adsorption: Kinetic and thermodynamic studies. *Journal of Environmental Chemical Engineering,* 5, 955-963.

HONG, M., YU, L., WANG, Y., ZHANG, J., CHEN, Z., DONG, L., ZAN, Q. & LI, R., 2019. Heavy metal adsorption with zeolites: The role of hierarchical pore architecture. *Chemical Engineering Journal* 359, 363-372.

HOSSAIN, A., 2013. Development of novel biosorbents in removing heavy metals from aqueous solution. PhD Thesis. University of Technology, Sydney (UTS). Sydney, Australia.

HU, X., SONG, J., WANG, H., ZHANG, W., WANG, B., LYU, W., WANG, Q., LIU, P., CHEN, L. & XING, J., 2019. Adsorption of Cr(VI) and Cu(II) from aqueous solutions by biochar derived from Chaenomeles sinensis seed. *Water Science and Technology,* 80(12), 2260-2272.

HUSAIN, A., JAVED, I. & KHAN, N.A., 2014. Characterization and treatment of electroplating industry wastewater using Fenton's reagent, *Journal of chemical and pharmaceutical research*, 6(1), 622-627.

IBRAHIMI, M.M. & SAYYADI, A.S., 2015. Application of natural and modified zeolites in removing heavy metal Cations from aqueous media: an overview of including parameters affecting the process. *International Journal of Geology, Agriculture and Environmental Sciences*, 3(2), 1-7.

INGLEZAKIS, V.J., LOIZIDOU, M.M. & GRIGOROPOULOU, H.P., 2004. Ion exchange studies on natural and modified zeolites and the concept of exchange site accessibility, *Journal of Colloid Interface Sciences*, 275, 570-576.

ISLAM, A., SABAR, S., BENHOURIA, A., KHANDAY, W.A., ASIF, M. & HAMEED, B.H., 2017. Nanoporous activated carbon prepared from karanj (Pongamia pinnata) fruit hulls for methylene blue adsorption. *Journal of the Taiwan Institute of Chemical Engineers*, 74, 96-104.

KETSELA, G., ANIMEN, Z. & TALEMA, A., 2020. Adsorption of lead (II), cobalt (II) and iron (II) from aqueous solution by activated carbon prepared from white lupine (GIBITO) HUSK. *Journal of Thermodynamics and Catalysis*, 11, 203.

KHAMIS, M., JUMEAN, F. & ABDO, N., 2009. Speciation and removal of chromium from aqueous solution by white, yellow and red UAE sand. *Journal of Hazardous Materials*,169, 948-952.

KUANG, Y., ZHANG, X. & ZHOU, S., 2020. Adsorption of methylene blue in water onto activated carbon by surfactant modification. *Water*, 12(587), 1-19.

LACH, J., 2019. Adsorption of chloramphenicol on commercial and modified activated carbons. *Water*, 11(1141).

LAKHERWAL, D., 2014. Adsorption of heavy metals: A review. *International Journal of Environmental Research Development*, 4(1), 41-48.

LI, G. X., XUE, P. Y., YAN, C. Z. & LI, Q. Z., 2010. Copper biosorption by Myriophyllum spicatum: Effects of temperature and pH. *Korean Journal of Korean Journal of Chemical Engineering*, 27(4), 1239-1245.

LIU, Y., WANG, G., WANG, L., LI, X., LUO, Q. & NA, P., 2019. Zeolite P synthesis based on fly ash and its removal of Cu(II) and Ni(II) ions. *Chinese Journal of Chemical Engineering*, 27, 341-348.

MARTIN-LARA, M.A. BLAZQUEZ, G., CALERO, M., ALMENDROS, A.I. & RONDA, A., 2016. Binary biosorption of copper and lead onto pine cone shell in batch reactors and in fixed bed columns. *International Journal of Mineral Processing*, 148, 72-82.

MATHEW, B.B., JAISHANKAR, M., BIJU, V.G. & BEEREGOWDA, K.N., 2016. Role of bioadsorbents in reducing toxic metals. *Journal of Toxicology*, 2016, 1-13.

MISHRA, A. & TRIPATHI, B.D., 2008. Utilization of fly ash in adsorption of heavy metals from wastewater, *Toxicological and Environmental Chemistry*, 90(6), 1091-1097.

OLJIRA, L., 2016. Adsorption of heavy metal from constituent waste water by tea waste adsorbent. Master's Thesis. Addis Ababa University. Addis Ababa-Ethiopia.

PANG, F. M., KUMAR, P., TENG, T. T., OMAR, A.K. M. & WASEWAR, K.L., 2011. Removal of lead, zinc and iron by coagulation-flocculation. *Journal of the Taiwan Institute of Chemical Engineers*, 42, 809-815.

PARMAR, M. & SINGH, T.L., (2013) Heavy metal Cu, Ni and Zn: toxicity, health hazards and their removal techniques by low cost adsorbents: a short overview. *International Journal Plant Animal and Environmental Sciences,* 3, 143-147.

RAFATULLAH, M., SULAIMAN, O., HASHIM, R. & AHMAD, A., 2010. Adsorption of methylene blue on low-cost adsorbents: a review. *Journal of Hazardous Materials,* 177, 70-80.

RAJASULOCHANA, P. & PREETHY V., 2016. Comparison on efficiency of various techniques in treatment of waste and sewage water-A comprehensive review. *Resource-Efficient Technologies,* 2, 175-184.

RANASINGHEA, S.H., NAVARATNEA, A.N. & PRIYANTHA, N., 2018. Enhancement of adsorption characteristics of Cr(III) and Ni(II) by surface modification of jackfruit peel biosorbent. *Journal of Environmental Chemical Engineering*, 6, 5670-5682.

REGTI, A., EL KASSIMI, A., LAAMARI, M.R. & EL HADDAD, M., 2017. Competitive adsorption and optimization of binary mixture of textile dyes: a factorial design analysis, *Journal of the Association of Arab Universities for Basic and Applied Sciences*, 24, 1-9.

RICHARDS, S., DAWSON, J. & STUTTER, M., 2019. The potential use of natural vs commercial biosorbent material to remediate stream waters by removing heavy metal contaminants. *Journal of Environmental Management*. 231, 275-281.

ROMANA, M., VAN DIJK, L.H., GUTIERREZ, L., VANOPPEN, M., POST, J.W., WOLS, B.A., CORNELISSEN, E.R. & VERLIEFDE, A.R.D., 2019. Key physicochemical characteristics governing organic micropollutant adsorption and transport in ion-exchange membranes during reverse electrodialysis, *Desalination*, 468,114084.

SAEED, A., IQBAL, M. & WAHEED AKHTAR, M., 2002. Application of biowaste materials for the sorption of heavy metals in contaminated aqueous medium. *Pakistan Journal of Scientific and Industrial Research*, 45, 206-211.

SHARMA, B. & SHWETA TYAGI, S., 2013. Simplification of metal ion analysis in fresh water samples by atomic absorption spectroscopy for laboratory students. *Journal of Laboratory Chemical Education*, 1(3), 54-58.

SITI NUR, A.A., MOHD HALIM, S.I., LIAS KAMAL, M.D. & IZHAR, S., 2013. Adsorption Process of heavy metals by low-cost adsorbent: A Review. *World Applied Sciences Journal* 28: 1518-1530.

SONG, D., PAN, K., TARIQ, A., AZIZULLAH, A., SUN, F., LI, Z. & XIONG, Q., 2016. Adsorptive removal of toxic chromium from waste-water using wheat straw and eupatorium adenophorum. *PLOS ONE*. 1-15.

SUGANYA, S. & KUMAR, P.S., 2018. Influence of ultrasonic waves on preparation of active carbon from coffee waste for the reclamation of effluents containing Cr(VI) ions. *Journal of Industrial and Engineering Chemistry*, 60, 418-430.

TANG, X., ZHENG, H., TENG, H., SUN, Y., GUO, J., XIE, W., YANG, Q. & CHEN, W., 2014. Chemical coagulation process for the removal of heavy metals from water: a review. *Desalination and Water Treatment*,1-16.

TIAN, H., WANG, Y., PEI, Y. & CRITTENDEN, J.C., 2020. Unique applications and improvements of reverse electrodialysis: A review and outlook. *Applied* Energy, 262, 114482.
TRIPATHI, A. & RANJAN, M.R., 2015. Heavy metal removal from wastewater using low cost adsorbents. *Journal of Bioremediation & Biodegradation,* 6(6), 1000315.

YANG, S., LI, J., SHAO, D., HU, J. & WANG, X., 2009. Adsorption of Ni (II) on oxidized multi-walled carbon nanotubes: effect of contact time, pH, foreign ions and PAA. *Journal of Hazardous Materials*, 166(1), 109-116.

YARKANDI, N. H., 2014. Removal of lead (II) from waste water by adsorption. *International Journal of Current Microbiology and Applied Sciences,* 3(4), 207-228.

YUAN, M., XIE, T., YAN, G., CHEN, Q. & WANG, L., 2018. Effective removal of Pb^{2+} from aqueous solutions by magnetically modified zeolite. *Powder Technology*, 332, 234-241.

ZHANG, D., CAO, J., WU, G. & CUI, L., 2018. Dynamic adsorption model fitting studies of typical VOCs using commercial activated carbon in a fixed bed. *Water Air and Soil Pollution* 229(178), 1-10.

CHAPTER 3: EXPERIMENTAL

This chapter is divided into four sections. The first section indicates chemicals used, their chemical names and their manufacturers. All chemicals obtained were used without further purification. The second section describes the methods of preparation for each adsorbent used and batch experiments. The third describe the adsorption procedure throughout the study. The last section shows instrumentation and their general description and their use.

3.1 Reagents

Lead nitrate [$Pb(NO_3)_2$]-99.95%, A.R grade, copper sulphate pentahydrate ($CuSO_4.5H_2O$)-98% A.R grade, 99.95%, iron(III)nitrate nonahydrate [$Fe(NO_3)_3.9H_2O$]-99.95%, cobalt(II)nitrate [$Co(NO_3)_2$]-99.95%, A.R grade, nickel(II)nitrate [$Ni(NO_3)_2$]-99.95%, A.R grade, Cadmium acetate [$Cd(CH_3COO)_2$]-99.95%, Iron(II) chloride ($FeCl_2 \cdot 4H_2O$)-98.95% and Iron(III) chloride ($FeCl_3 \cdot 6H_2O$)-98.95% were purchased from Sigma-Aldrich. Liquid chemicals such as nitric acid (HNO_3)-70%, A.R grade, Hydrochloric acid (HCl)-32%, A.R grade, phosphoric acid (H_3PO_4)-75%, sulphuric acid (H_2SO_4)-98% A.R grade and *N*,*N* dimethylformamide (C_3H_7NO) were purchased at Associated Chemical Enterprises. Other chemical salts namely; hydroxide (NaOH) pallets-98.5% A.R grade, potassium permanganate ($KMnO_4$)-99%, potassium dichromate salt ($K_2Cr_2O_7$)-99.5%, methylene blue ($C_{16}H_{18}N_3SCl$) 82%, Sucrose ($C_{12}H_{22}O_{11}$), sodium thiosulfate ($Na_2S_2O_3$) and ammonium hydroxide (NH_4OH) were purchased from Sigma-Aldrich. Unprocessed Black Cumin (*Nigella Sativa* L.) seeds were procured at the health shop in Vanderbijlpark, South Africa. The metal ion chemicals used as pollutants found in the environment. Acids were used as chemical activation of black cumin

seeds in order to enhance their adsorption capacity. Acetone and *N,N* dimethylformamide were used as solvents to remove and extract the fatty acids in in the black cumin seeds.

3.2 Untreated black cumin seeds (UT-BCS) adsorbent preparation

Black seed also known as black cumin (Nigella sativa) is a yearly flowering plant belonging to the family Ranunculaceae and is refined in the Northern India, Middle Eastern Mediterranean region, Iran, Turkey, Southern Europe, Pakistan, Syria and Saudi Arabia (Srinivasan 2018). Black cumin seeds (Fig. 2) were bought from Vanderbijlpark, Vaal triangle, South Africa health shop. The raw Black Cumin (*Nigella Sativa L.*) seeds were rinsed in distilled water several times to get rid of dust and dirt then weighed. Thereafter, they were dried at 40 °C for 24 hr. After drying the seeds were grounded with a mortar and piston. The grounded seeds were used to prepare other adsorbents.

Figure 2: Black Cumin Seeds (*Nigella Sativa* L.)

3.3 Instrumentation

Several instrumental techniques were used to characterize the adsorbents and some instruments were used to determine the remaining concentration of toxic ions in the solution.

3.3.1 Atomic Absorption Spectroscopy (AAS)

The metal ion concentration was determined using atomic adsorption spectrometry (AAS) Shimadzu ASC 7000 instrument with auto sampler. Atomic Absorption Spectrophotometer is an analytical instrument based on the principle of atomic absorption spectroscopy and is very useful to detect the metal ion concentration present in water samples. The instrument shown in Fig. 3 was used to determine the remaining metal ions concentration in solution before and after adsorption. Calibration was conducted using prepared calibration standards with concentrations of 20, 40, 60, 80 and 100 ppm for Co(II), Ni(II), Cu(II), Cr(VI), Pb(II) and Cd(II).

Figure 3: Atomic adsorption spectrometry (AAS)

3.3.2 Thermogravimetric analysis (TGA)

Thermal studies were determined using Perkin Elmer, TGA 4000 (Fig. 4) with scan temperature from 30 to 900 °C. Temperature ramp rate was 10 °C min^{-1} with nitrogen gas flow of 20 mL min^{-1}. Thermogravimetric analysis technique was used to determine the adsorbents thermal stability and volatile components by checking the weight change that occurred as the adsorbents were heated at constant rate.

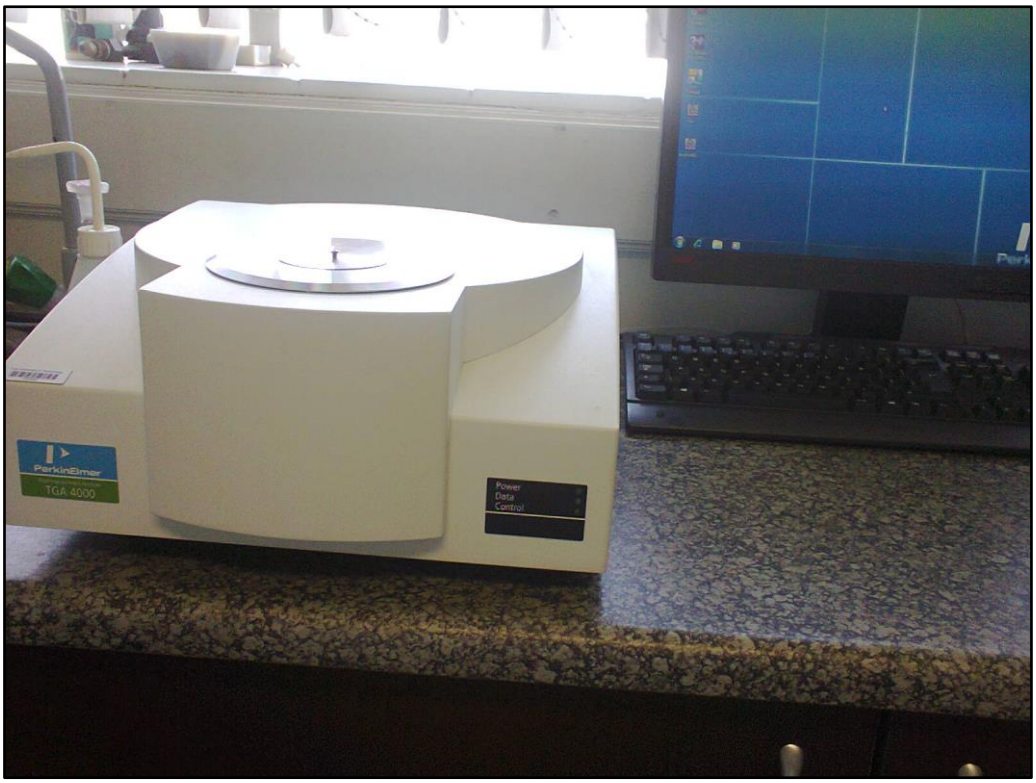

Figure 4: Thermogravimetric Analyser (TGA)

3.3.3 Scanning electron microscopy (SEM)

A scanning electron microscope (SEM) is a form of microscope using a focused beam of electrons to photograph the surface of a sample to create a high-resolution image. The images were obtained from JSM IT500 SEM operated at 10.0 kV. SEM (Fig. 5) was used to take images that show the information on the adsorbent's surface composition and topography. In the study the equipment was used to evaluate and study the surface morphology of the adsorbents before and after adsorption of the cations and the dye.

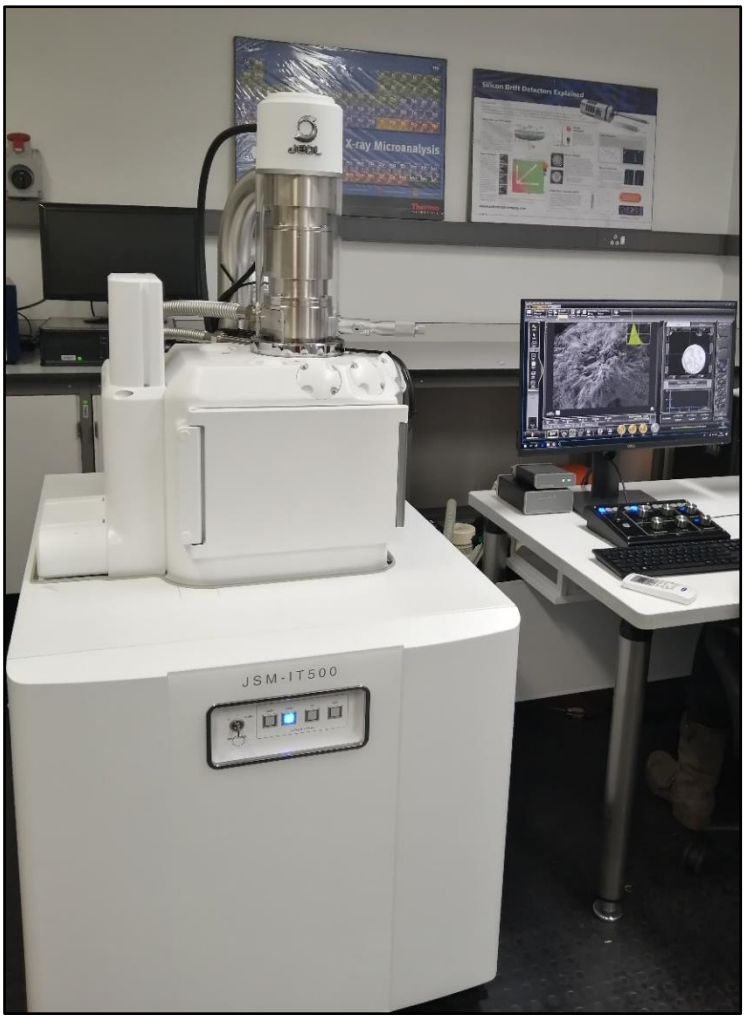

Figure 5: Scanning electron microscopy (SEM)

3.3.4 X-ray diffraction (XRD)

Fig. 6 show the X-ray diffractometer (XRD) Shimadzu XRD 7000 which was used to identify diffraction patterns, composition and structure of the adsorbents with a scanning range from (2θ) values from 10 to 80° with scan speed set at 10°/min.

Figure 6: X-ray diffractometer (XRD)

3.3.5 Fourier transformed infrared (FTIR) spectroscopy

The FTIR spectrum was obtained using Fourier transform infrared (FTIR) spectrometer (Nicolet iS50 FTIR) from Thermo Fischer Scientific using with a diamond detector at wavelength from 4000 to 650 cm^{-1}. No sample preparation was required. The instrument was used to determine the functional groups present on the surface of the adsorbents were established by FTIR. The instrument is shown in Fig. 7.

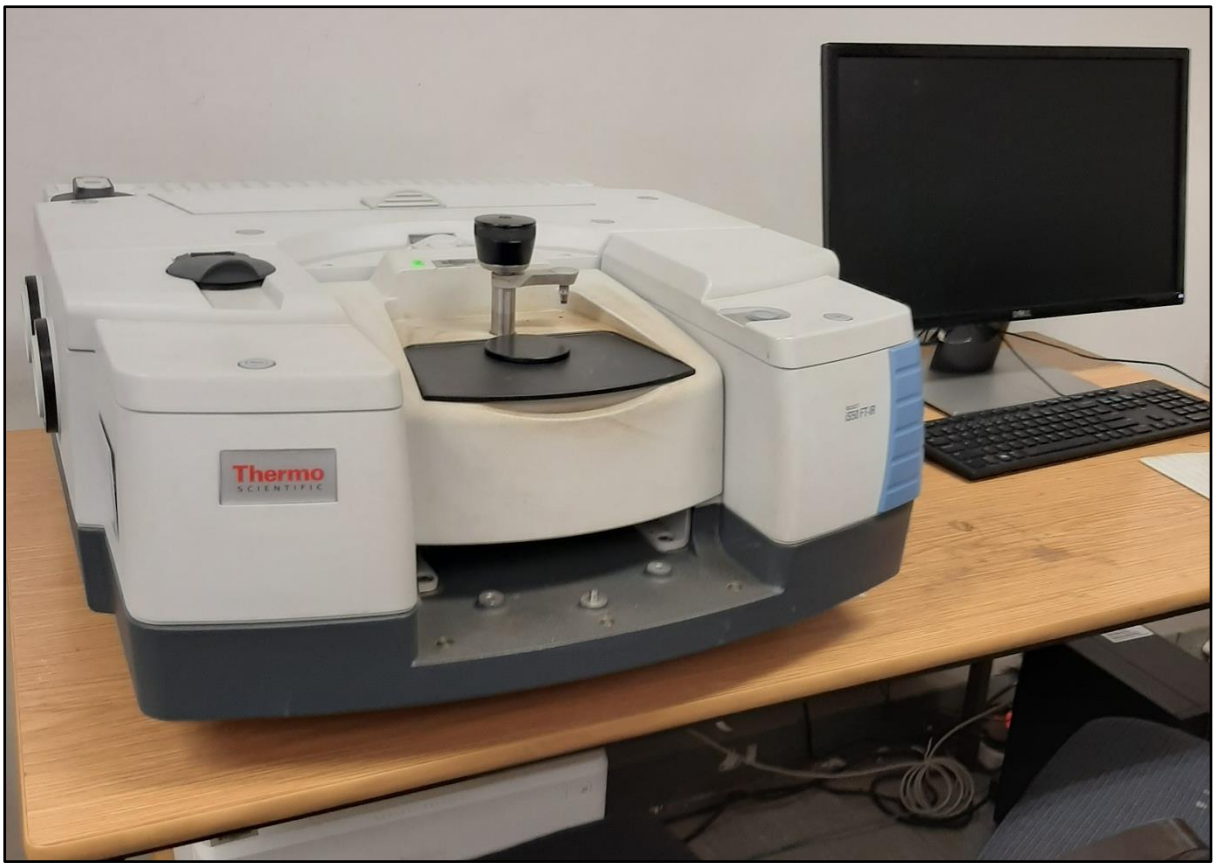

Figure 7: Fourier transformed infrared (FTIR) spectrophotometer

3.3.6 pH meter

Metrohm pH meter was used to measure pH of the solutions and the pH at point of zero charge (pH_{PZC}) using the pH drift method. Calibration of the instrument was performed using buffer solutions of pH 4.00, 7.00 and 10.00. The used instrument is shown in Fig. 8.

Figure 8: pH/Conductometer

3.3.7 Shaker

Shaker Labcon 3100U (Fig. 9) was used to equilibrate the adsorbents and the adsorbates at 200 rmp. The same ramp was used throughout the adsorption studies for the effect of time, initial concentration, pH and temperature. The equipment was used for rocking and agitating metal ion solutions and dyes for the adsorption tests namely; time effect, pH effect and initial concentration determination.

Figure 9: Shaker

3.3.8 Furnace

Elite furnace was used to produce carbon from the black cumin seeds. The furnace consisted of a horizontal ceramic tube (diameter of 4.5 cm and length of 62 cm) located in an electric furnace. The activated carbon was prepared by carbonization of biomass in a quartz tube and under nitrogen atmosphere, the biomass was heated up to 600 °C and maintained at that temperature for 1 h. Fig. 10 indicates the instrument used for carbonization.

Figure 10: Furnace

3.3.9 Ultraviolet-visible (UV-Vis) spectroscopy

UV-Vis analyses were accomplished by T80 PG Instruments (Fig. 11) with a double beam spectrometer which collects spectra from 180-1100 nm UV and visible range using a bandwidth of 1 nm with a fixed slit and Tungsten and deuterium lamps used for illumination. Adsorption capacity was conducted by determining the remaining metal ions and dye in the solution. The calibration of the instrument was conducted by laboratory prepared standard solutions with a concentration of 20, 40, 60, 80 and 100 mg/L.

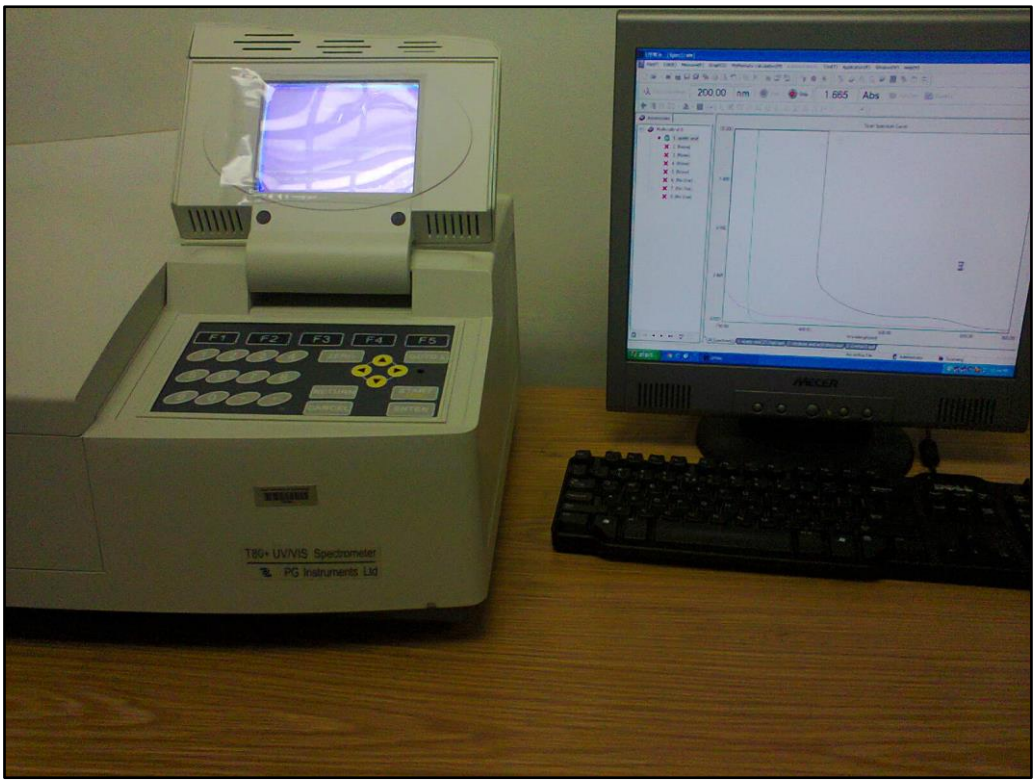

Figure 11: Ultraviolet-visible (UV-Vis) spectrophotometry

3.3.10 Brunauer Emmet Teller (BET)

The nitrogen adsorption-desorption isotherm and specific surface area of the adsorbents were acquired by Brunauer-Emmette-Teller (BET) analysis using Micromeritics ASAP 2020 plus (Micromeritics Instrument, Georgia, Corporation, USA) as indicated in Fig. 12.

Figure 12: Brunauer Emmet Teller (BET)

3.3.11 Drying Oven

An oven purchased from Scientific (Fig. 13) was used to dry the black cumin seeds. The drying oven is designed to remove moisture from the oven chamber so as to dry the samples as rapidly as possible. The drying oven process introduces fresh dry air to the chamber and expels the warm moist air instantaneously allowing fast drying of the seeds.

Figure 13: Drying oven

3.3.12 Weighing balance

AE Adam PW 124 weighing balance (Fig. 14) was used to determine the weight or mass of the adsorbents.

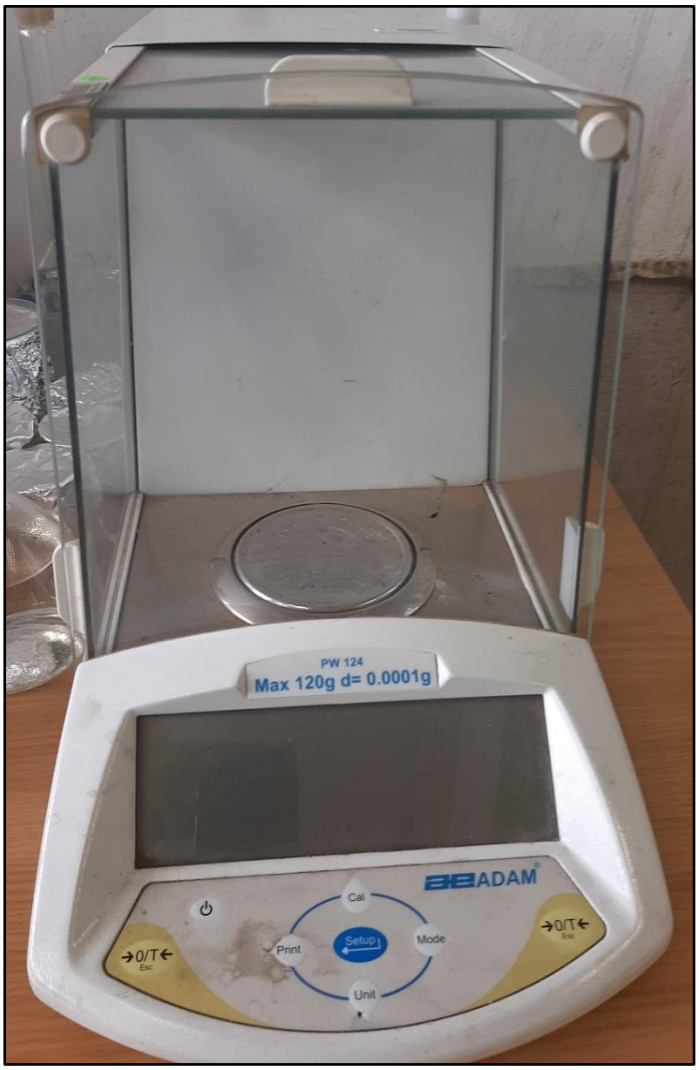

Figure 14: Weighing Balance

3.3.13 Water Bath

A Labcon laboratory water bath (Fig. 15) was used to heat samples in the lab during the study of temperature effect at 25, 30, 40, 60 and 80 °C. A water bath consisted of a stainless-steel chamber that holds the water and samples, heating unit and a control interface which was used to set the temperature.

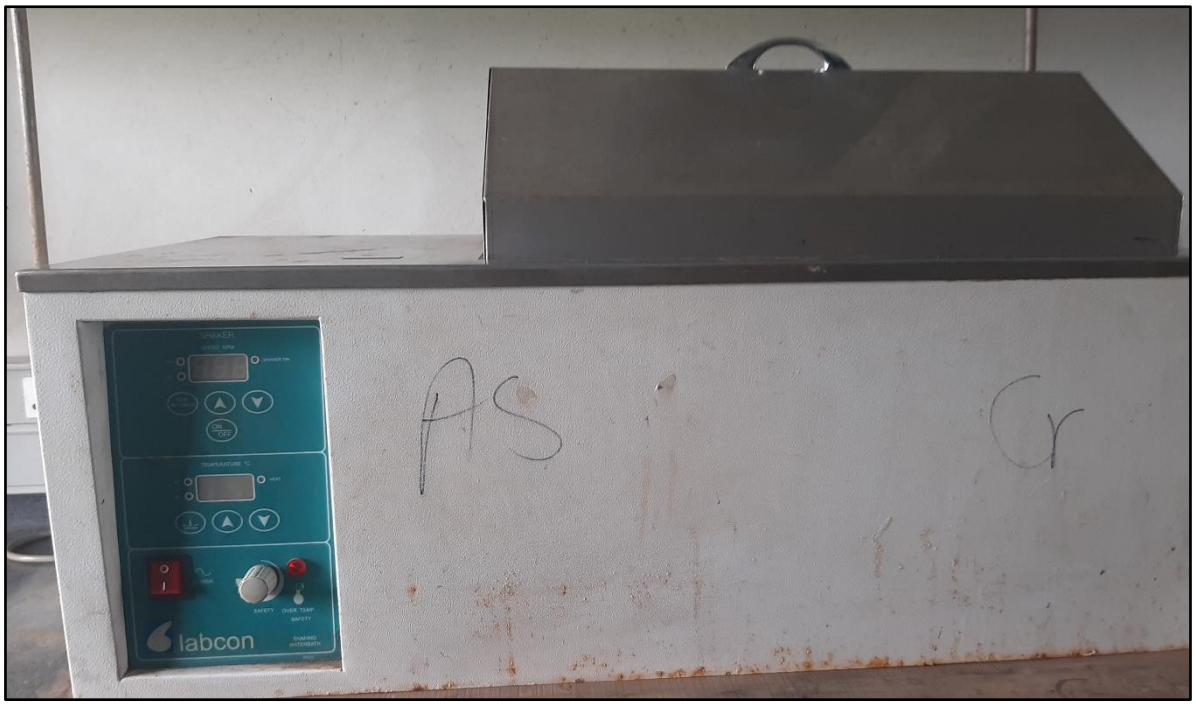

Figure 15: Water Bath

3.3.14 Inductively coupled plasma (ICP) spectroscopy

Fig. 16 shows a thermo scientific iCAP 7000 series inductive couple plasma (ICP) spectrometer with an ASX-520 auto sampler. This equipment was used to determine the concentration of the metal ion solutions before and after adsorption.

Figure 16: Inducive couple plasma (ICP) spectrometer

CONTRIBUTION OF THE CANDIDATE

Performed all the experimental work, conducted data analysis and interpretation, wrote the draft of the manuscripts, data collections, writing original draft, revision of the manuscript.

CHAPTER 4

Simultaneous adsorptive study of toxic metal ions in quaternary system from aqueous solution using low cost black cumin seeds (*Nigella Sativa*) adsorbents

This chapter is published as follows:

Ntaote David Shooto, Patience Mapule Thabede, Eliazer Bobby Naidoo. 2019. Simultaneous adsorptive study of toxic metal ions in quaternary system from aqueous solution using low-cost black cumin seeds (Nigella Sativa) adsorbents. South African Journal of Chemical Engineering 30, 15-27.

This chapter is addressing objective (a), (b), (g) and (h) which read as follows:

To characterize the untreated black cumin seeds (UT-BCS), acid treated (AT-BCS) and base treated (BT-BCS) using SEM, TGA, XRD and FTIR spectroscopy.

To conduct simultaneous (quaternary) adsorption of cobalt [Co(II)], nickel [Ni(II)], copper [Cu(II)] and lead [Pb(II)] using UT-BCS, AT-BCS and BT-BCS while varying time, pH, temperature and concentration.

To determine the point of zero charge (pH_{PZC}) of the UT-BCS, AT-BCS, BT-BCS, functionalized and activated adsorbents.

To determine the reusability of the UT-BCS, AT-BCS, BT-BCS, modified and the carbonized seeds.

4.1 Abstract

A new adsorbent obtained from alkaline treatment of black cumin seeds (BCS) has been developed for the adsorption of cation pollutants [cobalt Co(II), lead Pb(II), copper Cu(II) and nickel Ni(II)] from aqueous solutions. The alkaline treated black cumin seeds were labeled; base treated black cumin seeds (BT-BCS), acid treated black cumin seeds (AT-BCS) and untreated black cumin seeds (UT-BCS). The absorbents were analyzed by scanning electron microscope (SEM), Fourier-transform infrared spectroscopy (FTIR) and X-ray diffraction spectroscopy (XRD). The SEM images showed that UT-BCS is composed of spherical shaped particles. AT-BCS and BT-BCS images showed irregular surface morphology. AT-BCS and BT-BCS -IR spectra observed new bands. Pseudo First Order kinetic (PFO) model gave consistent fit in describing the adsorption of all the cations. The PFO good fit suggest that the adsorption mechanism involved, Van der Waal forces. The estimated pore adsorption (EPA) was more dominant than estimated surface adsorption (ESA). Equilibrium data had a good fit for Langmuir isotherm model for all cations this indicates that adsorption took place on active sites having equal affinity for these ions and further suggests that monolayer adsorption occurred on adsorbents surface at the end of adsorption process. BT-BCS was the best performing adsorbent with capacity of 190.7 mg/g for Cu(II), AT-BCS and UT-BCS with capacities of 180.1 and 135 mg/g respectively for Pb(II). Adsorption trend is BT-BCS>AT-BCS>UT-BCS. Reusability data suggests that (BCS) adsorbents retained ≥ 90% of their initial cations adsorption, these adsorbents may be reusable in wastewater treatment.

Keywords: Adsorption, isotherms, kinetic, thermodynamic, black cumin seeds

4.2 Introduction

An accelerated urbanization and industrialization growth in the last century have caused the discharge of wastewater into fresh water bodies without proper pretreatment. This poses a serious threat to the environment, human health and natural aquatic system (Myers et al. 2013). The scope of wastewater pollutants is too large and includes; toxic metal ions, pesticides, organic pollutants, dyes, etc (Shooto et al. 2016; Munze et al. 2017; Nagpal & Kakkar, 2018; Tran et al. 2019). Many of these pollutants are toxic to human and the ecosystem. They accumulate in human body and are non-biodegradable (Atique et al. 2017). The current study focused on four toxic metals that are being characterized as the priority pollutants from the various health organizations; Co(II), Pb(II), Cu(II) and Ni(II) ions (Veli & Alyuz, 2007).

Copper is needed only in small quantities by human body to support some biological processes. It is a commonly used metal by many municipalities and industries. Upon long term exposure even at lower concentrations, Cu(II) contaminated water has toxic effects on vital organs such as the brain, heart and liver (Jaishankar et al. 2014). It is also reported to cause vomiting, stomach cramps and kidney failure (Potera, 2004). Pb(II) is a slow, pernicious, but most malignant poison. Via any route or level of exposure it replaces calcium on the bones and accumulates in the skeletal system (Puzas et al. 2004). It further causes neurodevelopmental effects, brain damage (Wani et al. 2015), kidney, liver disorders as well as reproduction and development (Adham, 1997; Luo et al. 2012; Savic et al. 2014). Exposure to higher concentrations of Co(II) causes neurological problems such as changes in brain structure, cognitive function impairment and depression (Clark et al. 2014). Co(II) toxicity also affect all major organ systems and causes respiratory problems and fatigue (Pelclova et al. 2012). Long

term Ni(II) exposure is associated with headaches, dyspnea, carcinogenic, cytotoxicity and genotoxicity (Kasprzak et al. 2003).

Therefore, it is necessary to remove such toxic metal ions from the water, before discharging into drainage system, sewer, river and/or sea. Advance conventional technologies have been developed, for this very reason. Technologies such as; chemical-precipitation (Yu et al. 2017), nano-filtration (Wu et al. 2019), ion exchange (Zhang et al. 2014), membrane separation (Mikusova et al. 2014), reverse osmosis (Anis et al. 2019), coagulation and flocculation (Kuokkanen et al. 2013), and photo-degradation/photo catalyzed degradation of organic dyes (Saravanan et al. 2014; Soleiman et al. 2016; Mousavinia et al. 2016; Mosleh et al. 2016; Mosleh et al. 2017; Mosleh et al. 2018;) are some of the developed technologies for water treatment. However, these technologies have limitations that make them unsuitable for everyday use, such as technical challenges, high operational costs and methods effectiveness (Malaeb et al. 2011). However, a non-conventional method; adsorption is the most promising. It is sustainable, affordable, eco-friendly and effective (Kyzas et al. 2014).

Numerous research groups worldwide have shown great interest in the adsorption studies of low-cost materials as potential wastewater pollutants adsorbents. Therefore, many biomaterials have been used to remove toxic metal ions and dyes from water such as de-oiled soya (Mittal et al. 2010), canola residues (Balarak et al. 2014), bagasse fly ash (Gupta & Sharma, 2003) and dead cells of Yarrowia lipolytica (Asfaram et al. 2018). Other researched materials are Fe_3O_4 nanoparticles (Ghaedi et al. 2015), carbon based materials such as carbon nanotubes and fullerene (Gupta & Saleh, 2013), activated carbon from waste rubber tyre (Gupta et al. 2013), ZnS:Cu nanoparticles loaded on activated carbon (Asfaram et al. 2015), graphene oxide (Gupta et al. 2014), magnetic activated carbon loaded with gold nanoparticles (Dashtian et al. 2016),

Fertilizer plant waste carbon (Gupta et al. 2016) and ZnO nanorod-loaded activated carbon (Ghaedi et al. 2016).

Selection of black cumin seeds as potential absorbent in this work was based on their; abundance in nature, accessibility, eco-friendliness, low cost, not selective towards pollutants, reusability, easy generation and their surface have several functional groups (carboxyl, hydroxyl and amide). Such attributes put the seeds in an advantageous position for adsorption technology. However, few adsorptive studies of black cumin seeds material are available in the literature (El-Said et al. 2009; Ahmad et al. 2014; Siddiqui et al. 2018; Addala et al. 2018). To the best of our knowledge this work is the first of its kind ever to report on alkaline/base treated BCS for water treatment application. Also, it is the first time ever that a study reports the evaluation of quaternary adsorptive study of toxic metal ions (Pb(II), Ni(II), Cu(II) and Co(II)) by UT-BCS, BT-BCS and AT-BCS. In this work the efficiency of BCS adsorbents to adsorb toxic metal ions from aqueous solution in quaternary system is presented. The adsorption studies were conducted under varying experimental parameters such as concentration, contact time, temperature and pH.

4.3 Experiments

4.3.1. Materials and methods

Black cumin seeds (BCS) were purchased from a local health shop in Vanderbijlpark, Vaal Triangle, South Africa. BCS were washed several times with ultra-pure water and then oven dried. Hydrochloric acid (HCl)-32%, A.R grade, nitric acid (HNO_3)-70%, A.R grade, sodium hydroxide (NaOH) pallets-98.5% A.R grade, lead nitrate ($Pb(NO_3$)-99.95%, A.R grade, copper sulfate pentahydrate ($CuSO_4.5H_2O$)-98% A.R grade, cobalt(II)nitrate ($Co(NO_3)_2$)-99.95%,

A.R grade and nickel(II)nitrate ($Ni(NO_3)_2$)-99.95%, A.R grade were purchased from Merck South Africa LTD.

4.4. Preparation of bio-adsorbents

4.4.1 Untreated black cumin seeds (UT-BCS) adsorbent preparation

Black cumin seeds (BCS) were washed dried and grounded, the seeds were then labeled untreated black cumin seeds (UT-BCS). Moreover UT-BCS were used to prepare other adsorbents, such as AT-BCS and BT-BCS.

4.4.2 Acid treated black cumin seeds (AT-BCS) adsorbent preparation

Adsorbent's preparation procedure was adopted from (Shooto et al. 2019). UT-BCS was acid treated with a mixture of 100 ml, 1M inorganic acids (HCl and HNO_3, ratio 1:1) to remove some of the elements and compounds attached on their surface. The obtained brownish-black material was oven dried (40 °C) overnight and then labeled; acid treated black cumin seeds (AT-BCS) as shown in scheme 1.

4.4.3 Base treated black cumin seeds (BT-BCS) adsorbent preparation

UT-BCS were treated with 100 ml of 1M NaOH solution to remove some of the elements and organic compounds attached on their surface. After 60 min the material was filtered and washed several times. The obtained greyish-black material was labeled; base treated black cumin seeds (BT-BCS) as shown in scheme 1. During alkaline/base solution treatment large amount of oil was noticed however saponification was not observed. Previous studies on BCS chemical

content reported that the composition is primarily; fatty acids (oil), fibers, carbohydrates and proteins. The fatty acids (oil) in BCS are linoleic acid, oleic acid and palmitic acid (Al-Jassir et al. 1992).

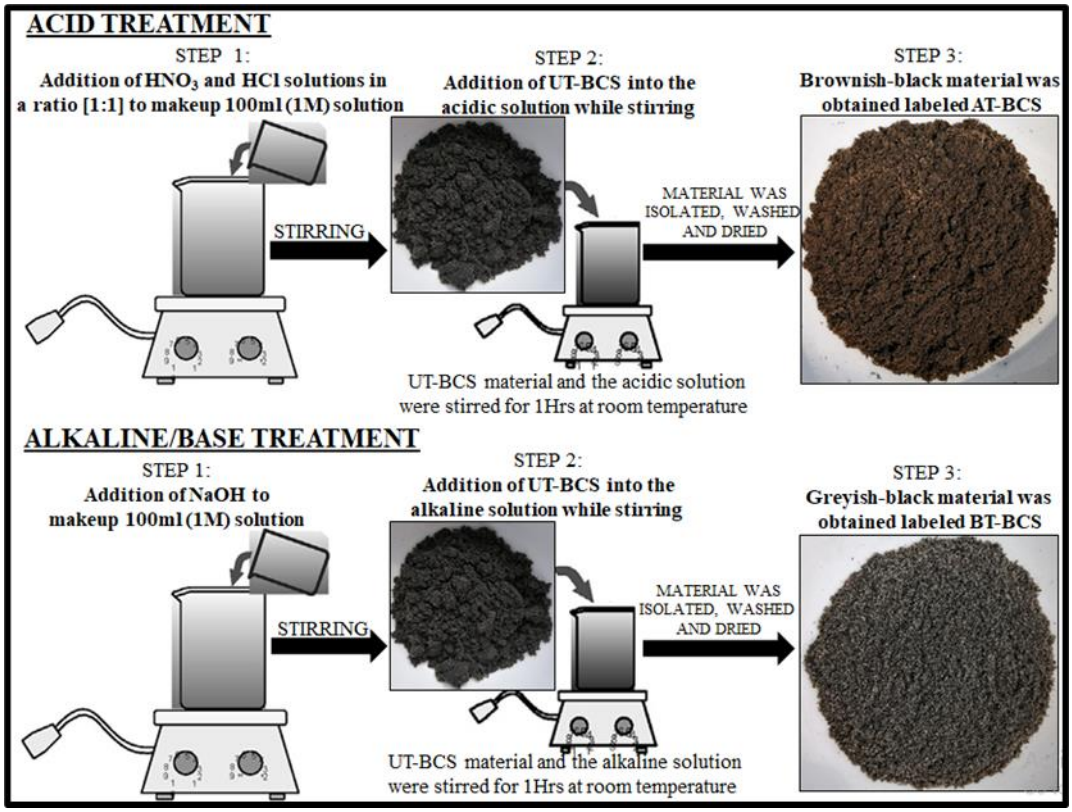

Scheme 1: Preparation of AT-BCS and BT-BCS.

4.5 Adsorption experiments

Lead nitrate ($Pb(NO_3)$), copper (II) sulfate pentahydrate ($CuSO_4.5H_2O$), cobalt (II) nitrate ($Co(NO_3)_2$) and nickel (II) nitrate ($Ni(NO_3)_2$), all were used for the preparation of stock solution (200 mg/L). These metals were all mixed in one solution.The effect of contact time; was studied at different time intervals (1, 5, 10, 30, 60 and 120 min) with working standard concentration of 100 mg/L at pH of 5.56. 20 mL of working standard was transferred into capped bottles

containing 0.1 g of the adsorbent. The effect of different concentration; (20, 40, 60, 80 and 100 mg/L) at time interval of 120 min was studied. 20 mL of the specified working standards were transferred into capped bottles containing 0.1 g of the adsorbent. The effect of pH on the solution was studied at different pH (1, 3, 5, 7 and 8.5) using 20 mL of the working standard (100 mg/L) which was transferred into capped bottles containing 0.1 g of the adsorbent. Temperature effect was studies at 288, 298, 308, 318 and 328 K with working standard (100 mg/L and pH of 5.56). 20 mL of the working standard was transferred into capped bottles containing 0.1 g of the adsorbent. An orbital shaker was used for each parameter (concentration, temperature, contact time and pH) to equilibrate the working standard and adsorbent at 200 rpm. After each experiment, respective capped bottles were removed, and then centrifuged for 5 min at 4500 rpm. The solution was taken for analysis of metal ions remaining. The concentrations of working standards before adsorption and supernatant solutions after adsorption were confirmed by ICP.

4.6 Data analysis

Equations (1) and (2) were used to calculate *(q_e)* the amounts of metal ions adsorbed *(mg/g)* and *(Rp)* removal percentage (Soleiman et al., 2016) respectively; where *(C_o)* is the initial and *(C_e)* is final metal ion concentrations in solution *(mg/L)*. *(v)* volume of working standard *(ml)* and (*m)* mass of the adsorbent in *(g)*.

$$q_e = \frac{(C_o - C_e)\,V}{m} \qquad (1)$$

$$R_p = \frac{(C_o - C_e)}{C_o}\ X\ 100 \qquad (2)$$

The nonlinear forms equations (3) and (4) were applied to evaluate the kinetic models; pseudo-first order (PFO) and pseudo-second order (PSO) respectively. *(q_e)* and *(q_t)* are the amounts of

metal ions adsorbed *(mg/g)* at equilibrium and at time *(t)*. k_1 is rate constant of the PFO in *(min^{-1})* and k_2 is rate constant of the PSO *(g mg^{-1} min^{-1})*.

$$q_e = q_t(1 - e^{-k_1 t}) \quad (3)$$

$$q_e = \frac{1 + k_2 q_e t}{k_2 q_e^2 t} \quad (4)$$

The experimental data was integrated into equation (5) to evaluate the intra-particle diffusion (IPD) model. The amounts adsorbed *(q_t)* and rate constant *(k_i)* were determined using the KyPlot software. *(k_i)* the rate constant *(g g^{-1} min$^{1/2}$)* and *C* is the concentration of metal ions on the adsorbent surface.

$$q_t = k_i\left(t^{1/2}\right) + C \quad (5)$$

Equations (6), (7) and (8) were employed to determine the adsorption isotherm for Langmuir, Freundlich and Temkin models respectively. $(Q_o)_{max,}$ maximum capacity of the adsorbent *(mg/g)*, (*b)* solute surface interaction energy, (k_f) Freundlich capacity factor and (*1/n)* is the isotherm linearity parameter. (*R)* Gas constant 8.314 J K^{-1}mol^{-1}, (*T)* temperature in (K), b_T and k_T are rate constants for Temkin model.

$$q_e = \frac{Q_o b C_e}{1 + b C_e} \quad (6)$$

$$q_e = k_f C_e^{1/n} \quad (7)$$

$$q_e = \frac{RT}{b_T} In(k_T C_e) \quad (8)$$

Thermodynamic function; equilibrium constant *(K_c)*, values were evaluated using equation (9)

$$K_c = \frac{q_e}{C_e} \quad (9)$$

Equations (10) and (11) were applied to equilibrium adsorption data at 288, 298, 308, 318 and 328 K to determine other thermodynamic functions; enthalpy *(ΔH^o)*, entropy *(ΔS^o)* and Gibbs free energy *(ΔG^o)*.

$$In\ K_c = -\frac{\Delta H^o}{RT} - \frac{\Delta S^o}{R} \quad (10)$$

$$\Delta G^o = -RT\ In\ K_c \quad (11)$$

4.7 Regeneration of the adsorbents

The regeneration of UT-BCS, AT-BCS and BT-BCS was conducted by taking 0.1 g of the pre-used (cations-loaded) adsorbent. The adsorbed cations were removed from adsorbents surface by agitating twice in 20 mL of 0.3 M HCl at 200 rpm for 30 min and then rinsed several times with ultra-pure water at 200 rpm for 60 min before reuse.

4.8. Characterization

The morphology, chemical features and phase purity of UT-BCS, AT-BCS and BT-BCS were affirmed by SEM, FTIR and XRD techniques. Scanning electron microscopy (SEM) images were taken on a Nova Nano SEM 200 from FEI operated at 10.0 kV. Perkin Elmer Fourier transformed infrared spectroscopy FT IR/FTNIR spectrometer, spectrum 400 was used. X-ray diffractometer (XRD), Shimadzu XRD 7000 was used to identify crystalline phase of the

sample, scan range was set from 10 to 80 (2θ °), scan speed was set at 10 °/min. Inductive couple plasma spectroscopy (ICP), thermo scientific iCAP 7000 series, ICP spectrometer, using ASX-520 auto sampler, was used to measure the metal ion solutions before and after adsorption.

4.9 Results and discussion

4.9.1 Adsorbents characterization

4.9.1.1 SEM analysis

The SEM images (Figs. 17a-l) were evaluated to study the surface morphology of the adsorbents before and after adsorption of the cations. UT-BCS (Figs. 17a-b) images show that the raw biomaterial before adsorption is composed of more or less spherical shaped particles. However, after adsorption the surface morphology of the raw biomaterial (UT-BCS) had cavities and irregular in nature (Figs. 17c-d). AT-BCS and BT-BCS images before adsorption of cations are Figs. 17e-f and Figs. 17i-j respectively. AT-BCS and BT-BCS images show that after the acid and alkaline/base treatment the spherical shaped particles observed in UT-BCS (Figs. 17a-b) were not observed for the treated adsorbents. The SEM images of AT-BCS and BT-BCS after adsorption of cations are shown in Figs. 17g-h and Figs. 17k-l respectively. AT-BCS and BT-BCS after adsorption show that the surfaces had porous and cavities, which may easily trap and adsorb the cations.

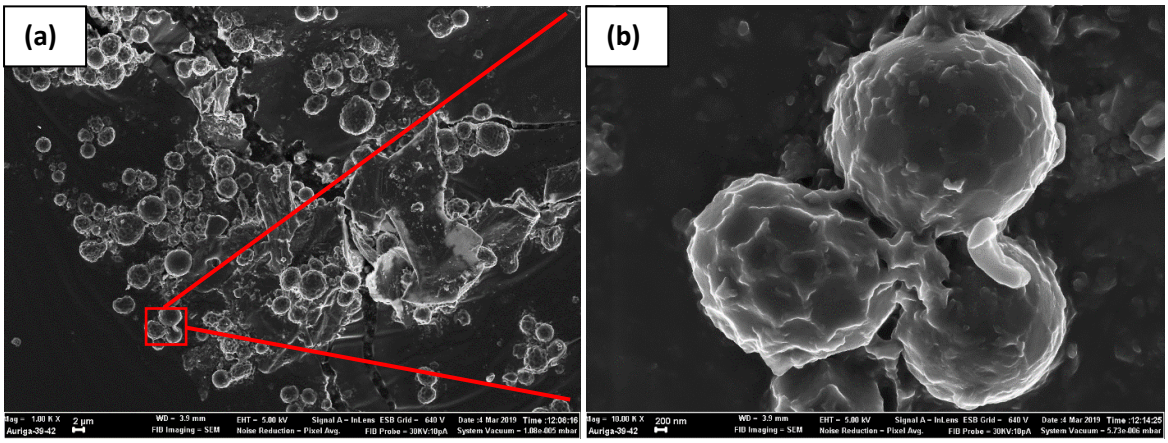

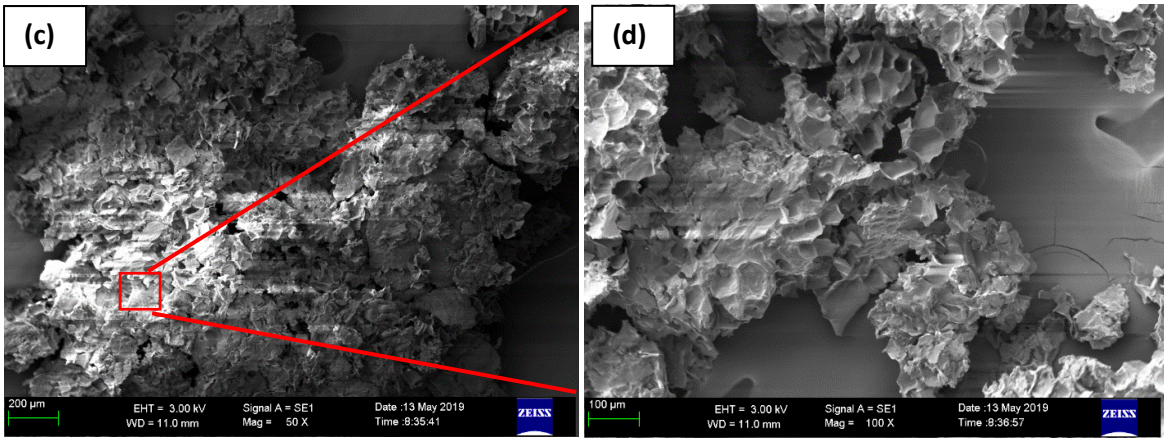
(c)
200 µm
EHT = 3.00 kV
WD = 11.0 mm
Signal A = SE1
Mag = 50 X
Date :13 May 2019
Time :8:35:41
ZEISS

(d)
100 µm
EHT = 3.00 kV
WD = 11.0 mm
Signal A = SE1
Mag = 100 X
Date :13 May 2019
Time :8:36:57
ZEISS

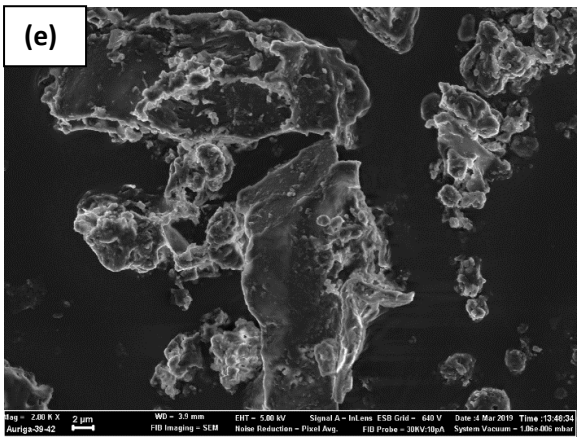
(e)

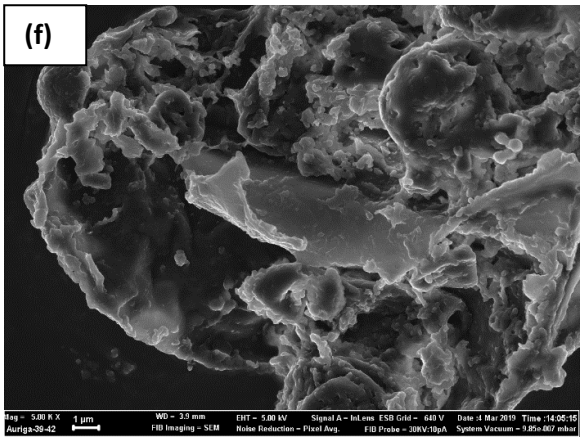
(f)

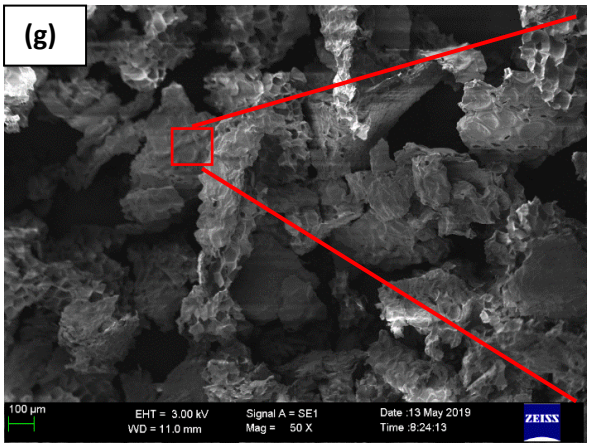
(g)
100 µm
EHT = 3.00 kV
WD = 11.0 mm
Signal A = SE1
Mag = 50 X
Date :13 May 2019
Time :8:24:13
ZEISS

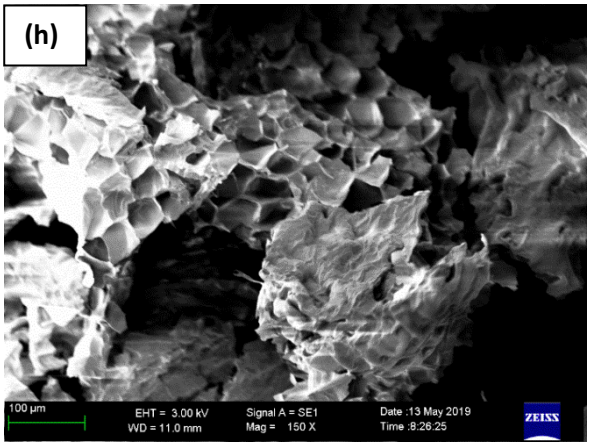
(h)
100 µm
EHT = 3.00 kV
WD = 11.0 mm
Signal A = SE1
Mag = 150 X
Date :13 May 2019
Time :8:26:25
ZEISS

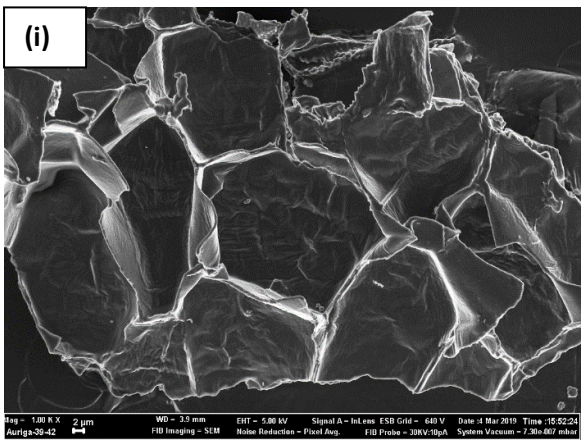
(i)

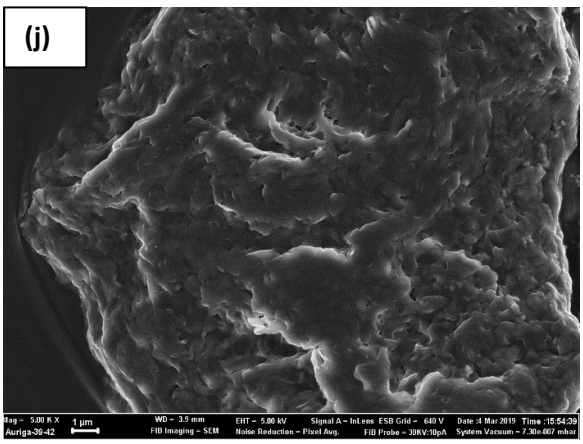
(j)

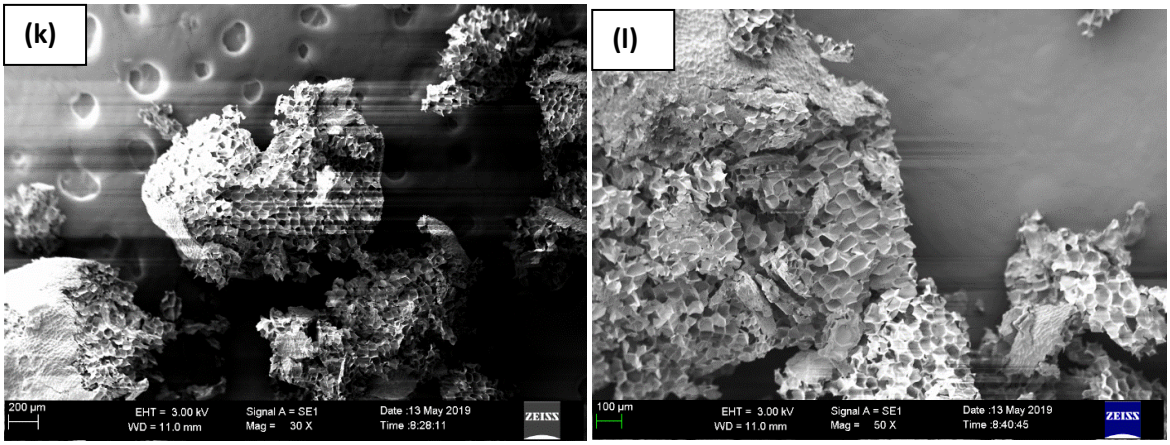

Figure 17: SEM images: (a-b) UT-BCS before adsorption, (c-d) UT-BCS after adsorption, (e-f) AT-BCS before adsorption, (g-h) AT-BCS after adsorption, (i-j) BT-BCS before adsorption and (k-l) BT-BCS after adsorption

4.9.1.2 FTIR

The IR plots confirmed the functional groups present on UT-BCS, AT-BCS and BT-BCS adsorbents as shown in Fig. 18. The broad band at 3282 cm^{-1} on UT-BCS spectrum is assigned to (-OH) stretching. AT-BCS and BT-BCS (-OH) stretching bands slightly shifted to 3288 and 3347 cm^{-1} respectively. The small band at 2978 cm^{-1} was observed only in UT-BCS and AT-BCS, however it dropped off in BT-BCS. The two bands in UT-BCS, AT-BCS and BT-BCS at 2923 and 2853 cm^{-1} were attributed to (-CH) stretch of ($-CH_3$) and ($-CH_2$) respectively. The band (-C=O) for ketonic group was observed at 1743 cm^{-1} for all adsorbents. Two sharp bands on UT-BCS and AT-BCS at 1637 and 1541 cm^{-1} were assigned to (-C=O) and ($-NH_2$) of amide group respectively. However, on BT-BCS, (-C=O) band was recorded at 1624 cm^{-1} and ($-NH_2$) band dropped off. The (-COOH) group stretching band was assigned at 1413 cm^{-1} for UT-BCS and slightly shifted to 1453 for AT-BCS and BT-BCS. The band at 1239 cm^{-1} on UT-BCS and BT-BCS was assigned to (-CO) group. On AT-BCS the (-CO) group shifted to 1236 cm^{-1}. New band was observed at 1147 cm^{-1} on AT-BCS and BT-BCS spectra respectively. Most bands

indicated massive oxygen containing group's presence on UT-BCS, AT-BCS and BT-BCS surfaces.

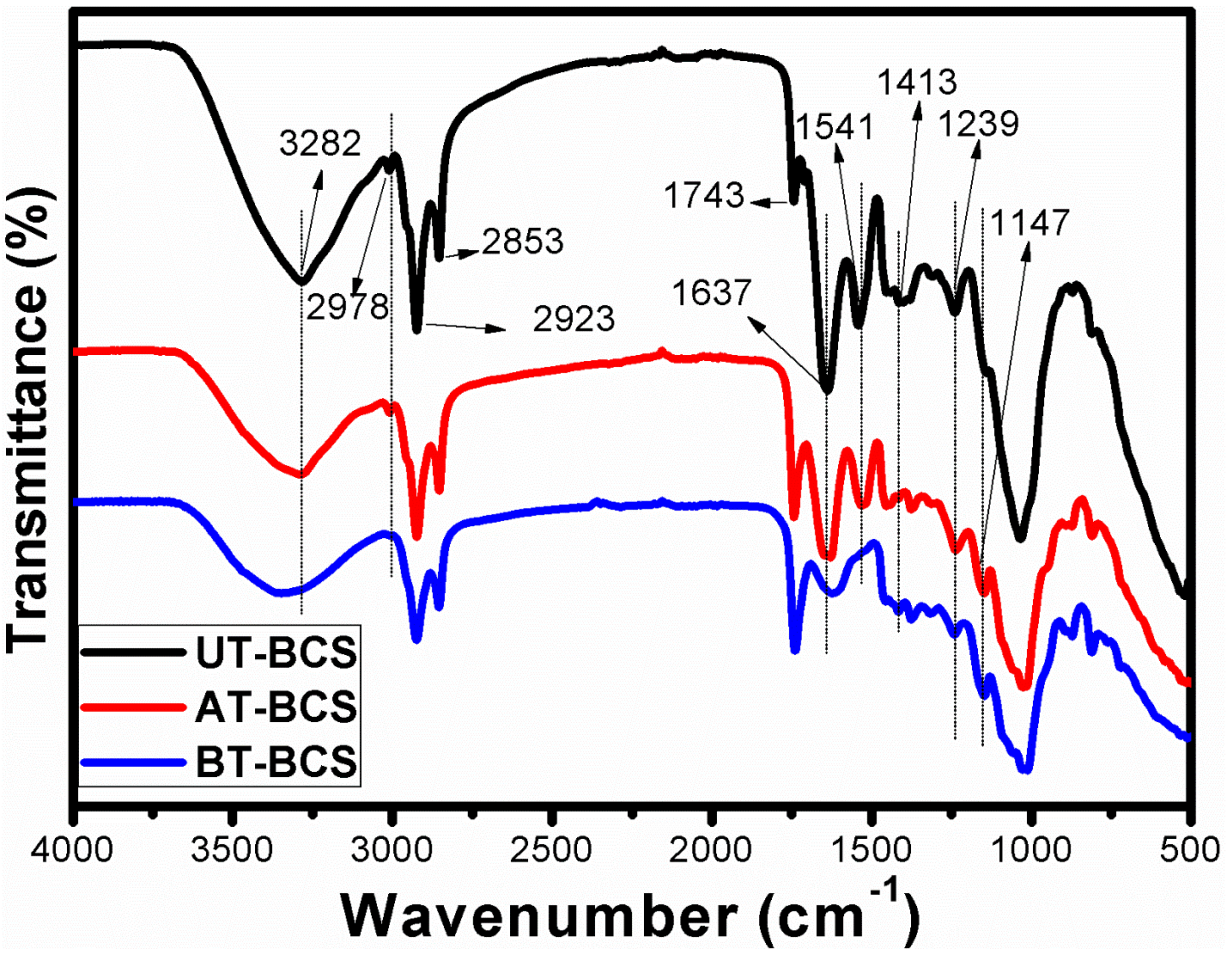

Figure 18: IR spectra of UT-BCS, AT-BCS and BT-BCS adsorbents

4.9.1.3 XRD

The X-ray diffraction spectra of UT-BCS, AT-BCS and BT-BCS before and after adsorption are shown in Figs. 19a-b respectively. The pattern trends of spectra were similar for all adsorbents before and after adsorption. The exhibited broad peaks in Fig. 19a-b between (2θ) 17 and 21° represent cellulosic content in the adsorbents. The weak peaks are assigned to the

amorphous nature of adsorbents. However, the only change observed was a peak in Fig. 19a at (2θ) = 64° before cations adsorption, it disappeared in Fig. 19b for all adsorbents after adsorption.

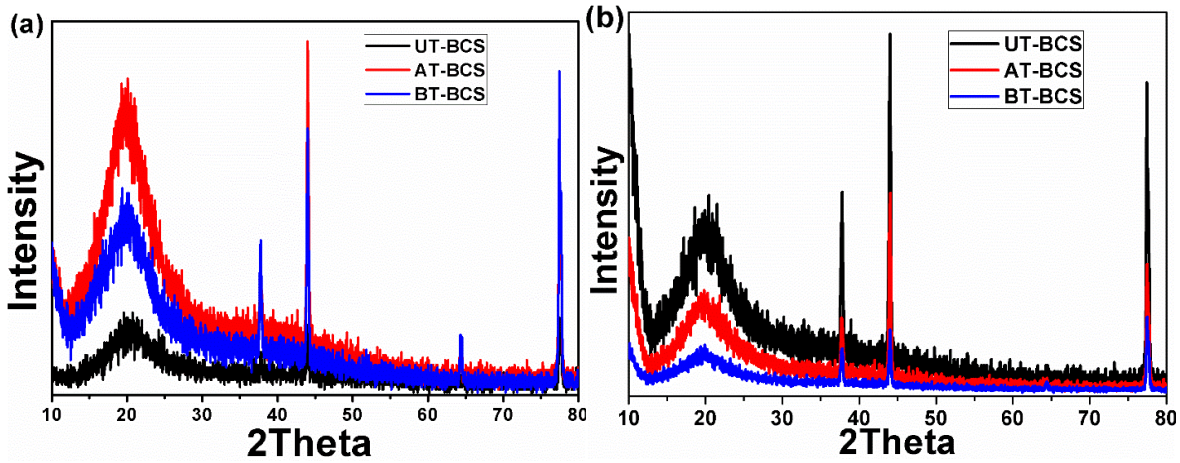

Figure 19: XRD spectra of UT-BCS, AT-BCS and BT-BCS; (a) before adsorption and (b) after adsorption.

4.9.2 Adsorption studies

4.9.2.1 Concentration effect and modeling studies

Figs. 20a-c shows the adsorption ability of UT-BCS, AT-BCS and BT-BCS for cations in aqueous solution at varying cations concentration. The trend of the plots recorded an increase in adsorption with increasing cations solutions concentration. This may be attributed to the fact that initial concentration of the cation solution provides an important driving force to overcome mass transfer resistance of the cations between the aqueous and solid phases, hence higher initial concentration of cations will result in higher adsorption.

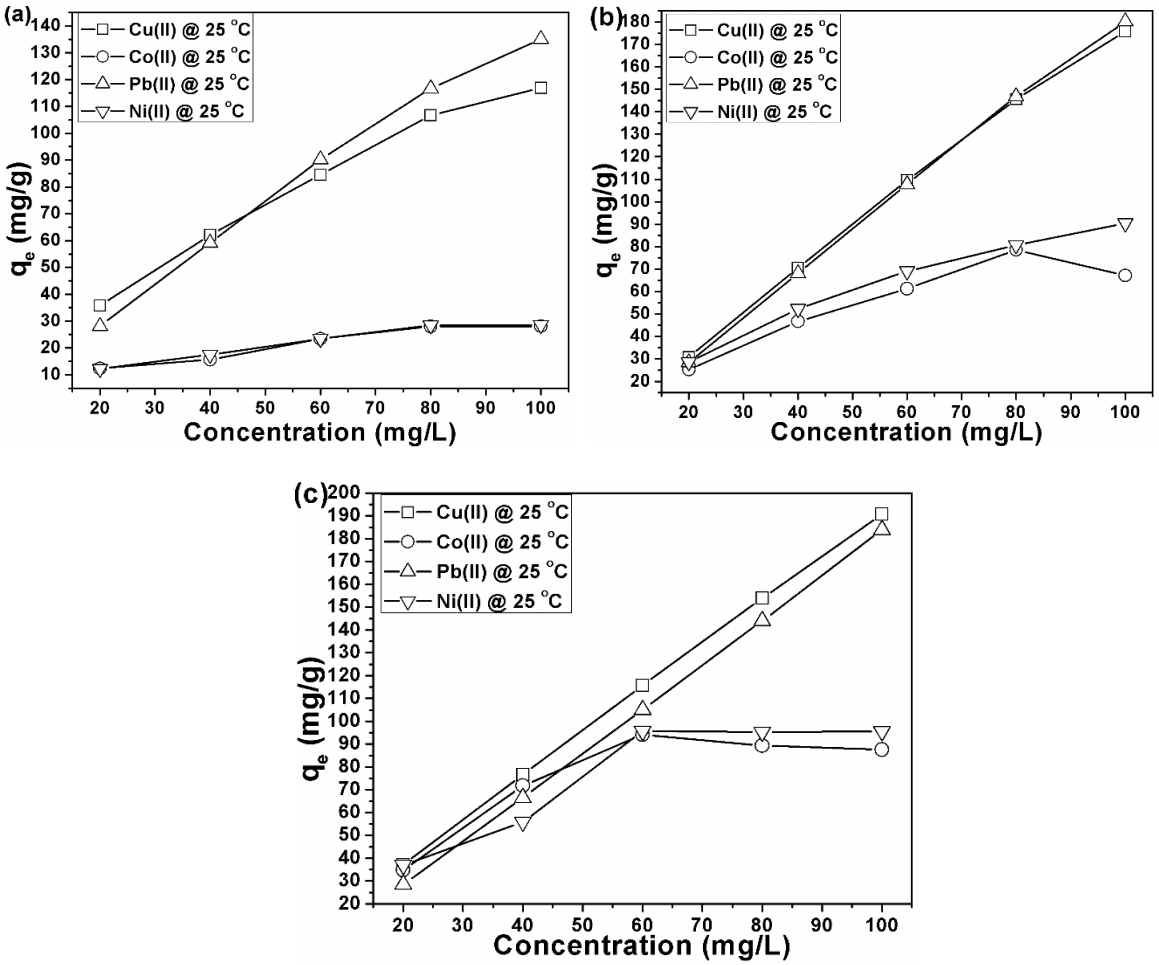

Figure 20: Concentration effect studies onto (a) UT-BCS, (b) AT-BCS and (c) BT-BCS for the adsorption of Cu(II), Co(II), Pb(II) and Ni(II)

Langmuir, Freundlich and Temkin isotherms shown in (Table 1) were evaluated by means of equilibrium data obtained at 288 K to determine the maximum capacity and interaction behaviour (adsorption mechanism) of cations onto UT-BCS, AT-BCS and BT-BCS. It is shown in the table that all adsorption equilibrium data fitted Langmuir isotherm model; higher r^2 values between (0.983-0.999) close to unity (1) and Q_o values closer to the experimental. This data indicates that the adsorption of cations onto UT-BCS, AT-BCS and BT-BCS took place on active sites having equal affinity for these ions and further suggests that monolayer adsorption occurred on adsorbents surface at the end of adsorption process. Freundlich and Temkin isotherm models could not be used to explain the adsorption processes. Freundlich and

Temkin isotherms gave (r^2) values between (0.837-0.990) and (0.544-0.982) respectively. Both models could not be used to explain the adsorption processes on to adsorbents.

Table 1: Isotherm models

Isotherms		UT-BCS				AT-BCS				BT-BCS			
		Cu(II)	**Co(II)**	**Pb(II)**	**Ni(II)**	**Cu(II)**	**Co(II)**	**Pb(II)**	**Ni(II)**	**Cu(II)**	**Co(II)**	**Pb(II)**	**Ni(II)**
Langmuir	Q_o	115.0	27.92	134.1	29.81	174.0	77.54	178.1	91.28	191.2	89.62	181.2	99.92
	B	0.100	0.059	0.021	0.068	0.013	0.067	0.462	0.055	0.034	0.394	0.542	0.325
	r^2	0.991	0.996	0.990	0.989	0.993	0.983	0.996	0.999	0.996	0.988	0.992	0.985
Freundlich	**1/n**	106.6	15.65	110.8	16.09	170.8	75.96	185.0	95.11	114.8	48.05	135.2	39.38
	k_f	2.471	2.78	1.348	2.886	1.064	2.645	0.636	2.205	8.555	5.774	0.185	4.145
	r^2	0.975	0.905	0.969	0.967	0.850	0.937	0977	0.990	0.943	0.948	0.976	0.837
Temkin	k_T	1.296	5.74	1.091	1.070	1.119	1.028	1.247	1.075	19.65	1.384	1.530	1.388
	b_T	-2.39	-16.8	-2.88	-4.40	-1.56	-3.95	-1.34	-3.58	-1.055	-2.15	-0.76	-2.22
	r^2	0.752	0.833	0.725	0.544	0.852	0.912	0.965	0.934	0.982	0.947	0.923	0.632
Experimental (q_e)		116.8	28.05	135.0	28.55	175.7	78.58	180.1	90.41	190.7	87.54	183.9	95.59

4.9.2.2 Temperature effect and modeling studies

The effect of temperature was studied at 288, 298, 308, 318 and 328 K temperatures; the data are shown in Figs. 21a-c. The trend in UT-BCS adsorbent (Fig. 21a), shows a significant increase in adsorption capacity as temperature increased from 288 to 298 K; Cu(II) 98.2 to 116 mg/g, Pb(II) 112 to 134 mg/g, Co(II) 4.24 to 29.4 mg/g and Ni(II) 2.18 to 28.9 mg/g respectively. A further increase in temperature to 308 K; resulted in Cu(II) increasing to 163 mg/g, Pb(II) 151 mg/g, Co(II) to 33.5 mg/g and Ni(II) to 41.2 mg/g. However, at higher temperatures of 318 and 328 K, lower adsorption capacities were exhibited for all cations, Cu(II) decreased from 161 to 160 mg/g, Pb(II) 143 to 139 mg/g, Co(II) 29.2 to 21.0 mg/g and Ni(II) 24.4 to 23.4 mg/g. Data obtained showed that higher temperatures of 318 and 328 K were detrimental to the process. This trend suggests, escaping of the adsorbed cations on UT-

BCS at higher temperatures, indicating physical nature of the adsorption. The same trends were observed in Figs. 21b-c, for AT-BCS and BT-BCS respectively.

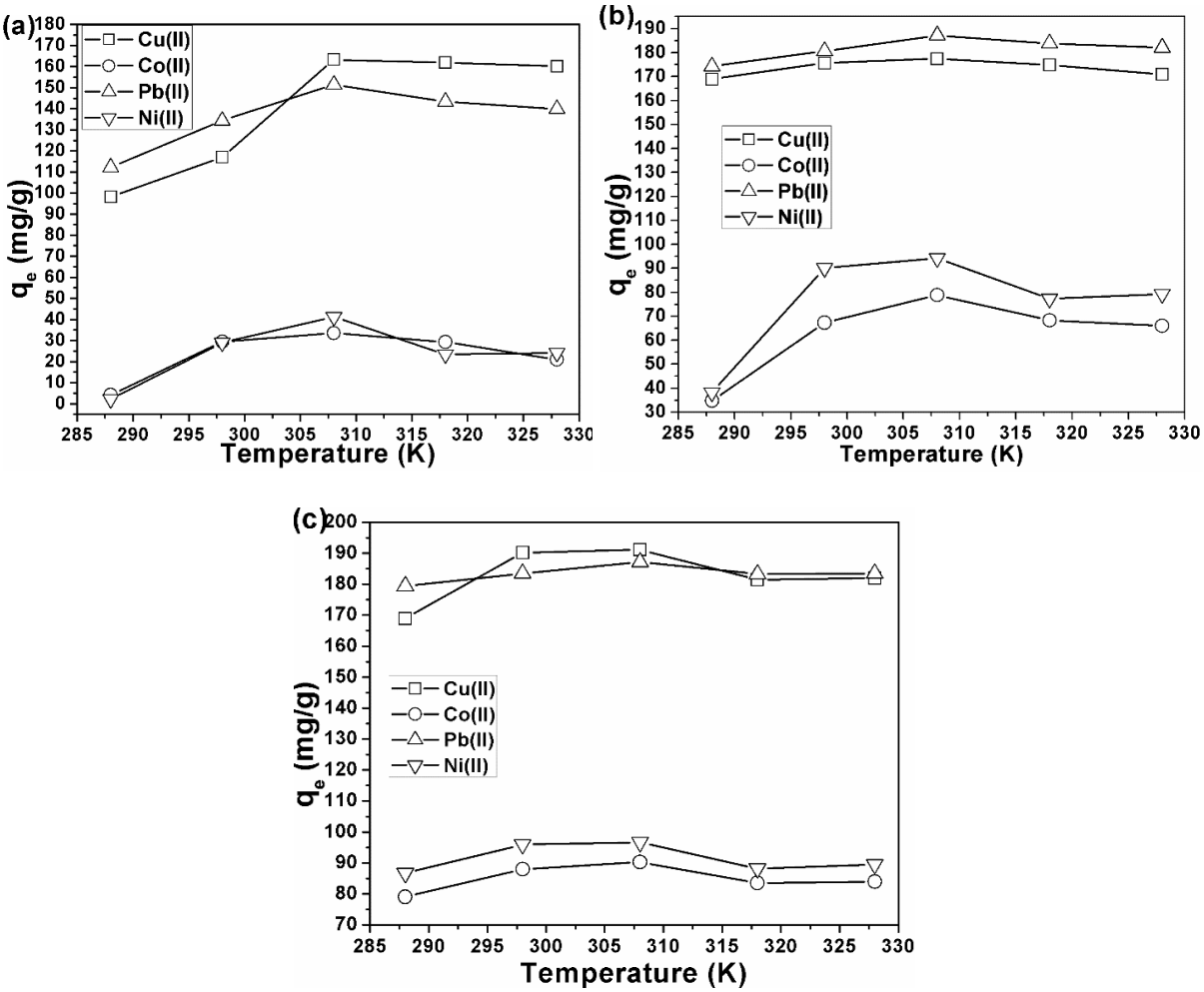

Figure 21: Temperature effect studies onto (a) UT-BCS, (b) AT-BCS and (c) BT-BCS for the adsorption of Cu(II), Co(II), Pb(II) and Ni(II)

The thermodynamic parameters; Gibbs free energy *(ΔG°)*, enthalpy *(ΔH°)*, and entropy *(ΔS°)* were evaluated to determine the spontaneity and feasibility of Cu(II), Pb(II), Co(II) and Ni(II) ions sorption onto UT-BCS, AT-BCS and BT-BCS (Table 2). The parameters were evaluated at different temperatures (288, 298, 308, 318 and 328 K). *ΔS°* gave positive values this indicates increased randomness and degree of freedom for cations in aqueous solution during sorption process. Both *ΔG°* and *ΔH°* gave negative values suggesting that all sorption processes were

spontaneous and exothermic respectively. Therefore, it was observed that at higher temperatures sorption ability of cations was reduced. However, Fig. 19a-c plots recorded an increase in sorption capacity of the cations as temperature increased from 288 to 308 K. This is significant, as small amounts of energy may be required to terminate the hindering repulsive forces preventing further sorption of the cations. Higher temperatures from 318 to 328 K recorded less sorption of the cation compared to 308 K, as such temperatures 318 and 328 K were detrimental to the process. This could be linked to kinetic energy causing the ions to move more rapidly in the solution and not staying long enough at the active sorption sites to be adsorbed resulting in lower sorption.

Table 2: Thermodynamic studies and their parameters

Parameter	UT-BCS				AT-BCS				BT-BCS			
	Cu(II)	**Co(II)**	**Pb(II)**	**Ni(II)**	**Cu(II)**	**Co(II)**	**Pb(II)**	**Ni(II)**	**Cu(II)**	**Co(II)**	**Pb(II)**	**Ni(II)**
ΔH^o (KJ mol^{-1})	-4.64	-1.95	-2.14	-3.16	-1.63	-1.06	-2.71	-0.857	-5.87	-0.311	-2.29	-0.251
ΔS^o (KJ mol^{-1}K^{-1})	1.27	0.743	0.519	1.12	0.25	0.352	0.549	0.306	1.55	0.059	0.411	0.0283
ΔG^o (KJ mol^{-1}) 288 K	-1.57	-7.51	-2.24	-9.13	-5.71	-2.06	-6.24	-1.79	-0.503	-0.640	-6.84	-1.01
298 K	-2.56	-2.63	-3.49	-2.68	-6.60	-0.034	-7.24	-1.22	-9.06	-1.11	-7.68	-1.51
308 K	-5.59	-2.32	-4.68	-1.67	-7.06	-0.675	-8.64	-1.47	-7.86	-1.27	-8.64	-1.60
318 K	-5.66	-2.82	-4.29	-3.50	-6.96	-0.387	-8.25	-0.610	-7.86	-0.952	-8.16	-1.20
328 K	-5.68	-3.94	-4.19	-3.53	-6.71	-0.289	-8.21	-0.744	-8.19	-1.00	-8.45	-1.31

4.9.2.3 Rate and kinetic studies of cations removal from aqueous solution

The rate at which pollutants are removed from aqueous solution is imperative and it was evaluated in order to determine the efficiency of UT-BCS, AT-BCS and BT-BCS for wastewater treatment**.** The rate of removal trends of cations; Cu(II), Co(II), Pb(II) and Ni(II) onto UT-BCS, AT-BCS and BT-BCS absorbents are shown in Figs. 22a-c. In Fig. 22a the removal rate was much rapid for Cu(II) and Pb(II) than Co(II) and Ni(II) ions, hence equilibrium was reached faster in just 30 min for Cu(II) and Pb(II) ions and 60 min for Co(II)

and Ni(II) ions. In Fig 22b it was observed that Pb(II) ions removal rate was faster, therefore attaining equilibrium in 10 min, followed by Cu(II) ions that attained equilibrium in 30 min. Co(II) and Ni(II) ions had slower removal rate, attained equilibrium in 60 min. In Fig. 22c Cu(II) and Pb(II) ions removal rate was faster and attained equilibrium in 10 min compared to Co(II) and Ni(II) ions, adsorption which attained equilibrium in 60 min.

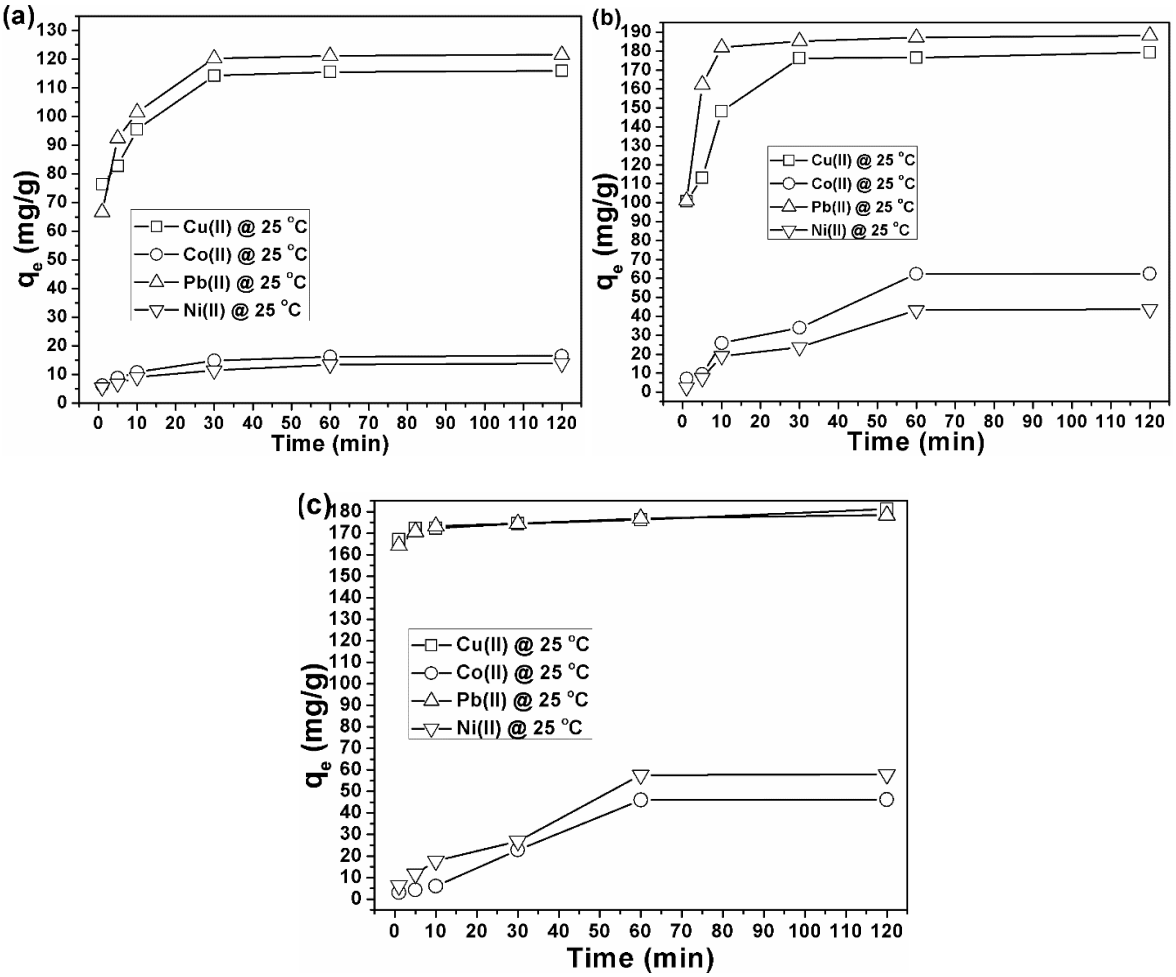

Figure 22: Time effect studies onto (a) UT-BCS, (b) AT-BCS and (c) BT-BCS for the adsorption of Cu(II), Co(II), Pb(II) and Ni(II)

The kinetic studies of Cu(II), Co(II), Pb(II) and Ni(II) removal onto UT-BCS, AT-BCS and BT-BCS were determined using pseudo first order (PFO), pseudo second order (PSO), and intra particle diffusion (IPD) models. Different kinetic models and their parameters are shown

in Table 3. To determine whether the adsorption had a good fit for the PFO or PSO it requires either the values of correlation coefficient r^2 to be close to 1 (unity) and the values of adsorption capacity (q_e) close to the experimental values. It was shown in Table 3 that the PFO model gave consistent fit in describing the adsorption of all the cations onto UT-BCS, AT-BCS and BT-BCS than PSO model. The r^2 values were closer to 1, (0.990-0.998) for PFO unlike PSO values (0.919-0.983). The calculated capacities (q_e) values were closer to the obtained experimental values for PFO, unlike PSO. PFO good fit suggests that the adsorption mechanism for all cations onto adsorbents in this study involved Van der Waal forces attraction.

IPD kinetic model estimates the nature of the process, either surface or pores adsorption. The parameter; *C (mg/g)* values measure the degree of thickness of the accumulated cations adsorbate on the adsorbents surface. It is shown in Table 3 that estimated pore adsorption (EPA) was dominant in all adsorption processes than estimated surface adsorption (ESA). EPA ranged between 81.39-95.87% and ESA between 5.201-26.42%.

Table 3: Kinetic model types and their parameters

Models		**UT-BCS**				**AT-BCS**				**BT-BCS**			
		Cu(II)	**Co(II)**	**Pb(II)**	**Ni(II)**	**Cu(II)**	**Co(II)**	**Pb(II)**	**Ni(II)**	**Cu(II)**	**Co(II)**	**Pb(II)**	**Ni(II)**
PFO	$\mathbf{q_e}$	116.1	16.47	130.5	10.31	185.8	63.02	187.6	42.14	183.9	46.01	173.02	57.92
	$\mathbf{K_1}$	1.00	1.00	1.00	1.00	2.765	1.00	3.745	1.00	2.351	1.00	1.993	1.00
	$\mathbf{r^2}$	0.991	0.992	0.998	0.992	0.998	0.995	0.996	0.995	0.998	0.994	0.990	0.996
PSO	$\mathbf{q_e}$	97.26	3.554	92.25	7.384	102.2	21.91	125.6	31.75	173.9	46.65	124.0	54.55
	$\mathbf{K_2}$	0.610	1.582	0.965	0.096	0.102	3.787	0.880	3.559	0.663	4.519	0.429	2.621
	$\mathbf{r^2}$	0.978	0.972	0.957	0.983	0.919	0.973	0.979	0.957	0.980	0.957	0.948	0.958
IPD	**C**	13.32	1.283	14.52	1.055	25.33	3.802	35.02	2.758	47.90	2.561	46.84	3.092
	$\mathbf{K_i}$	10.59	1.514	10.47	1.314	14.05	7.139	13.99	5.851	12.18	6.518	12.01	5.146
	$\mathbf{r^2}$	0.996	0.987	0.981	0.989	0.929	0.987	0.936	0.940	0.9427	0.932	0.940	0.942

EPA[a]	**%**	89.69	92.81	88.75	93.16	85.86	95.36	81.39	95.87	73.57	96.53	73.73	94.79
ESA[a]	**%**	10.30	7.183	11.24	6.83	14.14	4.640	18.61	4.126	26.42	3.470	26.27	5.201
Experimental (q_e)		115.9	17.86	129.1	15.44	179.2	62.52	188.2	43.69	181.3	46.25	178.3	57.90

*EAP- Estimated pore adsorption of IPD and *ESA - Estimated surface adsorption of IPD.

4.9.2.4. pH effect on the adsorption of cations

The effect of the pH of the solution was studied at pH 1, 3, 5, 7 and 8.5 as shown in Figs. 23a-c. The adsorption of cations onto all adsorbents was largely pH dependent. It was observed that UT-BCS, AT-BCS and BT-BCS adsorption capacities increased with increasing pH. However, this could be explained based on; at low pH 1 to 5 the functional groups (-COOH, -OH and -NH_2) on adsorbents surface were protonated. This restricted the adsorption of cations because of repulsive forces. Haug (1961), reported that at low pH below 4.5 (-COOH) groups are protonated therefore, electrostatic attraction between adsorbent surface and positively charged cations is negligible. However, at high pH values from 7 to 8.5 functional groups (-COOH, -OH and -NH) on adsorbents surface got deprotonated and increased the adsorption of cations. This increased the negative charges on the adsorbents surface and improved attraction forces and adsorption capacity.

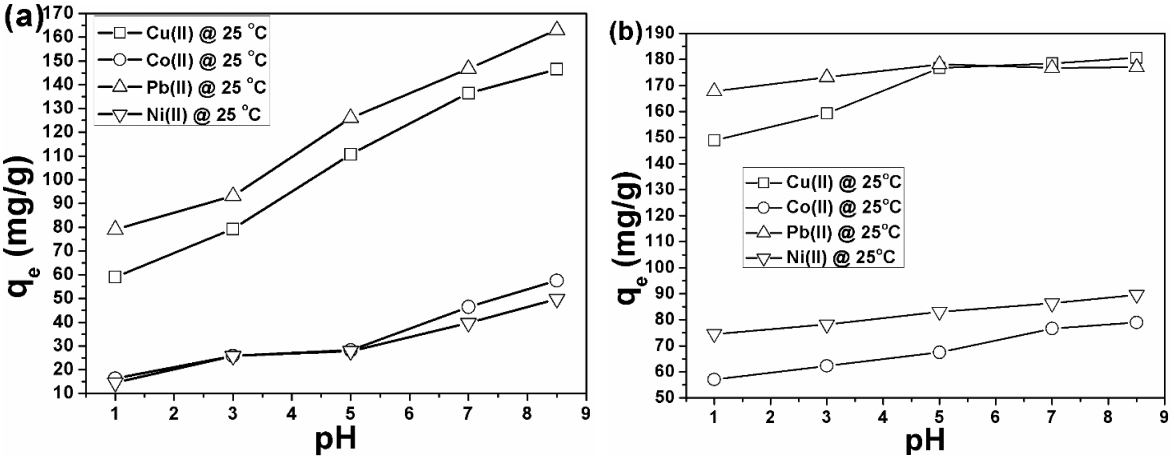

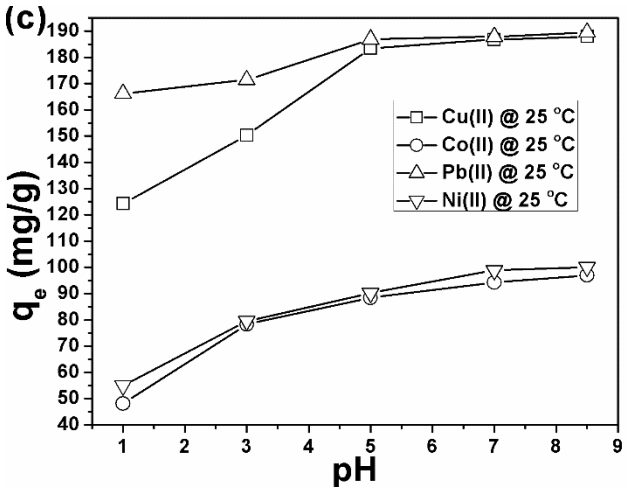

Figure 23: Effect of pH onto (a) UT-BCS, (b) AT-BCS and (c) BT-BCS for the adsorption of Cu(II), Co(II), Pb(II) and Ni(II)

4.9.2.5 Point of zero charge for adsorbents

Fig. 24 shows plots of ΔpH vs. pH_i of adsorbents. From the plots point of zero charge (pH_{ZPC}) of UT-BCS, AT-BCS and BT-BCS is 5.7, 3.7 and 5.5 respectively. It is shown that ΔpH values were negative before pH values of 3.7, 5.5 and 5.7 for AT-BCS, BT-BCS and UT-BCS respectively; this indicated that the adsorbents surface acquired negative charge from initial pH_i up until (pH_{ZPC}). pH values above (pH_{ZPC}) 3.7, 5.5 and 5.7 the adsorbents surface acquired positive charge ΔpH vales became positive. However, at pH values of 3 to 5.5 for BT-BCS and 3 to 5.7 for UT-BCS a buffering effect is observed, this is in agreement with Demeny et al. (2018) findings. They reported that the buffering effect is linked to the protonation of carboxylic groups (-COOH), which affect the adsorption capacity

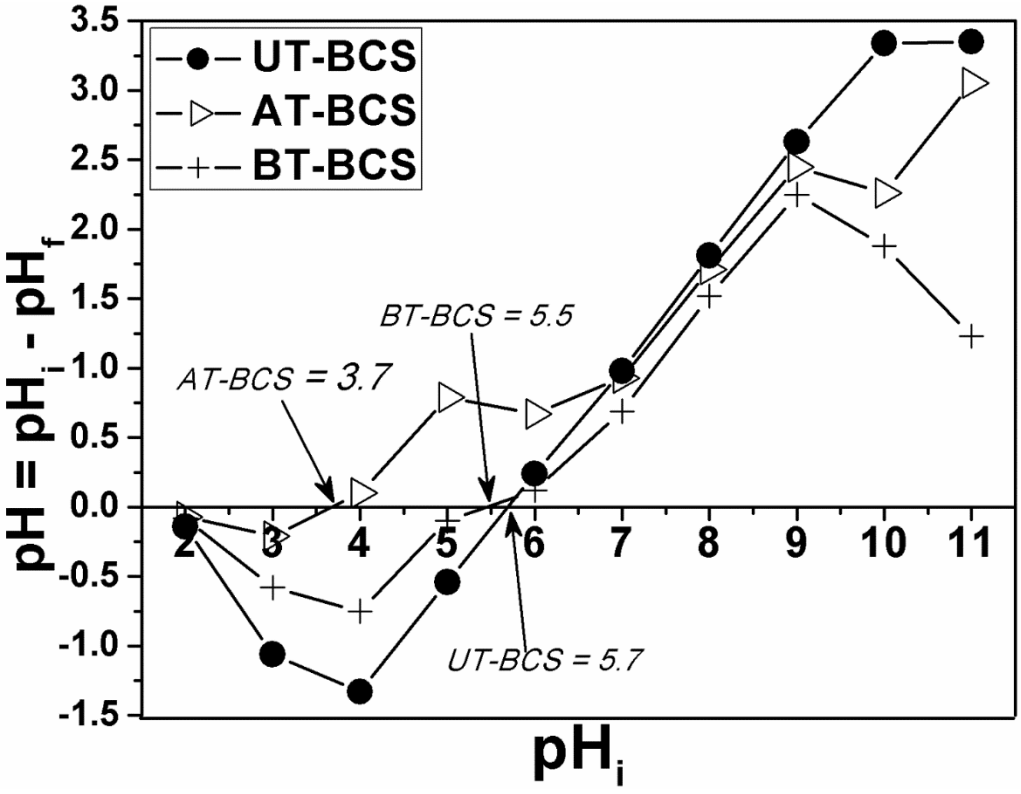

Figure 24: Point of zero charge of adsorbents

4.9.3 Mechanism of adsorption

Black cumin seeds (UT-BCS, AT-BCS and BT-BCS) FTIR spectra (Fig 18) confirmed the presence of several functional groups such as carboxyl (-COOH), hydroxyl (-OH) and amide ($-NH_2$) on the adsorbents surface. The presence of these functional sites could have possibly governed the adsorption processes (see the proposed mechanism in scheme 2). The interaction behaviour between adsorbents surface and metal ions was through electrostatic attraction.

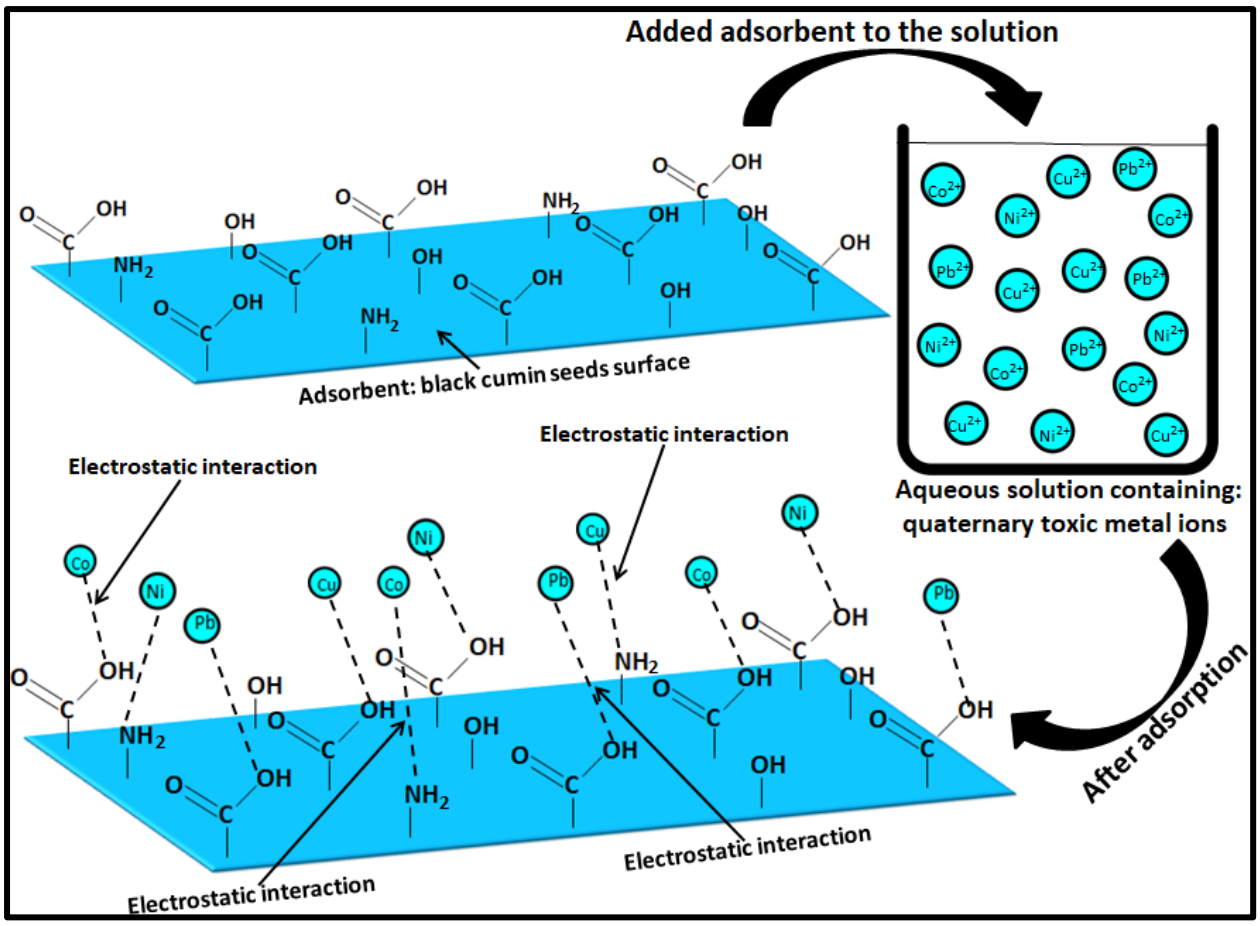

Scheme 2: Proposed adsorption mechanism of Cu(II), Pb(II), Ni(II) and Co(II) ions onto UT-BCS, AT-BCS and BT-BCS.

4.9.4 Reusability studies

Economic benefits of UT-BCS, AT-BCS and BT-BCS were estimated by investigating the reusability of the biosorbents. The adsorption/desorption result of five cycles of biosorbents used in this study towards cations are shown in (Figs. 25a-c). The biosorbents adsorption capabilities (Figs. 25a-c) show a slow downward trend with increasing cycle numbers to five. UT-BCS; Cu(II) decreased from 83.7 to 78.0 %, Co(II) 65.3 to 60.9 %, Pb(II) 84.6 to 77.9 % and Ni(II) 62.6 to 59.2 %. AT-BCS; Cu(II) decreased from 95.3 to 85.9 %, Co(II) 80.9 to 72.9 %, Pb(II) 98.3 to 88.6 % and Ni(II) 79.3 to 69.9 %. BT-BCS; Cu(II) decreased from 96.6 to 91.0 %, Co(II) 85.5 to 77.9 %, Pb(II) 98.5 to 91.5 % and Ni(II) 85.9 to 77.1 %. At the end of

the fifth cycle, UT-BCS, AT-BCS and BT-BCS adsorbents retained ≥90 % of their initial cation's adsorption capacities. The obtained reusability data suggest that UT-BCS, AT-BCS and BT-BCS adsorbents may be reusable in wastewater treatment.

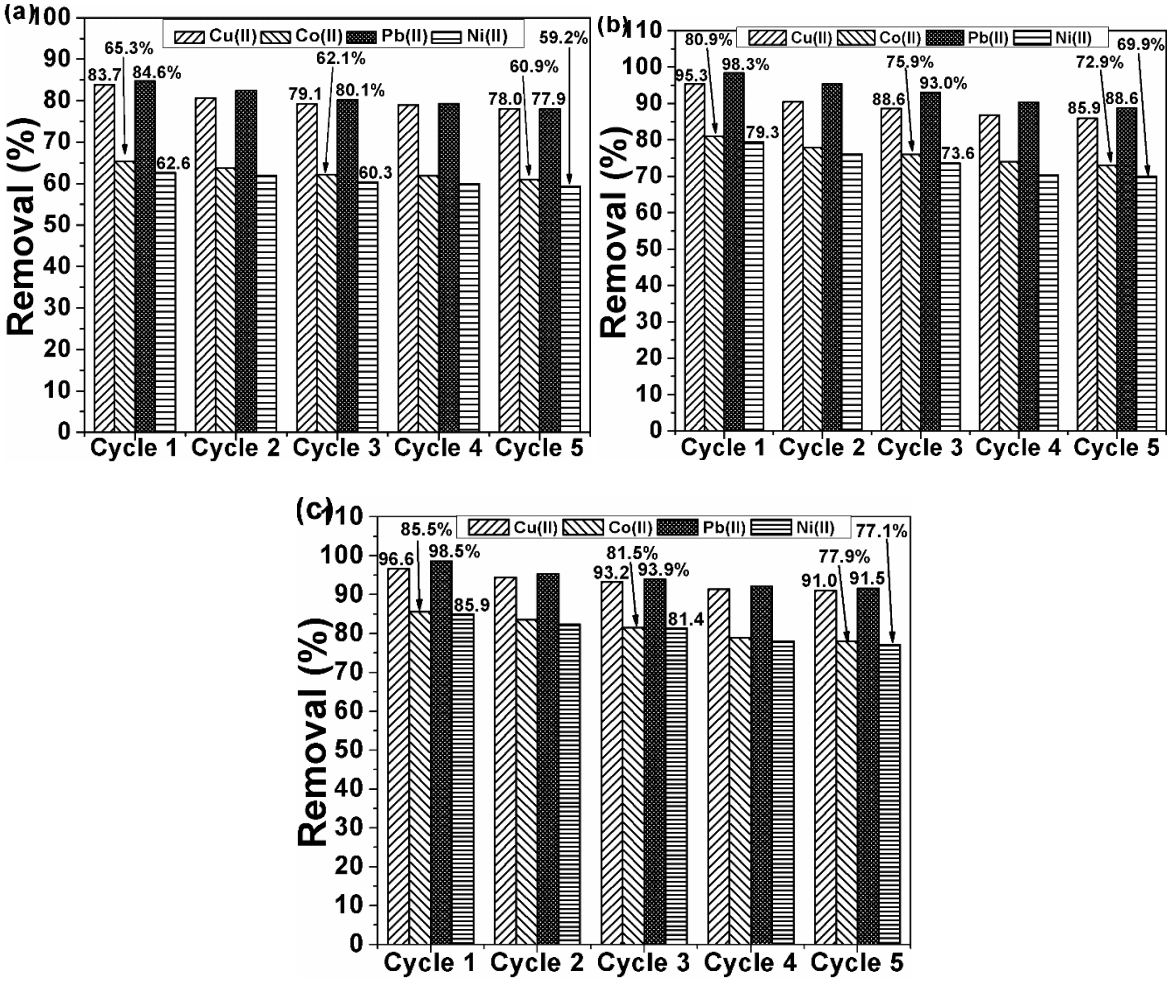

Figure 25: Reusability data of (a) UT-BCS (b) AT-BCS and (c) BT-BCS

4.9.5 Comparative studies

Black cumin seeds (AT-BCS and BT-BCS) adsorption studies showed high potential and possess good removal capacity in comparison to previously reported seeds biosorbents as

shown in Table 4. The results show the potential of treated black cumin seeds; AT-BCS and BT-BCS have in wastewater treatment.

Table 4: Seed's adsorbents comparative study

Biosorption capacities study of Co(II), Ni(II), Pb(II) and Cu(II)					
Biomass adsorbent	**$q_{(max)}$ (mg/g)**				**Reference**
	Ni(II)	**Co (II)**	**Pb(II)**	**Cu(II)**	
Black sapote seeds	-	-	5.50	8.20	Cid et al. 2019
Defatted papaya seeds	-	-	53.02	17.29	Garba et al. 2016
Caryota urens seeds	-	-	-	27.39	Rao et al. 2016
Peganum harmala seeds	91.74	-	-	-	Ghasemi et al. 2014
Litchi chinensis seeds	66.62	-	-	-	Flores-Garnica et al. 2013
Doum seeds	-	13.51	-	-	El-Sadaawy et al. 2014
Citrus limettioides seeds	-	35.54	-	-	Sudha et al. 2015
Moringa stenopetala seeds	-	-	16.13	10.20	Kebede et al. 2018
Chili seeds	-	-	11.78	-	Medellin-Castillo et al. 2017
Cotton seeds	-	-	-	156	Thirugnanasambandham et al. 2015
Black cumin seeds	-	-	-	85.49	Ahmad et al. 2014
Acid treated BCS	90.41	78.58	180.1	175.7	This study
Base treated BCS	95.59	87.54	183.9	190.7	This study

4.9.6. Conclusion

The low cost acid and base treated black cumin seeds adsorbents; AT-BCS and BT-BCS were successfully utilized for quaternary adsorption study of Cu(II), Co(II), Pb(II) and Ni(II) ions from aqueous solution. The adsorption processes were depended on system parameters such as; initial concentration of the metal ions, contact time, temperature and initial pH of the solution. Adsorbents maximum capacity trend was BT-BCS>AT-BCS>UT-BCS. Isotherm models were evaluated for; Langmiur, Freundlich and Temkin, the best fit was found to be

Langmiur model. Kinetic studies were tested for pseudo first order (PSO) and pseudo second order (PSO). The PFO good fit suggest that the adsorption mechanism involved, electrostatic attractions and Van der Waal forces. Thermodynamic analysis revealed that the adsorption processes were spontaneous and exothermic in nature. The reusability data, suggests that the low-cost black cumin seeds adsorbents can be reused for the adsorption of cations from solution. Advantages of the present study are; easy generation of the biosorbents and their ability to be reused several times. Disadvantages of the study are; black cumin seeds modification by acid and base can only be carried at low concentrations. At high concentrations black cumin seeds dissolve in acid and base solutions.

4.9.7 Acknowledgment

We acknowledge the supports of the Department of Chemistry and Research Directorate, Vaal University of Technology, Vanderbiljpark, South Africa.

References

ADHAM, M.L., 1997. Renal effects of environmental and occupational lead exposure. *Environmental Health Perspectives*, 105, 928-938.

ADDALA, A., BELATTAR, N. & ELEKTOROWICZ, M., 2018. Nigella sativa L. Seeds Biomass as a Potential Sorbent in Sorption of Lead from Aqueous Solutions and Wastewaters. *Oriental Journal of Chemistry*, 34, 638-647.

AHMAD, R. & HASEEB, S., 2013. Adsorption of Pb(II) on Mentha piperita carbon (MTC) in single and quaternary systems. *Arabian Journal of Chemistry*.

AL-JASSIR, M.S., 1992. Chemical composition and microflora of black cumin (Nigella sativa L.) seeds growing in Saudi Arabia. *Food Chemistry*, 45, 239-242.

ANIS, S.F., HASHAIKEH, R.& HILAL, N., 2019. Reverse osmosis pretreatment technologies and future trends: A comprehensive review. *Desalination*, 452, 159-195.

ASFARAM, A., GHAEDI, M., AGARWAL, S., TYAGIB, I. & GUPTA, V.K., 2015. Removal of basic dye Auramine-O by ZnS:Cu nanoparticles loaded on activated carbon: optimization of parameters using response surface methodology with central composite design. *RSC Advances*, 5, 18438-18450.

ASFARAM, A., GHAEDI, M., DASHTIAN, K. & GHEZELBASH, G.R., 2018. Preparation and Characterization of $MnO.4ZnO.6Fe_2O_4$ Nanoparticles Supported on Dead Cells of Yarrowia lipolytica as a Novel and Efficient Adsorbent/Biosorbent Composite for the Removal of Azo Food Dyes: Central Composite Design Optimization Study *ACS Sustainable Chemistry & Engineering*, 6, 4549-4563.

ATIQUE ULLAH, A.K.M., MAKSUD, M.A., KHAN, S.R., LUTFA, L.N. & QURAISHI, S.B., 2017. Dietary intake of heavy metals from eight highly consumed species of cultured fish and possible human health risk implications in Bangladesh. *Toxicology Reports*, 4, 574-579.

BALARAK, D., JAAFARI, J., HASSANI, G., MAHDAVI, Y., TYAGI, I., AGARWAL, S. & GUPTA, V.K., 2014 The use of low-cost adsorbent (Canola residues) for the adsorption of methylene blue from aqueous solution: Isotherm, kinetic and thermodynamic studies. *Colloids Interface and Science Communications*, 7, 16-19.

CID, A.A.P., HERNANDEZ, V.R., GONZALEZ, A.M.H., HERNANDEZ A.B. & ALONSO, O.C., 2019. Synthesis of activated carbon from black sapote seeds characterized and application in the elimination of heavy metals and textile dyes. *Chinese Journal of Chemical Engineering.*

CLARK, M.J., PRENTICE, J.R., HOGGARD, N., PALEY, M.N., HADJIVASSILIOU, M. & WILKINSON, J.M., 2014. Brain structure and function in patients after metal-on-metal hip resurfacing. *American Journal Neuroradiology*, 2014, 1753-1758.

DASHTIAN, K., NASIRI AZAD, F., GHAEDI, M., JAMSHIDI, A, HASSANI, G., MONTAZEROZOHORI, M., HAJATI, S., RAJABI, M. & BAZRAFSHAN, A.A. 2016. Preparation and characterization of AC-Fe_3O_4-Au hybrid for simultaneous removal of Cd^{2+}, Pb^{2+}, Cr^{3+} and Ni^{2+} ions from aqueous solution via complexation with 2-((2, 4-Dichloro-benzylidene)-amino)-benzenethiol: Taguchi optimization. *RSC Advances.*

DEMEY, H., VINCENT, T. & GUIBAL, E., 2018. A novel algal-based sorbent for heavy metal removal. *Chemical Engineering Journal*, 332, 582-595.

DENG, Y., HUANG, D.S., LAIRD, D.A., WANG, X. & MENG, Z., 2019. Adsorption behaviour and mechanisms of cadmium and nickel on rice straw biochars in single- and binary-metal systems. *Chemosphere*, 218, 308-318.

EL-SADAAWY, M. & ABDELWAHAB, O., 2014. Adsorptive removal of nickel from aqueous solutions by activated carbons from doum seed (Hyphaenethebaica) coat. *Alexandria Engineering Journal*, 53, 399-408.

EL-SAID, S.M., ALAMRI, M.B.S. & EL-BARAK, A.B.S. & Alsogair, O., 2009. Adsorptive removal of arsenite as (III) and arsenate as (V) heavy metals from waste water using *Nigella sativa* L. *Asian Journal of Scientific Research* 2, 96-104.

FLORES-GARNICA, J.G., MORALES-BARRERA. L., PINEDA-CAMACHO, G. & CRISTIANI-URBINA, E., 2013. Biosorption of Ni(II) from aqueous solutions by Litchi chinensis seeds. *Bioresource Technology,* 136, 635-643.

GARBA, Z.N., BELLO, I., GALADIMA, A. & LAWAL, A.Y., 2016. Optimization of adsorption conditions using central composite design for the removal of copper (II) and lead (II) by defatted papaya seed. *Karbala International Journal Modern Science,* 2, 20-28.

GHAEDI, M., AZAD, F.N., DASHTIAN, K., HAJATI, S., GOUDARZI, A. & SOYLAK, M., 2016. Central composite design and genetic algorithm applied for the optimization of ultrasonic-assisted removal of malachite green by ZnO nanorod-loaded activated carbon. *Spectrochimica Acta,* A.167, 157-164.

GHAEDI, M., HAJJATI, S., MAHMUDI, Z., TYAGI, I., AGARWAL, S., MAITY, A. & Gupta, V.K., 2015. Modeling of competitive ultrasonic assisted removal of the dyes-Methylene blue and Safranin-O using Fe_3O_4 nanoparticles. *Chemical Engineering Journal* 268, 28-37.

GHASEMI M., GHASEMI, N. & AZIMI-AMIN, J., 2014. Adsorbent ability of treated Peganum harmala-L seeds for the removal of Ni (II) from aqueous solutions: kinetic, equilibrium and thermodynamic studies. *Indian Journal of Material Science.*

GUPTA, V.K., ALI, I., SALEH, T.A., SIDDIQUI, M.N. & AGARWAL, S., 2013. Chromium removal from water by activated carbon developed from waste rubber tires. *Environmental Science and Pollution Research*, 20, 1261-1268.

GUPTA, V.K., ATAR, N., YOLA, M.L., USTUNDAG, Z. & UZUN, L., 2014. A novel magnetic Fe@Au coreshell nanoparticles anchored graphene oxide recyclable nanocatalyst for the reduction of nitrophenol compounds. *Water Research*, 48, 210-217.

GUPTA, V.K. & SALEH, T.A., 2013. Sorption of pollutants by porous carbon, carbon nanotubes and fullerene. *Environmental Science and Pollution Research*, 20, 2828-2843.

GUPTA, V.K. & SHARMA, S., 2003. Removal of zinc from aqueous solutions using Bagasse Fly ash-a low cost adsorbent. *Industrial & Engineering Chemistry Research*, 42, 6619-6624.

GUPTA, V.K., SUHAS, TYAGI, I., AGARWAL, S., SINGH, R., CHAUDHARY, M., HARIT, A. & KUSHWAHA, S., 2016. Column operation studies for the removal of dyes and phenols using a low-cost adsorbent. *Global Journal of Environmental Science and Management*. 2, 1-10.

HAUG, A., 1961. Dissociation of alginic acid, *Acta Chemica Scandinavica*, 15, 950-952.

JAISHANKAR, M., TSETEN, T., ANBALAGAN, N., MATHEW, B.B. & BEEREGOWDA, K.N., 2014. Toxicity, mechanism and health effects of some heavy metals. *Interdisciplinary toxicology*, 7, 60-72.

KASPRZAK, K.S., SUNDERMAN JR, F.W. & SALNIKOW, K., 2003. Nickel carcinogenesis. Mutat. *Research-Fundamental and Molecular Mechechanism. Mutation*, 533, 67-97.

KEBEDE, T.G., MENGISTIE, A.A., DUBE, S., NKAMBULE, T.T.I. & NINDI, M.M., 2018. Study on adsorption of some common metal ions present in industrial effluents by Moringa stenopetala seed powder. *Journal of environmental chemical engineering*, 6, 1378-1389.

KUOKKANEN, V., KUOKKANEN, T., RAMO, J. & LASSI, U., 2013. Recent Applications of Electrocoagulation in Treatment of Water and Wastewater. *Green and Sustainable Chemistry*, 3, 89-121.

KYZAS, G.Z. & KOSTOGLOU, M., 2014. Green Adsorbents for Wastewaters: A Critical Review Materials. *Materials*, 7, 333-364.

LUO, W., RUAN, D., YAN, C., YIN, S. & CHEN, J., 2012. Effects of chronic lead exposure on functions of nervous system in Chinese children and developmental rats. *Neurotoxicology*. 33, 862-871.

MALAEB, L.& AYOUB, G.M., 2011. Reverse osmosis technology for water treatment: State of the art review. *Desalination.* 267, 1-8.

MEDELLIN-CASTILLO, N.A., PADILLA-ORTEGA, E., REGULES-MARTÍNEZ, M.C., LEYVA-RAMOS, R., OCAMPO-PEREZ, R. & CARRANZA-ALVAREZ, C., 2017. Single and competitive adsorption of Cd(II) and Pb(II) ions from aqueous solutions onto industrial chili seeds (Capsicum annuum) waste. *Sustainable environment research*, 27, 61-69.

MIKUSOVA, V., LUKACOVICOVA, O., HAVRANEK, E. & MIKUS, P., 2014. Radionuclide X-ray fluorescence analysis of selected elements in drug samples with 8-hydroxyquinoline preconcentration. *Journal of Radioanalytical and Nuclear Chemistry*, 299, 1645-1652.

MITTAL, A., MITTAL, J., MALVIYA, A. & GUPTA, V.K., 2010. Removal and recovery of Chrysoidine Y from aqueous solutions by waste materials. *Journal of Colloid and Interface Science*, 344, 497-507.

MOSLEH, S., RAHIMI, M.R., GHAEDI, M., DASHTIAN, K. & HAJATI, S., 2018. Sonochemical-assisted synthesis of $CuO/Cu_2O/Cu$ nanoparticles as efficient photocatalyst for simultaneous degradation of pollutant dyes in rotating packed bed reactor: LED illumination and central composite design optimization. Ultrasonics-Sonochemistry 40, 601-610.

MOSLEH, S., RAHIMI, M.R., GHAEDI, M DASHTIAN, K. & HAJATI, S., 2016. Photocatalytic degradation of binary mixture of toxic dyes by HKUST-1 MOF and HKUST-1-SBA-15 in a rotating packed bed reactor under blue LED illumination: central composite design optimization. *RSC Advances*, 2016, 6, 17204-17214.

MOSLEH, S., RAHIMI, M.R., GHAEDI, M., DASHTIAN, K., HAJATI, S. & WANG, S., 2017. Ag_3PO_4/AgBr/Ag-HKUST-1-MOF composites as novel blue LED light active photocatalyst for enhanced degradation of ternary mixture of dyes in a rotating packed bed reactor. *Chemical Engineering and Processing*, 114, 24-38.

MOUSAVINIA, S.E., HAJATI, S., GHAEDI, M. & DASHTIAN, K., 2016. Novel nanorose-like Ce(III)-doped and undoped Cu(II)-biphenyl-4,4-dicarboxylic acid (Cu(II)-BPDCA) MOSs as visible light photocatalysts: synthesis, characterization, photodegradation of toxic dyes and optimization. *Physical Chemistry Chemical Physics.*

MUNZE, R., HANNEMANN, C., ORLINSKIY, P., GUNOLD, R., PASCHKE, A., FOIT, K., BECKER, J., KASKE, O., PAULSSON, E., PETERSON, M., JERNSTEDT, H., KREUGER, J., SCHUURMANN, G. & LIESS, M., 2017. Pesticides from wastewater treatment plant effluents affect invertebrate communities. *Science of the Total Environment*, 599-600, 387-399.

MYERS, S. S., GOLDEN, D. RICKETTS, T., TURNER, OSTFELD, W. R., REDFORD, R., K. H. GAFFIKIN, L & OSOFSKY, S. A. 2013. Human health impacts of ecosystem alteration.- Proceedings of the National Academy of Sciences, U.S.A. 110, 18753-18760.

NAGPAL, M.& KAKKAR, R., 2018. Use of metal oxides for the adsorptive removal of toxic organic pollutants. *Separation and Purification Technology*, 211, 522-539.

PELCLOVA, D., SKLENSKY, M., JANICEK, P. & LACH, K., 2012. Severe cobalt intoxication following hip replacement revision: clinical features and outcome. *Clinical Toxicology* (Phila). 50, 262-265.

POTERA, C., 2004. Silent advances. *Environmental Health Perspective* 112.

PUZAS, J.E., CAMPBELL, J., O'KEEFE, R.J. & ROSIER, R.N., 2004. Lead Toxicity in the Skeleton and Its Role in Osteoporosis. *Nutrition and Bone Health. Nutrition and Health.* 363-376.

RAO R.A.K & KHATOON, A., 2016. Adsorption characteristics of chemically modified Caryota urens seeds for the removal of Cu(II) from aqueous solution: Isotherms and kinetic studies. *Groundwater for Sustainable Development,* 2-3, 42-52.

SARAVANAN, R., GUPTA, V.K., NARAYANAN, V. & STEPHEN, A., 2014. Visible light degradation of textile effluent using novel catalyst ZnO/g-Mn_2O_3. *J.ournal of the Taiwan Institute of Chemical Engineers* 45, 1910-1917.

SAVIC, I.M., SAVIC, I.M. & STOJILJKOVIC, S.T., Gajic, D.G., 2014. Modeling and optimization of energy-efficient procedures for removing lead (II) and zinc (II) ions from aqueous solutions using the central composite design. *Energy*, 77, 66-72.

SHOOTO, N.D., DIKIO, C.W., WANKASI, D., SIKHWIVHILU, L.M., MTUNZI, F.M & DIKIO, E.D., 2016. Novel PVA/MOF Nanofibres: Fabrication, evaluation and adsorption of Lead ions from aqueous solution. *Nanoscale Research Letters*.

SHOOTO, N.D., NAIDOO, E.B. & MAUBANE, M., 2019. Sorption studies of toxic cations on ginger root adsorbent. *Journal of Industrial and Engineering Chemistry* 76, 133-140.

SIDDIQUI, S.I., RATHI, G. & CHAUDHRY, S.A., 2018. Acid washed black cumin seed powder preparation for adsorption of methylene blue dye from aqueous solution: Thermodynamic, kinetic and isotherm studies. *Journal of Molecular Liquids*, 264, 275-284.

SOLEIMAN, M., RAHIMI, M.R., GHAEDI, M., DASHTIAN, K. & HAJATI, S., 2016. $BiPO_4$/Bi_2S_3-HKUST-1-MOF as novel blue light-driven photocatalyst for simultaneous degradation of toluidine blue and auramine-O dyes in new rotating packed bed reactor: optimization and comparison to conventional reactor. *RSC Advances.*

SUDHA, R., SRINIVASAN, K. & PREMKUMAR, P., 2015. Removal of nickel(II) from aqueous solution using citrus limettioides peel and seed carbon. *Ecotoxicology and Environmental Safety,* 117, 115-123.

THIRUGNANASAMBANDHAM, K. & SIVAKUMAR, V., 2015. An ecofriendly approach for copper(II) ion adsorption onto cotton seed cake and its characterization: Simulation and validation. *Journal of the Taiwan Institute of Chemical Engineers*. 50, 198-204.

TRAN, B.L., CHIN, H.Y., CHANG, B.K. & CHIANG, A.S.T., 2019. Dye adsorption in ZIF-8: The importance of external surface area. *Microporous and Mesoporous* Materials. 277, 149-153.

VELI, S.& ALYUZ, B., 2007. Adsorption of copper and zinc from aqueous solutions by using natural clay. *Journal of Hazardous Materials,* 149, 226233.

WANI, A.L., ARA, A. USMANI, J.A., 2015. Lead toxicity. Interdiscip Toxicol. 8, 55-64.

WEBER JR, W.J., MCGINLEY, P.M.& KATZ, L.E., 1992. A distributed reactivity model for sorption by soils and sediments. 1. Conceptual basis and equilibrium assessments. *Environmental Science and Technology*, 26, 1955-1962.

WU, Y., PANG, H., LIU, Y., WANG, X., YU, S., FU, D., CHEN, J. & WANG, X., 2019. Environmental remediation of heavy metal ions by novel-nanomaterials. *Eenvironmental Pollution*, 246, 608-620.

YU, S., WANG, X., YAO, W., WANG, J., JI, Y., AI, Y., ALSAEDI, A., HAYAT, T. & WANG, X., 2017. Macroscopic, Spectroscopic, and Theoretical Investigation for the Interaction of Phenol and Naphthol on Reduced Graphene Oxide. *Environmental Science Technology*, 51, 3278-3286.

ZHANG, S., LI, J., WANG, X., HUANG, Y., ZENG, M. & XU. J., 2014. *In Situ* Ion exchange synthesis of strongly coupled Ag@AgCl/g-C_3N_4 porous nanosheets as plasmonic photocatalyst for highly efficient visible-light photocatalysis. *ACS Applied Materials Interfaces*, 6, 22116-22125.

CHAPTER 5

Adsorption studies of toxic cadmium(II) and chromium(VI) ions from aqueous solution by activated black black cumin (*Nigella Sativa*) seeds

This chapter is published as follows:

Patience Mapule Thabede, Ntaote David Shooto, Thokozani Xaba, Eliazer Bobby Naidoo. 2020. Adsorption studies of toxic cadmium(II) and chromium(VI) ions from aqueous solution by activated black cumin (*Nigella Sativa*) seeds. Journal of Environmental Chemical Engineering 8, 104045.

This chapter is addressing objective (c) which read as follows:

To activate black cumin seeds by potassium permanganate ($KMnO_4$) and phosphoric acid (H_3PO_4) for the removal of chromium Cr(VI) and cadmium Cd(II) ions from aqueous solution by varying time, pH, temperature and concentration.

5.1 Abstract

This work studied the adsorptive capability of activated black seeds to remove cadmium (Cd(II)) and chromium (Cr(VI)) ions from aqueous solution. The use of activated black seeds by potassium permanganate ($KMnO_4$) and phosphoric acid (H_3PO_4) to remove Cd(II) and Cr(VI) ions from aqueous solution is largely unexplored therefore, it is fair to conduct a study on the effect of activating agents on black seeds. Pristine black seeds were designated (PBS), the H_3PO_4 and $KMnO_4$ activated seeds (H_3BS) and (KMBS) respectively. The seeds were characterized by SEM, BET, XRD and FTIR and. SEM micrographs revealed that H_3BS and KMBS were more porous than PBS. The BET surface area of H_3BS and KMBS increased to 10.1 and 9.3 m^2/g respectively. FTIR spectra confirmed the presence of -OH, -COOH, -C=O and $-NH_2$ functional groups attached to the surface of all adsorbents. Adsorption batch studies were conducted to investigate the effect of contact time, initial concentration, temperature and pH of the solution. It was found that the adsorption capacities of all adsorbents increased with increasing Cd(II) and Cr(VI) initial concentration in the solution. The isotherm data revealed that Cd(II) ions uptake onto all adsorbents found good fit for Langmiur. This implies that the uptake processes occurred on active sites having equal affinity and further suggest monolayer adsorption. Whilst the isotherm data for Cr(VI) ions uptake onto PBS and KMBS found good fit for Freundlich. This is indicative that the uptake processes involved multi-layer adsorption formation. It was observed that all adsorbents had higher uptake for Cd(II) than Cr(VI) ions. It was found that the maximum adsorption capacity for Cr(VI) ions was 17.70 mg/g obtained at pH 1 at temperature 353 K whilst for Cd(II) ions it was 19.79 mg/g onto KMBS at pH 9 and temperature 298 K. The sorption rate of Cr(VI) ions onto PBS increased sharply from 5 until 60 min thereafter it stabilized and attained equilibrium from 60. The same sorption rates were observed for KMBS and H_3BS rapid from 5 min however the processes were much faster

stabilized in 30 min. The sorption rates of Cd(II) ions were rapid from 5 min and remained significant until 60, 30 and 20 min mark for PBS, KMBS and H_3BS adsorbents respectively. Afterwards, little to no sorption was recorded for either adsorbent. Increasing the temperature of the solution had a negative effect on the uptake of Cd(II) ions onto KMBS and H_3BS, this was indicative of the exothermic nature of the processes. However, temperature increase had a positive effect of the uptake of Cr(VI) ions onto all adsorbents, this was indicative of the endothermic nature of the processes. It was observed that the uptake removal of Cd(II) and Cr(VI) ions found a good fit for PSO kinetic model.

Keywords: modified black seeds, hexavalent chromium, divalent cadmium, adsorption

5.2 Introduction

Pollution of water by metal ions of Cd(II) and Cr(VI) has become a serious challenge worldwide. These water contaminants mainly originate from accelerated industrialization. The challenge with metal ions of Cd(II) and Cr(VI) in particular within water bodies is from the fact that they are toxic, non-biodegradable and persistent. Cd(II) and Cr(VI) ions enter water through careless disposal of compounds containing cadmium and chromium by mines, paint, electroplating, plastic and cadmium-nickel battery manufacturing factories (Rao et al. 2010; Bhatnaga & Minocha, 2009).

Cd(II) and Cr(VI) ions are harmful to the living organisms and the environment (Singh et al. 2011). They are highly toxic even at low concentration and detrimental to human health and well-being (Zeng et al. 2019). Exposure to cadmium (Cd(II)) ions through drinking contaminated water causes irreparable multiple organ damage, such as skeletal, kidneys, reproductive, cardiovascular, central and peripheral nervous, lungs and it is highly carcinogenic

(Yang et al. 2018; Rafati et al. 2017; Kellen et al. 2007). Drinking chromium Cr(VI) ion contaminated water is likewise toxic, it is reported to cause physical health problems that are irreversible such as cancer (Neolaka et al. 2018), damage to the kidneys (Qi et al. 2017) and nervous system (Taghizadeh & Hassanpour, 2017).

Several conventional treatment technologies have been developed for the remediation of toxic contaminants such as precipitation, membrane, ion exchange, reverse osmosis, adsorption, coagulation and flocculation (Amuda et al. 2006, Bai & Bartkiewicz, 2009; Rao et al. 2010, Barbooti et al. 2011; Lin et al. 2014; Daci-Ajvazi et al. 2016). However, adsorption method is the most preferred because it has significant advantages over other methods. It is effective, inexpensive, easy to conduct, not selective, and does not generate harmful by-products (Yarkandi, 2014). In the last decade agricultural (biomass) materials have gained much attention as potential candidates in water treatment (Bharathi & Ramesh, 2013). Agricultural materials are abundant in nature, inexpensive, accessible, and can be regenerated. Some of the extensively researched biomass include papaya seeds (Shooto & Nadioo, 2019; Yadav et al. 2014), ginger root (Shooto et al. 2019a), mucuna beans (Shooto et al. 2020a; Shooto et al. 2020b), coffee beans (Kaikake et al. 2007) pine cone (Dawood et al. 2017), moringa (Kebede et al., 2018), coconut shell (Zhao et al. 2018), orange peels (Safari et al. 2019), sugarcane bagasse (Xiong et al. 2019), etc.

Treatment of agricultural materials by strong to mild oxidizing substances such as phosphoric acid (H_3PO_4), potassium permanganate (KMnO4), hydrochloric acid (HCl), nitric acid (HNO_3) and sulfuric acid (H_2SO_4) (Lesaoana et al. 2019; Yao et al., 2016) reported to increase the oxygen containing functional groups like carboxyl (COOH) and carbonyl (C=O) (Gupta &

Saleh, 2013) on the materials surface therefore that improving the adsorption capacity of the material.

Black seeds have shown great potential in water application. However, only several research groups worldwide have exploited the feasibility of black seeds in waste water treatment. Consequently, only very few documents were found that reported on black seeds in water treatment. Shooto et al. (2019b) conducted a study on HCl and NaOH activated black seeds for the removal of Pb(II), Cu(II), Ni(II) and Zn(II) ions quaternary adsorption. Siddiqui and Chaudhry (2019) modified black seeds surface with Fe_2O_3-ZrO_2 nano composite for the removal of arsenic ions and methylene blue. Siddiqui et al. (2019) reported on black seeds functionalized with the nano hybrid composite Fe_2O_3-SnO_2 for the adsorption of methylene blue. Siddiqui et al. (2018a) employed black seeds-MnO_4 composite for the removal of methylene blue. Siddiqui et al. (2018b) used HCl washed black seeds for the adsorption of methylene blue. Addala et al. (2018) reported on defatted black seeds by hexane for the removal of lead ions. Ahmad & Haseeb (2014) used pristine black seeds to remove copper ions. Black seeds are largely unexploited. Therefore, it is be fair to conduct further studies.

Black seeds are inexpensive, abundant, accessible and nontoxic agricultural material used as home medicine for anti-inflammatory and anti-oxidant. The seeds also support the immune system, stomach and intestinal health, kidney and liver functions, prevent diabetes, cancer, and neutralize toxins, increases concentration and memory (Ahmad & Haseeb 2014). In this work black seeds were activated by $KMnO_4$ and H_3PO_4 for the removal of Cd(II) and Cr(VI) ions from aqueous solution. To the best of our knowledge activation of black seeds by $KMnO_4$ and H_3PO_4 is the first time being reported. Likewise the sorption of Cd(II) and Cr(VI) ions from aqueous solution by black seeds is not documented until now. The influence of varying system

parameters such as; initial concentration, contact time, temperature and pH of the solution were also investigated.

5.3 Experiments

5.3.1. Materials and methods

Black seeds (BCS) were obtained from a pharmacy in Vaal, South Africa. Potassium permanganate salt ($KMnO_4$)-99%, phosphoric acid (H_3PO_4)-75%, cadmium acetate salt $Cd(CH_3COO)_2$-99.95%, potassium dichromate salt ($K_2Cr_2O_7$)-99.5% all reagents were ACS grade and purchased from Merck South Africa LTD.

5.4 Preparation of adsorbents

5.4.1 Pristine black seeds (PBS)

The black seeds were stirred in distilled water several times to get rid of dirt then dried in an oven and ground by a blender with steel blades. Thereafter grounded pristine black seeds were labelled (PBS).

5.4.2 Potassium permanganate ($KMnO_4$) activated black seeds

PBS, 50 g was stirred in a solution of $KMnO_4$ 500 ml at 0.5 M for 5 hours. Thereafter the material was isolated and soaked in distilled water several times to get rid of excess $KMnO_4$. The material was transferred in a beaker and dried in oven at 313 K, thereon the material was labelled $KMnO_4$ activated black seeds (KMBS).

5.4.3 Phosphoric acid (H_3PO_4) activated black seeds

PBS, 50 g was stirred in H_3PO_4 solution of 500 ml, 0.5 M for 5 hours. Thereafter the treated material was isolated and washed in distilled water several times to get rid of excess H_3PO_4. The material was transferred in a beaker and dried in oven at 313 K, thereon the material was labelled H_3PO_4 activated black seeds (H_3BS).

5.5 Adsorption procedure

Stock solutions of 500 mg/L of Cr(VI) and Cd(II) ions were prepared using potassium dichromate and cadmium acetate salts respectively. Thereafter working solutions of Cr(VI) and Cd(II) were prepared by serial dilution of the stock solutions. Subsequently, preliminary studies on PBS to remove Cr(VI) and Cd(II) ions from aqueous solution were conducted while varying systematic parameters such as concentration, contact time, temperature and pH. Concentration effect was studied on working solutions 20, 40, 60, 80 and 100 mg/L equilibrium time used 120 min. Contact time effect was examined at 5, 10, 15, 20, 30, 40, 60, 90 and 120 min on working solution 100 mg/L. Temperature effect was evaluated at 298, 303, 313, 333 and 353 K on working solution 100 mg/L and equilibrium time 120 min. pH effect was studied at pH 1, 3, 5, 7 and 9 on working solution 100 mg/L and equilibrium time 120 min. Each adsorption experiment was carried out by addition of 20 mg of PBS into 20 ml of the specified working standard in capped bottles. The solutions containing PBS were agitated on an orbital shaker at 300 rpm until equilibrium time was reached. Thereafter the solutions were centrifuged at 4500 rpm for 5 min. The remaining amount of Cd(II) and Cr(VI) in the solution were determined using AAS. The adsorption studies on KMBS and H_3BS adsorbents were also determined.

5.6 Adsorption data management

Equations 1 and 2 were employed to evaluate the removal capacity, q_e (in mg/g) and removal percentage, *%R* (in %) of Cd(II) and Cr(VI) ions at equilibrium.

$$q_e = \frac{(C_o - C_e)\,V}{W} \quad (1)$$

$$\%R = \frac{(C_o - C_e)}{C_o} \text{ x } 100 \quad (2)$$

where the removal capacity and percentage were designated *(q_e)* and *(%R)*, initial and final concentrations designated *(C_o)* and *(C_e)* in mg/L. Volume of the solution and mass of the adsorbent designated *(v)* and *(W)* respectively.

The adsorption mechanisms were evaluated using kinetic models namely; pseudo-first order (PFO) nonlinear equation (3), pseudo-second order (PSO) nonlinear equation (4) and intra-particle diffusion (IPD) nonlinear equation (5). The obtained adsorption contact time data was integrated into three kinetics models.

$$q_e = q_t(1 - e^{-k_1 t}) \quad (3)$$

$$q_e = \frac{1 + k_2 q_e t}{k_2 q_e^2 t} \quad (4)$$

$$q_t = k_i\left(t^{1/2}\right) + C \quad (5)$$

where *(q_e)* and *(q_t)* are the amounts removed (in mg/g) at time *(t)*. *(k_1)*, *(k_2)* and *(k_i)* are the rate constants of PFO (in min^{-1}), PSO (in g mg^{-1} min^{-1}) and IPD (in g g^{-1} $min^{1/2}$) respectively. (*C)*

is the concentration of Cr(VI) and Cd(II) on the surface of PBS, KMBS and H_3BS at equilibrium.

The equilibrium data was integrated into two isotherm models namely; Langmuir and Freundlich using nonlinear equations (6) and (7) respectively.

$$q_e = \frac{Q_o b C_e}{1 + bC_e} \quad (6)$$

$$q_e = k_f C_e^{1/n} \quad (7)$$

Where the parameters; (Q_o) represent Langmuir maximum adsorption capacity (in mg/g), (*b*) represent the interaction energy related constant, (k_f) represent Freundlich capacity factor constant and (*1/n*) is the isotherm linearity parameter constant.

Thermodynamic functions such as standard enthalpy change (ΔH^o), standard entropy change (ΔS^o), standard free energy change (ΔG^o) and the equilibrium constant (K_c) were obtained at 298, 303, 313, 333 and 353 K using equations (8), (9) and (10).

$$In\ K_c = -\frac{\Delta H^o}{RT} - \frac{\Delta S^o}{R} \quad (8)$$

$$\Delta G^o = -RT\ In\ K_c \quad (9)$$

$$K_c = \frac{q_e}{C_e} \quad (10)$$

5.7 Characterization

The PBS, KMBS and H_3BS surface characterization, thermal disintegration, functional sites attached, specific surface area and purity were affirmed using SEM, FTIR, BET and XRD respectively. SEM images were taken on a Nova Nano SEM 200 from FEI operated at 10.0 kV. Perkin Elmer FTIR/FTNIR spectrometer, spectrum 400 was used for the confirmation of the functional groups attached to the surface of the adsorbents. Shimadzu XRD 7000 was used to determine the purity of the adsorbents, scan range was set from 10 to 80 (2θ °), scan speed was set at 10 °/min. Micromeritics ASAP 2020 (Micromeritics Instrument Corporation, USA) was used to determine the BET surface area of the adsorbents under nitrogen adsorption/desorption. The pH of the samples was determined in deionized water, and pH at point of zero charge $pH_{(PZC)}$ was evaluated using the pH drift method. Inductive couple plasma spectroscopy (ICP), thermo scientific iCAP 7000 series, ICP spectrometer, using ASX-520 auto sampler, was used to measure the metal ion solutions before and after adsorption.

5.8. Results and discussion

5.8.1 Adsorbents characterization

5.8.1.1 SEM

The examination of PBS, H_3BS and KMBS by SEM offered vital surface morphological information. Figs. 26a-b show PBS images, it was observed that the pristine adsorbent exhibited cavities on the surface and irregular morphology. Whilst both activated adsorbents H_3BS and KMBS images in Figs. 26c-d and Figs. 26e-f respectively show improved surfaces in terms of more cavities and porosity. These attributes are therefore anticipated to enhance the adsorption processes of Cd(VI) and Cd(II) onto both activated adsorbents.

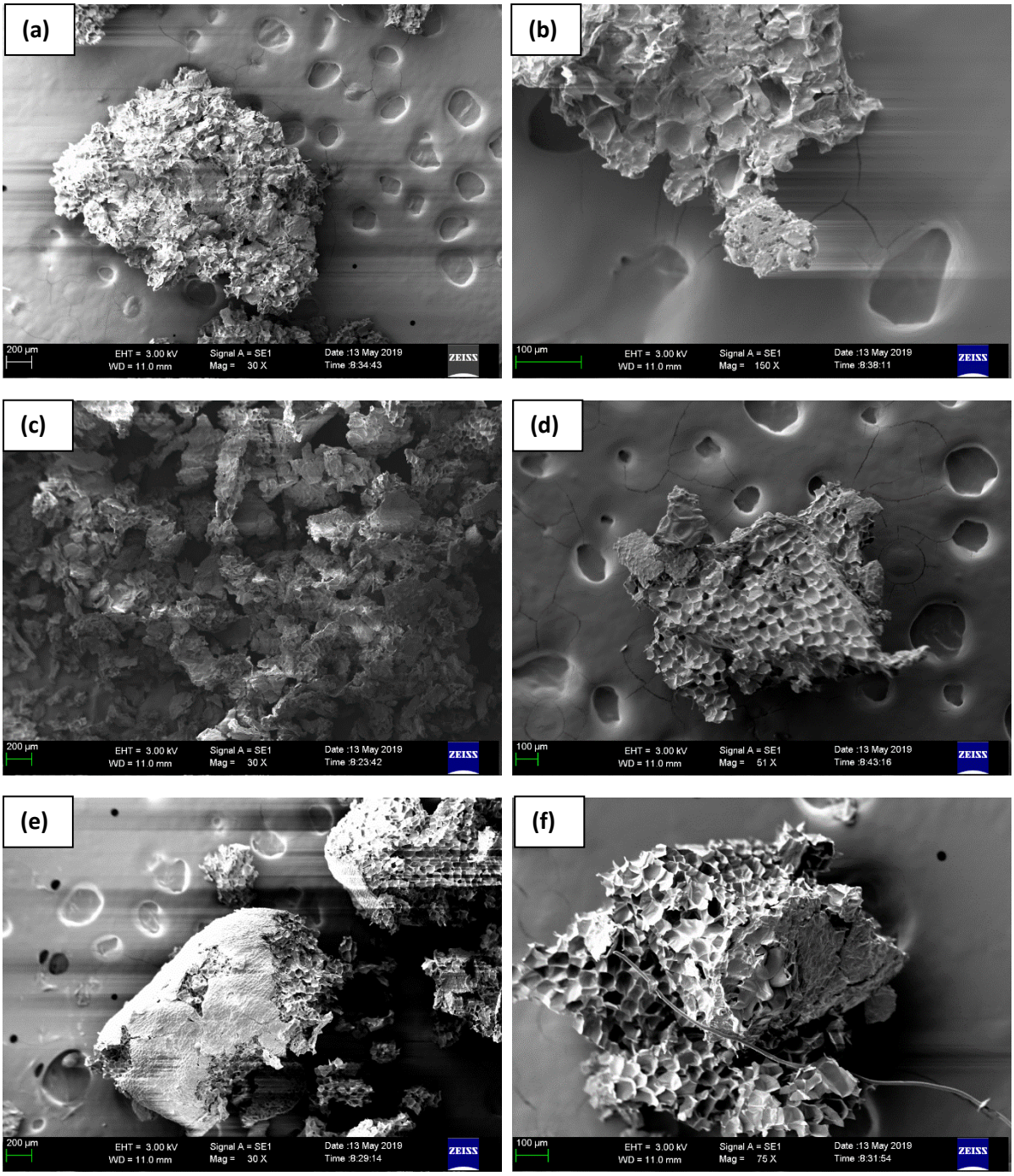

Figure 26: SEM micrographs; (a-b) PBS, (c-d) H_3BS and (e-f) KMBS

5.8.1.2 FTIR analysis

IR characterization of PBS, H_3BS and KMBS adsorbents are shown in Fig. 27. The peaks at wavenumber 3280 were attributed to hydroxyl (-OH) stretch of lignocellulose materials present in the biomass (Shooto et al., 2020). The hydroxyl (-OH) stretch peak was observed in all adsorbents however it almost vanished in KMBS spectrum. Two sharp peaks were observed in all adsorbents assigned to (-CH) stretch in methylidene ($=CH_2$) and methyl ($-CH_3$) groups at wavenumbers 2923 and 2853 respectively (Siddiqui et al. 2018b). The (-CH) stretch peaks intensified in KMBS and H_3BS compared to PBS. The ketonic group was assigned to the peak at wavenumber 1740 observed in all adsorbents (Addala et al. 2018). The peak at wavenumber 1413 on PBS disappeared on KMBS and H_3BS. The peaks at 1370 were observed only on the spectra of KMBS and H_3BS. All adsorbents had (-C=O) and ($-NH_2$) of amide group peaks at wavenumbers 1637 and 1541 respectively. The carboxyl (-COOH) group peaks were observed at wavenumber 1413 in all adsorbents. New peaks observed in phosphoric acid activated materials (H_3BS) at wavenumbers 1703, 887, 802 and 691 were attributed to the implanted phosphorus groups onto black seeds surface (Liou, 2010). Similarly, potassium permanganate activated materials (KMBS) recorded several new peaks at 1703, 802 and 691. All marked changes confirm successful functionalization of the black seeds by phosphoric acid and potassium permanganate.

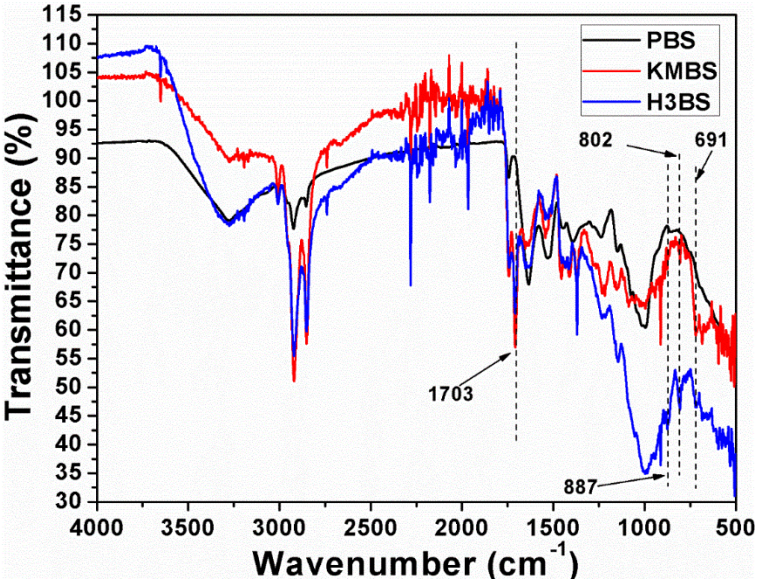

Figure 27: FTIR spectra of PBS, KMBS and H_3BS

5.8.1.3 XRD diffraction

The XRD spectra of PBS, KMBS and H_3BS are shown in Fig. 28. No changes were recorded on the spectra of the pristine black seeds (PBS) and the activated black seeds (KMBS and H_3BS) adsorbents. The characteristic broad peak observed in all adsorbents around (2θ) 17 and 21° indexed (002) was attributed to crystalline lignocellulose material (Siddiqui & Chaudhry, 2018; Shooto et al. 2020). Peaks at (2θ) 37.5, 44, 64 and 77.5° indexed (040) were assigned to the amorphous nature of the adsorbents.

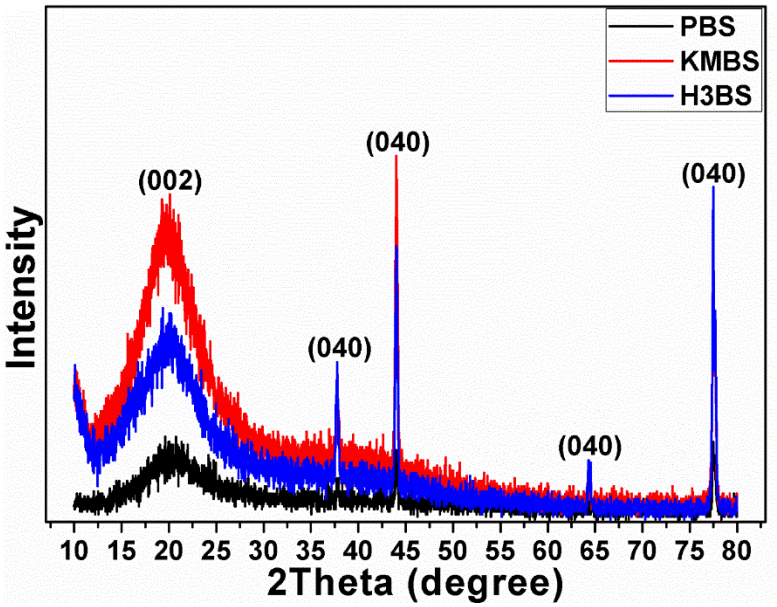

Figure 28: XRD diffraction of PBS, KMBS and H_3BS

5.8.2 Physicochemical characterization

5.8.2.1 Point zero charge and nitrogen adsorption/desorption studies

Table 5 shows $pH_{(PZC)}$, BET surface area, pore size and pore width data of adsorbents. The $pH_{(PZC)}$ values of PBS, KMBS and H_3BS were 5.7, 6.3 and 3.1 respectively. The BET surface area of PBS was 2.7 m^2/g and significantly increased for KMBS and H_3BS to 10.1 and 9.3 m^2/g respectively. Furthermore, PBS pore width was 6.02 nm and became fairly large in KMBS and H_3BS 14.7 and 16.3 nm respectively.

Table 5: Physicochemical parameters of the adsorbents.

Adsorbent	$pH_{(PZC)}$	BET surface area (m^2/g)	Pore size (cm^2/g)	Pore width (nm)
PBS	5.70	2.70	0.0387	6.02
KMBS	6.30	10.3	0.0469	14.7
H_3BS	3.10	9.30	0.0478	16.3

5.8.3 Adsorption studies

5.8.3.1 pH effect studies

pH effect on the adsorption of Cd(II) and Cr(VI) ions onto PBS, KMBS and H_3BS was studied at pH 1, 3, 5, 7 and 9 is shown in Figs. 29a-c. From the plots it was observed that the adsorption of Cr(VI) ions was pH dependant. Therefore, Cr(VI) ions adsorption capacities decreased as pH of the solution increased from 1 to 9 onto all adsorbents with the highest sorption's recorded at pH 1. The adsorbents performance trend at pH 1 was KMBS>H_3BS>PBS with adsorption capacities 16.12, 15.98 and 10.15 mg/g. High performance by KMBS and H_3BS adsorbents could be explained by the fact that black seeds activation with strong oxidising agent such as $KMnO_4$ increases the oxygen rich functional groups such as -OH and -COOH on the surface of the treated material (Fang et al. 2017). Mineral acid such as H_3PO_4 implants phosphorus related groups such as PO_4^{3-} (Liou, 2010). These function groups at low acidic medium (pH = 1) were protonated and acquired a positive charge like $-COOH^+$, $-OH^{2+}$ and $-C=OH^+$ this then enhanced the electrostatic attraction between Cr(VI) ions predominantly existing as negative species $HCr_2O_7^-$ (Huang et al. 2018) and led to higher adsorption capacity than in KMBS and H_3BS than PBS. Similarly it was observed that the adsorption of Cd(II) ions was pH dependant. Thus, Cd(II) ions adsorption capacities increased as pH of the solution increased onto all adsorbents with the highest sorption's recorded at pH 9. The adsorbents performance trend at

pH 9 was KMBS>H_3BS>PBS with adsorption capacities 19.15, 19.09 and 16.80 mg/g. This could be due to the fact that at high pH value (9) functional sites were deprotonated and acquired a negative charge like $-OH^-$ and $-COOH^-$ thus enhanced the electrostatic attraction between adsorbents surface and Cd(II) ions.

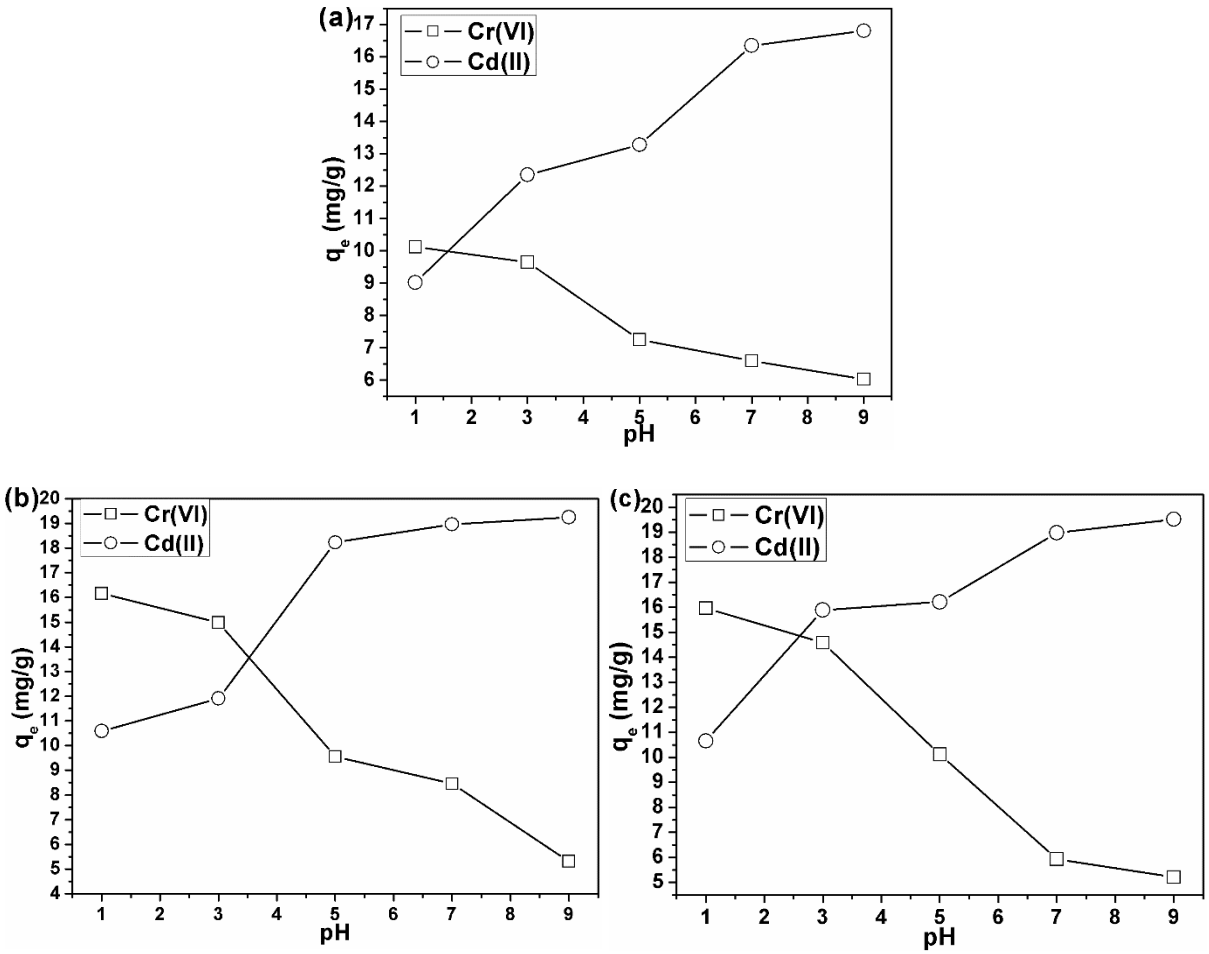

Figure 29: pH effect plots of (a) PBS, (b) KMBS and (c) H_3BS for the adsorption of Cr(VI) and Cd(II). [Conditions: adsorbent dosage (20 mg), volume of solution (20 ml), concentration of solution (100 m/L), temperature of the system (298 K), agitation speed (300 rpm) and agitation time (120 min)]

5.8.3.2 Contact time effect and kinetics

The rate and efficiency at which Cr(VI) and Cd(II) ions are removed from aqueous solution by PBS, KMBS and H_3BS were evaluated over a contact time range of 5-120 min the trends are shown in Fig. 30a-b. The sorption rate of Cr(VI) onto PBS increased sharply from 5 until 60 min thereafter it stabilized and no significant sorption was recorded. Therefore, the process attained equilibrium from 60 until 120 min. The same sorption rates were observed for KMBS and H_3BS rapid from 5 min however the processes were stable within 30 min. Thereafter little to no significant sorption was recorded (i.e.) the processes attained equilibrium from 30 until 120 min. Rapid sorption rate at the initial stage was due to abundant unoccupied active sites and pores available at the beginning of the process. However, as contact time increased the active sites were exhausted and pores filled up to a point were little or no adsorption was recorded (Shooto et al. 2019b). The sorption rates of Cd(II) ions were rapid from 5 min and remained significant until 60, 30 and 20 min mark for PBS, KMBS and H_3BS adsorbents respectively. Afterwards, little to no sorption was recorded for either adsorbent.

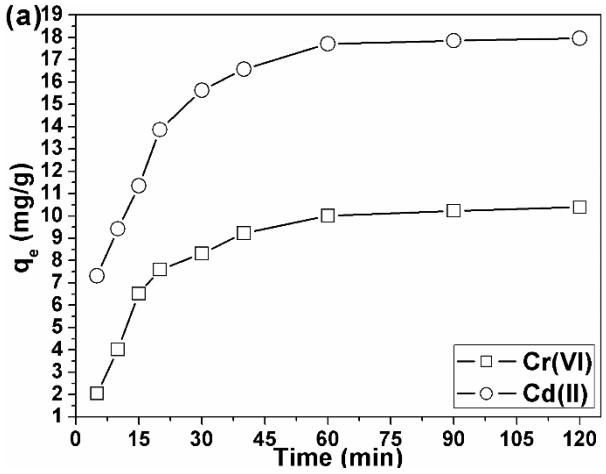

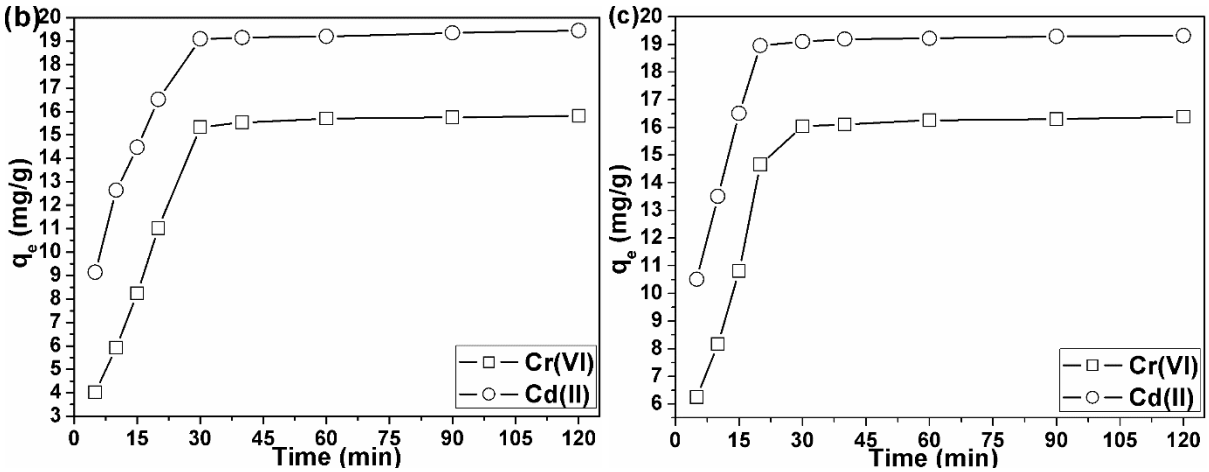

Figure 30: Contact time effect plots (a) PBS, (b) KMBS and (c) H_3BCS for the adsorption of Cr(VI) and Cd(II). [Conditions: adsorbent dosage (20 mg), volume of solution (20 ml), concentration of solution (100 m/L), temperature of the system (298 K), agitation speed (300 rpm), pH of Cr(VI) solution was (1) and Cd(II) solution was (9)]

Sorption rate data obtained for Cr(VI) and Cd(II) ions onto PBC, KMBS and H_3BCS were subjected to nonlinear kinetic models (PFO, PSO and IPD) in order to determine the mechanisms involved in the sorption processes. Table 6 shows the kinetic data parameters of PFO and PSO. To estimate the sorption process whether it could be best described by either PFO or PSO model, it was based (r^2) value closer to unity (1) and the projected (q_e) values. PFO and PSO (r^2) values were compared, and it was observed that all sorption processes gave better PSO (r^2) values which were closer to unity. Therefore, neither process could be described by the PFO model. The obtained PSO (r^2) values for Cr(VI) and Cd(II) onto PBS were 0.9990 and 0.9953, onto KMBS 0.9974 and 0.9987, onto H_3BC 0.9912 and 0.9973 respectively. The good fit for PSO model indicates that the sorption of Cr(VI) and Cd(II) ions was based on electrostatic interactions. The nature of Cr(VI) and Cd(II) ions removal uptake was evaluated by IPD kinetic model, whether the sorption processes occurred through surface (ESA) or pores (EPA). Cr(VI) and Cd(II) ions sorption onto PBS was dominated by (ESA) with estimated

percentages of 76.64 and 72.83 % respectively. Whilst Cr(VI) and Cd(II) ions sorption onto KMBS and H_3BS were more or less equal for (ESA) and (EPA).

Table 6: Kinetics and their parameters

Models		PBS		KMBS		H_3BC	
		Cr(VI)	**Cd(II)**	**Cr(VI)**	**Cd(II)**	**Cr(VI)**	**Cd(II)**
PFO	q_e	53.31	11.28	10.79	43.07	17.53	15.10
	K_1	3.91	3.63	3.78	4.07	3.71	3.51
	r^2	0.9428	0.9857	0.9526	0.9556	0.9167	0.9591
PSO	q_e	45.85	14.63	15.59	17.20	16.18	17.04
	K_2	0.0199	0.0886	1.016	0.0294	0.0683	0.5875
	r^2	0.9990	0.9953	0.9974	0.9987	0.9912	0.9973
IPD	**C**	7.48	13.32	6.29	8.49	8.08	9.24
	K_i	1.20	1.41	0.9874	0.547	2.27	0.5401
	r^2	0.9820	0.9925	0.9814	0.9989	0.9853	0.9835
EPA*	**%**	23.36	23.17	50.67	55.99	52.36	52.62
ESA*	**%**	76.64	72.83	49.33	44.01	47.64	47.38
Experimental (q_e)		10.16	17.92	15.59	19.40	16.23	19.21

5.8.3.3 Concentration effect and isotherms

The initial concentration of Cr(VI) and Cd(II) solutions is an important parameter that provides the required energy to overcome the hindering forces that prevent the mass transfer resistance of metal ions between liquid-solid interfaces. Therefore the effect of initial concentration of Cr(VI) and Cd(II) solutions was evaluated and the plots are shown in Figs. 31a-c. It was observed that the adsorption capacities of all adsorbents increased with increasing initial concentration of the solution (i.e.) at higher concentrations of the solutions of Cr(VI) and Cd(II)

the removal was significantly high than at lower concentration (Diagboya & Dikio, 2018). The sorption of Cr(VI) ions in solution with initial concentration 100 mg/L onto PBS, KMBS and H_3BS was higher at 9.98, 12.50 and 15.55 mg/g compared to solution with initial concentration 20 mg/L at 4.21, 8.51 and 9.35 mg/g respectively. Whilst the sorption of Cd(II) ions in solution with initial concentration 100 mg/L onto PBC, KMBS and H_3BCS was higher at 19.20, 19.65 and 19.60 mg/g compared to solution with initial concentration 20 mg/L at 8.32, 10.56 and 15.6 mg/g. This could be explained by the fact that high metal ions initial concentration in the solution means greater collision possibility between Cr(VI)/Cd(II) ions and adsorbent, which is associated with high mass transfer (Islam et al. 2015).

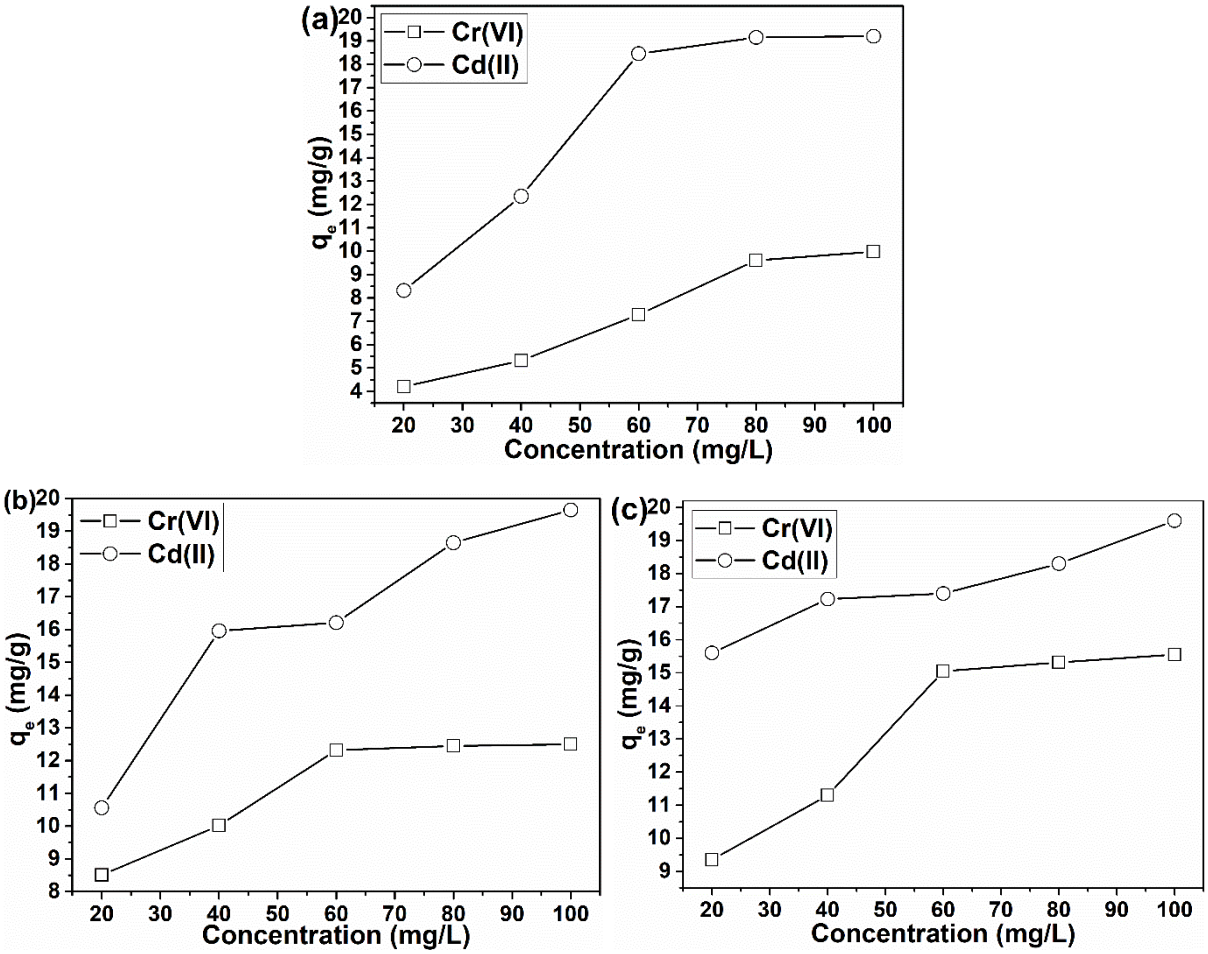

Figure 31: Initial concentration effect of (a) PBS, (b) KMBS and (c) H_3BCS for the adsorption of Cr(VI) and Cd(II). [Conditions: adsorbent dosage (20 mg), volume of solution (20 ml), temperature of the system (298 K), agitation speed (300 rpm), pH of Cr(VI) solution was (1) and Cd(II) solution was (9)]

In order to better understand the interaction behaviour between the Cr(VI) and Cd(II) ions and the adsorbents, concentration effect data were subjected to nonlinear isotherm models Langmuir and Freundlich. Isotherm models and their parameters are shown in Table 7. It is observed that the isotherm data of Cr(VI) ions onto PBS, KMBS and H_3BS had high (r^2) values of 0.9959, 0.9956 and 0.9987 for Langmuir model respectively. This is indicative that Cr(VI) ions adsorption could be better described by Langmuir than Freundlich isorthem. This implies that Cr(VI) ions uptake on adsorbents surface occurred on active sites having equal affinity and further suggest monolayer adsorption. The isotherm data of Cd(II) ions onto PBC and KMBS had high (r^2) values of 0.9980 and 0.9921 for Freundlich respectively. However, isotherm data of Cd(II) ions onto H_3BCS gave high (r^2) value for Langmuir. Cd(II) ions sorption with Freundlich model are indicative that the uptake process involved multi-layer adsorption formation.

Table 7: Isotherms studies and their parameters.

Isotherms		**PBS**		**KMBS**		**H_3BC**	
		Cr(VI)	**Cd(II)**	**Cr(VI)**	**Cd(II)**	**Cr(VI)**	**Cd(II)**
Langmuir	**Q_0**	15.81	18.16	16.06	23.87	17.25	19.48
	B	0.0204	3.29	0.0547	0.0434	0.1911	0.349
	r^2	0.9959	0.9717	0.9956	0.9980	0.9987	0.9858
Freundlich	**1/n**	1.096	3.50	3.74	4.299	10.06	13.98

	k_f	2.005	2.62	3.510	3.006	9.21	14.67
	r^2	0.9803	0.9980	0.9788	0.9793	0.9792	0.9921
Experimental (q_e)		9.98	19.20	12.50	19.65	15.55	19.60

5.8.3.4 Temperature effect and thermodynamics

The effect of temperature was studied at 298, 303, 313, 333 and 353 K on the sorption of Cr(VI) and Cd(II) ions onto all adsorbents the trends are shown in Figs. 32a-c. The data revealed that the sorption of Cr(VI) ions onto all adsorbents increased continuously in all temperature ranges from 298 to 353 K. This showed the endothermic nature of the sorption processes, the recorded adsorption capacities are 10.85 to 16.19 mg/g for PBS, 13.02 to 17.59 mg/g for KMBS and 16.47 to 17.70 mg/g for H_3BS. Similar trend was observed for Cd(II) ions sorption onto PBS, the removal uptake increased as temperature increased from 298 to 353 K revealing the endothermic nature of the process. However, the Cd(II) ions sorption onto KMBS and H_3BS were exothermic processes. Temperature increase was detrimental to the removal uptake from 298 throughout 353 K. Onto KMBS adsorption capacity decreased from 19.79 to 18.78 mg/g and H_3BS from 19.58 to 18.98 mg/g. This is indicative of desorption of Cd(II) ions on KMBS and H_3BS surfaces at temperatures above 298 K, because of the gained kinetic energy the ions moved rapid in the solution resulting in less interaction between Cd(II) ions and the active sites/pores on KMBS and H_3BS.

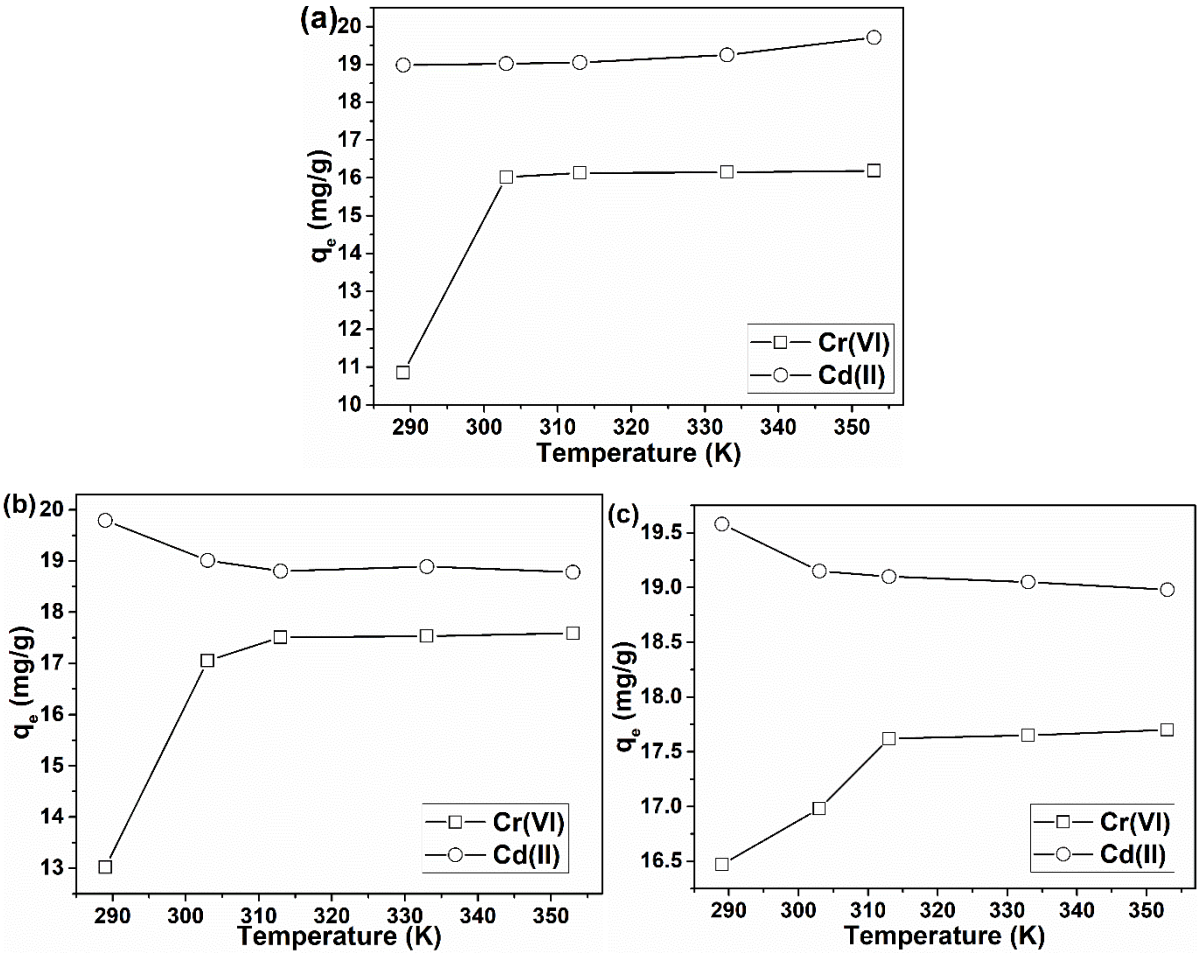

Figure 32: Temperature effect studies of (a) PBS, (b) KMBS and (c) H_3BS for the adsorption of Cr(VI) and Cd(II) [Conditions: adsorbent dosage (20 mg), volume of solution (20 ml), agitation speed (300 rpm), pH of Cr(VI) solution was (1) and Cd(II) solution was (9)]

Thermodynamic parameters (ΔH^o, ΔG^o and ΔS^o) for Cd(II) and Cr(VI) in Table 8 data were generated at temperatures 298, 303, 313, 333 and 353 K. The calculated (ΔG^o) values were negative for all the investigated temperatures, this indicated that Cd(II) and Cr(VI) ions uptake processes onto PBS, KMBS and H_3BS were spontaneous and feasible. The sorption processes of Cr(VI) and Cd(II) ions that gave positive (ΔH^o) values implying that reactions were endothermic, Typically an endothermic reaction, increases the adsorption uptake of metal ions as temperature of the system increases. Whilst the sorption of Cr(VI) and Cd(II) ions onto

KMBS and H_3BS gave negative (ΔH^o) values implying that the processes were exothermic in nature. All Cd(II) and Cr(VI) ions sorption processes had positive (ΔS^o) values which indicates the increased randomness of the metal ions in the solution as the uptake processes approached equilibrium.

Table 8: Thermodynamic studies and their parameters

Parameter	**PBS**		**KMBS**		**H_3BS**	
	Cr(VI)	**Cd(II)**	**Cr(VI)**	**Cd(II)**	**Cr(VI)**	**Cd(II)**
ΔH^o (KJ mol^{-1})	-1.68	-1.49	-1.57	-1.08	-0.937	-0.455
ΔS^o (KJ $mol^{-1}K^{-1}$)	4.93	3.12	-5.14	4.94	-3.17	3.10
ΔG^o (KJ mol^{-1}) 298 K	-3.59	-2.93	-3.16	-2.37	-3.40	-0.391
303 K	-0.314	-3.84	-3.37	-1.35	-4.31	-0.248
313 K	-0.229	-4.19	-4.02	-1.34	-4.45	-1.09
333 K	-0.199	-4.70	-4.83	-1.30	-4.83	-1.10
353 K	-0.141	-5.26	-5.39	-1.30	-5.39	-1.24

5.8.4 Comparative studies

Activated black seeds adsorbents KMBS and H_3BS adsorption capacities for Cd(II) and Cr(VI) ions were compared with other low cost biosorbents materials reported in literature as shown in Table 9. The comparison studies of both activated black seeds adsorbents showed higher performance than several reported low cost biosorbents for Cd(II) and Cr(VI) ions adsorption. Hence, KMBS and H_3BS are promising cost-effective biosorbents for Cd(II) and Cr(VI) ions from aqueous solution.

Table 9: Activated black seeds and other bioadsorbents comparative study of Cd(II) and Cr(VI) ions sorption

Adsorbents	**$q_{(max)}$ (mg/g)**	**References**
	Cd(II)	
$KMnO_4$ treated black seeds	19.79	This study
H_3PO_4 treated black seeds	19.58	This study
Pinus sylvesteris	19.10	Costodes et al., 2003
Phaseolus hulls	15.70	Rao et al., 2009
Cocoa pod husk	13.43	Njoku et al., 2012
Corn stalk	12.73	Zheng et al., 2010
Coconut shell	7.19	Vazquez et al., 2009
Wheat straw	3.83	Mahmood-ul-Hassan et al., 2015
Alhaji maurorum seed	3.74	Ebrahimi et al., 2015
Adsorbents	**$q_{(max)}$ (mg/g)**	**References**
	Cr(VI)	
H_3PO_4 treated black seeds	17.70	This study
$KMnO_4$ treated black seeds	17.59	This study
Almonds	10.61	Sharma et al., 2016
Garlic peel	9.22	Nag et al., 2017
Coconut shell	8.73	Nag et al., 2017
Orange peel	7.14	Khalifa et al., 2019
Litchi peel	7.05	Yunhong et al., 2017
Banana peel	3.35	Ali and Saeed, 2014
Potatoes peel	3.28	Mutongo et al., 2014

5.8.5 Conclusion

The purpose of this work was to develop activated bioadsorbents from abundant low cost black seeds for the sorption of Cd(II) and Cr(VI) ions from aqueous solution. The pristine black seeds

(PBS), $KMnO_4$ activated black seeds (KMBS) and H_3PO_4 activated black seeds (H_3BS) were characterized by SEM, FTIR, XRD and BET. Batch sorption studies were conducted by varying the following parameters; initial concentration of the solution, contact time, pH of the solution and temperature of the solution. It was found that the highest adsorption capacities for Cr(VI) and Cd(II) ions were recorded at pH 1 and 9 respectively. The adsorption capacity trend for Cr(VI) ions was KMBS>H_3BS>PBS (i.e.) 16.12, 15.98 and 10.15 mg/g and for Cd(II) ions it was KMBS>H_3BS>PBS (i.e.) 19.15, 19.09 and 16.80 mg/g respectively. This could be explained by the fact that functional groups on PBS, KMBC and H_3BS surface were either protonated/deprotonated depending on the pH therefore that enhanced the electrostatic attraction between Cr(VI)/Cd(II) ions and the functional groups on the adsorbents surface. Contact time effect revealed that the sorption rate of Cr(VI) ions onto PBS increased sharply from 5 until 60 min thereafter it stabilized and attained equilibrium from 60. The same sorption rates were observed for KMBS and H_3BS rapid from 5 min however the processes were much faster stabilized in 30 min. The sorption rates of Cd(II) ions were rapid from 5 min and remained significant until 60, 30 and 20 min mark for PBS, KMBS and H_3BS adsorbents respectively. It was observed that the adsorption capacities of all adsorbents increased with increasing initial concentration of the solution (i.e.) at higher concentrations solution of Cr(VI) and Cd(II) the removal was significantly high than at lower concentration. The data revealed that the sorption of Cr(VI) ions onto all adsorbents increased continuously in all temperature ranges from 298 to 353 K. This showed the endothermic nature of the sorption processes. Similar trend was observed for Cd(II) ions sorption onto PBS, the removal uptake increased as temperature increased from 298 to 353 K revealing the endothermic nature of the process. However, the Cd(II) ions sorption onto KMBS and H_3BS were exothermic processes. Temperature increase was detrimental to the removal uptake from 298 throughout 353 K. The obtained PSO (r^2) values for Cr(VI) and Cd(II) onto PBS were 0.9990 and 0.9953, onto KMBS

0.9974 and 0.9987, onto H_3BC 0.9912 and 0.9973 respectively. The good fit for PSO model indicates that the sorption of Cr(VI) and Cd(II) ions was based on electrostatic interactions. Cd(II) and Cr(VI) ions uptake processes onto PBS, KMBS and H_3BS were spontaneous and feasible. The sorption processes gave positive (ΔH^o) values implying that reactions were endothermic, Whilst the sorption of Cr(VI) and Cd(II) ions onto KMBS and H_3BS gave negative (ΔH^o) values implying that the processes were exothermic in nature.

5.8.6 Acknowledgment

We acknowledge the supports of National Research Fund-NRF (TTK190403426819) for funding this work, the Department of Chemistry, Vaal University of Technology, Vanderbiljpark, South Africa.

References

ADDALA, A., BELATTAR, N. & ELEKTOROWICZ, M., 2018. Nigella Sativa L. seeds biomass as a potential sorbent in sorption of lead from aqueous solutions and wastewater. *Oriental Journal of Chemistry,* 34, 638-647.

AHMAD, R. & HASEEB, S., 2014. Black Cumin Seeds (BCS): a non-conventional adsorbent for the removal of Cu (II) from aqueous solution. *Desalination and Water Treatment,* 1-10.

ALI, A. & SAEED, K., 2014. Decontamination of Cr (VI) and Mn (II) from aqueous media by untreated and chemically treated banana peel: a comparative study. *Desalination Water Treat*ment, 1-6.

AMUDA, O.S., AMOO, I.A. & IPINMOROTI, K.O., 2006. Coagulation/flocculation process in the removal of trace metals present in industrial wastewater. *Journal of Applied Science and Environmental Management*, 10, 159-162.

BAI, Y., BARTKIEWICZ, B., 2009. Removal of cadmium from wastewater using ion exchange resin amber jet 1200H columns. *Polish Journal of Environmental Studies*, 18, 1191-1195.

BARBOOTI, M.M., ABID, B.A. & AL-SHUWAIKI, N.M., 2011. Removal of heavy metals using chemical precipitation. *Journal of Engineering Technology*, 29, 595-612.

BHARATHI, K.S. & RAMESH, S.T., 2013. Removal of dyes using agricultural waste as low-cost adsorbents: a review. *Applied Water Science*, 3, 773-790.

BHATNAGA, A. & MINOCHA, A.K., 2009. Utilization of industrial waste for cadmium removal from water and immobilization in cement. *Chemical Engineering Journal*, 150, 145-151.

COSTODES, V.C.T., FAUDUET, H., PORTE, C. & DELACROIX, A., 2003. Removal of Cd(II) and Pb(II) ions from aqueous solutions by adsorption onto sawdust of Pinus sylvestris. *Journal of Hazardous Materials*, 105, 121-142.

DACI-AJAZI, M., THACI, M., DACI, N. & GASHI, S., 2016. Membrane and Adsorption Processes for Removing of Organics and Inorganics from Urban Wastewaters. *Oriental Journal of Chemistry*, l32, 2391-2400.

DAWOOD, S., SEN, T.K. & PHAN, C., 2017. Synthesis and characterization of slow pyrolysis pine cone bio-char in the removal of organic and inorganic pollutants from aqueous solution by adsorption: Kinetic, equilibrium, mechanism and thermodynamic. *Bioresource Technology*, 246, 76-81.

DIAGBOYA, P.N. & DIKIO, E.D., 2018. Scavenging of aqueous toxic organic and inorganic cations using novel facile magneto-carbon black-clay composite adsorbent. *Journal of cleaner production,* 180, 71-80.

EBRAHIMI, A., EHTESHAMI, M.& DAHRAZMA, B., 2015. Isotherm and kinetic studies for the biosorption of cadmium from aqueous solution by Alhaji maurorum seed. *Process Safety and Environmental Protection*, 98, 374-382.

FANG, R., HUANG, H., HUANG, W., JI, J., FENG, Q., SHU, Y., ZHAN, Y., LIU, G. & XIE, R., 2017. Influence of peracetic acid modification on the physicochemical properties of activated carbon and its performance in the ozone-catalytic oxidation of gaseous benzene. *Applications of Surface Science,* 420, 905-910.

GUPTA, V.K. & SALEH, T.A., 2013. Sorption of pollutants by porous carbon, carbon nanotubes and fullerene- an overview. *Environmental Science and Pollution Research*, 20 (5), 2828-2843.

ISLAM, M.A., BENHOURIA, A., ASIF, M. & HAMEED, B., 2015. Methylene blue adsorption on. factory-rejected tea activated carbon prepared by conjunction of hydrothermal.

carbonization and sodium hydroxide activation processes. *Journal of the Taiwan Institute of Chemical Engineers*, 52, 57-64.

KAIKAKE, K., HOAKI, K., SUNADA, H., DHAKAL, R.P. & BABA, Y., 2007. Removal characteristics of metal ions using degreased coffee beans: Adsorption equilibrium of cadmium(II). *Bioresource Technology*, 98, 2787-2791.

KEBEDE, T.G., MENGISTIE, A.A., DUBE, S., NKAMBULE, T.T.I. & NINDI, M.M., 2018. Study on adsorption of some common metal ions present in industrial effluents by Moringa stenopetala seed powder. *Journal of Environmental Chemical Engineering*, 6, 1378-1389.

KELLEN, E., ZEEGERS, M.P., HOND, E.D., BUNTINX, F., 2007. Blood cadmium may be associated with bladder carcinogenesis: The Belgian case-control study on bladder cancer. *Cancer Detection and Prevention*, 31, 77-82.

KHALIFA, E.B., RZIG, B., CHAKROUN, R., NOUAGUI, H. & HAMROUNI, B., 2019. Application of response surface methodology for chromium removal by adsorption on low-cost biosorbent. *Chemometrics and Intelligent Laboratory*, 189, 18-26.

LESAOANA, M., MLABA, R.P.V., MTUNZI, F.M., KLINK, M.J., EJIDIKE, P. & PAKADE, V.E., 2019. Influence of inorganic acid modification on Cr(VI) adsorption performance and the physicochemical properties of activated carbon. *South African Journal of Chemical Engineering*, 28, 8-18.

LIN, L., XU, X., PAPELIS, C., CATH, T.Y. & XU, P., 2014. Sorption of metals and metalloids from reverse osmosis concentrate on drinking water treatment solids. *Separation and Purification Technology*, 134, 37-45.

LIOU, T.H., 2010. Development of mesoporous structure and high adsorption capacity of biomass-based activated carbon by phosphoric acid and zinc chloride activation. *Chemical Engineering Journal*, 158, 129-142.

MAHMOOD-UL-HASSAN, M., SUTHAR, V., RAFIQUE, E., AHMAD, R., YASIN, M., 2015. Kinetics of cadmium, chromium, and lead sorption onto chemically modified sugarcane bagasse and wheat straw. *Environmental Monitoring and Assessment*, 187, 470.

MUTONGO, F., KUIPA, O. & KUIPA, P.K., 2014. Removal of Cr (VI) from aqueous solutions using powder of potato peelings as a low-cost sorbent. *Bioinorganic Chemistry and Applications*, 2014, 1-7.

NAG, S., MONDAL, A., BAR, N. & DAS, S.K., 2017. Biosorption of chromium (VI) from aqueous solutions and ANN modelling. *Environmental Science and Pollution Research international*, 23, 18817-18835.

NEOLAKA, Y.A.B., SUPRIYANTO, G. & KUSUMA, H.S., 2018. Adsorption performance of Cr(VI) imprinted poly(4-VP-co-MMA) supported on activated Indonesia (Ende-Flores) natural zeolite structure for Cr(VI) removal from aqueous solution. *Journal of Environmental Chemical Engineering*, 6, 436-3443.

NJOKU, V.O., AYUK, A.A., OGUZIE, E.E. & EJIKE, E.N., 2012. Biosorption of Cd(II) From Aqueous Solution by Cocoa Pod Husk Biomass: Equilibrium, Kinetic, and Thermodynamic Studies. *Separation Science and Technology,* 47, 753-761.

QI, X., GAO, S., DING, G. & TANG, A.N., 2017. Synthesis of surface Cr(VI)-imprinted magnetic nanoparticles for selective dispersive solid-phase extraction and determination of Cr(VI) in water samples. *Talanta*. 162, 345-353.

RAFATI, R.M., RAFATI, R.M., KAZEMI, S., MOGHADAMNIA, A.A., 2017. Cadmium toxicity and treatment: An update. *Caspian Journal of Internal Medicine*, 8(3), 135-145.

RAO, K.S., MOHAPATRA, M., ANAND, S. & VENKATESWARLU, P., 2010. Review on Cadmium removal from aqueous solutions. *International Journal of Engineering, Science and Technology,* 2, 81-103.

RAO, M.M., RAMANA, D.K., SESHAIAH, K., WANG, M.C., CHIEN, S.W., 2009. Removal of some metal ions by activated carbon prepared from Phaseolus aureus hulls. *Journal of hazardous materials,* 166(2-3),1006-1013.

SAFARI, E., RAHEMI, N., KAHFOROUSHAN, D., ALLAHYARI, S., 2019. Copper adsorptive removal from aqueous solution by orange peel residue carbon nanoparticles synthesized by combustion method using response surface methodology. *Journal of Environmental Chemical Engineering,* 7, 102847.

SHARMA, P.K., AYUB, S. & TRIPATHI, C.N., 2016. Isotherms describing physical adsorption of Cr(VI) from aqueous solution using various agricultural wastes as adsorbents. *Cogent Chemistry*, 3, 1-20.

SHOOTO, N.D., P.M. THABEDE. & NAIDOO, E.B., 2019b. Simultaneous adsorptive study of toxic metal ions in quaternary system from aqueous solution using low cost black cumin seeds (Nigella sativa) adsorbents. *South African Journal of Chemical Engineering*, 30, 15-27.

SHOOTO, N.D. & NAIDOO, E.B., 2019. Detoxification of wastewater by paw-paw (carica papaya) seeds adsorbents. *Asian Journal of Chemistry*, 31, 2249-2256.

SHOOTO, N.D., NAIDOO, E.B. & MAUBANE, M., 2019a. Sorption studies of toxic cations on ginger root adsorbent. *Journal of Industrial and Engineering Chemistry*,76, 133-140.

SHOOTO, N.D., NKUTHA, C.S., GUILANDE, N.R. & NAIDOO, E.B., 2020a. Pristine and modified mucuna beans adsorptive studies of toxic lead ions and methylene blue dye from aqueous solution. *South African Journal of Chemical Engineering*, 31, 33-43.

SHOOTO, N.D., THABEDE, P.M., BHILA, B., MOLOTO, H. & NAIDOO, E.B., 2020b. Lead ions and methylene blue dye removal from aqueous solution by mucuna beans (velvet beans) adsorbents. *Journal of Environmental Chemical Engineering*, 103557.

SIDDIQUI, S.I. & CHAUDHRY, S.A., 2018. Nigella sativa plant-based nanocomposite-$MnFe_2O_4$/BC: An antibacterial material for water purification. *Journal of Cleaner Production*, 200, 996-1008.

SIDDIQUI, S.I. & CHAUDHRY, S.A., 2019. Nanohybrid composite Fe_2O_3-ZrO_2/BC for inhibiting the growth of bacteria and adsorptive removal of arsenic and dyes from water. *Journal of Cleaner Production,* 223, 849-868.

SIDDIQUI, S.I., MANZOOR, O., MOHSIN, M. & CHAUDHRY, S.A., 2019. Nigella sativa seed-based nanocomposite-MnO_2/BC: An antibacterial material for photocatalytic degradation, and adsorptive removal of Methylene blue from water. *Environmental Research*,171, 328-340.

SIDDIQUI, S.I., RATHI, G. & CHAUDHRY, S.A., 2018b. Acid washed black cumin seed powder preparation for adsorption of methylene blue dye from aqueous: Thermodynamic, kinetic and isotherm studies. *Journal of Molecular Liquids*, 264, 275-284.

SIDDIQUI, S.I., ZOHRA, F. & CHAUDHRY, S.A., 2019. Nigella sativa seed based nanohybrid composite-Fe_2O_3-SnO_2/BC: A novel material for enhanced adsorptive removal of methylene blue from water. *Environmental Research*, 178, 108667.

SINGH, R., GAUTAM, N., MISHRA, A. & GUPTA, R., 2011. Heavy metals and living systems. *Indian Journal of Pharmacology*, 43, 247-253.

TAGHIZADEH, M. & HASSANPOUR, S., 2017. Selective adsorption of Cr(VI) ions from aqueous solutions using a Cr(VI)-imprinted polymer supported by magnetic multiwall carbon nanotubes, *Polymer* (Guildf), 132, 1-11.

VAZQUEZ, G., SONIA FREIRE, M. & GONZALEZ-ALVAREZ, J., 2009. Antorrena G. Equilibrium and kinetic modelling of the adsorption of Cd^{2+} ions onto chestnut shell. *Desalination,* 249, 855-860.

XIONG, W., ZHANG, J., YU, J. & CHI, R., 2019. Competitive adsorption behavior and mechanism for Pb^{2+} selective removal from aqueous solution on phosphoric acid modified sugarcane bagasse fixed-bed column. *Process Safety and Environmental Protection*, 124, 75-83.

YADAV, S.K. SINGH, D.K. & SINHA, S., 2014. Chemical carbonization of papaya seed originated charcoals for sorption of Pb(II) from aqueous solution. *Journal of Environmental Chemical Engineering,* 2, 9-19.

YAGUB, M.T., SEN, T.K., AFROZE, S. & ANG, H.M., 2014. Dye and its removal from aqueous solution by adsorption. *Advances Colloid and Interface Science* 209, 172-184.

YANG, T., SHENG, L., WONG, L., WYCKOFF, K.N., HE, C. & HE, Q., 2018. Characteristics of cadmium sorption by heat-activated red mud in aqueous solution. *Scientific Reports*, 8 (1), 13558.

YAO, S., ZHANG, J., SHEN, D., XIAO, R., GU, S., ZHAO, M. & LIANG, J., 2016. Removal of Pb(II) from water by the activated carbon modified by nitric acid under microwave heating. *Journal of Colloid Science***,** 463, 118-127.

YARKANDI, N.H., 2014. Removal of lead (II) from waste water by adsorption. *International Journal of Current Microbiology and Applied Sciences,* 3, 207-228.

YUNHONG, Y., JUNLIANG, L., YI, L. & GONGQING, W., 2017. Synthesis and application of modified Litchi peel for removal of hexavalent chromium from aqueous solutions. *Journal of Molecular Liquids*, 225, 28-33.

ZENG, L., GONG, J., RONG, P., LIU, C. 7 CHEN, J., 2019. A portable and quantitative biosensor for cadmium detection using glucometer as the point-of-use device. *Talanta*. 198, 412-416.

ZHAO, X., ZENG, X., QIN, Y., LI, X., ZHU, T. & TANG, X., 2018. An experimental and theoretical study of the adsorption removal of toluene and chlorobenzene on coconut shell derived carbon. *Chemosphere* 206, 285-292.

ZHENG, L., DANG, Z., YI, X., ZHANG, H., 2010. Equilibrium and kinetic studies on adsorption of Cd (II) from aqueous solution using modified corn stalk. *Journal of Hazardous Materials*, 176, 650-656.

CHAPTER 6

Sulfuric activated carbon of black cumin (*Nigella Sativa* L.) seeds for the removal of cadmium(II) and methylene blue dye

This chapter is published as follows:

Patience Mapule Thabede, Ntaote David Shooto, Thokozani Xaba, Eliazer bobby Naidoo. 2020. Sulfuric activated carbon of black cumin (*Nigella sativa* L.) seeds for the removal of cadmium(II) and methylene blue dye. Asian Journal of Chemistry 32(6), 1361-1369.

This chapter is addressing objective (d) which read as follows:

To activate BCS using sulfuric acid and carbonize the activated seeds at 200 °C and conduct single adsorption of MB and Cd(II) under different parameters (temperature, concentration, time and pH

6.1 Abstract

Carbon from black cumin seeds was modified with 10 % and 20 % sulfuric acid (H_2SO_4) to obtain the activated adsorbents. Pristine carbon from black cumin seeds, 10 and 20 % H_2SO_4 activated carbon from black cumin seeds were labelled CBC, ACBC-10 and ACBC-20 respectively. The adsorbents were characterized by SEM, XRD, FTIR, TGA and BET. The adsorbents maximum trend for Cd(II) was ACBC-10>ACBC-20> CBC. The maximum adsorption capacity trend for methylene blue (MB) dye was ACBC-20>ACBC-10>CBC. The kinetic model best fitted pseudo second order (PSO) for Cd(II) which gave r^2 values of 0.991-0.998. The MB adsorption equilibrium data fitted pseudo first order (PFO) model with r^2 values ranging from 0.993-0.997. PFO suggest that the adsorption mechanism for MB onto adsorbents involved Van der Waal forces of attraction. The equilibrium data fitted Langmuir isotherm model for CBC, ACBC-10 and ACBC-20 with r^2 of 0.994 to 0.998 for the removal of MB whilst the removal of Cd(II) followed Freundlich with r^2 ranging from 0.992 to 0.997. The Gibb's free energy ($\Delta G°$) for Cd(II) and methylene blue onto CBC, ACBC-10 and ACBC-20 suggested that the reaction was spontaneous. The adsorption of Cd(II) and MB was endothermic, positive values *($\Delta H°$)*. This suggested that the enthalpy, *($\Delta H°$)* had a weak interactive force process whose low energy is associated with electrostatic attraction.

Keywords: Activated carbon, methylene blue, cadmium(II), adsorption, sulfuric acid

6.2 Introduction

The presence of organic dyes in streams and rivers is an environmental problem (Albadarin et al. 2017). Hence its elimination is very important because it is toxic and have a potential of being carcinogenic. About 15% of dyes are found in industrial effluents during operations and

manufacturing processes (Pathania et al. 2017). Many synthetic dyes have been discovered and are usually used in pharmaceutical, chemical, leather, food, paper and textile industries and they are not easily degraded (Pandey, 2019). Excess of dyes leads to the change of aquatic life properties like; Chemical oxygen demand (COD), Biological oxygen demand (BOD), Dissolved oxygen (DO), taste, pH, colour and odour, which ultimately can damage aquatic life (Helmy et al. 2017). Methylene blue (MB) a cationic dye is not only carcinogenic it also pollutes water environment. MB can cause abdominal disorders, respiratory disease and blindness (Novais et al. 2018).

Cadmium is found in fruits, seafood, vegetables, rice and meats. Hence, it is important to control it to minimum especially in aqueous water (Kawasaki et al. 2010). The use of cadmium in industries and discarding of waste containing Cd (II) have led to an increase in the residual concentration of cadmium in water, soil, air and food and its exposure is associated with many health effects of acute exposure and chronic conditions (Al-Homaidan et al. 2015). Cd(II) is one of the most toxic metals, which has an extensive range of sources including, chemical, nuclear, electroplating and electronic industries (Zhang et al. 2018). Intake of water containing cadmium is harmful and has the risk of causing chronic diseases, such as gastrointestinal cancer, kidney damage, and liver disease also causes Itai-itai disease, hypertension and bone degradation (Sharififard et al. 2018; Basu et al. 2017). Due to toxic effects of metal ions and dyes on human health, the removal of these pollutants is compulsory before it adds in the environment and passes into the human food chain.

Reverse osmosis (Lin et al. 2014; Thaci et al. 2019) chemical precipitation (Brbooti et al. 2011), electro dialysis (Alliouxa et al. 2081), ion exchange (Zhao et al. 2019), and many others are conventional methods employed for the removal of dyes and metal ions from aqueous

solutions. Disadvantages of these conventional treatment technologies include partial removal of certain ions especially at low concentration and high cost often make these processes not to be ideal. Adsorption process is an alternative method in comparison with the other techniques, it provides many opportunities such efficiency, low cost, easy operation and control, high potential to bring about the separation more effectively (Sharififard et al. 2018).

Among the various adsorbents, studies have shown that low cost activated carbon obtained from biomass has a potential for removing toxic metals and dyes due to chemical interactions of polar functional groups, such as hydroxyl, carboxylic and amino groups and also due to their high surface area, high degree of porosity which leads to high adsorption capacity (Aghababaei et al. 2017). The use of biomass as a source of carbon has other advantages such as availability, low cost, renewability and ecological suitability (Zubrik et al. 2017). The aim of the study was to chemically activate and carbonize the black cumin seeds using 10 % and 20 % of sulfuric acid at 200 °C. Sorption properties towards methylene blue dye and Cd(II) of the prepared activated carbons are also discussed.

6.3 Experiments

6.3.1. Materials and methods

Black cumin seeds were bought from health shop in Vanderbijlpark, Vaal triangle, South Africa. Cadmium acetate $Cd(CH_3COO)_2$-99.995%, Sulphuric acid (H_2SO_4)-98% A.R grade and methylene blue ($C_{16}H_{18}ClN_3S$)-82% were purchased from Sigma Aldrich South Africa LTD.

6.4 Adsorbents preparation

6.4.1 Carbonized black cumin (CBC) seeds adsorbent

Adsorbent's preparation method was adopted from Shooto et al. (2019). The untreated black cumin seeds were washed dried and grounded. The grounded black cumin seeds were carbonized at 200 ^{o}C in catalytic vapour deposition (CVD) furnace in nitrogen atmosphere thereafter they were labelled (CBC).

6.4.2 Activated carbon black cumin (ACBC)-10 adsorbent

The carbonized (200 ^{o}C) black cumin seeds were activated with 10 % H_2SO_4 and labelled ACBC-10. The adsorbent was agitated for 24 hours then rinsed with distilled water several times and dried in the oven for 24 hours. The obtained brownish-black material was used for adsorption studies.

6.4.3 Activated Black Cumin (ACBC)-20 adsorbent

The carbonized adsorbent was activated with 20 % H_2SO_4 then agitated for 24 hours. After elapsed time the adsorbent was rinsed with distilled water then dried for 24 hours. This adsorbent was labelled ACBC-20. The obtained black material was ready for characterization.

6.5 Adsorption procedure

6.5.1 Concentration effect

Each adsorbents CBC, ACBC-10 and ACBC-20 (0.1 g) were weighed into sample vials. Methylene blue dye (20 mL) with standard solutions of 20, 40, 60, 80 and 100 mg/L was transferred into each vial containing 0.1 g. The solutions and the adsorbents were agitated for 60 min at 200 rpm on a shaker. The mixture was centrifuge at 200 rpm for 5 min and decanted. The decanted solutions were used for analysis. The same procedure was used for Cd(II).

6.5.2 Contact time effect

About 0.1 g of adsorbent was weighed and then transferred into nine vials. To each vial containing the weighed adsorbent was added to 20 mL Cd(II) solution with a standard concentration of 100 ppm from $Cd(CH_3COO)_2$ solution. The mixture was agitated on a shaker for each time interval of 1, 5, 10, 15, 20, 30, 60, 90 and 120 min, respectively. The solutions were centrifuge at 200 rpm for 5 min then decanted and stored for analysis. The same method was followed using methylene blue dye.

6.5.3 Temperature effect

Accurately weighed CBC, ACBC-10 and ACBC-20 (0.1 g each) were placed into five test tubes. Methylene blue solution (20 mL) with concentration of 100 mg/L was transferred into each vial containing the adsorbents. The effect of temperature was carried out at 25, 30, 40, 60 and 80 ^{o}C. The mixture was put in a water bath for 60 min. The solution with adsorbents were centrifuged and decanted. The decanted solutions were used for analysis. The same procedure was used for the metal ion.

6.5.4 pH effect

Each adsorbent (0.1 g) was weighed then placed into five sample vials. Cadmium acetate (20 mL) solution with a standard concentration of 100 ppm was transferred to each vial containing the weighed adsorbents. The initial pH of each solution was measured and thereafter adjusted with 0.1 M of HNO_3 and 0.1 M NaOH to pH of 1, 3, 5, 7 and 9. The mixtures were agitated on a shaker for 60 min. After 60 min, the mixtures were centrifuged then decanted. The solutions were collected and used for Cd(II) analysis. The same procedure was followed for methylene blue.

6.6 Data Analysis

The determination of the adsorption capacity for Cd(II) and methylene blue (MB) onto the adsorbents was determined using the following equation for batch dynamic studies:

$$q_e = \frac{V(C_o - C_e)}{m} \qquad (1)$$

q_e: Cd(II) and MB concentration sorbed onto the adsorbents at equilibria point (mg of metal ion/g of adsorbent)

(Co): Initial concentration of Cd(II) and MB in solution (ppm)

(Ce) Equilibria point concentrations Cd(II) and MB in solution (ppm)

V: Initial volume of Cd(II) and MB solutions used (L)

m: Weight of the adsorbents

Equation (2) and (3), non-linear forms which were used to determine the kinetics models; pseudo-first order (PFO) and pseudo-second order (PSO). The amounts of metal ions adsorbed *(mg/g)* are *(qe)* and *(qt)* at equilibrium and time *(t)*. The rate constant is k_1 of the PFO in *(min^{-1})* and k_2 is the rate constant of the PSO *(g mg^{-1} min^{-1})*.

$$q_e = q_t(1 - e^{-k_1 t}) \quad (2)$$

$$q_e \frac{1+k_2 q_e t}{k_2 q_e^2 t} \quad (3)$$

The data collected was integrated into equation (4) to calculate the intra-particle diffusion (IPD) model. The amounts adsorbed *(q_t)* and rate constant *(k_i)* were evaluate using the KyPlot software, *(k_i)* the rate constant *(g g^{-1} min$^{1/2}$)* and *C* is the concentration of metal ions on the adsorbent surface.

$$q_t = k_i\left(t^{1/2}\right) + C \quad (4)$$

To calculate the adsorption isotherm for Langmuir and Freundlich respectively equations (5) and (6) were used. Solute surface interaction energy *(b)*, *(Q_o) max*, is the maximum capacity of the adsorbent *(mg/g)*, Freundlich capacity factor (*kf*), and (*1/n*) is the isotherm linearity parameter. (*R*) Gas constant 8.314 J K-1mol^{-1} and (*T*) temperature in (K).

$$q_e = \frac{Q_0 b C_e}{1+bC_e} \quad (5)$$

$$q_e = k_f C_e^{1/n} \quad (6)$$

Equation (7) was used to evaluate the thermodynamic function values; equilibrium constant *(K_c)*.

$$K_c = \frac{q_e}{C_e} \quad (7)$$

Other thermodynamic functions namely; enthalpy *(ΔH^o)*, entropy *(ΔS^o)* and Gibbs free energy *(ΔG^o)* were determined using equations (8) and (9) at temperatures of 25, 30, 40, 60 and 80 °C.

$$ln\ K_c = -\frac{\Delta H^o}{RT} - \frac{\Delta S^o}{R} \quad (8)$$

$$\Delta G^o = -RT \ln K_c \quad (9)$$

6.7 Characterization

The chemical features of the adsorbent were determined by scanning electron microscope (SEM), Fourier transform infrared (FTIR), thermogravimetric analysis (TGA) and X-ray diffractometer (XRD). The surface morphology measurements were determined using field emission scanning microscopy (FE-SEM)-ZEISS ultra plus, Germany. Nicolet iS50 FTIR spectrometer 400 was used with measuring range from 4000 to 520 cm^{-1}. TGA 4000 thermogravimetric analyser, Perkin Elmer was used at a heating rate of 10 ^oC/min under a nitrogen atmosphere between 30-900 ^oC. Shimadzu XRD 7000 was used to identify crystalline phase of the samples with scan speed set at 10 °/min and scan range set from 10 to 80. Hach Precision pH meter was used to measure pH using deionized water and pH at point of zero charge $pH_{(PZC)}$ was evaluated using the pH drift method. Ultraviolet-visible (UV-Vis)

spectrometer spectroscopy Perkin Elmer Lambda 25 was used for methylene blue dye with the visible range using a slit of 1.0 and width of 0.1.

6.8 Results and discussion

6.8.1 Adsorbents characterization

6.8.1.1 SEM

Characterization of the surface morphology and physical properties of the adsorbents was carried out using SEM. Figs. 33a-f show the surface morphology of CBC, ACBC-10 and ACBC-20. Images of CBC (Figs. 33a-b) show that the adsorbent consist of cavities and tiny pores on the surface which may be taken as a sign that adsorption of Cd(II) and dye molecules can take place in the cavities and pores. A similar trend was observed in Figs. 33c-d and e-f for ACBC-10 and ACBC-20, respectively with shiny smooth surfaces that have small spots.

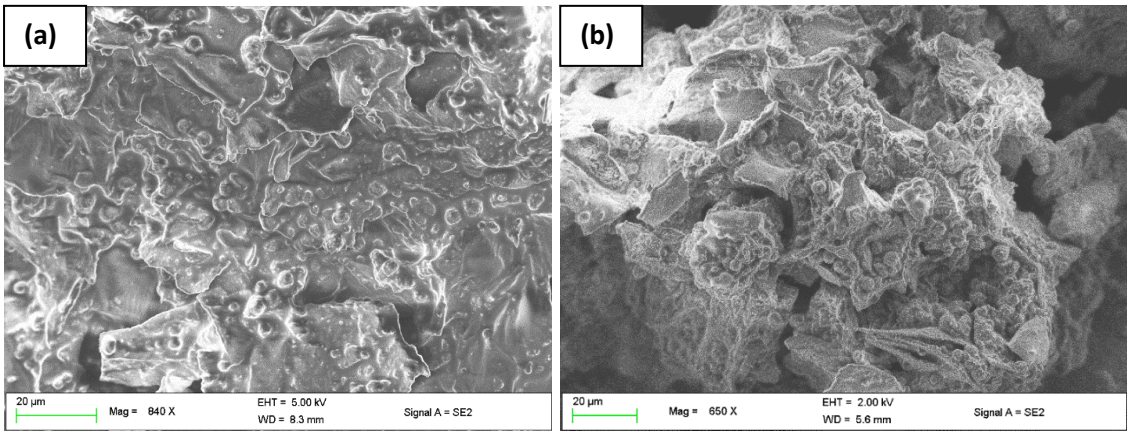

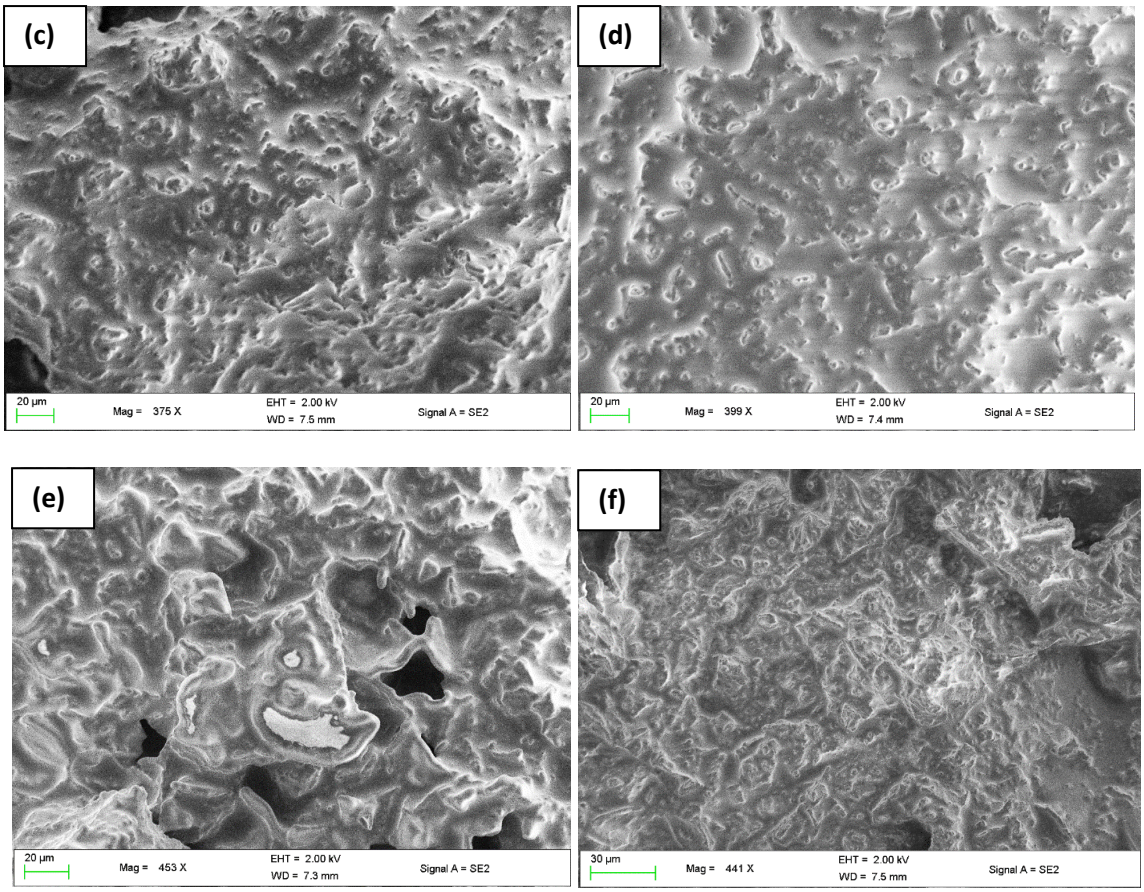

Figure 33: SEM images of (a-b) CBC, (c-d) ACBC-10, (e-f) ACBC-20 adsorbents.

6.8.1.2 FTIR analysis

The FTIR spectroscopy was used to track changes that has occurred after the activation. FTIR spectra of CBC, ACBC-10 and ACBC-20 are shown in Fig. 34 with broad peaks at 3287, 3279 and 3295 cm^{-1} which were due to (-OH) stretching respectively. The small peaks at 3008 cm^{-1} were observed in all spectra which were assigned to (-CH). These peaks were due to oil in the samples composition in fatty acids which was observed on the three adsorbents (Poiana et al., 2015). The two bands of ($-CH_3$) and ($-CH_2$) which were attributed to (-CH) stretch were observed at 2922 and 2853 cm^{-1} on CBC, 2923 and 2853 cm^{-1} on ACBC-10 and 2922 to 2853 cm^{-1} on ACBC-20 respectively. The sharp peak at 1743 cm^{-1} due to ketonic group (-C=O) (Zhou et al. 2019) was observed on all adsorbents. The band at 1651 cm^{-1} on ACBC-10 and

ACBC-20 was attributed to the vibration of (C=O) of the carbonyl structure (Zhou et al. 2015), the peak shifted to 1649 cm^{-1} on CBC. The peak at this region might be with (N-H) deformation of amino and amide groups along with C=O stretching vibration of amides (Barsainya et al. 2016). There was a new peak due to (N-H) (Li et al. 2018) at 1530 cm^{-1} on ACBC-10 which shifted to 1527 cm^{-1} on ACBC-20, then it dropped off on CBC. The peaks at 1457, 1455 and 1456 cm^{-1} were assigned to (-CO) group stretching band of CBC, ACBC-10 and ACBC-20 respectively. The band at 1377 cm^{-1} on CBC, ACBC-10 and ACBC-20 was due to (-CH) and is associated with the deformation of cellulose and hemicelluloses (Matos et al. 2017). The other bands at 1240 and 1157 cm^{-1} on all adsorbents were attributed to structures of hemicellulose and cellulose and lignin (Husseien et al. 2009).

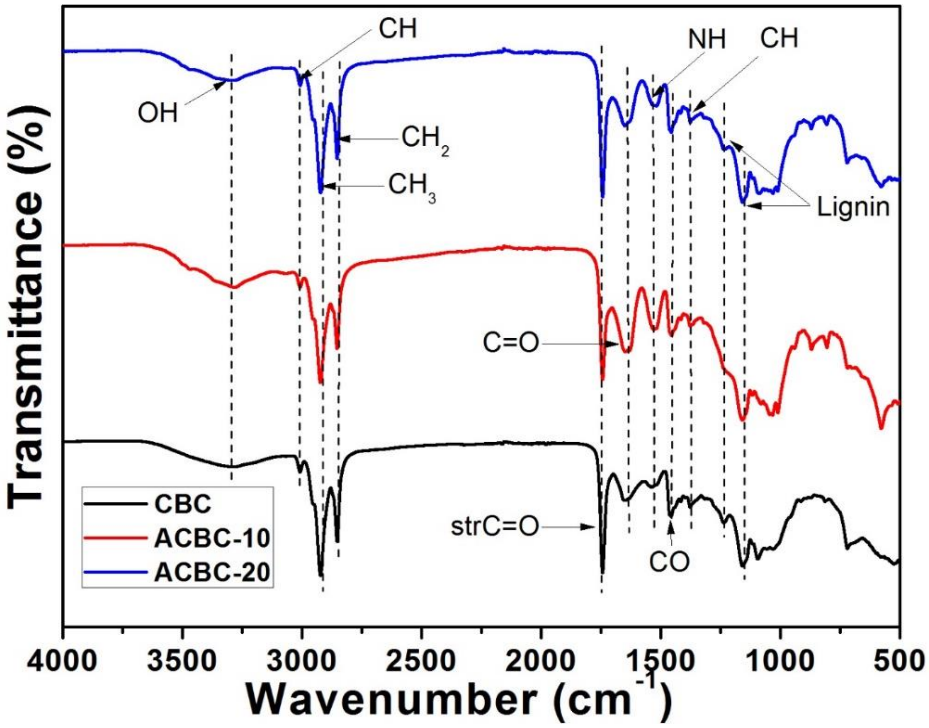

Figure 34: IR spectra of CBC, ACBC-10 and ACBC-20 adsorbents.

6.8.1.3 XRD analysis

The X-ray diffraction patterns of CBC, ACBC-10 and ACBC-20 are shown in Fig. 35. The broad peak at 2θ between 15 and 21° on CBC, ACBC-10 and ACB-20 is assigned to cellulosic content of the adsorbents. CBC shows a tall narrow peak at 2θ (62°) and disappeared on ACBC-10 and ACBC-20. The other peaks are assigned to the amorphous nature of adsorbents.

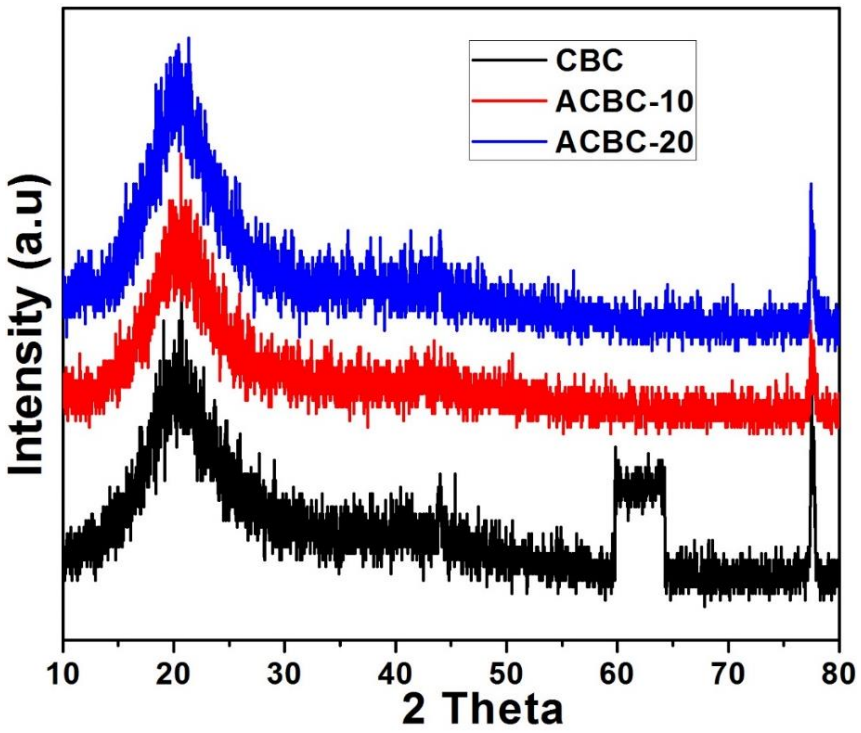

Figure 35: XRD spectra of CBC, ACBC-10 and ACBC-20 adsorbents.

6.8.1.4 Thermal analysis

Fig. 36 shows the thermal stability profiles of CBC, ACBC-10 and ACBC-20 conducted in nitrogen atmosphere. The plot shows two main decomposition steps namely, the first stage between 34 and 174 °C due to dehydration of water on the surface of the adsorbents. Samples weight loss percentages are 4, 2, and 1 % for CBC, ACBC-10 and ACBC-20 respectively. The second decomposition between 174 and 516 °C is attributed to the breaking down of lighter

volatiles hemicellulose, then the heavier cellulose and lignin (Shooto et al. 2016) with weight percentage of 81, 80 and 86 % for CBC, ACBC-10 and ACBC-20 respectively. After the degradation of lignocellulose materials, a long tail from 516-900 °C is due to pyrolysis of residues formed during the breaking down of cellulose, hemicellulose and lignin was observed.

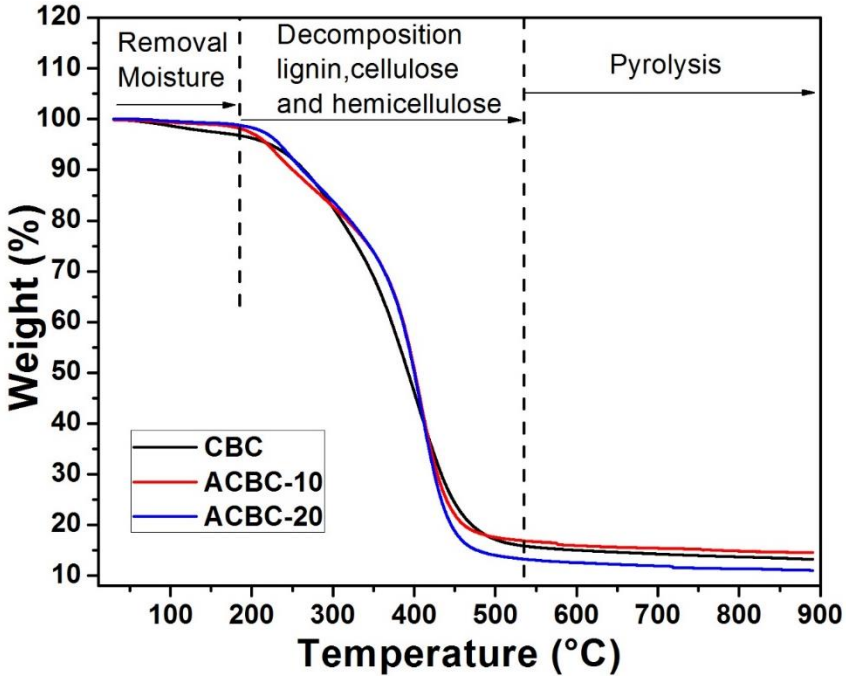

Figure 36*:* TGA of CBC, ACBC-10 and ACBC-20 adsorbents.

6.8.2 Adsorption studies

6.8.2.1 Effect of concentration

The effect of adsorption concentration at different concentrations (20, 40, 60 80 and 100 ppm) was studied to determine sorption ability of CBC, ACBC-10 and ACBC-20 at constant temperature of 25 °C for MB and Cd (II) in aqueous solution is shown in Figs. 37a-b. The adsorption rate was very rapid at lower concentrations between 20 and 60 ppm solutions. This might be attributed to the presence of vacant bounding sites and free pore space on the surface

of CBC, ACBC-10 and ACBC-20. As the concentration increased the sorption capability started to slow down indicating the saturation of vacant sites and pores (Liu & Hu, 2007). Thereafter, no further increase of capacity was observed which indicated that equilibrium was reached. Methylene blue maximum capacities are; 15.11 mg/g on CBC, 15.89 mg/g on ACBC-10 and 16.00 mg/g on BCAC-20 with maximum capacity trend as ACBC-20 > ACBC-10> BCC. The maximum adsorption capacities for the removal of Cd(II) are; 6.27 mg/g on CBC, 7.61 mg/g on ACBC-10 and 7.14 mg/g ACBC-20. Adsorbents maximum capacity trend for Cd(II) was ACBC-10>ACBC-20 >CBC. It was observed that the adsorbents were selective towards pollutants.

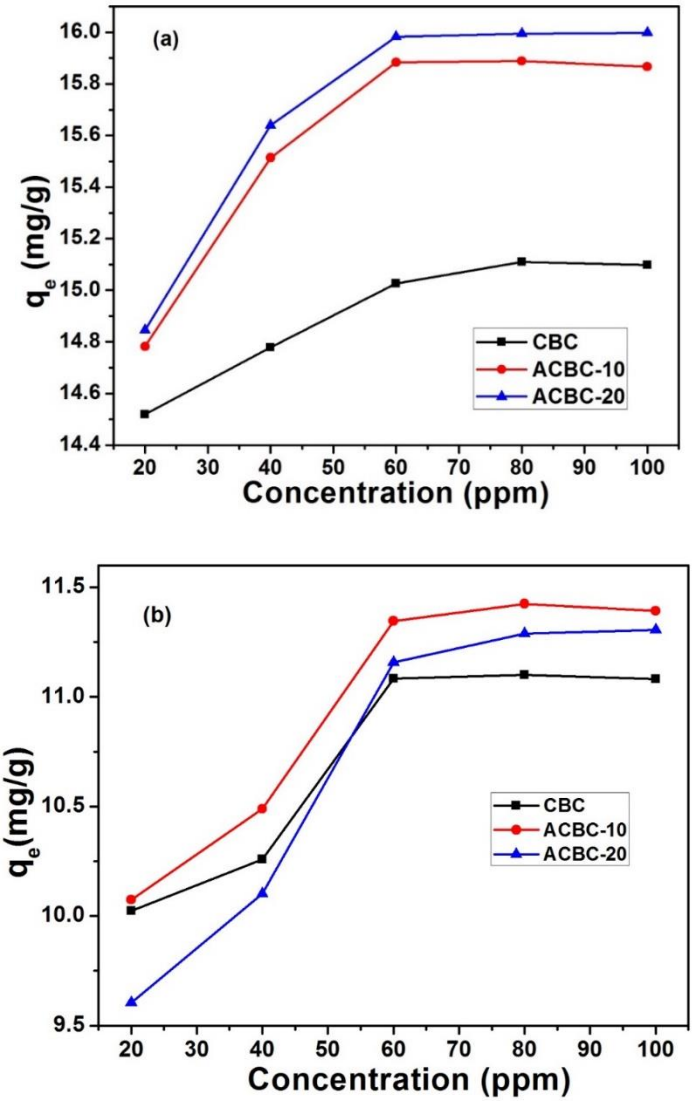

Figure 37: Concentration effect of (a) MB and (b) Cd(II) adsorption onto CBC, ACBC-10 and ACBC-20 adsorbents

Table 10 shows isotherm parameters of CBC, ACBC-10 and ACBC-20 which were evaluated at 25 °C in order to determine interaction behaviour and capacity of the adsorbents. The sorption of MB on all adsorbents followed Langmuir isotherm model with r^2 between 0.994-0.998 whilst Cd(II) fitted Freundlich isotherm model with r^2 between 0.992-0.997 which was close to the unity. The Langmuir isotherm model indicates that the adsorption took place on active sites and has equal attraction for adsorbates and also implies that there is monolayer adsorption occurring on dye surface. The Freundlich model suggest that the process involves multi-layer adsorption with interactions between the adsorbate and the adsorbent, it further proposes that surface is heterogeneous in nature.

Table 10: Isotherms studies and their parameters.

Isotherms		**CBC**		**ACBC-10**		**ACBC-20**	
		Cd(II)	**MB**	**Cd(II)**	**MB**	**Cd(II)**	**MB**
Langmuir	**Q_o**	13.34	15.47	15.68	23.03	13.16	21.54
	B	0.24	0.857	0.27	0.15	0.16	0.51
	r^2	0.902	0.998	0.904	0.994	0.914	0.997
Freundlich	**1/n**	53.34	25.67	45.68	23.03	46.15	21.54
	k_f	5.10	0.56	0.22	0.43	1.14	0.75
	r^2	0.992	0.821	0.995	0.903	0.997	0.911
Experimental (q_e)		11.09	15.11	11.31	16.00	11.36	16.01

6.8.2.2 Effect of time

The rate at which Cd(II) and MB was removed from aqueous solution was important, hence, the evaluation and determination of the efficiency of CBC, ACBC-10, ACBC-20 for wastewater treatment. The efficiency of the CBC, ACBC-10, ACBC-20 were determined using the time intervals of 5, 10, 15, 20, 30, 40, 60, 90 and 120 min as indicated in Figs. 38a-b. The plots show that sorption was rapid within the first 30 min, this is because of unoccupied active sites at the initial stage of the sorption process. However, as the time increased the sorption sites decreased in number and got saturated. The maximum capacities were 13.19 mg/g on CBC, 15.25 mg/g on ACBC-10 and 16.42 mg/g on BCAC-20 for MB and were 12.01 mg/g on CBC, 13.66 mg/g on ACBC-10 and 12.57 mg/g on BCAC-20 for Cd(II).

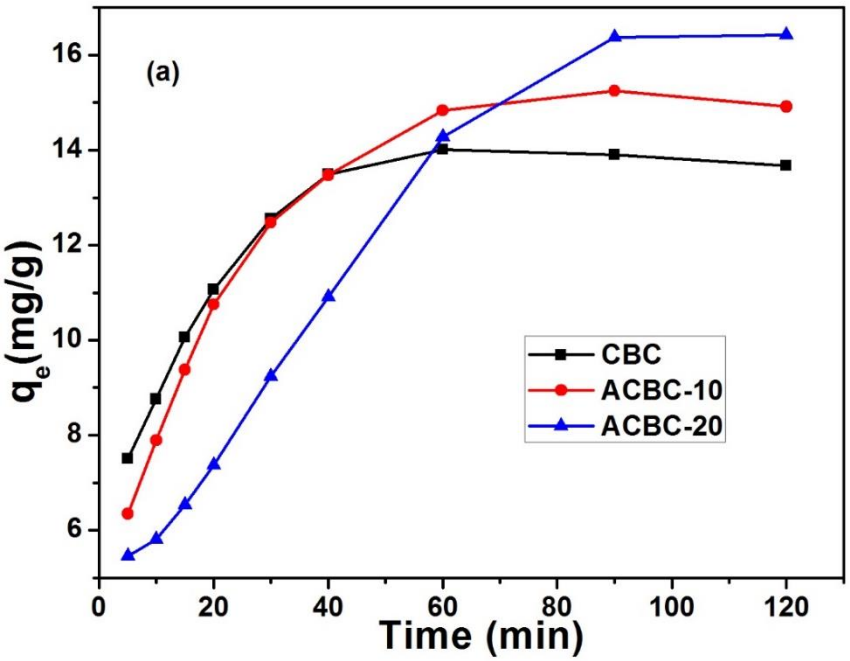

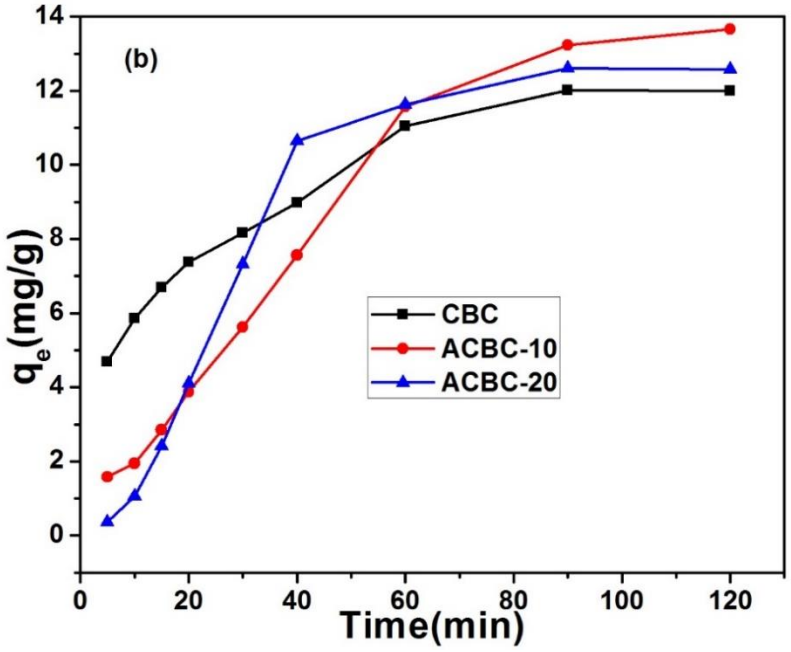

Figure 38*:* Time effect of (a) MB and (b) Cd(II)) adsorption onto CBC, ACBC-10 and ACBC-20 adsorbents

To calculate kinetic parameters three kinetic models were used and kinetic data are shown in Table 11 for MB and Cd(II) adsorption onto CBC, ACBC-10, ACBC-20. The three models were; pseudo first order (PFO), pseudo second order (PSO), and intra particle diffusion (IPD) models. In order to evaluate whether the adsorption has a good fit for the PFO or PSO, the values of coefficient of determination must be close to 1 and the values of adsorption capacity need to be close to the experimental data. The data show that the adsorption of MB on all adsorbents best fitted PFO model with r^2 values ranging from 0.993-0.997 whilst Cd(II) data fitted PSO with r^2 values of 0.991-0.998. The adsorption mechanism of PFO propose that Cd(II) on the adsorbents involved Van der Waal forces attraction and PSO indicates that the adsorption process on MB was dependent on the availability of the adsorption sites. The nature of the process was estimated using IPD kinetic model which evaluates whether adsorption takes

place on the surface (ESA) or pores (EPA). The estimated pore adsorption (EPA) was observed in all adsorbents.

Table 11: Kinetic models and their parameters

Models		CBC		ACBC-10		ACBC-20	
		Cd(II)	**MB**	**Cd(II)**	**MB**	**Cd(II)**	**MB**
PFO	q_e	13.07	14.66	14.05	14.72	12.16	17.66
	K_1	4.09	4.07	4.19	0.073	4.23	4.13
	r^2	0.808	0.993	0.877	0.997	0.838	0.996
PSO	q_e	9.87	4.83	8.44	8.14	6.08	4.08
	K_2	0.023	0.056	0.020	0.085	0.022	0.030
	r^2	0.998	0.872	0.991	0.895	0.993	0.874
IPD	C	4.177	5.097	3.515	4.556	7.54	5.39
	K_i	6.81	5.34	7.716	1.79	1.89	1.35
	r^2	0.933	0.715	0.909	0.769	0.976	0.759
EPA[a]	%	83.60	71.28	72.47	71.69	66.55	69.21
ESA[a]	%	16.40	28.72	27.52	28.31	33.45	30.79
Experimental (q_e)		13.37	14.01	13.23	15.24	12.57	16.42

[a] EPA - Estimated pore adsorption of IPD and *ESA - Estimated surface adsorption of IPD.

6.8.1.3 Effect of temperature

In this section, a sequence of experiments were accomplished at different temperatures to investigate the effect of temperature to the sorption of MB and Cd(II) dyes on CBC, ACBC-10 and ACBC-20. The effect of temperature was determined at 25 °C (298 K), 30 °C (303 K), 40 °C (313 K), 60 °C (333 K) and 80 °C (353 K) as indicated in Figs. 39a-b. The plots show that

there is an increase in adsorption capacities as the temperature increases from 25 to 60 °C in Fig. 39a for MB. As the temperature increased further from 60 to 80 °C resulted in reduced adsorption capacities and hence reaching equilibrium. This suggests that at high temperatures there is more kinetic energy which makes molecules to move fast in the solution which in turn decrease interaction with the active sites for adsorption to occur. Fig. 39b, shows slightly different patterns in that as the temperature increases the capacity increased as well. This suggests that the adsorption of Cd(II) in this study prefer a slight increase in temperature in order to improve the adsorption process.

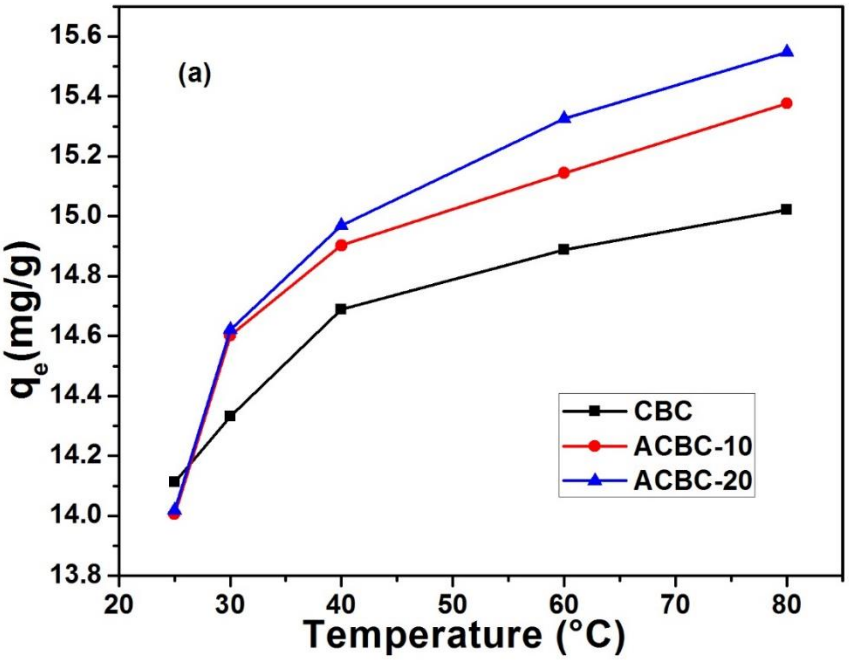

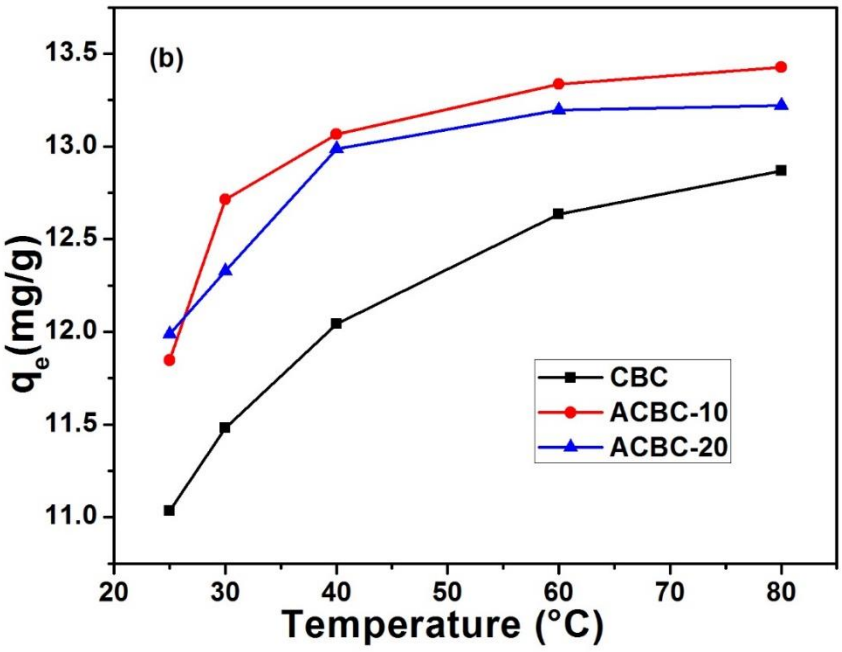

Figure 39: Temperature effect of (a) MB and (b) Cd(II) adsorption onto CBC, ACBC-10 and ACBC-20 adsorbents.

The thermodynamic parameters: enthalpy *(ΔH°)*, Gibbs free energy *(ΔG°)* and entropy *(ΔS°)* are shown in Table 12. The *ΔG*° for all CBC, ACBC-10 and ACBC-20 are negative indicating that the reaction was exothermic and spontaneous whereas *ΔH*° as well as *ΔS*° were positive. The positive value of Δ*H* indicates that Cd(II) biosorption is an endothermic process, which in turn explains the temperature-enhanced Cd(II) biosorption as shown in Fig. 39b (Mudyawabikwa et al. 2017).

Table 12: Thermodynamic studies and their parameters

Parameter	CBC		ACBC-10		ACBC-20	
	Cd(II)	**MB**	**Cd(II)**	**MB**	**Cd(II)**	**MB**
ΔH^o (KJ mol^{-1})	$1.3x10^{-3}$	$2.1x10^{-2}$	$1.4x10^{-3}$	$1.5x10^{-3}$	$1.3x10^{-3}$	$9.0x10^{-4}$
ΔS^o (KJ mol^{-1}K^{-1})	$1.6x10^{-3}$	$1.8x10^{-3}$	$1.6x10^{-3}$	$2.3x10^{-3}$	$1.8x10^{-3}$	$2.7x10^{-3}$
ΔG^o (KJ mol^{-1}) 298 K	-3.47	-1.82	-3.06	-1.88	-2.99	-1.87
303 K	-3.30	-1.72	-2.65	-1.55	-2.86	-1.72
313 K	-3.11	-1.54	-2.54	-1.40	-2.84	-3.39
333 K	-2.96	-1.49	-2.53	-1.31	-2.95	-0.85
353 K	-2.89	-1.48	-2.42	-1.21	-2.90	-0.61

6.8.1.4 Effect of pH

The effect of pH as shown in Figs. 40a-b was studied at pH 1, 3, 5, 7 and 9 for MB and Cd(II) on CBC, ACBC-10, ACBC-20. The adsorption capacity of MB and Cd(II) was largely dependent of pH. The adsorption of MB (Fig. 40a) was steadily increased with increasing pH 1 to 5. A similar trend was observed for Cd(II). This suggests that at low pH the solution is protonated due to functional groups (-COOH, -OH and-NH_2) on the adsorbent surface hence low adsorption due to repulsion force. At higher pH (7-9) there is less repulsion force between the adsorbent surface and the functional groups due to deprotonation hence an increase in adsorption capacity (Shooto et al. 2019). The increase in negative charges of the adsorbent surface benefits, improved the forces of attraction and the adsorption capacity.

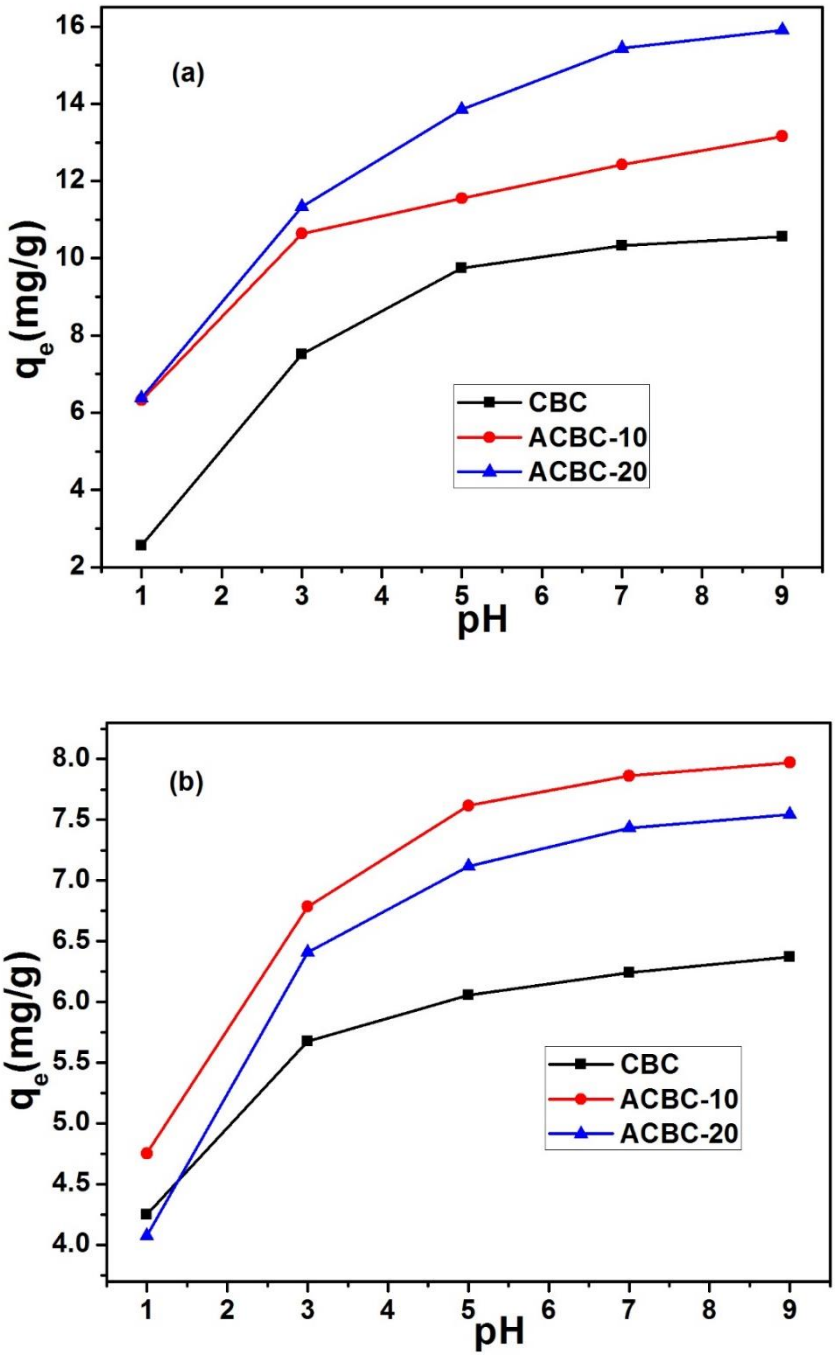

Figure 40: pH effect of (a) MB and (b) Cd(II) adsorption onto CBC, ACBC-10 and ACBC-20 adsorbents

6.8.1.5 pH at point zero charge (pH_{PZC})

Point of zero charge is an important characteristic which evaluates the point at which the adsorbent surface has net electrical neutrality (Zubrik et al. 2017). Fig. 41 shows the plots of

ΔpH vs. pHi of CBC, ACBC-10, and ACBC-20. The point of zero charge attained from the graphs is 5.7 on CBC and 2.3 for both ACBC-10, and ACBC-20. The pH_i-pH_f values are negative before 2.3 and 5.7. This indicates that the pHpzc is less than pH 7.00, causing an increase in the negative charge density on the surface of activated carbon for adsorption of MB and Cd(II). The pH values above pH_{ZPC} 2.3 and 5.7 show that CBC, ACBC-10, ACBC-20 surfaces acquired positive charge and ΔpH vales became positive.

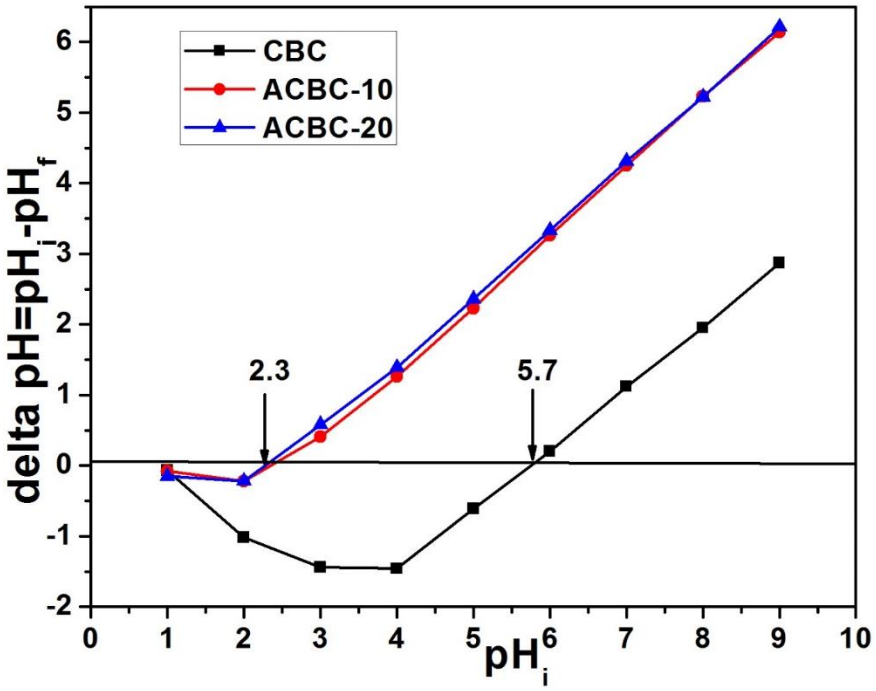

Figure 41: Point zero charge of MB and Cd(II) onto CBC, ACBC-10 and ACBC-20 adsorbents

6.8.3 Comparative study

The existing information in Table 13 indicates the previously adsorption capacities of some reported adsorbents. Table 13 show some of the literature where different adsorbents were used for removal of Cd(II) and methylene blue dye from aqueous solutions. From the data it is clear that activated black cumin seeds can be used for adsorption of Cd(II) and methylene blue dye.

Activated black cumin seeds (CBC, ACBC-10 and ACBC-20) adsorption studies showed a potential and good removal capacity in comparison to some of the previously reported bio sorbents.

Table 13: Comparison of Cd(II) adsorption capacity with other adsorbents

Adsorbents	**$q_{(max)}$ (mg/g)**	**References**
	Cd(II)	
Corn stalks	41.17	Zheng et al. 2018
Graphene oxide	23.9	Biana et al. 2015
H. valentiae	17.0	Rathinam et al. 2010
Black cumin seeds	13.66	This study
Sugar cane bagasse	14.8	Garg et al. 2008
Cocoa pod husk biomass	13.4	Njoku et al. 2012
Acrylonitrile modified corn stalk	12.7	Zheng et al. 2010
Buffalo weed	11.6	Yakkala et al. 2013

Adsorbents	**$q_{(max)}$ (mg/g)**	**References**
	MB	
Lignin-chitosan	36.25	Albadarin et al. 2017
Fly ash	30.1	Novais et al. 2019
Palm Oil	22.4	Zaini et al. 2013
Black cumin seeds	16.42	This study
Coconut shell	15.1	Aljeboree et al. 2017
Palygorskite clay	14.0	Al-Futaisi et al. 2007
Fly ash	9.8	Rao et al. 2006

Sugar spent rice biomass	8.1	Ur-Rehman et al. 2012
Yellow passion fruit shell	6.8	Pavan et al. 2008
Caulerpa racemose var.cylindracea	5.2	Cengiz & Cavas, 2008

6.8.4 Conclusion

In this work, the low-cost black cumin seeds were carbonized and activated with 10 and 20 % H_2SO_4 for the adsorption of methylene blue dye and cadmium ions. Adsorption processes was evaluated using different parameters such as time, concentration and pH. The results showed that maximum capacity trend for Cd(II) was ACBC-10>ACBC-20 >CBC and for methylene blue was ACBC-20>ACBC-10>CBC. Adsorption kinetics of CBC, ACBC-10 and ACBC-20 both Cd(II) ions and methylene blue was fast. The data show that the adsorption of MB on all adsorbents best fitted PFO whilst Cd(II) data fitted PSO model. Isotherms best fitted Freundlich model for Cd(II) and methylene blue fitted Langmuir model. The entropy, ($\Delta S°$) was positive which indicated randomness and degree of freedom for MB and Cd(II) in the solution during sorption process whilst ($\Delta G°$) with negative values suggest that the sorption processes for CBC, ACBC-10 and ACBC-20 was spontaneous. This work affirms the use of black cumin seeds as adsorbents for the adsorption of methylene blue dye and Cd(II) from aqueous solution.

6.8.5 Acknowledgement

We would like to thank National Research Fund for funding this work and the support of the Department of Chemistry Vaal University of Technology, Vanderbiljpark, South Africa.

References

AGHABABAEI, A., NCIBI, M.C. & SILLANPAA, M., 2017. Optimized removal of oxytetracycline and cadmium from contaminated waters using chemically-activated and pyrolyzed biochars from forest and wood-processing residues. *Bioresource. Technology,* 239, 28-36.

ALBADARIN, A.B., COLLINS, M.N., NAUSHAD, M., SHIRAZIAN, S., WALKER, G. & MANGWANDI, C., 2017. Activated lignin-chitosan extruded blends for efficient adsorption of methylene blue. *Chemical Engineering Journal*, 307, 264-272.

ALBADARIN, A.B., COLLINS, M.N., NAUSHAD, M., SHIRAZIAN, S., WALKER G. AND MANGWANDI, C., 2017. Activated lignin-chitosan extruded blends for efficient adsorption of methylene blue. *Chemical Engineering Journal*, 307, 264-272.

AL-FUTAISI, JAMRAH, A., J. & AL-HANAI, R. 2007. Aspects of cationic dye molecule adsorption to palygorskite *Desalination*, 214, 327-342.

AL-HOMAIDAN, A.A., ALABDULLATIF, J.A., AL-HAZZANI, A.A., AL-GHANAYEM, A. & ALABBAD, A.F., 2015. Adsorptive removal of cadmium ions by Spirulina platensis dry biomass. *Saudi Journal of Biological Sciences,* 22(6), 795-800.

ALJEBOREE, M., ASHRAFI, A.N. & ALKAIM. A.F., 2017. Kinetics and equilibrium study for the adsorption of textile dyes on coconut shell activated carbon. *Arabian Journal of Chemistry*, 10, S3381-S3393.

ALLIOUXA, F.M., KAPRUWANA, P., MILNE, N., KONGA, L., FATTACCIOLI, J., CHEN, Y. & DUMEE, L.F., 2018. Electro-capture of heavy metal ions with carbon cloth integrated microfluidic devices. *Separation and Purification Technology*, 194, 26-32.

BARSAINYA, M., CHANDRA, P. & SINGH, D.P., 2016. Investigation of Cr (VI) Uptake in Saline Condition Using Psychrophilic and Mesophilic Penicillium sp. *International Journal of Current Microbiology and Applied Sciences*, 5(1), 274-288.

BASU, M., GUHA, A.K. & RAY, L., 2017. Adsorption behavior of cadmium on husk of lentil. *Process Safety and Environ*mental *Protection*, 106, 11-22.

BIAN, Y., BIAN, Z.Y., ZHANG, J. X., DING, A.Z., LIU S.L. & WANG, H., 2015. Effect of the oxygen-containing functional group of graphene oxide on the aqueous cadmium ions removal *Applied Surface Science*, 329, 269-275.

BRBOOTI, M. M., ABID, B.A. & AL-SHUWAIKI, N.M., 2011. Removal of Heavy Metals Using Chemicals Precipitation. *Engineering and Technology Journal,* 29(3).

CENGIZ, S. & CAVAS, L., 2008. Removal of methylene blue by invasive marine seaweed: Caulerpa racemosa var. cylindracea. *Bioresource Technology*, 99(7), 2357-2363.

EBRAHIMI, A., EHTESHAMI, M. & DAHRAZMA, B. 2015. Isotherm and kinetic studies for the biosorption of cadmium from aqueous solution by Alhaji maurorum seed. *Process Safety and Environmental Protection*, 98, 374-382.

GARG, U. KAUR, M.P. JAWA, G.K. SUD D. & GARG, V.K. 2008. Removal of cadmium (II) from aqueous solutions by adsorption on agricultural waste biomass. *Journal of Hazardous Materials*, 154, 1149-1157.

HELMY, Q., NOTODARMOJO, S., ARUAN, I.A. & APRILAWATI, R., 2017. The Third International Conference on Civil Engineering Research *(ICCER)* 474.

HUSSEIEN, M. AMER, A.A. EL-MAGHRABY A. & N. HAMEDALLAH, 2009. A comprehensive characterization of corn stalk and study of carbonized corn stalk in dye and gas oil. sorption *Journal of Analytical and Applied Pyrolysis*, 86(2), 360-363.

KAWASAKI, N., TOMINAGA, H., OGATA, F. & KAKEHI, K., 2010. Removal of cadmium and copper by vegetable biomass treated with hydrochloric acid. *Chemical Engineering Journal*, 157, 249-253.

LI, X., WEI, Y., XU, J., XU N. AND HE, Y., 2018. Quantitative visualization of lignocellulose components in transverse sections of moso bamboo based on FTIR macro-and micro-spectroscopy coupled with chemometrics. *Biotechnology for Biofuels,* 11, 263.

LIN, L., XU, X., PAPELIS, C., CATH, T.Y. & XU, P., 2014. Sorption of metals and metalloids from reverse osmosis concentrate on drinking water treatment solids. *Separation and Purification Technol*ogy, 134, 37-45.

LIU, Y. & XU, H., 2007. Equilibrium, thermodynamics and mechanisms of Ni^{2+} biosorption by aerobic granules. *Biochemical. Engineering Journal,* 35(2), 174-182.

MATOS, T.T.S. SCHULTZ, J. KHAN, M.Y. ZANOELO, E.F. MANGRICH, MANGRICH, A.S. ARAUJO, B.R. NAVICKIENE S. & ROMAO, L.P.C. 2017. Using magnetized (Fe_3O_4/Biochar Nanocomposites) and activated biochar as adsorbents to remove two neuro-active pesticides from waters Romao, *Journal of the Brazilian Chemical. Society,* 28(10), 1975-1987.

MUDYAWABIKWA, B., MUNGONDORI, H.H., TICHAGWA L. & KATWIRE, D. M., 2017. *Water Science & Technology,* 75(10), 2390-2402.

NJOKU, V.O., AYUK, A.A., OGUZIE E.E. & EJIKE, E.N., 2012. Biosorption of Cd(II) From Aqueous Solution by Cocoa Pod Husk Biomass: Equilibrium, Kinetic, and Thermodynamic Studies. *Separation Science and Technol*ogy, 47(5), 753-761.

NOVAIS, R.M., ASCENSAO, G., TOBALDI, D.M., SEABRA, M.P. & LABRINCHA, J.A., 2018. Biomass fly ash geopolymer monoliths for effective methylene blue removal from wastewaters. *Journal of Cleaner Prod*uction, 171,783-794.

NOVAIS, R.M., CARVALHEIRAS, J., TOBALDI, D.M., SEABRA, M.P., PULLAR, R.C. & LABRINCHA, J.A. 2019. Synthesis of porous biomass fly ash-based geopolymer spheres for efficient removal of methylene blue from wastewaters. *Journal of Cleaner Production,* 207, 350-362.

PANDEY, R.L.M., 2019. Enhanced adsorption capacity of designed bentonite and alginate beads for the effective removal of methylene blue. *Applied Clay Science*, 169, 102-111.

PATHANIA, D., SHARMA, S. & SINGH, P., 2017. Removal of methylene blue by adsorption onto activated carbon developed from *Ficus carica* bast. *Arabian Journal of Chemistry*, 10, S1445-S1451.

PAVAN, F.A., MAZZOCATO, A.C. & GUSHIKEM, Y., 2008. Removal of methylene blue dye from aqueous solutions by adsorption using yellow passion fruit peel as adsorbent. *Bioresource Technology*, 99(8), 3162-3165.

POIANA, M.A., ALEXA, E., MUNTEANU, M.F., GLIGOR, R., MOIGRADEAN D. & MATEESCU, C. 2015. Use of ATR-FTIR spectroscopy to detect the changes in extra virgin olive oil by adulteration with soybean oil and high temperature heat treatment. *Open Chem*istry,13, 689-698.

RAO, V.V.B. & RAO, S.R.M.,2006. Adsorption studies on treatment of textile dyeing industrial effluent by flyash. *Chemical Engineering, Journal*, 116, 77-84.

RATHINAM, A., MAHARSHI, B., JANARDHANAN, S.K., JONNALAGADDA R.R. & NAIR, B.U., 2010. Biosorption of cadmium metal ion from simulated wastewaters using Hypnea valentiae biomass: A kinetic and thermodynamic study. *Bioresource Technology*, 101(5), 1466-1470.

SHARIFIFARD, H. SHAHRAKI, Z.H. REZVANPANAH E. & RAD, S.H., 2018. A novel natural chitosan/activated carbon/iron bio-nanocomposite: Sonochemical synthesis, characterization, and application for cadmium removal in batch and continuous adsorption process *Bioresource Technology*, 270; 562-569.

SHOOTO, N.D., DIKIO, C.W., WANKASI, D., SIKHWIVHILU, L.M., MTUNZI F.M. & DIKIO, E.D., 2016. Novel PVA/MOF nanofibres: fabrication, evaluation and adsorption of lead ions from aqueous solution. *Nanoscale Research. Letters*, 11, 414.

SHOOTO, N.D., THABEDE, P.M. & NAIDOO, E.B., 2019. Simultaneous adsorptive study of toxic metal ions in quaternary system from aqueous solution using low cost black cumin seeds (Nigella sativa) adsorbents. *South African Journal of Chemical.* Engineering, 30(1), 15-27.

THACI, B.S. & GASHI, S.T., 2019. Reverse osmosis removal of heavy metals from wastewater effluents using biowaste materials pretreatment. *Polish Journal of Environmental Stud*ies, 28, 337-341.

UR-REHMAN, M.S., KIM, I. & HAN, J.I., 2012. Adsorption of methylene blue dye from aqueous solution by sugar extracted spent rice biomass. *Carbohydrate Polymer*, 90(3), 1314-1322.

YAKKALA, K., YU, M.R., ROH, H., YANG, J.K. & CHANG, Y.Y., 2013. Buffalo weed (Ambrosia trifida L. var. trifida) biochar for cadmium (II) and lead (II) adsorption in single and mixed system. *Desalination and Water Treat*ment, 51, 7732-7745.

YIN, W., ZHAO, C., XU, C., ZHANG, J., GUO, Z. & SHAO, Y., 2019. Removal of Cd(II) and Ni(II) from aqueous solutions using activated carbon developed from powder-hydrolyzed-feathers and Trapa natans husks. *Colloid Surfaces A*, 560, 426-433.

ZAINI, M.A.A., ZAKARIA, M., MOHD-SETAPAR S.H. &. CHE-YUNUS, M.A. 2013. Sludge-adsorbents from palm oil mill effluent for methylene blue removal. *Journal of Environmental Chemical Engineering*, 1(4), 1091-1098.

ZHANG, Y. HE, Q. XIA, L. LI Y. & SONG, S., 2018. Algae cathode microbial fuel cells for cadmium removal with simultaneous electricity production using nickel foam/graphene electrode. *Biochemical Engineering Journal*, 138, 179-187.

ZHAO, C. GE, R. ZHEN, Y. WANG, Y., LI, Z., SHI, Y. & CHEN, X., 2019. A hybrid process of coprecipitation-induced crystallization-capacitive deionization-ion exchange process for

heavy metals removal from hypersaline ternary precursor wastewater, *Chemical Engineering Journal*, 378, 122136.

ZHENG, L. PENG D. AND MEN, P. 2018. Promotion effects of nitrogenous and oxygenic functional groups on cadmium (II) removal by carboxylated corn stalk. *Journal of Cleaner Production*, 201, 609.

ZHENG, L., DANGA, Z. YI, X. & ZHANG, H., 2010. Equilibrium and kinetic studies of adsorption of Cd(II) from aqueous solution using modified corn stalk. *Journal of Hazardous Materials*, 176, 650-656.

ZHOU, N., WANG, Y., YAO, D., LI, S., TANG, J., SHEN, D., ZHU, X., HUANG, L., ZHONG M. & ZHOU, Z., 2019. Novel wet pyrolysis providing simultaneous conversion and activation to produce surface-functionalized biochars for cadmium remediation. *Journal of Cleaner Production*, 221, 63-72.

ZUBRIK, A., MATIK, M. HREDZAK, S. LOVAS, M. DANKOVA, Z. KOVACOVA, M. & J. BRIANCIN, 2017. Preparation of chemically activated carbon from waste biomass by single-stage and two-stage pyrolysis. *Journal of Cleaner Prod*uction, 143, 643-653.

CHAPTER 7

Removal of methylene blue dye and lead ions from aqueous solution using activated carbon from black cumin seeds

This chapter is published as follows:

Patience Mapule Thabede, Ntaote David Shooto, Eliazer Bobby Naidoo. 2020. Removal of methylene blue dye and lead ions from aqueous solution using activated carbon from black cumin seeds. South African Journal of Chemical Engineering 33, 39-50.

This chapter is addressing objective (d) which read as follows:

To activate BCS using sulfuric acid and carbonize the activated seeds at 300 °C and conduct single adsorption of MB and Pb(II) under different parameters (temperature, concentration, time and pH).

7.1 Abstract

This work reports the preparation of carbon from black cumin seeds (BCC) and then activated with 10 and 20 % sulfuric acid (H_2SO_4) to obtain new adsorbents designated black cumin activated carbon (BCAC-10) and (BCAC-20) respectively for the adsorption of lead (Pb(II)) ions and methylene blue (MB) dye from aqueous solution. The adsorbents were characterized by scanning electron microscopy (SEM), Fourier transformed infrared (FIR), thermogravimetric analyzer (TGA), X-ray diffractometer (XRD) and Brunauer, Emmett and Teller (BET) analysis. The SEM images show that both activated carbon adsorbents (BCAC-10 and BCAC-20) have rough irregular surfaces with cavities. FTIR results show the ($-COO^-$), ($-NH_2$), ($-HSO^-_4$), (-C=O) functional groups were involved in the adsorption processes of Pb(II) ions and methylene blue (MB) dye . Nitrogen adsorption studies show that there is an increase in surface area and pore size for both BCAC-10 and BCAC-20 in comparison with BCC. The operational parameters (concentration, contact time, temperature and pH) of Pb(II) ions and MB dyes adsorption were assessed in batch mode. It was observed that the trends for Pb(II) ions and MB dye adsorption increased with increasing initial concentration of the solution, (i.e.) greater uptake was observed in solutions with higher initial concentration. Therefore the adsorption of Pb(II) ions with initial concentration of 100 mg/L was 17.19, 17.71 and 17.98 mg/g onto BCC, BCAC-10 and BCAC-20 respectively. Whilst for MB dye it was 11.63, 12.71 and 16.85 mg/g onto BCC, BCAC-10 and BCAC-20 respectively. The equilibrium data for Pb(II) ions and MB dye fitted Freundlich isotherm model onto BCC, BCAC-10 and BCAC-20. This suggested that the process involves multi-layer adsorption with interactions between the adsorbate and the adsorbents. The results show that the adsorption processes of Pb(II) ions and MB dye were rapid in the first 20 min. It was observed that the maximum adsorption trend of Pb(II) ions and MB dye was obtained at pH 9 which made the surface of black cumin seeds to be negatively charged and therefore making it easier to be attracted to positively charged Pb

(II) ions and MB dye. Kinetic studies showed that the adsorption of Pb(II) ions and MB dye onto BCC best fitted; pseudo-first order model whilst BCAC-10 and BCAC-20 data fit; pseudo-second order. The estimated pore adsorption for Pb(II) ions onto BCC, BCAC-10 and BCAC-20 was 65.85, 94.28 and 78.43 % respectively whilst MB dye was 73.37, 70.82 and 95.74 % respectively. Temperature and thermodynamics data indicated that the adsorption capacities of adsorbents increase with increasing temperature and the enthalpy *(ΔH°)* values indicated that the adsorption of Pb(II) ions and MB dye on the adsorbents was endothermic reaction. The entropy (*ΔS*°) gave positive values which indicated the randomness and degree of freedom for Pb(II) ions and MB dye in aqueous solution. The free energy (*ΔG*°) values for the adsorption of Pb(II) ions and methylene blue dye onto BCC, BCAC-10 and BCAC-20 show an increase in negative values as the temperature increases.

Keywords: Black cumin activated carbon, adsorption, kinetics, isotherms, thermodynamic

7.2 Introduction

Water pollution is an environmental problem facing the world today due to various industries such mining and smelting, fertilizers and pesticide, metallurgy, iron and steel, electrolysis, energy and fuel production, etc discharging waste that contain toxic metals (Wang et al. 2009). The disposal of toxic metals from industrial effluent without treatment is a matter of great concern (Dargahi et al. 2016). Toxic metals are one of the dangerous materials found in water. They are pathogenic and has the ability to accumulate in living organisms over a long period of time. There are many toxic metals, this study will focus on Pb(II) ions and MB dye.

Dyes are intensely coloured and consume dissolved oxygen (Zhang et al. 2011). Generally, dyes have the ability to penetrate light and destroy aquatic life and their degradation products

may be carcinogens and toxic (Enenebeaku et al. 2017). Dyes are usually used in leather, paper-making, textile, food additive, cosmetic and many other industries (Wang et al. 2019). MB dye is the most discharged dye in water which is associated with vomiting, high heart rate, nausea, tissue necrosis, jaundice and quadriplegia. Therefore, it is important to remove MB from the effluents, before discharging into environment. According to the Environmental Protection and Management (Trade Effluent) Regulations, no trade effluent shall be discharged into any stream or land without a written permission approved by the Director-General. Therefore, the allowable levels for methylene blue will vary by regulatory agency and municipality, but the Environmental Protection Agency (EPA) general guidelines recommend limit value of 0.2 mg/L (Environmental Protection Agency, 2001). Pb(II) is released with effluent from batteries, paint, and automobiles industrial units (Yarkandi 2014). It is one of the toxic metals and can affect peripheral, nervous and the central system (Chand & Pakade, 2013; Moyo et al. 2013). Other toxic effects of Pb(II) includes visual disturbances, convulsions, constipation, abdominal pains, paralysis in muscles, anemia and loss of appetite, nausea and antisocial behaviours. The World Health Organization (WHO) document set the limit of lead ion concentration in the blood to be 0.1 gm^{-3} (WHO, 2018). It is therefore crucial to treat polluted water.

Various methods have been used to treat contaminated water. Some of the methods used includes chemical precipitation (Barbooti et al. 2011; Os et al. 2016), ion-exchange (Bai & Bartkiewicz, 2009; Zewail & Yousef, 2015) and membrane technology (Algureiri & Abdulmajeed, 2006; Thaci & Gashi, 2018), etc. Compared to these techniques, adsorption method is widely used because it is cheap, highly efficient, and able to regenerate the sorbent material and recover metals (Boeykens et al. 2019). Different adsorbents have been used to remove toxic pollutants from aqueous solutions like; Fe(III)-Sn(IV) mixed oxide-coated sand, Iron-Zirconium binary oxide-coated sand, graphene oxide, nanomaterials, avocado seed, coffee

husks, banana peels, pumice stone, fruit shells, eucalyptus seeds, rape straw, spent-coffee-grounds and many others (Osakwe et al. 2014; Chaudhry et al. 2016; ; Kumar et al. 2016; Wu & Wang, 2016; Chaudhry et al. 2017, Siddiqui & Chaudhry, 2018a, Yu et al. 2018; Siddiqui 2019a, Boeykens et al. 2019; Cheruiyot et al. 2019; Soleimani et al. 2019; Torres-Caban et al. 2019).

Commercial activated carbon is also used as an adsorbent in wastewater treatment due to its high surface area and high adsorption capacity (Moyo et al. 2013). Activated carbon is prepared by pyrolysis and activation of organic compounds. However, pyrolysis and activation have drawbacks such as high energy consumption and large quantities of waste gas emission (Bai et al. 2017). Due to the highlighted problems including the high costs associated with activated carbon, deriving activated carbon from sorbent materials seem to be an ideal method to use. Activated carbon adsorbent in adsorption have shown to be carbonaceous including large surface area, high porosity and better mechanical strength (Krishnamoorthy et al. 2019). As compared to biosorbents, activated carbon have better stability, high surface area, excellent thermal resistance, better adsorption capacity and inertness to adsorption conditions making them an excellent choice. Researchers have used carbonized agricultural materials like apricot kernel shell, banana peel, black satope seeds, walnut shell and maze tassel for the removal of toxic metal ions and dyes from aqueous solutions (Jankovic et al. 2019; Thuan et al. 2017; Cid et al. 2019; Zbair et al. 2019; Moyo et al. 2013).

Application of black cumin seeds in wastewater treatment has shown great potential. Therefore, several research groups have modified the surface of black cumin seeds by incorporating with nano composite of Fe_2O_3-ZrO_2 (Siddiqui & Chaudhry, 2019) for the adsorption of arsenic ions and methylene blue; Fe_2O_3-SnO_2 (Siddiqui et al. 2019b) for the removal of methylene blue;

MnO_2 (Siddiqui et al. 2019c) composite for the adsorption of methylene blue; $MnFe_2O_4$/BC (Siddiqui & Chaudhry, 2018b) for water purification. To further improve the adsorption capacity other researchers have activated the black cumin seeds by HCl and NaOH (Shooto et al. 2019a) for the quaternary removal of Pb(II), Cu(II), Ni(II) and Zn(II) ions; HCl washed (Siddiqui et al. 2018) for the adsorption of methylene blue; defatted black seeds by hexane (Addala et al. 2018) for the adsorption of lead ions; pristine black seeds (Ahmad & Haseeb, 2014) for the removal of copper ions. Therefore, few activated black cumin seeds studies have been documented. Hence, it is necessary to further investigate the effect of other activating agents on black cumin seeds using quaternary removal of Pb(II), Cu(II), Ni(II) and Zn(II) ions which has never been investigated before.

Black cumin seeds are fairly available, cheap and nontoxic. They are used as home remedy to alleviate inflammation, lower cholesterol and blood pressure, have cancer fighting properties, kill off bacteria, protect the liver, regulate blood sugar and prevent stomach ulcer. In this research work black cumin seeds were carbonized then activated with 10 and 20 % H_2SO_4 solution for the adsorption of Pb(II) ions and MB dye from water. To the best of our knowledge the activated black cumin seeds by H_2SO_4 has never been reported hence this study aims to investigate the feasibility of activated black cumin seeds to remove Pb(II) ions and MB dye from aqueous solution whilst varying different experimental parameters such as contact time, concentration, temperature and pH.

7.3 Materials and methods

7.3.1 Chemicals

Black cumin seeds (BCS) were purchased from health shop in Vanderbijlpark, Vaal triangle, South Africa. Sulphuric acid (H_2SO_4)-98% A.R grade, lead nitrate $Pb(NO_3)_2$-99.95% A.R grade and methylene blue ($C_{16}H_{18}ClN_3S$)-82% were purchased from Sigma Aldrich South Africa LTD.

7.3.2 Preparation of adsorbents

The untreated black cumin seeds (BCS) were washed, dried and grounded. The grounded black cumin seeds were carbonized at 300 ^oC in catalytic vapour deposition (CVD) furnace in nitrogen atmosphere as shown in scheme 2. Thereafter, they were labelled BCC. The carbonized black cumin (BCC) seeds were mixed with H_2SO_4 (10%) in order to activate them and then agitated at 200 rpm in a shaker for 24 hours at room temperature. After the time has elapsed, the BCC was rinsed with distilled water, and then dried in an oven for 48 hours at temperature of 40 °C. After drying the BCC were labelled BCAC-10. This method was also used when preparing (20%) H_2SO_4 carbon BCC and then they were labelled BCAC-20. This method was adopted from Shooto et al. (2019a).

7.4 Batch adsorption studies

Stock solutions (100 ppm) of MB dye and Pb(II) ions were made by dissolving 0.1 g $Pb(NO_3)_2$ and ($C_{16}H_{18}ClN_3S$) separately in 1 L of ultrapure water. To study the effect of contact time, different time intervals of 1, 5, 10, 15, 20, 30, 60, 90 and 120 min were used with a standard solution of 100 ppm. In the typical method, 0.1 g of each adsorbent was weighed into a weighing then transferred into 50 mL capped sample bottles. The metal ion (Pb(II)) solution of

20 mL was added to the sample bottles and equilibrated by agitation at 200 rpm. Thereafter, the samples were centrifuged at 5000 rpm for 5 min then decanted. The decanted solutions were stored for Pb(II) ions analysis. The same procedure was followed during the effect of concentration (20, 40, 60, 80 and 100 mg/L) and temperature (298, 303, 313, 333 and 353 K) by agitation at 200 rpm for 60 min. In order to determine the effect of pH, 100 mL of the metal ion solution was poured into 5 beakers. The initial pH of each solution was measured and then the solution pHs were adjusted to 1, 3, 5, 7 and 9. The adjustment of pH was conducted using 0.1 M HCl for acidic medium and 0.1 M of NaOH for basic medium. A 20 mL of the adjusted pH solution with the respective acid and base was added to 0.1g of the adsorbents and equilibrated for 60 min. For MB dye the same procedure was used. The determination of the point of zero charge (pH_{pzc}) of BCC, BCAC-10 and BCAC-20 carbon was conducted using 1M $NaNO_3$ concentration series of 100 mL. The solution pH was adjusted between 1.0 and 9 by adding 0.1 M HCl for acidic medium and 0.1 M NaOH for basic medium. Then adjusted pH solutions were added to 0.1 g of sample and shaken at 200 rpm for 48 h. After the time elapse the final pH was measured.

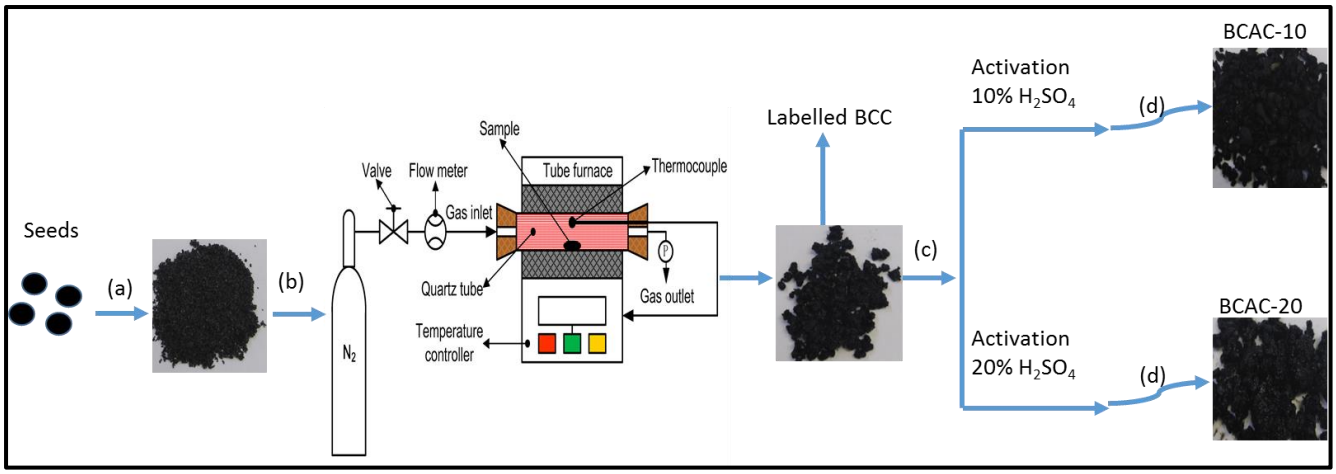

Scheme 3: Preparation of black cumin activated carbon (a) crushing (b) carbonization (c) activation (d) labelling

7.5 Data analysis

Adsorption capacity, q_e was used to determine the amount of ions adsorbed in (*mg/g*) and removal percentage *(%R)* was used in equations (1) and (2) where *(Co)* and *(Ce)* are the initial and final concentrations of the pollutants in the solution *(mg/L)* respectively. Volume *(v)* of the working solution in *(ml)* and mass (*m)* of the adsorbent in *(g)*.

$$q_e = \frac{(C_o - C_e)V}{m} \quad (1)$$

$$\%R = \frac{(C_o - C_e)}{C_o} X100 \quad (2)$$

Equation (3) and (4) non-linear forms were used to evaluate the kinetics models; pseudo-first order (PFO) and pseudo-second order (PSO). The amounts of metal ions adsorbed in *(mg/g)* are *(qe)* and *(qt)* at equilibrium and time *(t)*. The rate constant is k_1 of the PFO in *(min^{-1})* and k_2 is the rate constant of the PSO *($g\ mg^{-1}\ min^{-1}$)*.

$$q_e = q_t(1 - e^{-k_1 t}) \quad (3)$$

$$q_e \frac{1 + k_2 q_e t}{k_2 q_e^2 t} \quad (4)$$

The experimental data was incorporated into equation (5) to calculate the intra-particle diffusion (IPD) model. The amounts adsorbed *(q_t)* and rate constant *(k_i)* were determined using the KyPlot software. *(k_i)* the rate constant in *($g\ g^{-1}\ min^{1/2}$)* and *C* is the concentration of metal ions on the adsorbent surface.

$$q_t = k_i\left(t^{1/2}\right) + C \quad (5)$$

Equations (6), and (7) and were used to calculate the adsorption isotherm for Langmuir and Freundlich respectively. (Q_o) *max,* is the maximum capacity of the adsorbent *(mg/g),* solute surface interaction energy *(b),* Freundlich capacity factor (*kf),* and (*1/n)* is the isotherm linearity parameter. (*R)* Gas constant 8.314 J K-1mol^{-1} and (*T)* temperature in (K).

$$q_e = \frac{Q_0 b C_e}{1+bC_e} \quad (6)$$

$$q_e = k_f C_e^{1/n} \quad (7)$$

Thermodynamic function; equilibrium constant *(K_c),* values were determined using equation (8)

$$K_c = \frac{q_e}{C_e} \quad (8)$$

Equations (9) and (10) were used to equilibrium adsorption data at 298, 303, 313, 333 and 353 K and other thermodynamic functions namely; enthalpy *(ΔH^o),* entropy *(ΔS^o)* and Gibbs free energy *(ΔG^o).*

$$ln\ K_c = -\frac{\Delta H^o}{RT} - \frac{\Delta S^o}{R} \quad (9)$$

$$\Delta G^o = -RT \ln K_a \quad (10)$$

7.6 Characterization

Thermal stability, surface morphology, functional groups, phase purity and surface area were determined by TGA, SEM, FTIR, XRD and BET techniques respectively. Perkin Elmer TGA 4000 thermogravimetric analyser (TGA) was used at a heating rate of 10 ^{o}C/min under a nitrogen atmosphere between 30-900 ^{o}C. Scanning electron microscopy (SEM) images were taken with Field emission scanning microscopy (FE-SEM)-ZEISS ultra plus, Germany. Thermo Fischer Scientific Fourier transformed infrared spectroscopy, Nicolet iS50 FTIR spectrometer, spectrum 400 was used. X-ray diffractometer (XRD), Shimadzu XRD 7000 was used to identify crystalline phase of the sample with scan speed set at 10 °/min and scan range set from 10 to 80. The nitrogen adsorption/desorption of the adsorbents was evaluated using Micromeritics ASAP 2020 MtC accelerated surface area analyser (Micromeritics Instrument Corporation, USA). Ultraviolet-visible spectroscopy (UV-Vis) analyses were conducted with Perkin Elmer Lambda 25 UV/Vis spectrometer that collects spectra from 180-1100nm UV and visible range using a slit of 1.0 and width of 0.1. The pH was measured with Hach Precision pH meter using deionized water and pH at point of zero charge $pH_{(PZC)}$ was evaluated using the pH drift method.

7.7 Results and discussion

7.7.1 Adsorbents characterization

7.7.1.1 SEM analysis

Figs. 42a-f show the surface morphology of BCC, BCAC-10 and BCAC-20 which was investigated by SEM images. Images of BCC in Figs. 42a-b show that the carbonized black cumin seeds constitute of irregular surface morphology whilst the activated carbon in Figs.

42c-d (BCAC-10) and Figs. 42e-f (BCAC-20) show rough irregular surfaces with cavities and disintegrated surface morphologies. The use of sulfuric acid may have resulted in the improvement of BCAC-10 and BCAC-20 surfaces texture during activation. The changes observed on the surfaces of BCAC-10 and BCAC-20 adsorbents could have occurred due to the oxidation of sulfuric acid which may have imparted the surface with active cavities. These openings are anticipated to enhance the adsorption of Pb(II) ions and MB dye (Kumari et al. 2020).

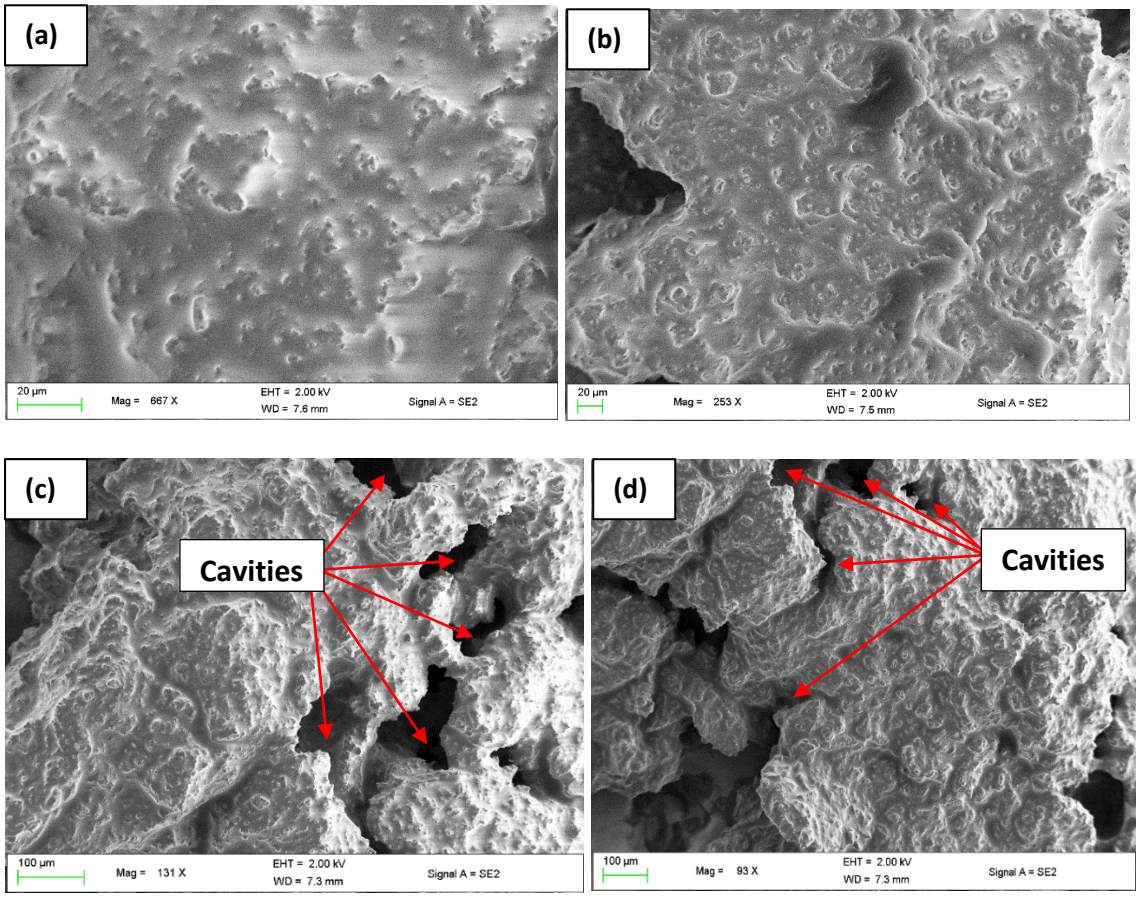

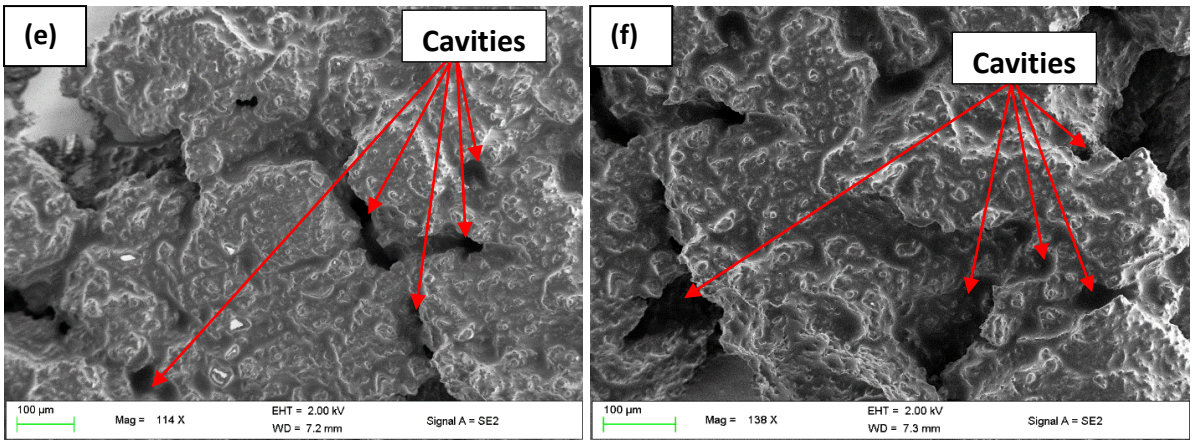

Figure 42: SEM images of (a-b) BCC, (c-d) BCAC-10 and (e-f) BCAC-20 adsorbents.

7.7.1.2 FTIR analysis

The FTIR spectra show the functional groups on the surface of the adsorbents (pristine black cumin seeds (PBCS), BCC, BCAC-10 and BCAC-20 as shown in Fig. 43a. The broad peak on PBCS at 3428 cm^{-1} was due to (-OH) stretching of the hydroxyl groups, this peak was not observed on BCC, BCAC-10 and BCAC-20. The small peak observed at 3003 cm^{-1} due to (-CH=CH) on PBCS shifted on BCC, BCAC-10 and BCAC-20 to 3008 cm^{-1} (Bouyanfif et al. 2017). The two bands at 2922 and 2853 cm^{-1} on all adsorbents, were attributed to (-CH) stretch of ($-CH_3$) and ($-CH_2$) respectively (Oliveira et al. 2016). The sharp peak for ketonic group (-C=O) at 1743 cm^{-1} was observed on all adsorbents (Shooto et al. 2019a). The peak at 1641 cm^{-1} on PBCS was attributed to (-C=O) of amide, however on BCC, BCAC-10 and BCAC-20 the peak shifted to 1658 cm^{-1} (Boeykens et al. 2019). A peak at 1545 cm^{-1} was due to ($-NH_2$) of the amide group on PBCS (Oliveira et al. 2016; Shooto et al. 2019) whilst on BCAC-10 and BCAC-20 the peak shifted to 1528 and 1523 cm^{-1} respectively. The peak on PBCS at 1459 cm^{-1} due to (-COOH) (Shooto et al. 2019a) slightly shifted to 1461 cm^{-1} on BCC and 1455 cm^{-1} on BCAC-10 and BCAC-20. The peaks at 1238, 1153 and 1038 cm^{-1} on all adsorbents are due to (-CO) group (Wang et al. 2013). The newly developed peak at 853 cm^{-1} only on BCAC-10

and BCAC-20 was associated bisulfate group (Li & Jang, 2013). This group was imparted to the surface of BCAC-10 and BCAC-20 during H_2SO_4 modification.

To better understand the mechanism that took place between black cumin adsorbents and both pollutants (Pb(II) ions and MB dye), FTIR spectra before and after was conducted. Fig 43b shows FTIR spectra of BCAC-20 before and after adsorption for Pb(II) ions and MB dye. The changes noted was for the ketonic group (-C=O) at 1743 cm^{-1} on BCAC-20 shift to lower wavenumber of 1736 and 1737 cm^{-1} in BCAC-20 after Pb(II) ions and MB dye adsorption respectively. This may suggest that the ketonic group (-C=O) maybe be involved in the adsorption process (Shooto et al. 2019b). The amide ($-NH_2$) peak at 1529 cm^{-1} before adsorption on BCAC-20 disappeared after the adsorption of both Pb(II) ions and MB dye which suggest that the amide group was involved in the adsorption process. The carboxyl group (-COOH) in BCAC-20 before adsorption at 1455 cm^{-1} shifted to higher wavenumber of 1458 cm^{-1} after Pb(II) ions and MB dye adsorption. The peaks associated with (-CO) at 1153 cm^{-1} remained the same in all three samples. The peak at 853 cm^{-1} was due to bisulfate (HSO^-_4) on BCAC-20 before adsorption and shifted higher to 869 cm^{-1} after adsorption of Pb(II) ions whilst after the adsorption of MB dye it shifted to 881 cm^{-1}. Therefore, (HSO^-_4) was involved in the adsorption process. Shifts observed in Fig. 43b suggest that functional groups such as ($-CCO^-$), ($-NH_2$), (-C=O), (HSO^-_4) interacted with Pb(II) ions and MB dye (Siddiui et al. 2018). The shifting of peaks indicates that there was strong interaction between the adsorbate and the adsorbents through electrostatic (Wang et al. 2016). New peaks were observed in BCAC-10 and BCAC-20 at 1097 cm^{-1}. The proposed attachment of Pb(II) ions and MB dye onto the adsorbents is shown in scheme 4.

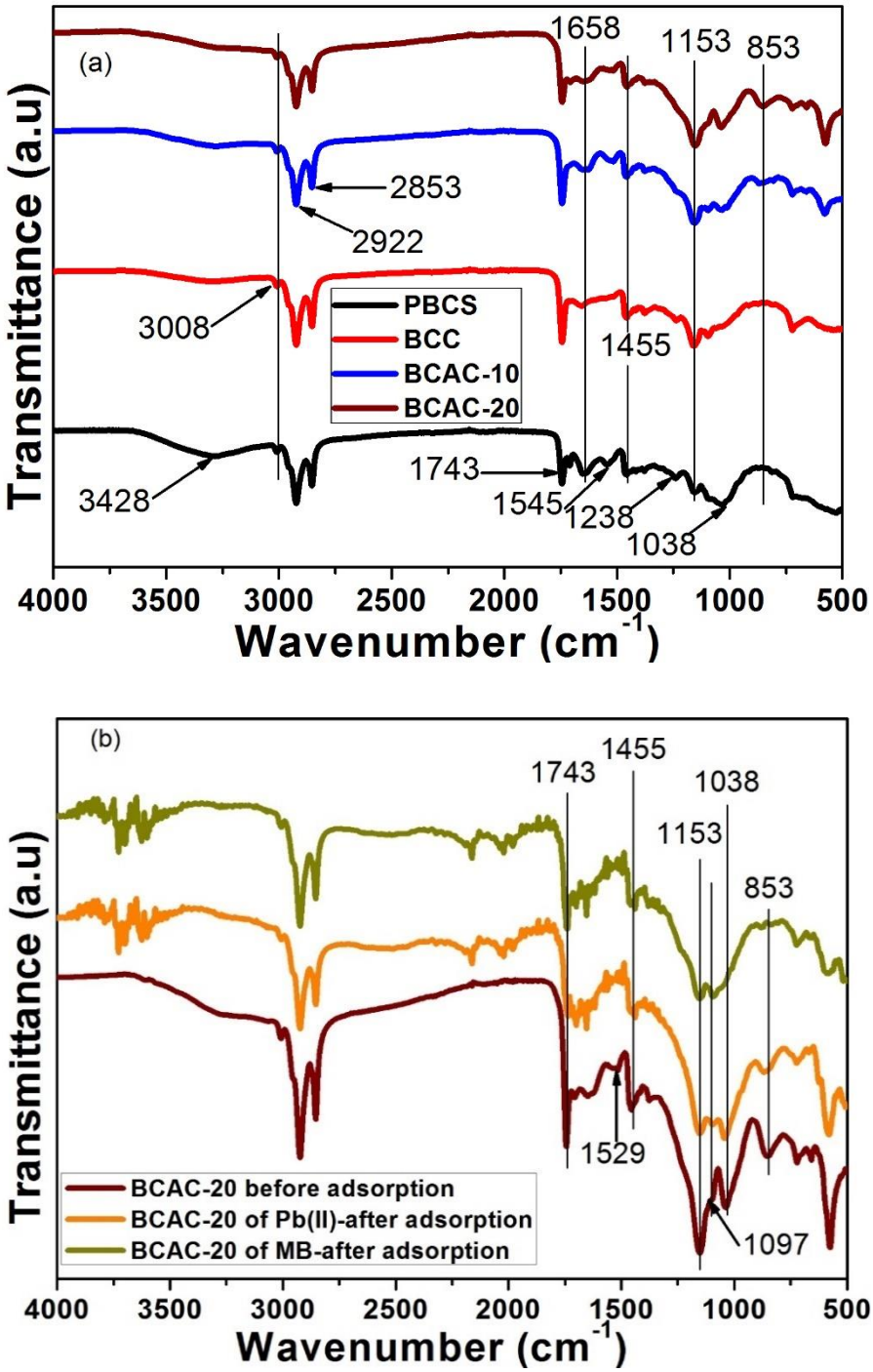

Figure 43: IR spectra of (a) PBCS, BCC, BCAC-10 and BCAC-20 adsorbents before adsorption, (b) BCAC-20 adsorbent before adsorption, BCAC-20 after adsorption for Pb(II) ions and BCAC-20 after adsorption MB dye.

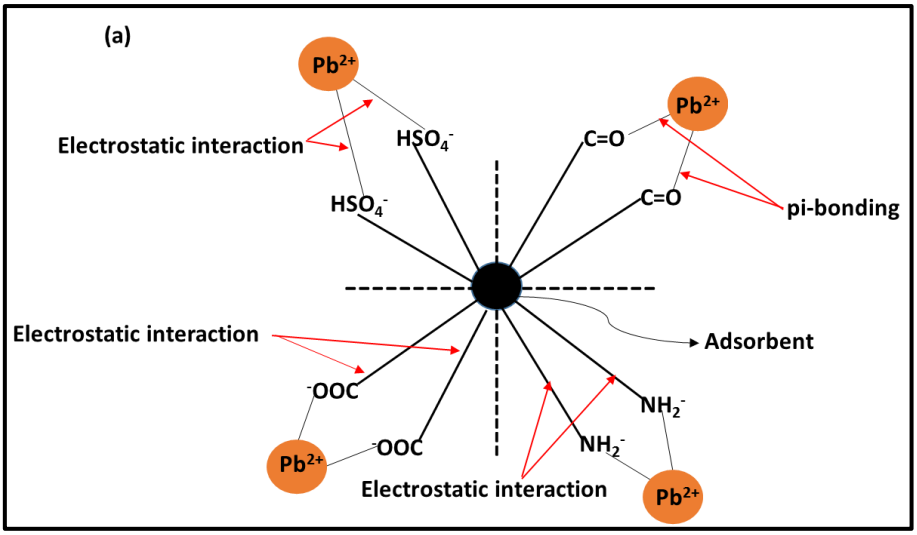

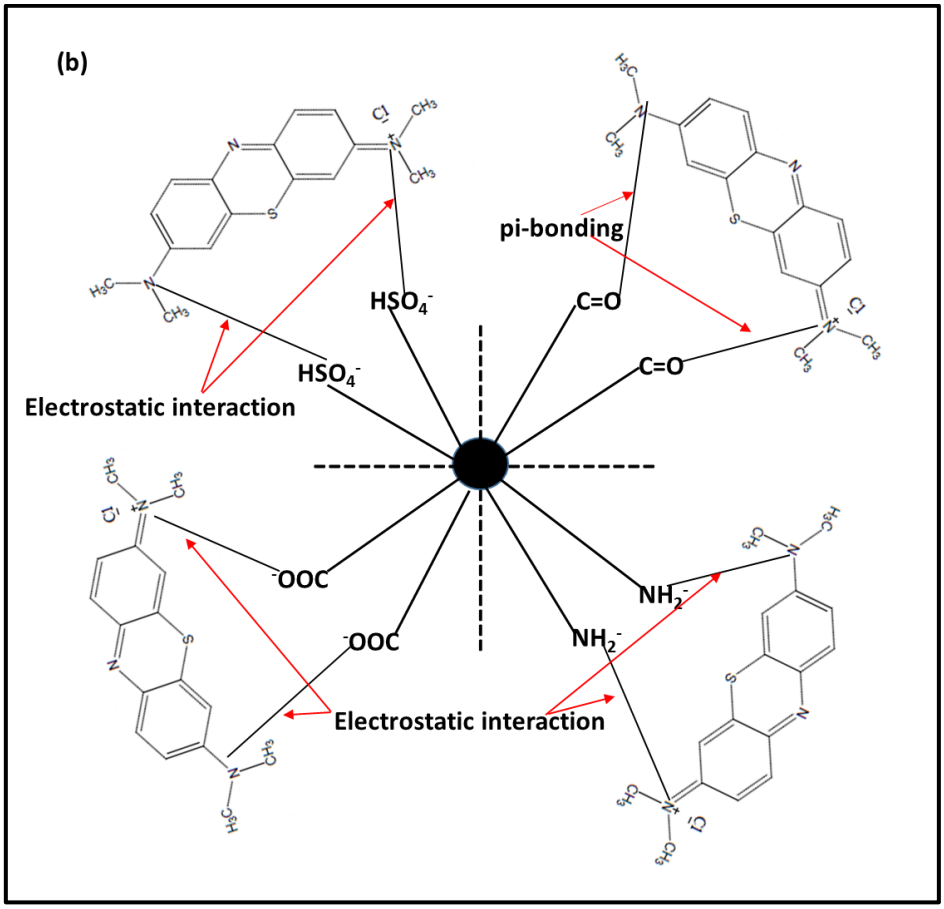

Scheme 4: Propose pathway for (a) Pb(II) ions and (b) MB dye interaction with the adsorbents.

7.7.1.3 XRD analysis

The X-ray diffraction spectra of BCC, BCAC-10 and BCAC-20 are shown in Fig. 44. The broad peak at 2θ value of 21° from BCC is assigned to crystalline lignocellulose content in the adsorbent and this peak disappeared for BCAC-10 and BCAC-20. New peaks were observed on BCAC-20 at 26 and 59° these peaks are assigned to amorphousness of the adsorbent.

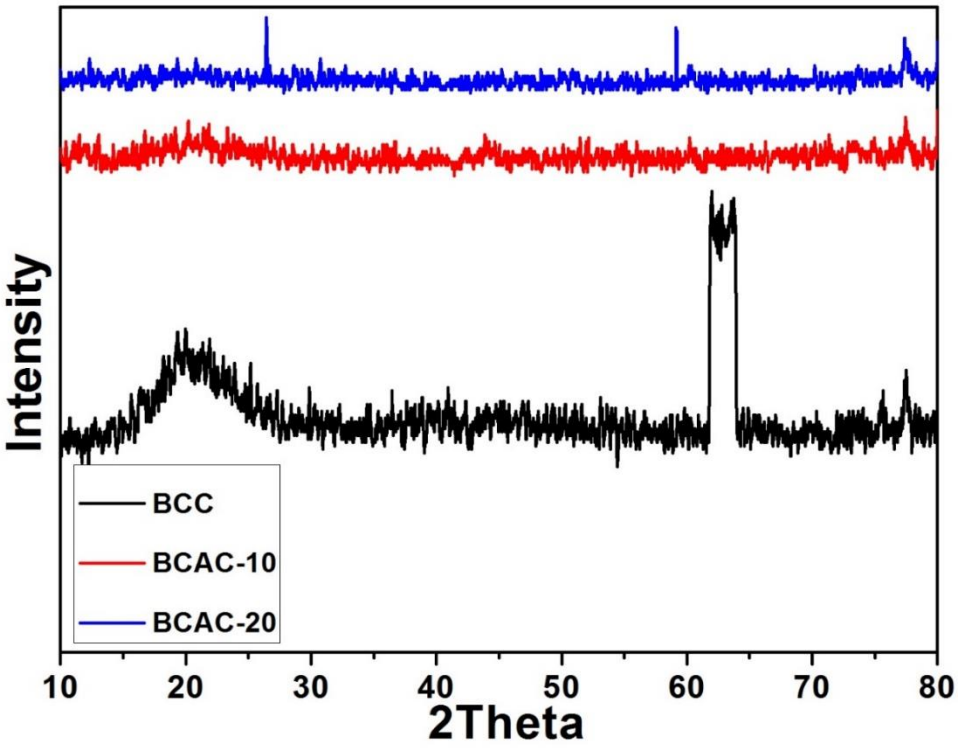

Figure 44: XRD spectra of BCC, BCAC-10 and BCAC-20 adsorbents.

7.7.1.1 TGA analysis

Fig. 45 shows the TGA profiles of the adsorbents which were conducted in nitrogen atmosphere. The profile shows that there are two decomposition steps. The first weight loss of BCC, BCAC-10 and BCAC-20 is observed between 30 and 198 °C. This loss is due to the adsorbed moisture on the surface. The adsorbents weight loss percentages are 2,1 and 2 % for

BCC, BCAC-10 and BCAC-20 respectively. The major weight is between 198-487 °C which is due to cellulose, lignin and hemicellulose (Ceylan & Topcu, 2014) and the percentages of 80, 79 and 78 %. The long tailing after major weight loss between 498-891°C, represented decomposition of the residues formed during disintegration of lignocellulose.

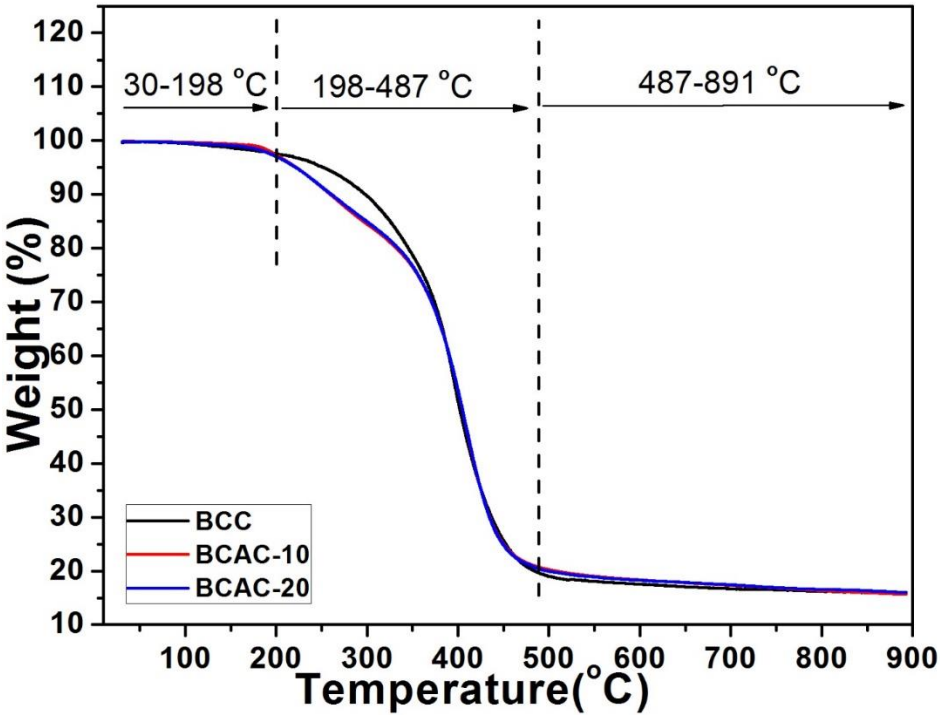

Figure 45: TGA of BCC, BCAC-10 and BCAC-20 adsorbents.

7.7.2 Adsorption studies

7.7.2.1 Concentration effect and modeling studies

The adsorption capacity of BCC, BCAC-10 and BCAC-20 was studied at different initial concentrations (20, 40, 60, 80 and 100 mg/L) at constant temperature of 298 K for Pb(II) ions and MB dye in aqueous solution are plotted in Figs. 46a-b. The trend for Pb(II) ions adsorption increased with increasing initial concentration of the solution, that is greater uptake was observed in solutions with higher initial concentration. Therefore the adsorption capacities of

Pb(II) ions was greater in solutions with initial concentration of 100 mg/L it was 17.19, 17.71 and 17.98 mg/g onto BCC, BCAC-10 and BCAC-20 respectively compared to adsorption capacities of solutions with initial concentration of 20 mg/L it was 17.07, 17.45 and 17.46 mg/g respectively. This might be due to that, at initial concentration 100 mg/L solution, collision chances between Pb(II) ions and the adsorbent surface are greater, and this is associated with high mass transfer (Aichour et al. 2019). The same trend was observed for MB dye, adsorption capacity increased with increasing initial concentration of the solution. Therefore, the adsorption capacities of MB dye were greater in solutions with initial concentration of 100 mg/L. It was 11.63, 12.71 and 16.85 mg/g onto BCC, BCAC-10 and BCAC-20 respectively compared to adsorption capacities of solutions with initial concentration of 20 mg/L which was 10.13, 10.83 and 15.22 mg/g respectively. The maximum adsorption capacity trend for Pb(II) ions was BCAC-10>BCAC-20>BCC whilst adsorption capacity trend for MB was BCAC-20 > BCAC-10> BCC.

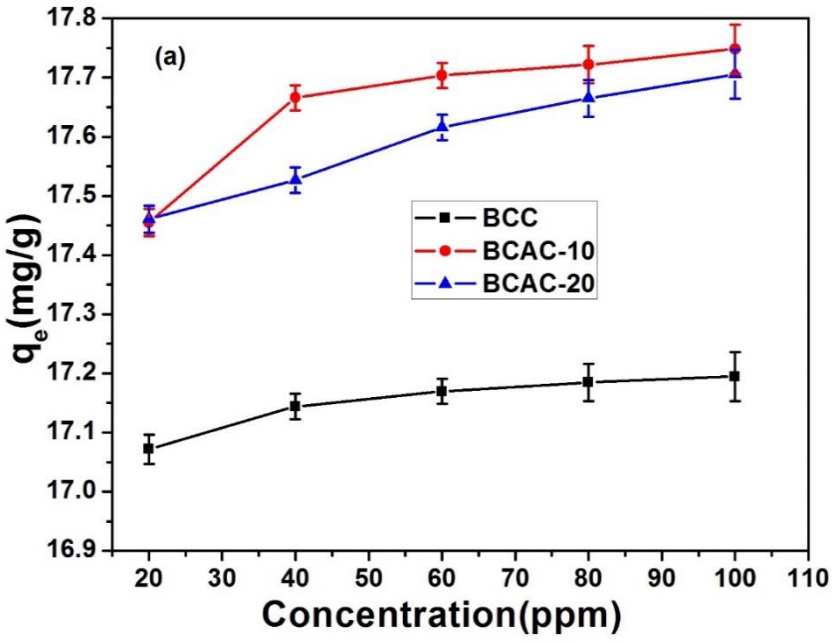

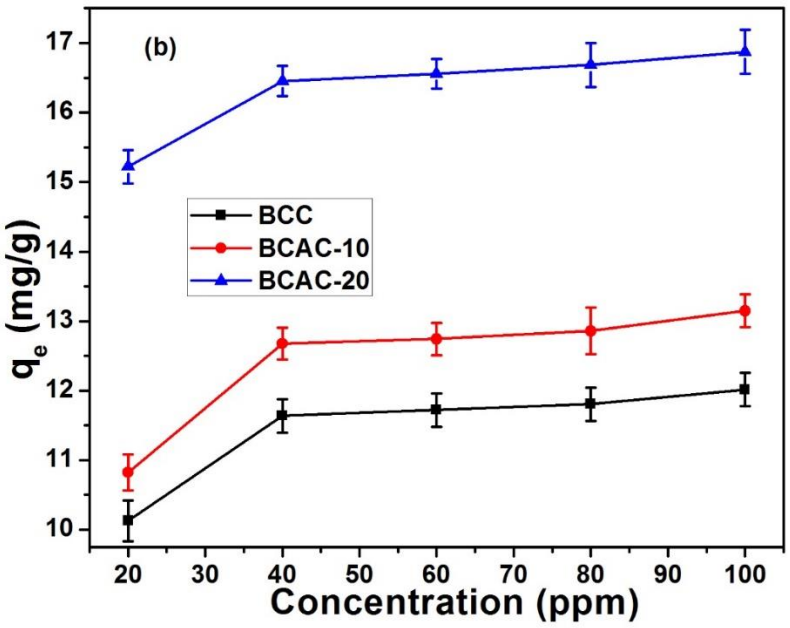

Figure 46: Concentration effect of (a) Pb(II) ions and (b) MB dye adsorption Onto BCC, BCAC-10 and BCAC-20 adsorbents [Experimental conditions: volume of solution (20 mL), time (60 min), adsorbent dosage (0.1 g), temperature of the system (298 K), agitation rate (200 rpm), pH of solutions during Pb(II) ions and MB dye sorption (4.8)]

Different isotherms; Langmuir and Freundlich as shown in Table 14 were used to determine equilibrium data obtained at 298 K in order to determine capacity and interaction behavior of BCC, BCAC-10 and BCAC-20. The data in Table 14 show that it fitted Freundlich isotherm model with (r^2) values close to 1. The model suggests that the process involves multi-layer adsorption with interactions between the adsorbate and the adsorbents, this also implies heterogeneous nature of the adsorbent surface. Langmuir isotherm models could not be used to explain the adsorption process.

Table 14: Isotherms studies and their parameters.

Isotherms		BCC		BCAC-10		BCAC-20	
		Pb(II)	MB	Pb(II)	MB	Pb(II)	MB
Langmuir	**Q_o**	14.32	16.24	15.70	18.56	12.37	26.32
	B	0.79	2.17	0.77	1.09	0.56	1.09
	r^2	0.91	0.91	0.90	0.90	0.90	0.90
Freundlich	**1/n**	15.81	12.25	11.70	34.72	22.37	15.31
	k_f	0.128	0.109	0.100	0.106	0.813	2.401
	r^2	0.99	0.99	0.99	0.99	0.99	0.99
Experimental (q_e)		17.16	11.71	17.75	12.68	17.54	16.56

7.7.2.2 Effect of contact time and kinetic studies of cations removal from aqueous solution

The effect of time was determined in order to evaluate the rate at which pollutants are adsorbed. The efficiency of the adsorbents (BCC, BCAC-10 and BCAC-20) was evaluated using the time intervals of 5, 10, 15, 20, 30, 40, 60, 90 and 120 min as shown in Figs. 47a-b. Fig.47a shows a rapid uptake of Pb(II) ions within from 5-10 min for BCC, 5-15 min for BCAC-10 and BCAC-20 thereafter equilibrium was reached. The uptake capacity of BCAC-10 towards Pb(II) ions was greater than BCAC-20 and BCC. Similarly, for MB dye as indicated in Fig.47b with uptake was rapid from 5-15 min for BCC and BCAC-10 whilst BCAC-10 reached 20 min. In both instances the results show that there was a fast adsorption at the beginning due to the available active sites being accessible on the surface of the adsorbents and after certain time the adsorption becomes slow because of saturation of the active sites (Aichour & Zaghouane, 2019a).

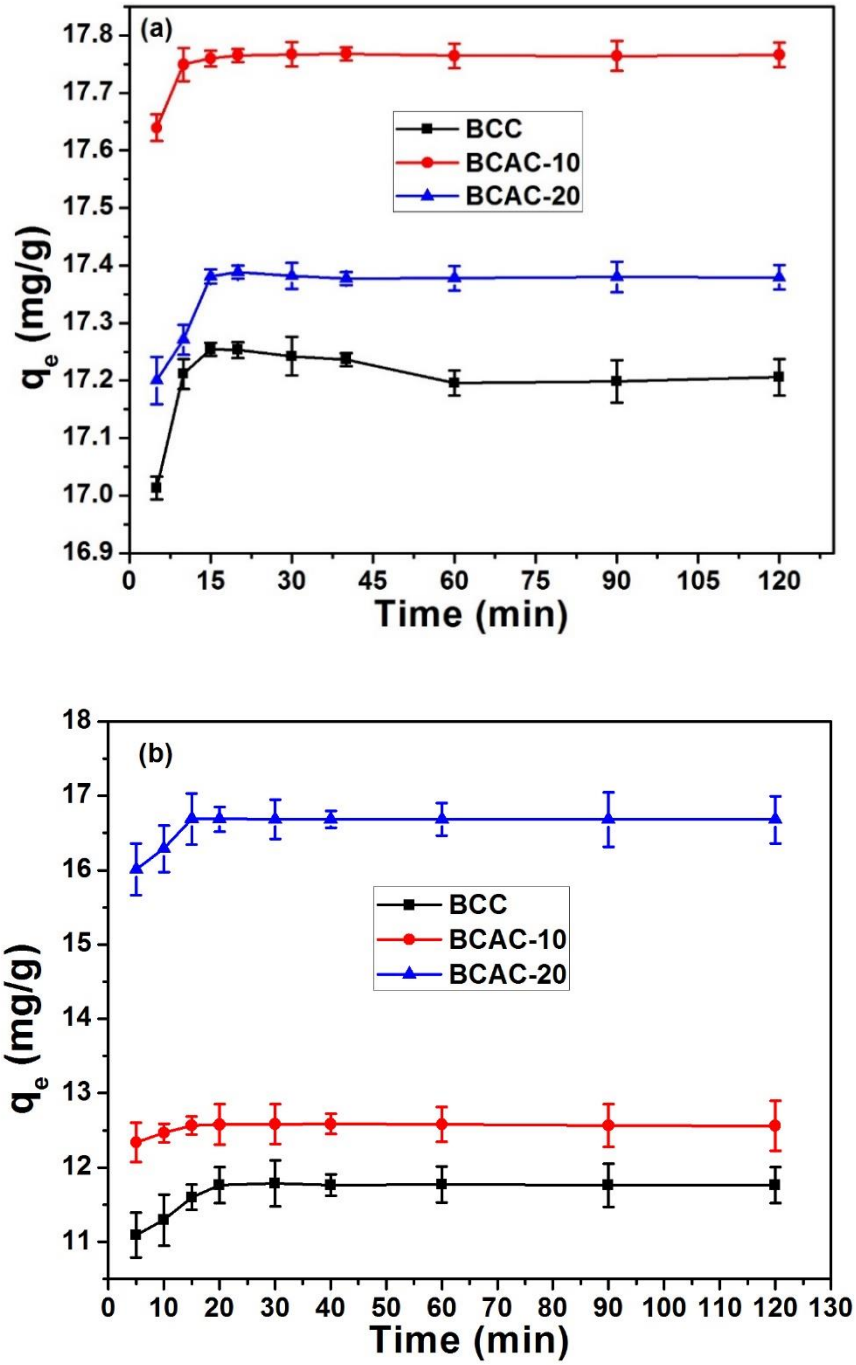

Figure 47: Time effect of (a) Pb(II) ions and (b) MB dye adsorption Onto BCC, BCAC-10 and BCAC-20 adsorbents. [Experimental conditions: volume of solution (20 mL), concentration (100 ppm), adsorbent dosage (0.1 g), temperature of the system (298 K), agitation rate (200 rpm), pH of solutions during Pb(II) ions and MB dye sorption (4.8)]

The kinetic data (Table 15) of Pb(II) ions and MB dye removal onto BCAC-20, BCAC-10 and BCC was studied using pseudo first order (PFO), pseudo second order (PSO), and intra particle diffusion (IPD) models. In order to determine whether the adsorption had a good fit for the PFO or PSO it requires that the values of coefficient of determination r^2 to be close to 1 and the values of adsorption capacity (q_e) need to be close to the experimental values. The data show that the adsorption of Pb(II) ions and MB dye onto BCC best fitted PFO model with (r^2) values of 0.99 including both BCAC-10 and BCAC-20. The calculated capacities (q_e) values were closer to the obtained experimental values for PFO (BCC) and PSO for BCS-10 and BCAC-20. The adsorption mechanism of PFO suggests that Pb(II) and MB onto BCC involves Van der Waal forces attraction. Unlike adsorption of Pb(II) ions and MB dye onto BCAC-10 and BCS-20, PSO indicates that the adsorption process was dependent on the availability of the adsorption sites. The nature of the process was evaluated using IPD kinetic model which determines whether adsorption takes place on the surface (ESA) or pores (EPA). The data in table 2 shows that the (EPA) for Pb(II) ions onto BCC, BCAC-10 and BCAC-20 was 65.85, 94.28 and 78.43 % respectively and the remaining was due to (ESA). The MB dye (EPA) onto BCC, BCAC-10 and BCAC-20 was 73.37, 70.82 and 95.74 % respectively.

Table 15: Kinetic models and their parameters

Models		**BCC**		**BCAC-10**		**BCAC-20**	
		Pb(II)	**MB**	**Pb(II)**	**MB**	**Pb(II)**	**MB**
PFO	$\mathbf{q_e}$	16.08	11.89	16.25	13.31	16.25	16.61
	$\mathbf{K_1}$	0.82	3.63	3.11	3.43	3.22	3.08
	$\mathbf{r^2}$	0.99	0.99	0.90	0.90	0.90	0.99
PSO	$\mathbf{q_e}$	14.71	84.28	39.11	12.94	33.37	17.91
	$\mathbf{K_2}$	0.071	0.024	0.090	0.060	0.077	0.060
	$\mathbf{r^2}$	0.88	0.89	0.99	0.99	0.99	0.99

IPD	**C**	11.34	5.96	11.79	8.74	11.77	8.22
	K_i	1.95	1.71	1.54	1.12	1.81	0.082
	r^2	0.98	0.93	0.98	0.95	0.99	0.98
EPA[a]	**%**	65.85	73.37	94.28	70.82	78.43	95.74
ESA[a]	**%**	34.14	46.63	35.71	29.18	31.56	49.26
Experimental (q_e)		17.22	11.78	17.20	12.58	17.38	16.68

7.7.2.3 Temperature effect and thermodynamic studies

The effect of temperature was evaluated at (298 K), (303 K), (313 K), (333 K) and (353 K). The obtained experimental data for Pb(II) ions and MB dye was plotted as shown in Figs. 48a-b respectively. The results of BCC, BCAC-10 and BCAC-20 for both Pb(II) ions and MB dye show that there increase in adsorption capacities as the temperature increases. The plot in Fig. 48a indicated that as temperature increased from 298 K to 313 K, the adsorption capacity of Pb(II) ions also increased for BCC and BCAC-20, however for BCAC-10 the temperature increased up to 333 K before reaching equilibrium. This indicated that the adsorption of Pb(II) ions and MB dye was through chemisorption (Jin et al. 2019). Fig. 48b showed that the adsorption of MB dye increased with increasing temperature (298- 313 K) of BCC, BCAC-10 and BCAC-20.

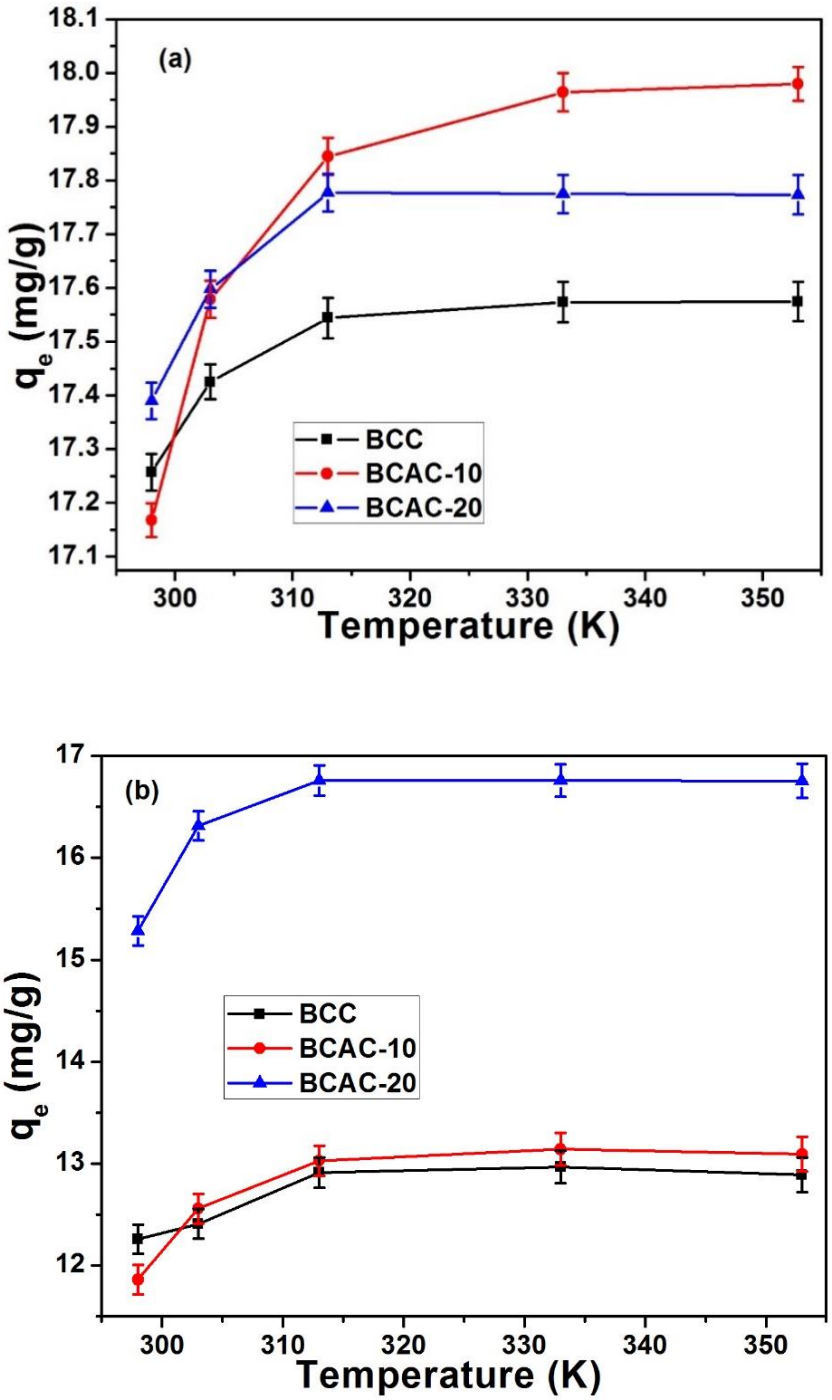

Figure 48: Temperature effect of (a) Pb(II) ions and (b) MB dye adsorption Onto BCC, BCAC-10 and BCAC-20 adsorbents. [Experimental conditions: volume of solution (20 mL), time (60 min), adsorbent dosage (0.1 g), concentration (100 ppm), agitation rate (200 rpm), pH of solutions during Pb(II) ions and MB dye sorption (4.8)]

The thermodynamic parameters; enthalpy *(ΔH°)*, Gibbs free energy *(ΔG°)* and entropy *(ΔS°)* were determined at different temperatures (298, 303, 313, 333 and 353 K) for Pb(II) ions and MB dye onto BCC, BCAC-10 and BCAC-20 as shown in Table 16. The calculated enthalpy *(ΔH°)* gave positive values. This indicated that the adsorption of Pb(II) ions and MB dye on the adsorbents was endothermic process. (*ΔS°*) gave positive values which indicates the randomness and degree of freedom for Pb(II) ions and MB dye in aqueous solution during the adsorption process. The Gibb's free energy (*ΔG°*) values for MB dye and Pb(II) ions show negative values for BCC, BCAC-10 and BCAC-20 at different temperatures which implies that the process of Pb(II) ions and MB dye adsorption has physical characteristics and spontaneous (Oussalah et al. 2019).

Table 16: Thermodynamic studies and their parameters

Parameter	**BCC**		**BCAC-10**		**BCAC-20**	
	Pb(II)	**MB**	**Pb(II)**	**MB**	**Pb(II)**	**MB**
ΔH^o (KJ mol^{-1})	2.9×10^{-3}	1.9×10^{-2}	1.5×10^{-3}	2.4×10^{-3}	3.3×10^{-3}	1.9×10^{-3}
ΔS^o (KJ mol^{-1}K^{-1})	4.10×10^{-3}	3.7×10^{-3}	1.6×10^{-3}	6.0×10^{-4}	4.6×10^{-3}	3.7×10^{-3}
ΔG^o (KJ mol^{-1}) 298 K	-0.57	-0.31	-0.41	-2.84	-0.90	-0.51
303 K	-0.76	-0.27	-0.93	-2.81	-0.96	-0.81
313 K	-0.93	-0.25	-1.31	-2.62	-1.22	-0.88
333 K	-1.03	-0.26	-1.57	-2.76	-1.29	-0.92
353 K	-1.09	-0.28	-1.69	-2.97	-1.37	-0.93

7.7.2.4 pH effect on the adsorption

Figs. 49a-b show the effect of pH studied at pH 1, 3, 5, 7 and 9. The adsorption of Pb (II) ions and MB dye was largely dependent of pH. The adsorption capacities of BCC, BCAC-10, BCAC-20 towards Pb(II) ions and MB dye steadily increases with increasing pH. This could be due to the fact that at low pH (1-5) the surface of the adsorbent is protonated resulting in increased repulsion force between positively charged Pb(II)/MB dye (Aichour et al. 2018). However, as the pH of the solution is increased to pH (7), the surface is progressively been deprotonated that is, enhancing the attractive forces between the adsorbent and Pb(II)/MB dye. At pH (9) the surface was totally deprotonated, hence the adsorption capacities reached maximum for Pb(II) and MB dye. The increase in negative charges of the adsorbent surface improved forces of attraction.

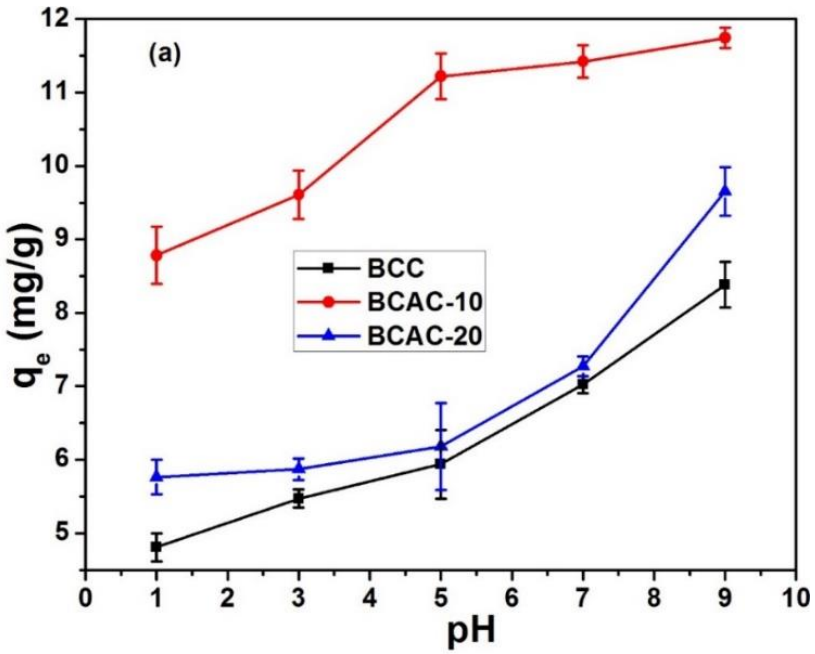

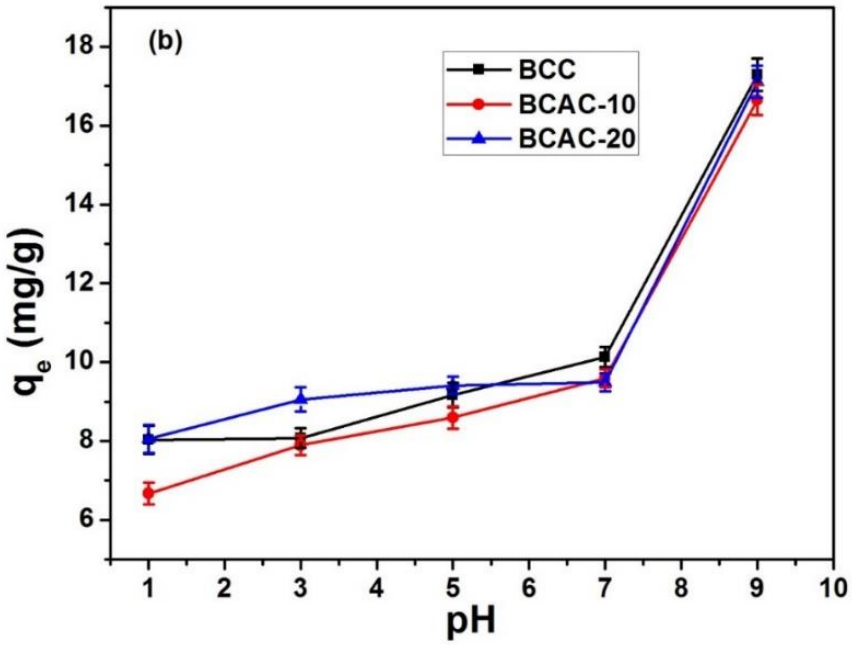

Figure 49: pH effect of (a) Pb(II) ions and (b) MB dye adsorption Onto BCC, BCAC-10 and BCAC-20 adsorbents. [Experimental conditions: volume of solution (20 mL), time (60 min), adsorbent dosage (0.1 g), temperature (298 K), agitation rate (200 rpm), concentration (100 ppm)]

7.7.2.5 Physicochemical studies of the adsorbents

pH and $pH_{(pzc)}$ are two important parameters that directly affect the adsorption of metal ions and dyes in aqueous solution, they determine the charge state of the adsorbent (Bardestani et al. 2019). The $pH_{(pzc)}$ plots of ΔpH vs. pH_i of adsorbents are shown in Fig 50. From the plots the point of $pH_{(pzc)}$ of BCC, BCAC-10, and BCAC-20 is 6.22, 2.10 and 2.00 respectively. It is shown that ΔpH values are negative before $pH_{(pzc)}$ values of 2.00, 2.10 and 6.22 for BCAC-20, BCAC-10 and BCC respectively. This indicates that the adsorbents surface acquired negative charge from initial pHi until $pH_{(pzc)}$. pH values above $pH_{(pzc)}$ 2.00, 2.10 and 6.22 show the adsorbents surface acquired positive charge and ΔpH values became positive. The values of pH_{pzc} show that the surface of BCC, BCAC-10 and BCAC-20 are acidic. At pH of solution

above pH_{pzc} values adsorbents are cation attractors whereas for pH values lower they repel cations (Aichour et al 2018). The tabulated BET data (Table 17) shows that the surface area of BCC was 11.67 m^2/g whilst BCAC-10 and BCAC-20 show 20.14 and 21.54 m^2/g respectively. BCAC-20 show larger pore width of 7.13 nm compared to 6.81 and 3.78 nm for BCAC-10 and BCC respectively. The results show that there is an increase in surface area and pore size for both BCAC-10 and BCAC-20 in comparison with BCC.

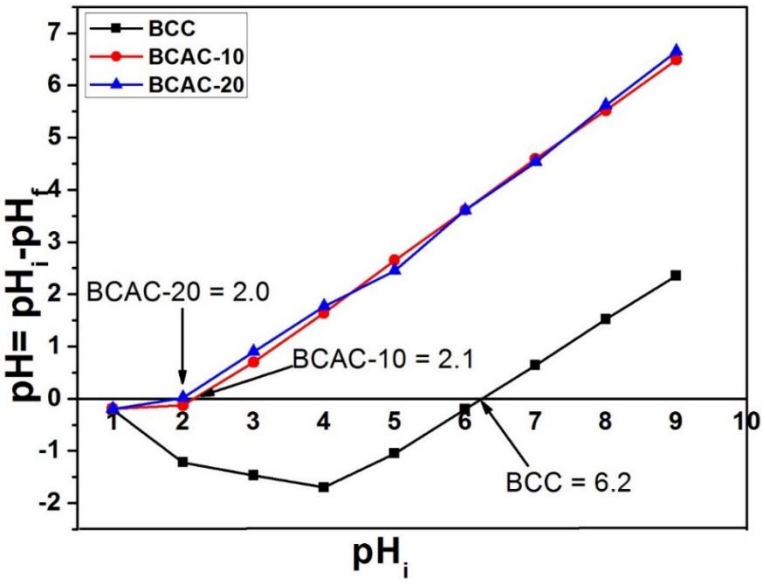

Figure 50: Point zero charge of adsorbents. [Experimental conditions: volume of solution (20 mL), time (720 min), adsorbent dosage (0.1 g), temperature (298 K), agitation rate (200 rpm), concentration (100 ppm)].

Table 17: Physicochemical parameters of the adsorbents

Adsorbent	**$pH_{(PZC)}$**	**BET surface area (m^2/g)**	**Pore size (cm^2/g)**	**Pore width (nm)**
BCC	6.22	11.67	0.0153	3.78
BCAC-10	2.10	20.14	0.0195	6.81

BCAC-20	2.00	21.54		0.0236	7.13

7.7.3 Regeneration and reusability

The regeneration of BCC, BCAC-10 and BCAC-20 was conducted by taking 0.1 g of the pre-used carbonized adsorbent. The adsorbed Pb(II) ions and MB dye were removed from adsorbent surface by agitating twice in 20 mL of 0.3 M HNO_3 for 30 min at 200 rpm and then rinsed several times with ultra-pure water at 200 rpm for 60 min before reuse. The reusability study of BCC, BCAC-10 and BCAC-20 was conducted in order to establish if black cumin seeds adsorbents are economically beneficial. The adsorption/desorption results of the used and regenerated black cumin seeds adsorbents of three cycles are shown in Figs. 51a-b. The results show that the first adsorption cycle recorded for both Pb(II) ions and MB dye the highest adsorption percentage. However, the following adsorption cycles decreased slightly in adsorption capabilities. The highest adsorption observed in the first cycle was due to abundant active sites and pores. However the lower adsorption observed in cycle 2 and 3 was because of incapability of desorbing the previously adsorbed Pb(II) ions and MB dye during regeneration.

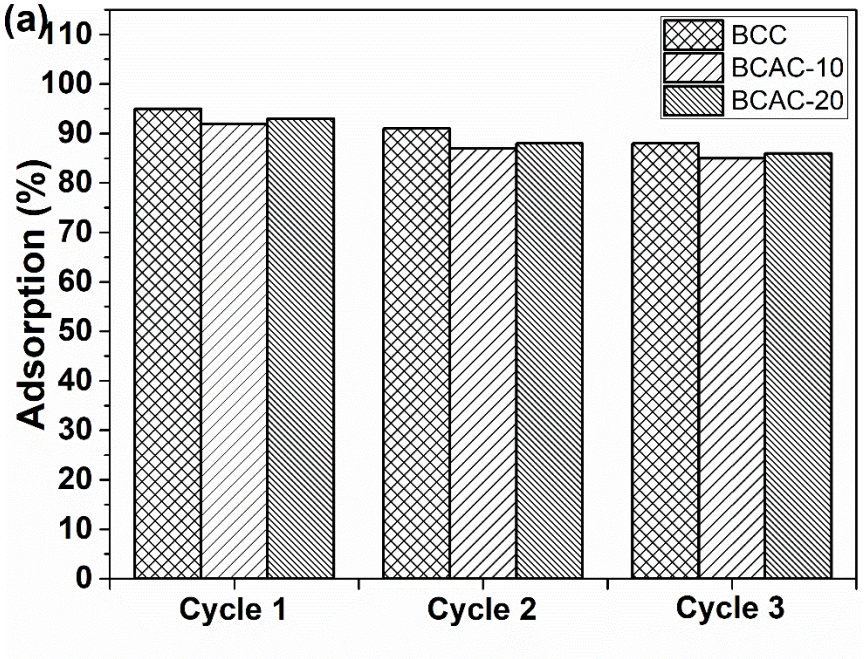

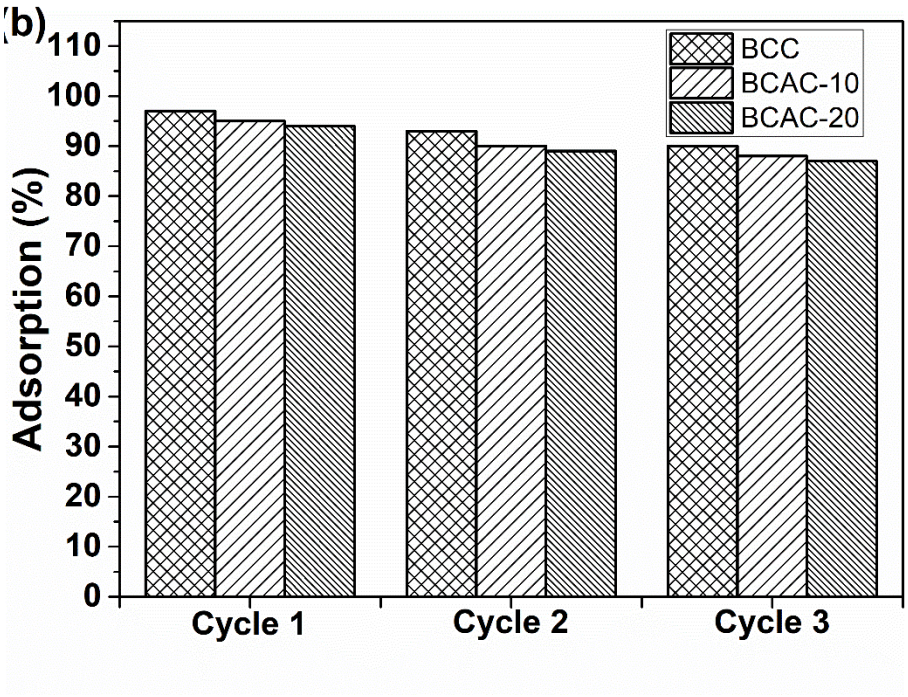

Figure 51: Reusability studies of the adsorption of (a) Pb(II) ions and (b) MB dye [Experimental conditions: volume of solution (20 mL), time (60 min), adsorbent dosage (0.1 g), temperature (298 K), agitation rate (200 rpm), concentration (100 ppm), pH(5)].

7.7.4 Comparative study

The presented information in Table 18 shows the previously adsorption capacities of some of the reported adsorbents in literature compared with activated black cumin seeds. The data shows that activated black cumin seeds can be used for adsorption of Pb(II) ions and MB dye.

Table 18: Adsorption capacities of different adsorbents for Pb(II) ions

Adsorbent	Maximum capacity (mg/g)	Dosage (g)	Solution pH	Temperature (°C)	Reference
Apricot stone	21.38	0.1	6	20	Mouni et al. 2011
Avocado seeds	18.20	0.15	5	25	Boeykens et al. 2019
Black cumin seeds	17.98	0.1	4.8	25	This study
Seed powder	16.42	0.1	5	28	Jayaram & Prasad, 2009
Aspergillus flavus	13.46	0.1	5	25	Akar & Tunali, 2006

Peanut shell	11.41	1.0	5	25	Lee et al. 2019
Oak wood	10.10	1.0	5	25	Mohan et al. 2007
Wood	7.90	0.5	5	25	Bardestani et al. 2019
Carbon nanotubes	7.10	0.2	7	25	Mahar et al. 2019

Adsorption capacities of different adsorbents for MB

Adsorbent	**Maximum capacity (mg/g)**	**Dosage (g)**	**Solution pH**	**Temperature (°C)**	**Reference**
Commercial AC	21.50	1	7	20	Yener et al. 2008
Black cumin seeds	16.85	0.1	4.8	25	This study
Sunflower oil cake	16.43	0.2	6	25	Karago et al. 2008
Morocca cactus	14.04	1	5	25	Sakr et al. 2019
Freeze-dried agarose	10.40	1	5	25	Seow & Hauser, 2016
Rice husk	9.83	0.5	7	30	Sharma & Uma, 2010
Glass wool	8.82	1	9	35	Chakrabati & Dutt, 2005
Hyacinth root powder	8.04	1	8	25	Soni et al. 2019
Leaginous microalga,S	7.80	100	7	25	Chandra et al. 2015

7.7.5 Conclusion

The effectiveness of carbonization and activation of black cumin seeds was evaluated for the removal of Pb(II) ions and methylene blue (MB) dye from aqueous solution. A series of adsorption experiments were conducted as a function of concentration, time, temperature and pH. The batch experiments indicated that the adsorption of Pb(II) ions and MB was influence by the pH of the solution. It was found that the adsorption capacity for Pb(II) ions and MB dye increased with increasing initial concentration of the solutions. The results show that the adsorption processes were rapid between 5-20 min. The temperature data showed that the sorption of Pb(II) ions and MB dye on all adsorbents increased with increasing temperature. The adsorption kinetics were well described by pseudo-first order for the carbonized black

cumin (BCC) seeds and pseudo-second order for the activated carbon of 10 and 20 % H_2SO_4 (BCAC-10 and BCAC-20). Freundlich isotherm data defined the equilibrium better than Langmuir model which suggested heterogeneous nature of the adsorbent surfaces. The results of this study show the feasibility of BCC, BCAC-10 and BCAC-20 adsorbents as alternative for removing Pb(II) ions and MB dye from aqueous solution.

7.7.6 Acknowledgement

We acknowledge the supports of National Research Fund-NRF (TTK190403426819) for funding this work and the Department of Chemistry, Vaal University of Technology, Vanderbiljpark, South Africa.

References

ADDALA, A., BELATTAR, N. & ELEKTOROWICZ, M., 2018. Nigella Sativa L. seeds biomass as a potential sorbent in sorption of lead from aqueous solutions and wastewater. *Oriental Journal of Chemistry,* 34, 638-647.

AHMAD, R. & HASEEB, S., 2014. Black Cumin Seeds (BCS): a non-conventional adsorbent for the removal of Cu (II) from aqueous solution. *Desalination and Water Treatment,* 1-10.

AICHOUR, A. & ZAGHOUANE-BOUDIAF, H., 2019a. Highly brilliant green removal from wastewater by mesoporous adsorbents: Kinetics, thermodynamics and equilibrium isotherm studies. *Microchemical Journal,* 146, 1255-1262.

AICHOUR, A. & ZAGHOUANE-BOUDIAF, H., 2019b. Single and competitive adsorption studies of two cationic dyes from aqueous mediums onto cellulose-based modified citrus peels/calcium alginate composite. *International Journal of Biological Macromolecules,* 154, 1227-1236.

AICHOUR, A., ZAGHOUANE-BOUDIAF, H., IBORRA, C.V. & POLO, M.S., 2018. Bioadsorbent beads prepared from activated biomass/alginate for enhanced removal of cationic dye from water medium: Kinetics, equilibrium and thermodynamic studies. *Journal of Molecular Liquids,* 256, 533-540.

AICHOUR, A., ZAGHOUANE-BOUDIAF, H., ZUKI, F.B.M., AROUA, M.K. & IBBORA, C.V., 2019a. Low-cost, biodegradable and highly effective adsorbents for batch and column fixed bed adsorption processes of methylene blue. *Journal of Environmental Chemical Engineering*, 7, 103409.

AKAR, T. & TUNALI, S., 2006. Biosorption characteristics of Aspergillus flavus biomass for removal of Pb(II) and Cu(II) ions from an aqueous solution. *Bioresource Technology,* 97, 1780-1787.

ALGUREIRI, A.H. & ABDULMAJEED, Y.R., 2016. Removal of heavy metals from industrial wastewater by using RO membrane. *Iraqi Journal of Chemical and Petroleum Engineering*, 17, 125-136.

BAI, C.X., SHEN, F.& QI, X.H., 2017. Preparation of porous carbon directly from hydrothermal carbonization of fructose and phloroglucinol for adsorption of tetracycline. *Chinese Chemical Letters,* 28, 960-962.

BAI, Y. & BARTKIEWICZ, B., 2009. Removal of Cadmium from wastewater using ion exchange resin Amberjet 1200H Columns. *Polish Journal of Environmental Studies*, 18, 1191-1195.

BARBOOTI, M., ABID, B.A. & AL-SHUWAIKI, N.M., 2011. Removal of heavy metals using chemicals precipitation. *Journal of Engineering and Technology*, 29, 595-612.

BARDESTANI, R., ROY, C. & KALIAGUINE, S., 2019. The effect of biochar mild air oxidation on the optimization of lead(II) adsorption from wastewater. *Journal of Environmental Management*, 240, 404-420.

BOEYKENS, S.P., REDONDO, N., OBESO, R.A., CARACCIOLO, N. & VAZQUEZ, C., 2019. Chromium and lead adsorption by avocado seed biomass study through the use of total reflection X-Ray fluorescence analysis. *Applied Radiation and Isotopes*, 153, 108809.

BOUYANFIF, A., LIYANAGE, S., HEWITT, J.E., VANAPALLI, S.A., MOUSTAID-MOUSSA, N., HEQUET, E. & ABIDI, N., 2017. FTIR imaging detects diet and genotype dependent chemical composition changes in wild type and mutant C. elegans strains.

CEYLAN, S. & TOPCU, Y., 2014. Pyrolysis kinetics of hazelnut husk using thermogravimetric analysis. *Bioresource. Technology*, 156, 182-188.

CHAKRABARTI, S. & DUTTA, B.K., 2005. On the adsorption and diffusion of methylene blue in glass fibers. *Journal of Colloid and Interface Science*, 286, 807-811.

CHAND, P. & PAKADE, Y.B., 2013. Removal of Pb from water by adsorption on apple pomace: equilibrium, kinetics, and thermodynamics studies. *Journal of Chemical Science*, 1-8.

CHANDRA, T. S., MUDLIAR, S.N., VIDYASHANKAR, S., MUKHERJI, S., SARADA, R., KRISHNAMURTHI, K. & CHAUHAN, V.S., 2015. Defatted algal biomass as a non-conventional low-cost adsorbent: Surface characterization and methylene blue adsorption characteristics. *Bioresource Technology*, 184, 395-404.

CHAUDHRY, S. A., ZAIDI, Z. & SIDDIQUI, S. I., 2017. Isotherm, kinetic and thermodynamics of arsenic adsorption onto Iron-Zirconium Binary Oxide-Coated Sand (IZBOCS): Modelling and process optimization. *Journal of Molecular Liquids*, 229, 230-240.

CHAUDHRY, S.A., AHMED, M., SIDDIQUI, S.I. & AHMED, S., 2016. Fe(III)-Sn(IV) mixed binary oxide-coated sand preparation and its use for the removal of As(III) and As(V) from water: Application of isotherm, kinetic and thermodynamics. *Journal of Molecular Liquids*, 224, 431-441.

CHERUIYOT, G.K., WANYONYI, W.C., KIPLIMO, J.J. & MAINA, E. N., 2019. Adsorption of toxic crystal violet dye using coffee husks: equilibrium, kinetics and thermodynamics study. *Scientific African*, 5, 1-11.

CID, A.A.P., HERNANDEZ, V.R., GONZALEZ, A.M.H., HERNANDEZ, A.B. & ALONSO, O.C., 2019. Synthesis of activated carbons from black sapote seeds, characterization and application in the elimination of heavy metals and textile dyes. *Chinese Journal of Chemical Engineering*.

DARGAHI, A., GOLESTANIFAR, H., DARVISHI, P., KARAMI, A., HASAN, S.H., POORMOHAMMADI, A. & BEHZADNIA, A., 2016. An Investigation and Comparison of Removing Heavy Metals (Lead and Chromium) from Aqueous Solutions Using Magnesium Oxide Nanoparticles. *Polish Journal of Environmental Studies*, 25, 557-562.

ENENEBEAKU, C.K., OKOROCHA, N.J., ENENEBEAKU, U.E. & ONYEACHU, B.I., 2011. Adsorption of methylene blue dye onto bush cane bark powder. *International Letters of Chemistry, Physics and Astronomy*, 76, 12-26.

Environmental Protection Agency, 2001, Parameters of water quality interpretation and standards.

JANKOVIC, B., MANIC, N., DODEVSKI, V., RADOVIC, I., PIJOVIC, M., KATNIC, D. & TASIC, G., 2019. Physico-chemical characterization of carbonized apricot kernel shell as precursor for activated carbon preparation in clean technology utilization. *Journal of Cleaner Production*, 236, 1-15.

JAYARAM, K. & PRASAD, M.N.V., 2009. Removal of Pb(II) from aqueous solution by seed powder of prosopis juliflora DC. *Journal of Hazardous Materials*, 169, 991-997.

JIN, Y., ZENG, C., LU, Q-F. & YU, Y., 2019. Efficient adsorption of methylene blue and lead ions in aqueous solutions by 5-sulfosalicylic acid modified lignin. *International Journal of Biological Macromolecules,* 123, 50-58.

KARAGO, S., TAY, T., UCAR, S. & ERDEM, M., 2008. Activated carbons from waste biomass by sulfuric acid activation and their use on methylene blue adsorption. *Bioresource. Technology,* 99, 214-222.

KRISHNAMOORTHY, R., GOVINDAN, B., BANAT, F., SAGADEVAN, V., PURUSHOTHAMAN, M. & SHOW, P.L., 2019. Date pits activated carbon for divalent lead ions removal. *Journal of Bioscience and Bioengineering,* 128, 88-97.

KUMAR, P.S., SARAVANAN, A., KUMAR, K.A., YASHWANTH, R. & VISVESH, S., 2016. Removal of toxic zinc from water/wastewater using eucalyptus seeds activated carbon: non-linear regression analysis. IET Nanobiotechnology. 10, 244-253.

KUMARIA, U., BEHERAA, S.K., SIDDIQI, H. & MEIKAP, B.C., 2020. Facile method to synthesize efficient adsorbent from alumina by nitric acid activation: Batch scale defluoridation, kinetics, isotherm studies and implementation on industrial wastewater treatment. *Journal of Hazardous Materials*, 381, 20917.

LEE, M.E., PARK, J.H. & CHUNG, J.W., 2019. Comparison of the lead and copper adsorption capacities of plant source materials and their biochars. *Journal of Environmental Management*, 236, 118-124.

LI J. & JANG, M., 2013. Kinetic study of esterification of sulfuric acid with alcohols in aerosol bulk phase. *Atmospheric Chemistry and Physics*, 13, 23217-23250.

MAHAR, F.K., HE, L., WEI, K., MEHDI, M., ZHU, M., GU, J., ZHANG, K., KHATRI, Z. & KIM, I., 2019. Rapid adsorption of lead ions using porous carbon nanofibers. *Chemosphere*, 225, 360-367.

MOHAN, D., PITTMAN JR, C.U., BRICKA, M., SMITH, F., YANCEY, B., MOHAMMAD, J., STEELE, P.H., ALEXANDRE-FRANCO, M.F., GOMEZ-SERRANO, V. & GONG, H., 2007. Sorption of arsenic, cadmium, and lead by chars produced from fast pyrolysis of wood and bark during bio-oil production. *Journal of Colloid and Interface Science*, 310, 57-73.

MOUNI, L., MERABET, D., BOUZAZA, A. & BELKHIRI, L., 2011. Adsorption of Pb(II) from aqueous solutions using activated carbon developed from Apricot stone. *Desalination*, 276, 148-153.

MOYO, M., CHIKAZAZA, L., NYAMUNDA, B.C. & GUYO, U., 2013. Adsorption batch studies on the removal of Pb(II) using maize tassel based activated carbon. *Journal of Chemical Science*.

OLIVEIRA, R.N., MANCINI, M.C., OLIVEIRA, F.C.S., PASSOS, T.M., QUILTY, B., THIRE, R.M.S. & McGuinness, G.B., 2016. FTIR analysis and quantification of phenols and flavonoids of five commercially available plants extracts used in wound healing. *Revista Materia*, 21, 767-779.

OS, A., IA, A., KO, I. & OO, A., 2006. Coagulation/flocculation process in the removal of trace metals present in industrial wastewater. *Journal of Applied Sciences & Environmental Management*,10, 159-162.

OSAKWE, C.E., SANNI, I., SAID, S. & ZUBAIRU, A., 2014. Adsorption of heavy metals from wastewaters using Adonosia digitata fruit shells and Theobroma cacao pods as adsorbents: a comparative study. *Assumption University Journal of Technology*, 18(1), 11-18.

OUSSALAH, A., BOUKERROUI, A., AICHOUR, A. & DJELLOULI, B., 2019. Cationic and anionic dyes removal by low-cost hybrid alginate/ natural bentonite composite beads: Adsorption and reusability studies. *International Journal of Biological Macromolecules*, 124, 854-862.

SEOW, W.Y. & HAUSER, C.A.E., 2016. Freeze-dried agarose gels: A cheap, simple and recyclable adsorbent for the purification of methylene blue from industrial wastewater. *Journal of Environmental Chemical Engineering*, 4, 1714-1721.

SHARMA, Y.C. & UMA, 2010. Optimization of parameters for adsorption of methylene blue on a low-cost activated carbon. J*ournal of Chemical and Engineering Data*, 55, 435-439.

SHOOTO, N.D., NKUTHA, C.S., GUILANDE, N.R. & NAIDOO, E.B., 2019b. Pristine and modified mucuna beans adsorptive studies of toxic lead ions and methylene blue dye from aqueous solution. *South African Journal of Chemical Engineering*, 31.

SHOOTO, N.D., THABEDE, P.M. & NAIDOO, E.B., 2019a. Simultaneous adsorptive study of toxic metal ions in quaternary system from aqueous solution using low cost black cumin seeds (Nigella sativa) adsorbents. *South African Journal of Chemical Engineering*, 30, 15-27.

SIDDIQUI, S.I. & CHAUDHRY, S.A., 2018a. A review on graphene oxide and its composites preparation and their use for the removal of $As^{3+}$and As^{5+} from water under the effect of various parameters: Application of isotherm, kinetic and thermodynamics. *Process Safety and Environmental Protection*, 119, 138-163.

SIDDIQUI, S.I. & CHAUDHRY, S.A., 2018b. Nigella sativa plant-based nanocomposite-$MnFe_2O_4$/BC: An antibacterial material for water purification. *Journal of Cleaner Production*, 200, 996-1008.

SIDDIQUI, S.I. & CHAUDHRY, S.A., 2019. Nanohybrid composite Fe_2O_3-ZrO_2/BC for inhibiting the growth of bacteria and adsorptive removal of arsenic and dyes from water. *Journal of Cleaner Production*, 223, 849-868.

SIDDIQUI, S.I., MANZOOR, O., MOHSIN, M. & CHAUDHRY, S.A., 2019c. Nigella sativa seed based nanocomposite-MnO_2/BC: An antibacterial material for photocatalytic degradation, and adsorptive removal of methylene blue from water. *Environmental Research*, 171, 328-340.

SIDDIQUI, S.I., NAUSHAD, M. & CHAUDHRY, S.A., 2019a. Promising prospects of nanomaterials for arsenic water remediation: A comprehensive review. *Process Safety and Environmental Protection*, 126, 60-97.

SIDDIQUI, S.I., RATHI, G. & CHAUDHRY, S.A., 2018. Acid washed black cumin seed powder preparation for adsorption of methylene blue dye from aqueous solution: thermodynamic, kinetic and isotherm studies. *Journal of Molecular Liquids*, 264, 275-284.

SIDDIQUI, S.I., ZOHRA, F. & CHAUDHRY, S.A., 2019b. Nigella sativa seed based nanohybrid composite-Fe_2O_3-SnO_2/BC: A novel material for enhanced adsorptive removal of methylene blue from water. *Environmental Research*, 178, 108667.

SOLEIMANI, H., MAHVI, A.H., YAGHMAEIAN, K., ABBASNIA, A., SHARAFI, K., ALIMOHAMMADI, M. & ZAMANZADEH, M., 2019. Effect of modification by five different acids on pumice stone as natural and low-cost adsorbent for removal of humic acid from aqueous solutions-application of response surface methodology. *Journal of Molecular Liquids*, 290, 1-13.

SONI, M., SHARMA, A.K., SRIVASTAVA, J.K. & YADAV, J.S., 2012. Adsorptive removal of methylene blue dye from an aqueous solution using water hyacinth root powder as a low-cost adsorbent. *International Journal of Chemical Sciences*, 3, 338-345.

THACI, B.S. & GASHI, S.T., 2018. Reverse osmosis removal of heavy metals from wastewater effluents using biowaste materials pretreatment. *Polish Journal of Environmental Studies*, 28, 337-341.

TORRES-CABAN, R., VEGA-OLIVENCIA, C.A., ALAMO-NOLE, L., MORALES-IRIZARR, D., ROMAN-VELAZQUEZ, F. & MINA-CAMILDE, N., 2019. Removal of

copper from water by adsorption with calcium-alginate/spent-coffee-grounds composite beads. *Materials,* 12, 1-21.

VAN THUAN, T., QUYNH, B.T.P., NGUYEN, T.D., HO, V.T.T. & BACH, L.G., 2017. Response surface methodology approach for optimization of Cu^{2+}, Ni^{2+} and Pb^{2+} adsorption using KOH-activated carbon from banana peel. *Surfaces and Interfaces,* 6, 209-217.

WANG, H., YAO, Q., WANG, C., FAN, B., SUN, Q., JIN, C. & XIONG, Y., 2016. A simple, one-step hydrothermal approach to durable and robust superparamagnetic, superhydrophobic and electromagnetic wave-absorbing wood. *Scientific Reports*. 6, 35549-35558.

WANG, J. & CHEN, C., 2009. Biosorbents for heavy metals removal and their future. *Biotechnology Advances,* 27, 195-226.

WANG, S., NING, H., HU, N., HUANG, K., WENG, S., WU, X., WU, L., ALAMUSI, J.L., 2019. Preparation and characterization of graphene oxide/silk fibroin hybrid aerogel for dye and heavy metal adsorption. *Composites Part A,* 163, 716-722.

WHO, 2018, Lead Poisoning and Health, Jee. Report World Health Organization.

WU, Y. & WANG, L., 2016. Kinetic and thermodynamic studies of the biosorption of Ni(II) by modified rape straw. *Procedia Environmental Sciences*, 31, 75-80.

YARKANDI, N.H., 2014. Removal of lead (II) from waste water by adsorption. *International Journal of Current Microbiology and Applied Sciences*, 3, 207-228.

YENER, J., KOPAC, T., DOGU, G. & DOGU, T., 2008. Dynamic analysis of sorption of Methylene Blue dye on granular and powdered activated carbon. *Chemical Engineering Journal*, 144, 400-406.

YU, D., WANG, L.& WU, M., 2018. Simultaneous removal of dye and heavy metal by banana peels derived hierarchically porous carbons. *Journal of the Taiwan Institute of Chemical Engineers*, 93, 543-553.

ZBAIR, M., AHSAINE, H.A., ANFAR, Z. & SLASSI. A., 2019. Carbon microspheres derived from walnut shell: Rapid and remarkable uptake of heavy metal ions, molecular computational study and surface modeling. *Chemosphere*, 231, 140-150.

ZEWAIL, T.M. & YOUSEF, N.S., 2015. Kinetic study of heavy metal ions removal by ion exchange in batch conical air spouted bed. *Alexandria Engineering Journal*, 54, 83-9.

ZHANG, W., ZHOU, C., ZHOU, W., LEI, A., ZHANG, Q., WAN, Q. & ZOU, B., 2011. Fast and considerable adsorption of methylene blue dye onto graphene oxide. *Bulletin of Environmental Contamination and Toxicology*, 87, 86-90.

CHAPTER 8

Magnetite functionalized Nigella Sativa seeds for the uptake of chromium(VI) and lead(II) ions from synthetic wastewater

This chapter is published as follows:

Patience Mapule Thabede, Ntaote David Shooto, Thokozani Xaba, Eliazer Bobby Naidoo. 2021. Magnetite functionalized *Nigella Sativa* seeds for the uptake of chromium(VI) and lead(II) ions from synthetic wastewater. Adsorption Science and Technology 2021.6655227.

This chapter is addressing objective (e) which reads as follows:

To functionalized black cumin seeds using sucrose and iron oxide to form composites for the removal of Cr(VI) and Pb(II) ions in aqueous solution. Thereafter, conduct adsorption studies under different parameters (temperature, concentration, time and pH).

8.1 Abstract

The aim of the present study was to utilise pristine and magnetite-sucrose functionalized *Nigella Sativa* seeds as the adsorbents for the uptake of chromium(VI) and lead(II) ions from synthetic wastewater. Prestine *Nigella Sativa* seeds were labelled (PNS) and magnetite-sucrose functionalized *Nigella Sativa* seeds (FNS). The PNS and FNS composites were characterized by Fourier-transform infrared spectroscopy (FTIR), and X-ray powder diffraction (XRD). The FTIR analysis of both adsorbents revealed the presence of vibrations assigned to 1749 and 1739 cm^{-1} (-C=O) for ketonic group for both adsorbents. The amide (-NH) peak was observed at 1533 and 1527 cm^{-1} on FNS and PNS composites respectively whilst the carboxyl group (-COOH) were observed at 1408 cm^{-1} on both adsorbents. The XRD results of FNS and PNS composites showed a combination of spinel structure and *y*-Fe_2O_3 phase confirming the formation of iron oxide. The influence of operational conditions such as initial concentration, temperature, pH and contact time were determined in batch adsorption system. The kinetic data of Cr(VI) and Pb(II) ions on both adsorbents was described by pseudo-first order (PFO) model which suggested physisorption process. The sorption rate of Cr(VI) ions was quicker, it attained equilibrium in 20 min and the rate of Pb(II) ions was slow and reached equilibrium in 90 min. Freundlich isotherm described the mechanism of Pb(II) ions adsorption on PNS and FNS composites. Langmiur best fitted the uptake of Cr(VI) ions adsorption on PNS and FNS. The results for both adsorbents showed that the removal uptake of Pb(II) ions increased when the initial concentration was increased however, Cr(VI) uptake decreased when the initial concentration increased. The adsorption of Cr(VI) and Pb(II) ions on both adsorbents increased with temperature. The objective of this study is to investigate if magnetite-sucrose functionalized *Nigella Sativa* seeds has the ability to adsorb chromium(VI) and lead(II) ions from aqueous water.

Keywords: sorption, sucrose, *Nigella Sativa*, batch adsorption, composite

8.2 Introduction

Chromium compounds find their way into the natural water stream as a consequence of the industrialization and improper disposal of wastes which is usually from leather tanning, metal finishing, electroplating and pigments industries (Gueye et al., 2014). Hexavalent chromium is one of the most contaminant that has attracted extensive attention among researchers due to its toxicity**.** Shupack (1991) indicated that hexavalent chromium Cr(VI) species may occur in different ionic forms namely; chromate (CrO_4^{2-}), dichromate ($Cr_2O_7^{2-}$) or hydrogen chromate ($HCrO_4^-$) in aqueous solution meanwhile Cr(III) tends to form hydrated species such as hydrated trivalent chromium $[Cr(H_2O)_6]^{3+}$, chromium hydroxide complexes $[Cr(OH)(H_2O)_5]^{2+}$ or $Cr(OH)_2(H_2O)$. According to Dehghani et al. (2016), Cr(III) species are fairly less toxic as compared to Cr(VI) which is extremely toxic. The World Health Organisation (WHO) has restricted the limit of Cr(VI) to 0.05 mg/L in drinking water (Li et al. 2020a). On the other hand Chand & Pakade, (2013) reported that industries release effluent from batteries, automobiles manufacturing units and paint which contain lead Pb(II) ions. Pb(II) is one of the most toxic ions found in industrial wastewater (Alguacil et al. 2018). The presence of lead Pb(II) ions in water is another major concern because it affects human health, aquatic animals, peripheral nervous system, anaemia, loss of appetite, vomiting, severe abdominal pain and paralysis in the muscles (Chand & Pakade, 2013; Alguacil et al. 2018). Pb(II) is a slow, malicious, but most evil poison, any contact with the body, may result it replacing calcium on the bones and accrues in the skeletal system (Puzas et al. 2004). World Health Organization (WHO) assessment document indicated the safe level for lead ion concentration in blood to be 0.1 gm^{-3} (Bardestani et al. 2019).

Treatment of contaminated water using nanoparticles/composites materials has been investigated by other researches because magnetic composite adsorbents has become desirable materials for separating the loaded pollutant adsorbents from water post adsorption and also centrifugation and filtration can be time consuming and a costly process (Diagboya & Dikio, 2018; Abdulla et al. 2019). Particles of hydroxides and iron oxides occurs in natural aquatic system and can adsorb anions and cations from aqueous system due to surface defects besides high magnetic character (Zang et al. 2019). The following composites were used as adsorbents for removing different toxic ions in water. Some of the composites are; catalytic oxidation and adsorption of Cr(III) on iron-manganese nodules under toxic conditions (Hai et al., 2020), hematite iron oxide nanoparticles (α-Fe_2O_3): synthesis and modelling adsorption of malachite green (Dehbi et al. 2020), boron removal and reclamation by magnetic magnetite (Fe_3O_4) nanoparticle: an adsorption and isotopic separation study (Chen et al. 2020) and scavenging of aqueous toxic organic and inorganic cations using novel facile magneto-carbon black-clay composite adsorbent (Diagboya & Dikio, 2018).

However, there are few studies where composite material using *Nigella Sativa* seeds as adsorbents have been investigated. Some of these studies are; *Nigella Sativa* plant-based nanocomposite-$MnFe_2O_4$/BC: an antibacterial material for water purification (Siddiqui & Chaudhry, 2018) with maximum adsorption capacity of 10.07 mg/g for methylene blue. Nanohybrid composite Fe_2O_3-ZrO_2/BC for inhibiting the growth of bacteria and adsorptive removal of arsenic and dyes from water (Siddiqui & Chaudhry, 2019), the results showed that the removal of As(II) was 1.01 and 38.10 mg/g for methylene blue. *Nigella Sativa* seed based nanohybrid composite-Fe_2O_3-SnO_2/BC: A novel material for enhanced adsorptive removal of methylene blue from water (Siddiqui et al. 2019a) with maximum adsorption capacity between 58.82-84.74 mg/g and *Nigella Sativa* seed-based nanocomposite-MnO_2/BC: An antibacterial

material for photocatalytic degradation, and adsorptive removal of methylene blue from water which showed adsorption capacity of 185 mg/g (Siddiqui et al. 2019b).

Sucrose is a natural disaccharide which is formed from the combination of glucose and fructose (Vadi &Najafi, 2011). Kuznetsov et al. (2010) functionalized nanocarbons by one-step process of fluorine substitution reaction with sucrose-derived lithium monosucrate. This was achieved by sonication in dimethylyformamide at room temperature. Their results showed that sucrose bonded on the surface of the fluorinated nanoancarbons using covalent bonding. Functionalization of multi-walled carbon nanotubes (MWCNTs) with D-sucrose carbohydrate was done by Mallakpour & Behranvand, (2016) in water at room temperature. Their aim was to investigate the influence of sucrose on MWCNTs surface and morphology using poly amide-imide (PAI) nanocomposites. Obark & Obark, (2019) investigated the capability of activated carbon for the removal of chromium(VI) ions by adding sucrose in the adsorption as an organic matter.

Technologies can be more effective if and when the adsorbent could be prepared easily, cost effectively and effective for range of pollutants. They should also be effective for the removal of high and low level of pollutants (Santhosh et al. 2014). Also, WHO (World Health Organization) emphasised on the investigation of medicinal plant species for human care system benefit (Datta et al. 2012). Therefore, the present work was made to prepare a material, with low cost, which can remove chromium(VI) and lead(II) ions from aqueous solution. Plant materials are abundant, sustainable and may provide oxygenous groups which can interact with charged pollutants from water without harming water quality (Pugazhendhi et al. 2018). Black Cumin seeds (BCS) (*Nigella Sativa*) is used as home medicine and has bitter taste and smell (Ahmad & Haseeb, 2014). It is used primarily in confectionery and liquors as well for medicinal purposes. The efficiency of *Nigella Sativa* was investigated for adsorption by seeing

the challenges continuing in toxic ions removal and the benefits offered by the biomasses (Siddiqui et al. 2018). These seeds are readily available, inexpensive, and have a number of oxygenous groups (carboxyl and hydroxyl) at the surface, which make them advantageous for the adsorption technology (Al Jassir, 2005). Some studies available in the literature have shown that *Nigella Sativa* material has been used for the adsorption studies. However, there is a need for some type of modifications in order to get more important results for the removal of water contaminants (Siddiqui et al. 2017). Accommodation of nanoparticles onto adsorbent surface and large number of functional groups of the material can provide the large vacant sites to nanocomposite for charged pollutants (Siddiqui & Chaudhry, 2017). Inorganic nanomaterials have shown unique and extra ordinary properties for numerous applications including adsorption (Niasari et al. 2009; Esmaili et al. 2011). The preparation of such material is eco-friendly, has low production cost and non-toxic, this can be a better solution for water treatment. In view of these facts, magnetite was incorporated into the *Nigella Sativa* powder for the formation of magnetite *Nigella Sativa* seeds then functionalized with sucrose for chromium(VI) and lead(II) ions adsorption from aqueous solution.

Sucrose is an inexpensive, commercially available and easily renewable carbon source (Sivadas et al. 2016). Zhou et al. (2017) used magnetic ceramsite coated by functionalized nano carbon spheres. Their study shows that using ceramsite without functionalization had low porosity, insufficient active site and low adsorption capacity for the removal of Cr(VI). To improve the adsorption capacity, ceramsite was functionalized with magnetic nano carbon spheres using sucrose. Their study also showed that there was an increased removal of Cr(VI) with increased concentration of sucrose. Synthesis of graphene sand composite was achieved with the use of a sucrose (Dubey et al. 2015). Their composite exhibited a maximum adsorption capacity of 106.2 mg/g for the removal of Cr(VI) at pH 1.5. Mesoporous carbon was obtained

by (Goscianska et al. 2015) using a silica material as a template and sucrose as a carbon precursor for the adsorption of anionic azo dyes. The results showed that adsorption of dyes ranged from 128-172 mg/g. Bedin et al. (2016) prepared activated carbon from sucrose for the adsorption of methylene blue dye. Their work showed that the use of sucrose in conjunction with chemical activation (KOH) to synthesize activated carbon had a high adsorption capacity (704 mg/g) for methylene blue. Thus, the use of sucrose as one way of modifying the adsorbents may improve adsorption capacity for the removal of toxic ions and dyes.

Previous work on *Nigella Sativa* seeds showed that the material has good removal uptake towards pollutants in water. Therefore, it is fair to conduct further studies on the material. Hence the purpose of the present study was to develop functionalized *Nigella Sativa* seeds with enhanced removal uptake towards Cr(VI) and Pb(II) ions. In this study the seeds were incorporated with sucrose and iron oxide to produce a composite material. The magnetic-sucrose functionalized *Nigella Sativa* (FNS) composite was a one step process done at room temperature. Incorporation of sucrose and iron oxide has proven to enhance the adsorption capacity of the other materials; however, no document was found that investigated this for *Nigella Sativa* seeds.

8.3 Reagents and experimental

8.3.1 Reagents

Sucrose ($C_{12}H_{22}O_{11}$), Iron(II) chloride ($FeCl_2 \cdot 4H_2O$), Iron (III) chloride ($FeCl_3 \cdot 6H_2O$), sodium thiosulfate ($Na_2S_2O_3$), potassium dichromate $K_2Cr_2O_7$, lead nitrate $Pb(NO_3)_2$ were purchased Sigma-Aldrich, Johannesburg, South Africa. Other chemicals like ammonium hydroxide (NH_4OH), sodium hydroxide (NaOH), sodium nitrate ($NaNO_3$) and hydrochloric acid (HCl),

were purchased at Associated Chemical Enterprises, Johannesburg, South Africa. Unprocessed *Nigella Sativa* seeds were procured from health shop in Vanderbijlpark, South Africa.

8.3.2 Preparation of pristine *Nigella Sativa* (PNS) composite

100 g of pristine *Nigella Sativa seeds* were weighed thereafter rinsed in distilled water several times to get rid of dust and dirt. The seeds were dried in an oven at 40 °C for 24 hr. After drying the seeds were grounded with a mortar and piston. The grounded seeds were sieved on 60/200 mesh in order to get particle sizes ranging from 0.8-1 mm. the sieved pristine *Nigella Sativa* seeds were labelled (PNS).

8.3.3 Preparation of the sucrose functionalized *Nigella Sativa* (FNS) composite

Pristine *Nigella Sativa* (PNS) seeds (10 g) were poured in a beaker and 0.5 % sucrose solution (50 mL) was mixed with the seeds. The sucrose functionalized *Nigella Sativa* (FNS) was stirred for 2 hrs. Thereafter $FeCl_3$ (5 g) was added which was allowed to mix for 3 hrs followed by 5 g of $FeCl_2$. A 10 mL of 25 % NH_4OH solution was added. When the solution become homogenous 5 g $Na_2S_2O_3$ was added into the mixture. The resultant black yellowish magnetic FNS composite was continuously stirred for 3 hrs. The obtained product was rinsed with distilled water and dried for 24 hrs at 40 °C. The prepared composite is shown in scheme 5.

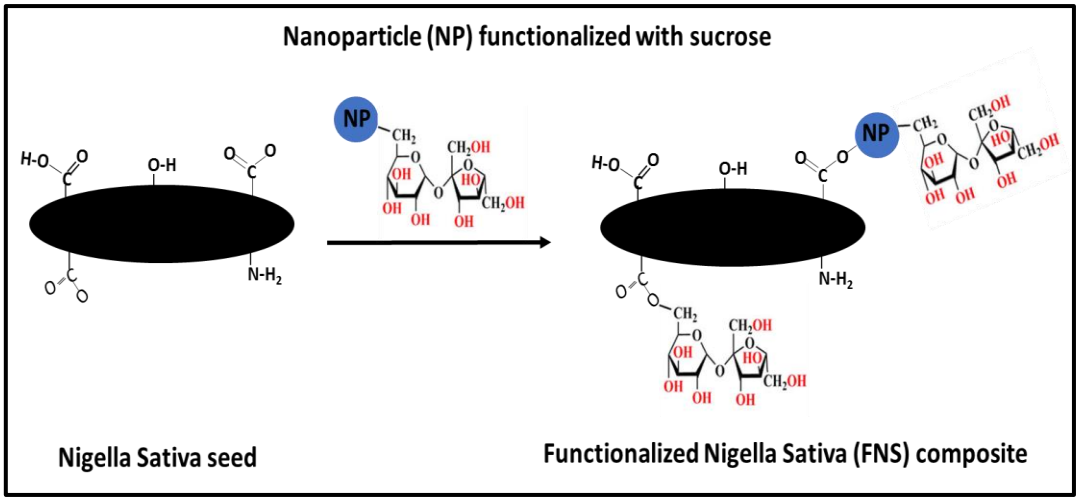

Scheme 5: Schematic of sucrose functionalized *Nigella Sativa* seeds (FNS) preparation

8.4 Batch adsorption studies

To better understand the adsorption behaviour of the adsorbents a number of batch studies were conducted to investigate the effect of pH, initial concentration, contact time and temperature. Lead nitrate and potassium dichromate were used to prepare the stock solutions of 100 mg/L. A 0.1 g of the adsorbent and 40 mL of the working standard solutions were transferred to 100 mL capped plastic tubes. The solutions were then placed on a shaker for 60 min. Thereafter, the composites were separated by centrifugation for 5 min at 5000 rpm. For all the parameters the supernatant was used for the analysis. The effect of pH was studied at 1, 3, 5, 7 and 9 using a standard solution of 100 mg/L and stirred for 60 min. Other adsorption studies conducted were time effect at 1, 5, 10, 15, 20, 30, 60, 90 and 120 min (using the same standard solution concentration for all other parameters). The effect of temperature was conducted at 298, 303, 313, 333 and 353 K whilst the concentration was studied at 20, 40 60, 80 and 100 mg/L. The solution pHs ranging from 1-9 were adjusted by adding 0.1 M NaOH for basic medium and 0.1 M HCl for acidic medium. Thereafter the adjusted pH solutions were added to 0.1 g adsorbents and agitated at 200 rpm for 24 hrs. The point of zero charge (pH_{pzc}) determination of FNS and PNS was conducted using 1M $NaNO_3$.

8.5 Data analysis

The percentage removal of Cr(VI) and Pb(II) ions from aqueous solution onto FNS and PNS composites surface was determined by using the following equation (1) and (2) (Behjati et al. 2018):

$$q_e = \frac{(C_o - C_e)\,V}{W} \quad (1)$$

$$\%R = \frac{(C_o - C_e)}{C_o} \text{ x } 100 \quad (2)$$

where C_o and C_e (mg/L) are initial and equilibrium concentrations of Cr(VI) and Pb(II) ions and q_e adsorption capacity (mgg^{-1}) and %R (%) of FNS and PNS composites at equilibrium. The volume of the solution and mass of the adsorbents are labelled (v) in L and (w) in g respectively.

8.5.1 Adsorption isotherm models

In order to better understand the interaction between the Cr(VI) and Pb(II) ions and the adsorbents surface, concentrations data were used in nonlinear isotherm models namely; Langmuir (3) (Langmuir 1918) and Freundlich (4) isotherms (Freundlich 1906).

$$q_e = \frac{Q_o b C_e}{1 + bC_e} \quad (3)$$

$$q_e = k_f C_e^{1/n} \quad (4)$$

(Q_o) represent Langmuir maximum adsorption capacity (in mg/g), (b) is the interaction energy related constant, where Ce (mgL^{-1}), (k_f) is Freundlich capacity factor constant and (1/n) represent isotherm linearity parameter constant.

8.5.2 Adsorption kinetics

Various kinetic models namely; pseudo-first order (PFO), pseudo-second order (PSO) rate models (Ho & McKay, 1999) and intra-particle diffusion (IPD) (Weber et al. 1963) nonlinear equations as shown in equations (5), (6) and (7) respectively, were used on the obtained experimental data of Cr(VI) and Pb(II) ions at different time intervals.

$$q_e = q_t(1 - e^{-k_1 t}) \quad (5)$$

$$q_e = \frac{1 + k_2 q_e t}{k_2 q_e^2 t} \quad (6)$$

$$q_t = k_i\left(t^{1/2}\right) + C \quad (7)$$

Where (q_e) and (q_t) represent the amounts removed (in mg/g) at time (t). (k_1), (k_2) and (k_i) are the rate constants of PFO (in min^{-1}), PSO (in g mg^{-1} min^{-1}) and IPD (in g g^{-1} $min^{1/2}$) respectively. (C) Represents the concentration of Cr(VI) and Pb(II) ions at equilibrium.

8.5.3 Thermodynamic functions

The investigation of the adsorption process was evaluated using thermodynamics calculation of enthalpy change (ΔH^o), entropy change (ΔS^o), Gibb's free energy change (ΔG^o) and the equilibrium constant (K_c) were determined at 298, 303, 313, 333 and 353 K by means of equations (8), (9) and (10) (Liu & Zhang, 2009).

$$In\ K_c = -\frac{\Delta H^o}{RT} - \frac{\Delta S^o}{R} \quad (8)$$

$$\Delta G^o = -RT\ In\ K_c \quad (9)$$

$$K_c = \frac{q_e}{C_e} \quad (10)$$

8.6 Instrumentation

The FNS and PNS composites were analysed for phase composition through the X-ray diffraction (XRD) with anode of Cu (Bruker, λ= 1.5406 Å) Shimadzu XRD 7000. The samples were scanned at 2θ=10-70° with a scan rate of 10 °/min. Thermo Fischer Scientific Fourier transform infrared (FTIR) spectroscopy was used to determine the spectra sorption materials from 4000 to 400 cm^{-1}. Atomic absorption spectroscopy (AAS) Shimadzu ASC 7000 with air-acetylene flame and auto sampler was used to determine the remaining Cr(VI) and Pb(II) ions in aqueous solutions.

8.7 Results and discussion

8.7.1 Characterization of the adsorbents

8.7.1.1 FTIR results

The FTIR spectra of prepared FNS and PNS composites characteristics absorption peaks at various wavenumbers ranging from 3238 to 812 cm^{-1} are shown in Fig.52a. The broad peaks around 3228 and 1625 cm^{-1} were attributed to hydroxyl (-OH) groups (Abdulla et al. 2019) on FNS composite. These groups shifted to higher frequency of 3238 and 1631 cm^{-1} on PNS composite. The two sharp peaks at 2918 and 2849 cm^{-1} were attributed to C-H stretching vibrations of $-CH_3$ and $-CH_2$ groups respectively (Oliveira et al. 2016). The bands at 1749 and 1739 cm^{-1} (-C=O) for ketonic group was observed for both FNS and PNS composites respectively (Shooto et al. 2019a). The shift of the C=O stretch showed that there is effective interaction between sucrose adsorbents and the functional groups on the surface (Mallakpour et al. 2016). The (-NH) peak due to the amide was observed at 1533 and 1527 cm^{-1} on FNS and PNS composites respectively which were close to the previously reported by (Shooto et al. 2019a). The carboxyl group (-COOH) on both adsorbents were observed at 1408 cm^{-1}. Other bands at 1243, 1157 and 1000 cm^{-1} of PNS and 1247, 1152 and 1001 cm^{-1} of FNS were attributed to structures of hemicellulose, cellulose and lignin (Husseien et al. 2009; Matos et al. 2017; Thabede et al. 2020a). Therefore, the changes obtained from the FTIR spectrum of the functionalization black cumin seeds have indicated a number of functional groups on the surface of FNS and PNS composites which may propose that these functional groups were responsible for the Cr(VI) and Pb(II) ions adsorption from aqueous solutions.

The FT-IR spectra of PNS and FNS composites loaded with Pb(II) and Cr(VI) ions are compared with composites before adsorption as shown in Figs.52b-c respectively. The FT-IR spectrum of PNS (Fig. 52b) after the adsorption of Pb(II) showed various functional groups at different frequencies. The peaks at 3238, 2918 and 2849 cm^{-1} shifted towards the 3273, 2921 and 2851 cm^{-1} after adsorption, whilst (-C=O) for ketonic group above 1700 cm^{-1} disappeared

and the hydroxyl group at 1625 cm^{-1} shifted to 1627 cm^{-1}. The amide (-NH) peak observed at 1527 cm^{-1} shifted to 1528 cm^{-1} whilst the (-COO) group shifted to 1405 cm^{-1} after the adsorption of Pb(II). The peaks associated with hemicellulose, cellulose and lignin shifted to 1234, 1148 and 1011 cm^{-1}. The peaks obtained from the FT-IR adsorption spectrum of PNS loaded Cr(VI) is shown in Fig. 52b. The adsorption of Cr(VI) (Fig. 52b) on the adsorbent showed that the functional groups had shifted to 3205, 2827 and 2757 cm^{-1}. However, the peak at 1739 cm^{-1} attributed to (-C=O) ketonic group and the peak due to hydroxyl group at 1631 cm^{-1} dropped off. On the other hand, the amide (-NH) at 1527 cm^{-1} shifted to 1535 cm^{-1} whilst carboxyl group (-COOH) shifted from 1408 to 1436 cm^{-1}. There is a new peak at 1315 cm^{-1} and the cellulosic framework shifted to 1153, 1061 and 930 cm^{-1} (Abdulla et al. 2019).

The FT-IR absorption spectra of FNS composites after adsorption of Pb(II) and Cr(VI) are shown in Fig. 52c. The peaks on FNS for Pb(II) at 3228 and 1625 cm^{-1} were assigned to hydroxyl (-OH) groups before adsorption, and the two sharp peaks at 2918 and 2849 cm^{-1} (-CH_3 and -CH_2) shifted to 3287, 1626, 2921 and 2852 cm^{-1} after adsorption respectively. The (-C=O) band at 1749 cm^{-1} disappeared. The amide group observed at 1533 cm^{-1} shifted to 1532 cm^{-1}. The carboxyl group (-COOH) observed at 1408 cm^{-1} shifted to 1405 cm^{-1} and the peak at 1247 disappeared. There was a new peak formed at 1308 cm^{-1}. The hemicellulose and cellulose peaks shifted to 1148 and 1009 cm^{-1}. The FNS spectrum loaded with Cr(VI) in Fig. 52c showed that the hydroxyl groups and (-CH_3 and -CH_2) shifted to 3298, 1620, 2920 and 2852 cm^{-1} respectively. The (-C=O) peak shifted to 1744 cm^{-1} with reduced intensity. The (-NH) peak at 1533 cm^{-1} shifted to 1535 cm^{-1} whilst the (-COOH) peak shifted to 1455 cm^{-1} after adsorption. The hemicellulose and cellulose peaks shifted to 1245, 1150 and 1029 cm^{-1}. The intensity of peaks on PNS and FNS after the adsorption, reduced significantly which may imply that, there

was interaction of oxygenous composites through electrostatic and hydrogen bonding (Siddiqui & Chaudhry, 2019).

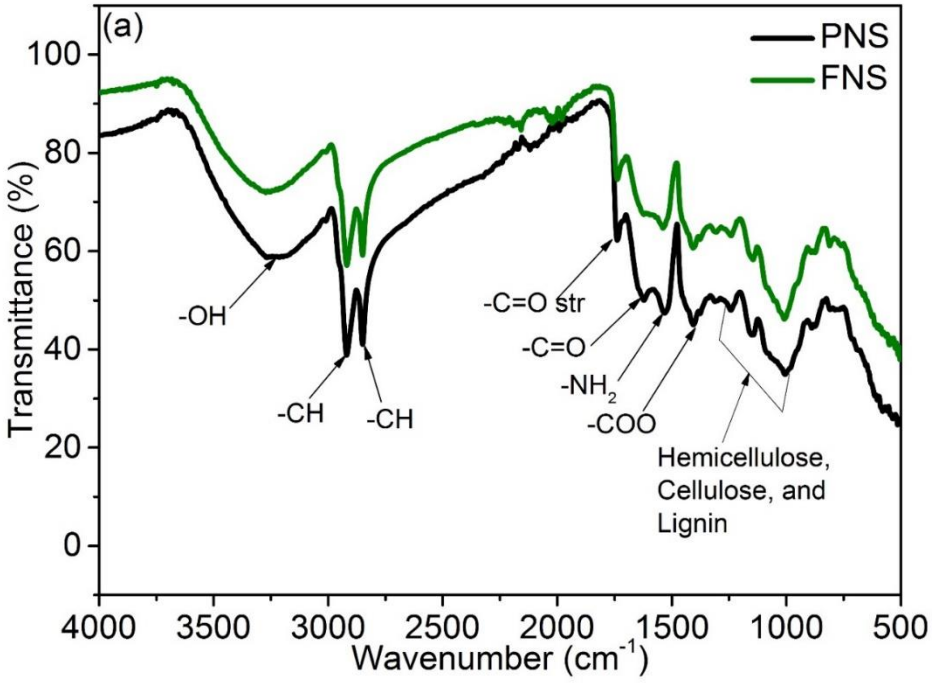

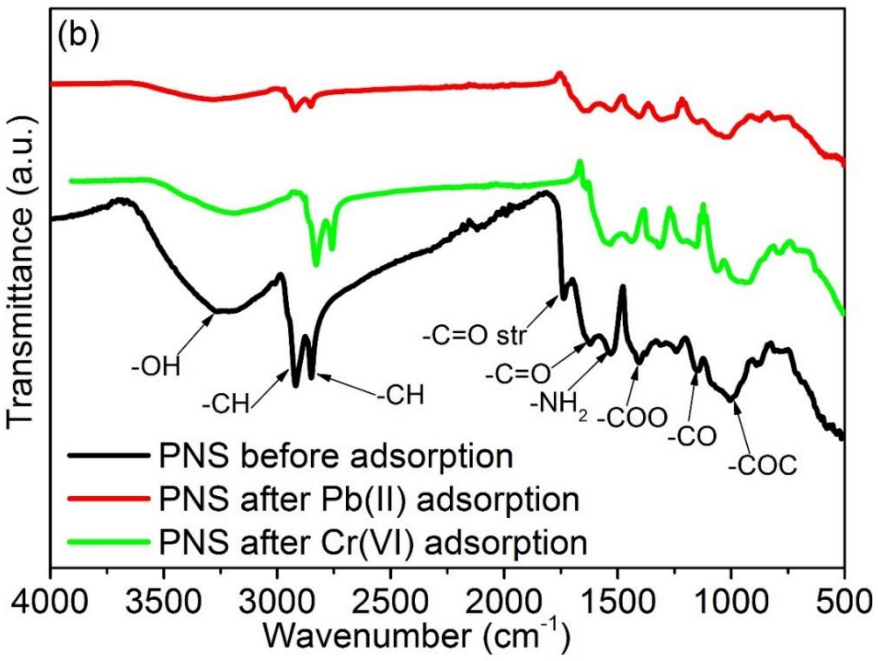

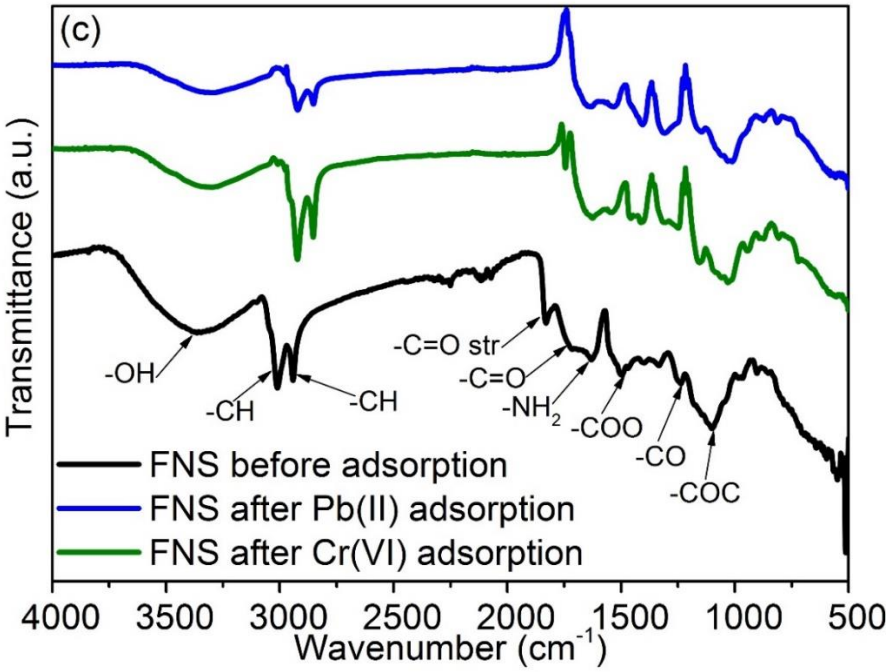

Figure 52: IR spectra of (a) PNS and FNS composites before adsorption, (b) PNS composite before and after adsorption and (c) FNS composite before and after adsorption of Pb(II) ions and Cr(VI).

8.7.1.2 XRD results

The X-ray diffraction pattern of FNS and PNS composites is illustrated in Fig.53. The broad peak at (2θ) value between 15 and 25° indicated the cellulosic structure of the black cumin seed material (Siddiqui & Chaudhry, 2018). The XRD spectrum of FNS and PNS composites show peaks around 23.73°, 30.84°, 35.27°, 41.24°, 43.41°, 62.43°and 77.48° corresponding to (210), (220), (311), (113), (400), (440) and (533) planes with combination of spinel structure and *y*-Fe_2O_3 phase confirming the formation of iron oxide (Abdulla et al. 2019; Li et al. 2020b). The FNS composite adsorbent showed that it had higher intensity peaks as compared to PNS composites.

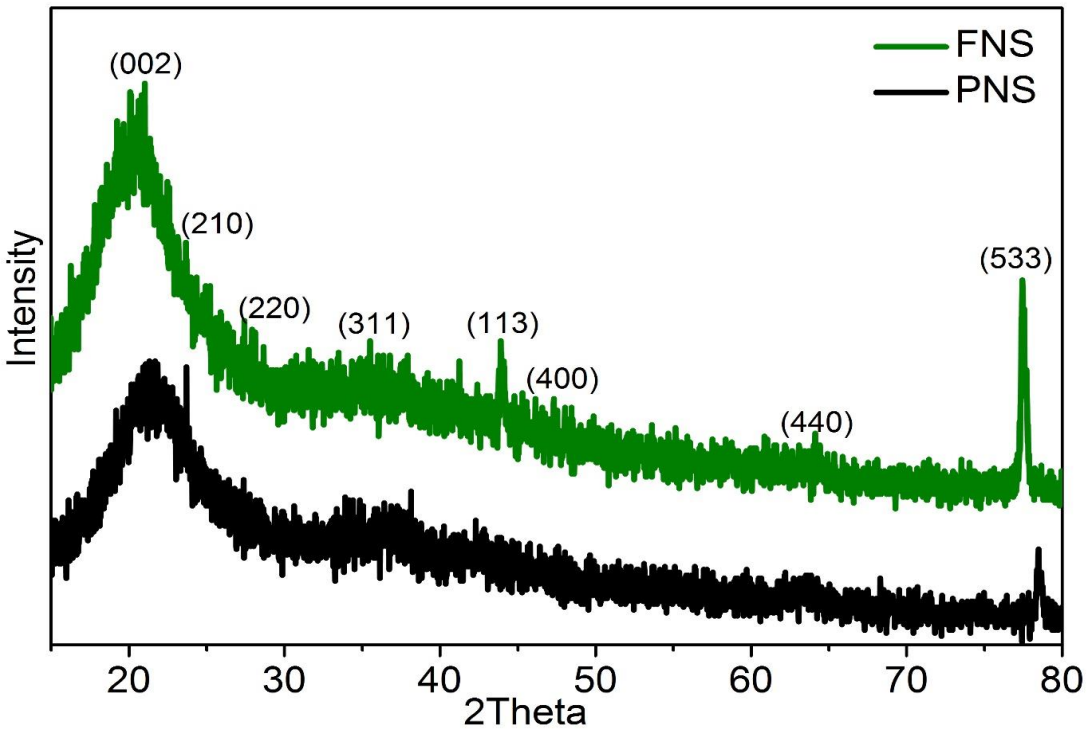

Figure 53: XRD spectra of FNS and PNS composites.

8.7.2 Adsorptions studies

8.7.2.1 Effect of pH solution

The adsorption of Cr(VI) and Pb(II) ions by FNS and PNS composites were evaluated at pH ranging from 1-9 as shown in Figs. 54a-b. The experimental data showed that the adsorption of Cr(VI) and Pb(II) ions was pH dependant. The sorption of Cr(VI) ions by PNS and FNS composites showed a decrease in capacity as the pH increased. A similar observation was recorded in the literature by (Pakade et al. 2016) using macadamia nutshells. Lesaoana et al. (2019); He et al. (2019) explained this trend by stating that at low pH (1-3) the hydrolysis reaction of dichromate ion ($Cr_2O_7^{2-}$) yield $HCrO_4^-$ which alternately becomes the main Cr(VI) species in acidic medium. However, at elevated pH $HCrO_4^-$ causes the equilibrium to shift towards creating CrO_4^{2-} and $Cr_2O_7^{2-}$ species. It is further mentioned that at lower pH, the

negatively charged dichromate or chromate binds electrostatically to the positively charged groups on the surface of the adsorbents because at low pH the surface of the adsorbents are positively charged due to protonation. Additionally, He et al. 2019 mentioned that this phenomenon was about the surface charge of the adsorbent and that the obtained modified adsorbent pHpzc ranged from 2-4. It is said that when the adsorbent is positively charged, it will adsorbs anions containing Cr(VI), such as $HCrO^{4-}$ and $Cr_2O_7^{2-}$. Otherwise, when the adsorbent is negatively charged it reduces the electrostatic interaction between the adsorbent and anionic Cr(VI). This means that pH is very important for the removal of Cr(VI) ions owing to its effects on the electrostatic interaction. A different trend was observed in the adsorption of Pb(II) ions whereby adsorption capacities of FNS and PNS composites increased as pH of the solution increased from pH 1 to pH 5, then beyond pH 5 the adsorbed amount remained the same with a slight decrease. This is due to the fact that, as the pH increases, the H^+ ion in the solution decreases therefore, the greater the number of negatively charged ions which makes the binding sites available for the metal adsorption to take place (Chand & Pakade, 2012). The adsorption of Cr(VI) ions on both adsorbents was lower compared to Pb(II) ions due to electrostatic repulsion of hydroxyl ions which are negatively charged (Pakade et al. 2016).

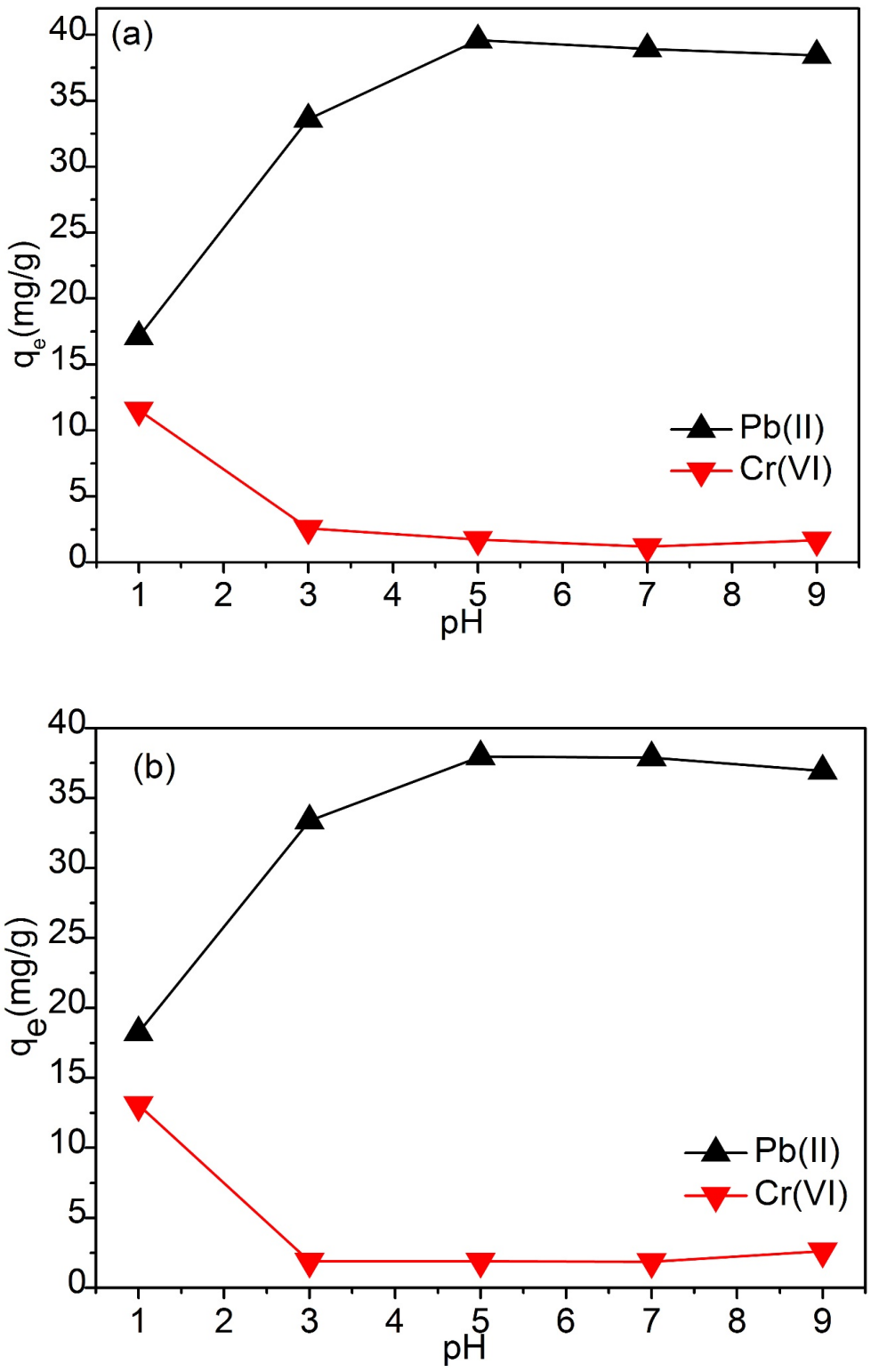

Figure 54: pH effect Onto (a) PNS and (b) FNS composites for Pb(II) ions and Cr(VI) sorption. [Experimental conditions: volume of solution (40 mL), time (60 min), adsorbent dosage (0.1 g), temperature (298 K), agitation rate (200 rpm), concentration (100 ppm)]

8.7.2.2 Speciation diagrams of Cr(VI) and Pb(II) ions

At different pH values chromium exist in aqueous solution in different anionic forms namely; hydrogen chromate ($HCrO_4^-$), chromate (CrO_4^{2-}), chromic acid (H_2CrO_4) and dichromate ($Cr_2O_7^{2-}$) (Unceta et al. 2010; Acharya et al. 2018; Zhang et al. 2020). The speciation of these Cr(VI) anions depends on concentration and pH of the solution (Gherasim et al. 2011; Acharya et al. 2017). Fig.55a show the speciation of Cr(VI) as a function of pH at concentration of 100 mg/L. H_2CrO_4 belong to the strong acids and is only observed below pH 1 (Markiewicz et al. 2014). However at pH >1 de-protonated form of Cr(VI) was observed, hence product $HCrO_4^-$ was formed at a pH from 1 to 6.5. The diagram shows that $HCrO_4^-$ was the major species at the experimental concentration and this was dominant between pH 1 and 6.5. According to (Dhal et al. 2013; Maremeni et al. 2018) $HCrO_4^-$ is usually the most predominant Cr(VI) species at acidic conditions. A similar observation was reported by (Sampaio et al. 2015; Jorge et al. 2019) stating that $HCrO_4^-$ species usually formed around pH below 6.8. In our study $HCrO_4^-$ form was obtained at pH 1 thereafter the capacity started decreasing. This indicated that $HCrO_4^-$ prevails in acidic medium. The decrease in sorption capacity could be due to the depletion of protons subsequently less protonated sites and more hydroxide groups that may result in competition with CrO_4^{2-} ions for adsorption (Maremeni et al. 2018). As the pH increased towards basic medium only CrO_4^{2-} ions were in the solution throughout the concentration range (McNeill et al. 2012; Markiewicz et al. 2014). On the other hand, $Cr_2O_7^{2-}$ is stable at weakly acidic and low oxidizing environments (Maremeni et al. 2018). In our study the metal ion concentration was ranging between 20 and 100 mg/L hence $Cr_2O_7^{2-}$ was not included in the diagram. Therefore this may suggest that Cr(VI) existed mainly as $HCrO_4^-$ anion. Bhowal & Datta, (2001); Markiewicz et al. (2014); Zhang et al. (2020) indicated that $Cr_2O_7^{2-}$ is dominant in more concentrated solution above 100 mg/L. Pakade et al. (2017) have shown that at low pH of 2 there is a possibility of Cr(III) forming when using macadamia nutshell. However, as

the pH increased from 3-9, Cr(III) and Cr(VI) also decreased. Yang & Chen (2008) also mentioned that at strongly acidic conditions Cr(VI) can be reduced to Cr(III). Therefore, it can be concluded that in this study only Cr(VI) was formed.

The pH of the solution is considered as the major parameter controlling metal speciation (Shahid et al. 2012). Fig.55b shows the species distribution diagram of Pb(II) in aqueous solution against pH at concentration of 100 mg/L. The results showed that higher sorption capacity was obtained between pH 2 and 5 where lead occurred only as Pb(II) species up to pH 6.0. This was also achieved in the research work done by (Vera et al. 2019). Since HCl was used to adjust pH it was suggested that there might be lead chloride complexes formation. From the diagram formation of lead chloride complexes were obtained between pH 7.0 and 8.0. Lukanin et al. (2013) showed that lead chloride species can be obtained around pH 7.3 and 8.3 whilst (Easley & Byrne, 2011) data showed that lead chloride formed from pH 7.2 to 7.6. Above pH 7.5 to alkaline conditions, there was production of hydroxyl groups and consequently increased the amount of lead hydroxide solution (Wang et al. 2017; Nicholaychuk, 2018). Byrne et al. (1981); Silwamba et al. (2020) have also shown that addition of hydrochloric acid can form Pb(II) and lead chloride complexes such as $PbCl^{+}$, $PbCl_2$ and $PbCl_3^{-}$.

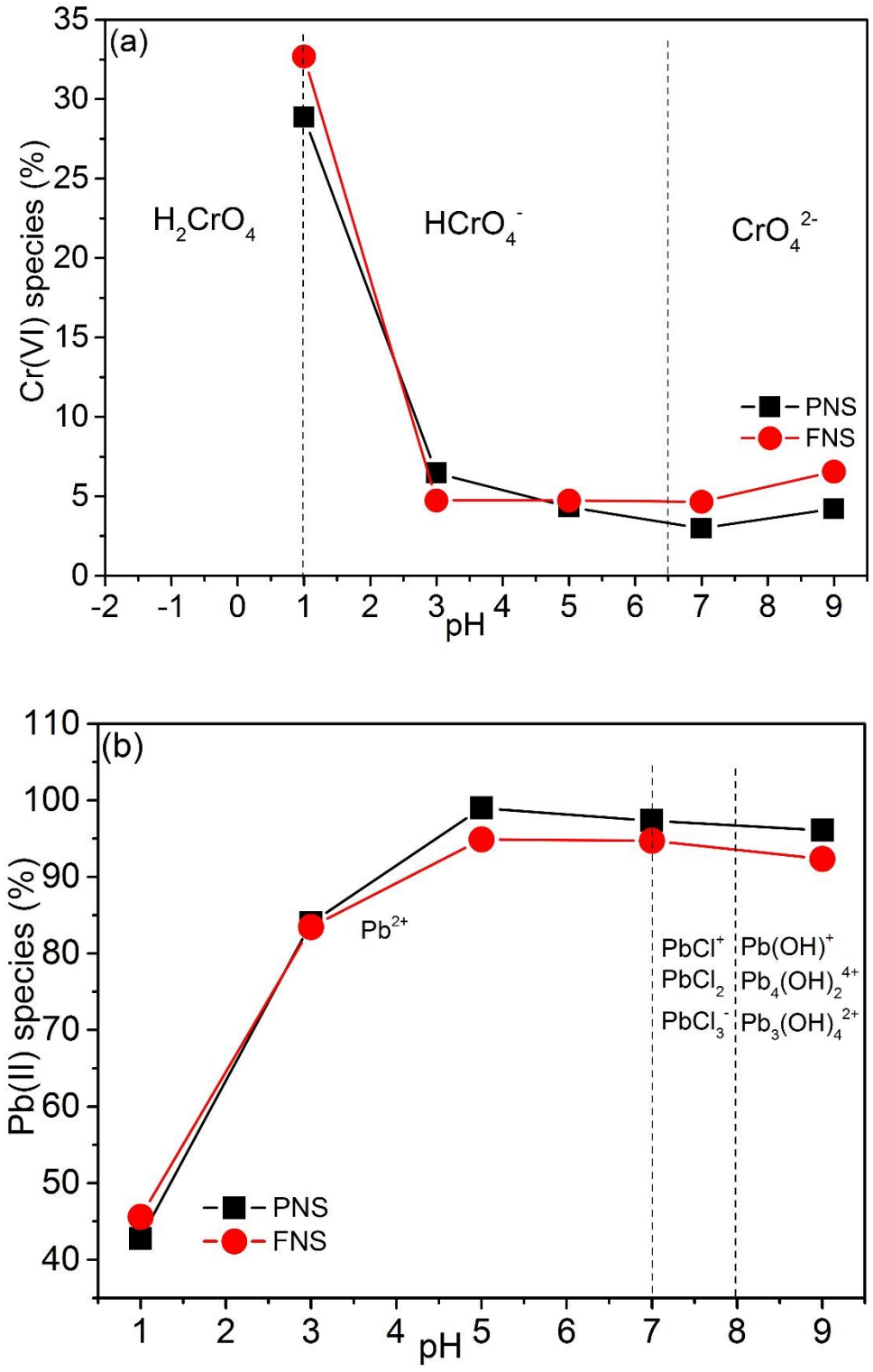

Figure 55: Speciation diagrams of **(a)** Cr(VI) and **(b)** Pb(II) ions Onto PNS and FNS composites at concentration of 100 mg/L at room temperature.

8.7.2.3 Concentration effect and adsorption isotherms

Figures 56a-b show the effect of initial concentrations on the adsorption of Cr(VI) and Pb(II) ions by PNS and FNS composites. The removal efficiency of both adsorbents was found to dependent on the initial concentration of chromium. The adsorption of Pb(II) by PNS in Fig.56a increased with increasing concentration from 20 to 80 mg/L, whilst the adsorption of Cr(VI) increased from 20 to 60 mg/L. Thereafter the removal efficacy slowly reached adsorption equilibrium and there was no further increase in the adsorption of Cr(VI). A similar adsorption trend was observed for FNS in Fig.56b whereby Pb(II) ions adsorption increased with increasing initial concertation (20-80 mg/L). However, the adsorption of Cr(VI) ions stays almost constant as the initial concentration increases. The maximum adsorption capacities at initial concentration of 20 mg/L onto FNS in Fig.56b was 4.34 and 6.14 mg/g for Cr(VI) and Pb(II) ions respectively, whereas on PNS it was only 0.26 mg/g and 5.98 mg/g for Cr(VI) and Pb(II) ions respectively. On the other hand the maximum adsorption capacities at 100 mg/L onto PNS in Fig.56a for Pb(II) and Cr(VI) ions were 29.47 and 15.74 mg/g respectively then onto FNS in Fig.56b was observed at 29.80 and 7.80 mg/g for Pb(II) and Cr(VI) respectively. The results in both Figs.56a-b showed that both adsorbents capacities increased with increased initial concentration especially for Pb(II) ions. The reason why Pb(II) ions were adsorbed more than Cr(VI) ions on PNS and FNS composites might be due negatively charged Cr(VI) ion electrostatically repelling the adsorbed ions resulting in decrease of the adsorption capacity (Santamarina et al. 2002). Also, as seen in Fig.54 the maximum adsorption for Cr(VI) took place at pH 1. Thereafter an increase in pH resulted to a decreased in adsorption due to $HCrO_4^-$, CrO_4^{2-} and $Cr_2O_7^{2-}$ and decreased in surface protonation (Rouibah et al. 2009).

The interaction of Cr(VI) and Pb(II) ions with PNS and FNS composites surfaces adsorption mechanism and surface affinities towards Cr(VI) and Pb(II) ions is described with the help of

non-linear Langmuir and Freundlich isotherms. The adsorption isotherms and their parameters are shown in Table 19. The data showed that Pb(II) ions on PNS and FNS composites had (r^2) of 0.996 and 0.997 for Freundlich isotherms whilst Langmuir isotherm showed r^2 of 0.903 and 0.935 respectively. This indicated that Pb(II) ions adsorption was best described by Freundlich than Langmuir isotherm which suggested that the surface was heterogeneous and also the ions bind physically and form multilayer (Thabede et al. 2020b). However, isotherm data of the adsorption of Cr(VI) ions onto PNS and FNS composites showed a high (r^2) value of 0.997 and 0.995 respectively for Langmuir which demonstrated formation of homogenous monolayer.

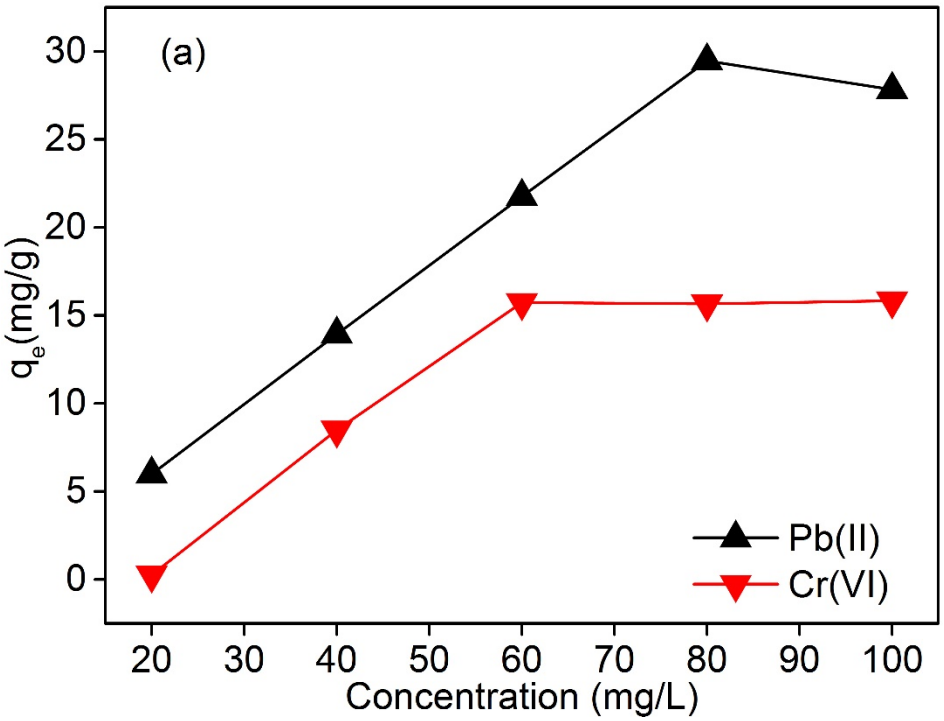

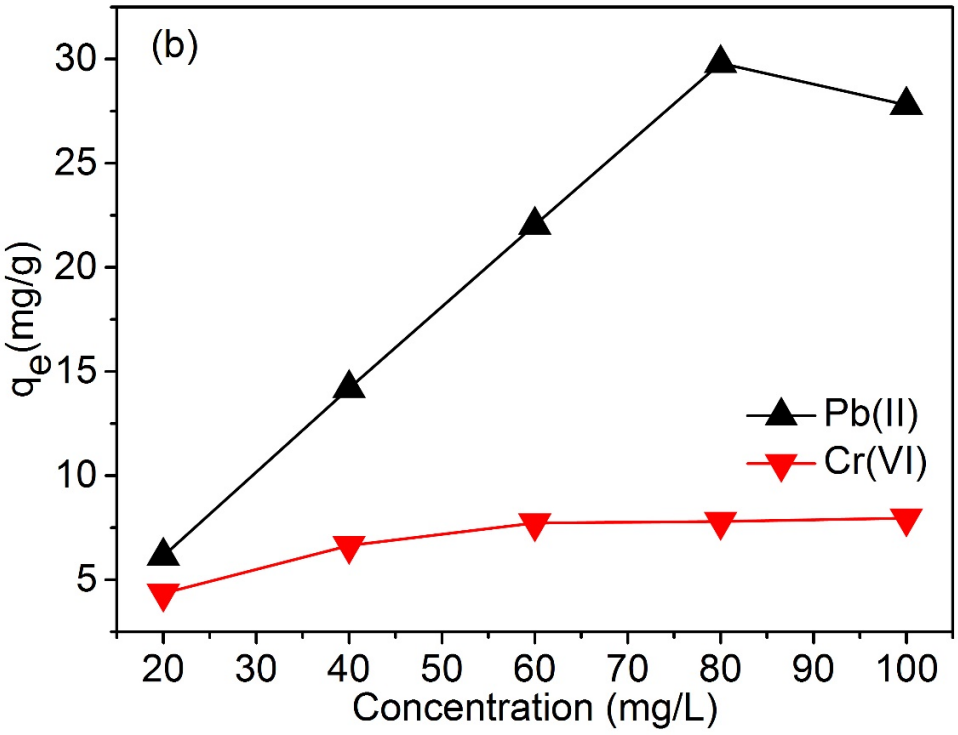

Figure 56: Concentration effect Onto (a) PNS and (b) FNS composites for Pb(II) ions and Cr(VI) sorption. [Experimental conditions: volume of solution (40 mL), time (60 min), adsorbent dosage (0.1 g), temperature of the system (298 K), agitation rate (200 rpm), pH of solutions during Pb(II) ions and Cr(VI) sorption (5.0)]

Table 19: Isotherms studies and their parameters

Isotherms		FNS		PNS	
		Pb(II)	Cr(VI)	Pb(II)	Cr(VI)
Langmuir	Q_o (mgg^{-1})	19.99	10.21	12.06	15.11
	b (Lmg^{-1})	6.6301	0.0412	1.0751	0.0642
	r^2	0.9031	0.9973	0.9355	0.9952
Freundlich	1/n	22.783	48.654	19.791	4.425
	k_f ($mg^{(1-n)}$ L^n g^{-1})	0.730	6.589	0.684	1.322
	r^2	0.9961	0.893	0.9975	0.8869
Experimental (q_e) (mg/g)		29.80	7.80	29.47	15.74

8.7.2.4 Time effect and adsorption kinetics

The sorption rates of Cr(VI) and Pb(II) ions were studied in the time intervals of 1-120 min as shown in Figs. 57a-b**.** The sorption rate of Cr(VI) ions was faster than Pb(II) ions for both PNS and FNS composites as shown in Figs. 57a-b. The maximum sorption for Cr(VI) ions was reached in 20 min in both Figs. 57a-b meanwhile adsorption rate of Pb(II) ions was slow and continue increasing up to 90 min of reaction. The slow adsorption stage was caused by the low concentration gradients then finally produced the equilibrium condition (Aichour & Zaghouane-Boudiaf, 2019). An increase in metal ions adsorption was observed in both adsorbents due to probability of Cr(VI) and Pb(II) ions occupying vacant sites on the adsorbents because there were plenty of unsaturated vacant sites that resulted in quick initial adsorption (Shooto et al. 2019b; Abdulla et al. 2019). However, as time continues vacant sites get exhausted and saturated therefore sorption ability of PNS and FNS composites decreased until equilibrium or decrease in sorption capacity. The maximum adsorption capacities of PNS composite for Cr(VI) and Pb(II) was found to be 15.75 and 35.36 mg/g respectively and FNS composite were 8.92 and 37.76 mg/g for Cr(VI) and Pb(II) respectively. These capacities were obtained under the following experimental conditions: 40 mL of solution at temperature of 298 K using adsorbent dosage of 0.1g with the concentration of 100 ppm at pH.

The kinetic study of PNS and FNS composites in removing Cr(VI) and Pb(II) ions was estimated using pseudo-first order (PFO) and pseudo-second order (PSO). The adsorption capacity (q_e), rate constants (k_1 and k_2), and coefficient of determination (r^2) values are shown in Table 20. The adsorption process was estimated based on the coefficient of determination value that is closer to unity (1). The data showed that (r^2) values of PFO model for PNS and FNS composites for both Cr(VI) and Pb(II) ions were ranging from 0.993-0.997 which was close to 1 whilst the (r^2) for PSO ranged from 0.741-0.902. Therefore, the good fit for PFO

data suggested that a physisorption mechanism was involved for all adsorbents fitting in PFO. The removal uptake of Cr(VI) and Pb(II) ions was also assessed using intra-particle diffusion (IPD) kinetic model by determining whether the sorption process has occurred through estimated surface adsorption (ESA) or estimated pores adsorption (EPA). The sorption of Cr(VI) and Pb(II) ions onto FNS composite occurred through pore adsorption with percentages of 59.00 and 53.92 % respectively. Similarly the sorption of Cr(VI) and Pb(II) ions onto PNS composite were 42.48 and 62.98 % respectively.

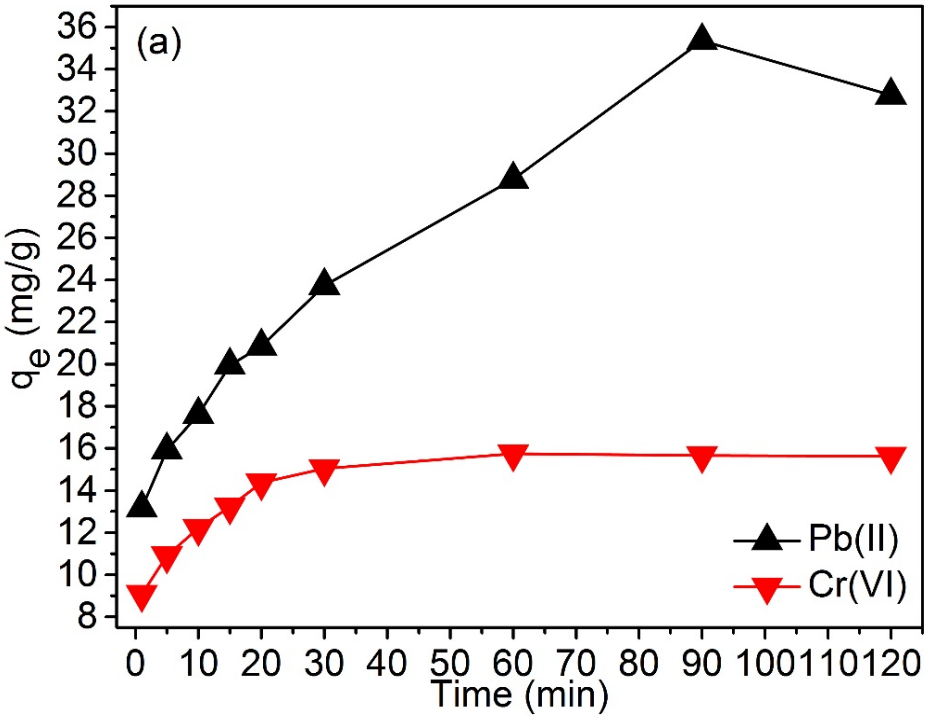

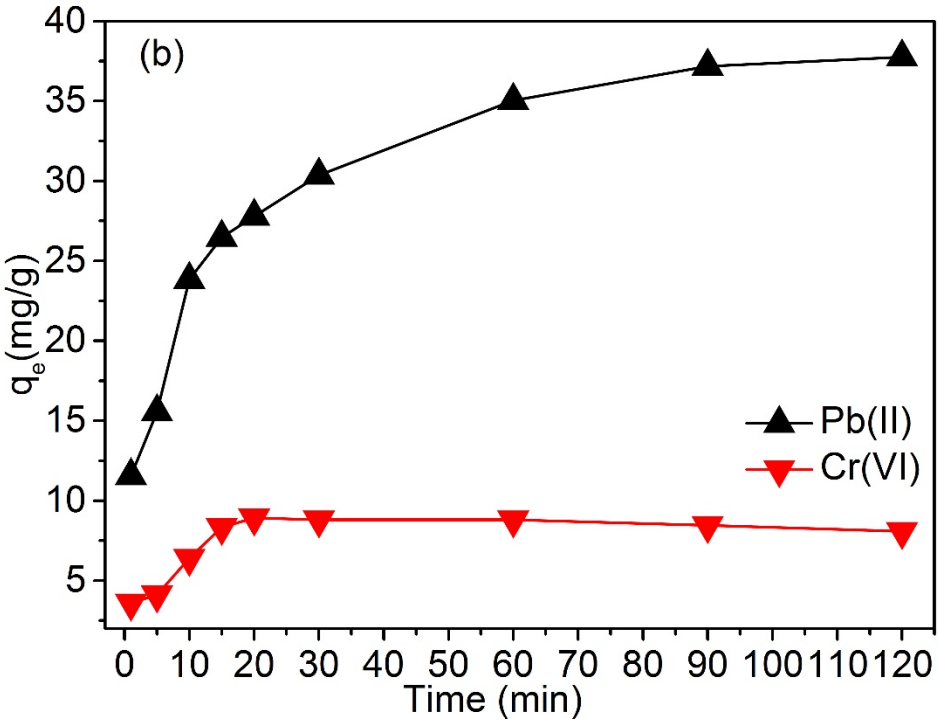

Figure 57: Time effect Onto **(a)** PNS and **(b)** FNS composites of Pb(II) ions and Cr(VI) sorption. [Experimental conditions: volume of solution (40 mL), concentration (100 ppm), adsorbent dosage (0.1 g), temperature of the system (298 K), agitation rate (200 rpm), pH of solutions during Pb(II) ions and Cr(VI) sorption (5)]

Table 20: Kinetic models and their parameters

Models		FNS		PNS	
		Pb(II)	Cr(VI)	Pb(II)	Cr(VI)
PFO	q_e (mgg^{-1})	35.20	8.64	30.98	14.15
	K_1(m^{-1})	0.10	0.17	0.07	0.96
	r^2	0.9979	0.9938	0.9947	0.9976
PSO	q_e (mgg^{-1})	33.24	18.32	23.71	20.67
	K_2 (gmg^{-1} min^{-1})	0.0377	0.1370	0.0419	0.0743
	r^2	0.9024	0.8481	0.7415	0.8969
IPD	C	15.48	4.11	13.09	9.06
	K_i (g g^{-1} min$^{0.5}$)	1.7716	0.4202	2.3475	0.6298
	r^2	0.917	0.719	0.941	0.876

EPA	%	59.00	53.92	62.98	42.48
ESA	%	41.00	46.08	37.02	57.52
Experimental (q_e) (mgg^{-1})		37.76	8.92	35.36	15.75

EPA-Estimated pore sorption and ESA-Estimated surface sorption.

8.7.2.5 Temperature effect and thermodynamic parameters

Figs. 58a-b show the effects of temperature on sorption on PNS and FNS composites. The graphs showed that the adsorption of Cr(VI) and Pb(II) ions are temperature depended. The adsorption of Cr(VI) ions on both adsorbents showed an increase in sorption capacity with increased temperature between 298 and 313 K in Figs.58a-b. At higher temperatures beyond 313 K no further increase of adsorption was observed, instead equilibrium was attained for both adsorbents. This suggests that the heat of adsorption of Cr(VI) ions onto FNS and PNS composite was small hence, changing the temperature could not change the thermodynamics of the system which may imply that only slight energy was needed to break the repulsive forces hindering the Cr(VI) ions adsorption (Diagboya & Dikio, 2018). Further increase in temperature to 308 K also confirmed that the adsorption process was physical (Dong et al., 2011). A different trend was observed for Pb(II) ions on PNS composite in Fig.58a whereby the adsorption capacity increased as the temperature increased from 298-353 K. However, the sorption of Pb(II) ions onto FNS composite in Fig.58b only increased as temperature increased from 298-313 K thereafter reached equilibrium. The uptake capacity increased with increasing the temperature on both adsorbents. This suggested that the reaction was endothermic and the increase in adsorption capacity was perhaps due to the diffusion and increase in the number of binding sites developed as a result of the breakage of internal bonds (Liu & Zhang, 2009; Bagbi et al. 2016). The maximum adsorption capacities of PNS at room temperature were 15.21 mg/g for Cr(VI) ions and 30.66 mg/g for Pb(II) ions. On the other hand the sorption capacities of

FNS were 12.76 and 30.54 mg/g for Cr(VI) and Pb(II) ions respectively. These results were obtained using an adsorbent dosage of 0.1 g with the solution volume of 40 mL for 60 min at pH of 5 and 100 ppm working solution.

The determination of thermodynamic parameters is very important in order to determine spontaneity and the heat change of the adsorption reactions. Thermodynamic parameters namely; enthalpy ($\Delta H°$), entropy ($\Delta S°$) and Gibb's free energy ($\Delta G°$) changes of adsorption are shown in Table 21. The negative values of ($\Delta G°$) indicate the feasibility of the adsorption process, physical characteristics nature of the process and the spontaneous nature of the sorption towards Cr(VI) and Pb(II) ions onto PNS and FNS composites (Yarkandi, 2014; Oussalah et al. 2019). The magnitude of the Gibbs free energy for Pb(II) ions onto PNS and FNS composite becomes more negative when temperature increased from 298 to 353 K, this suggests that adsorption process was favourable at higher temperature (Rodiguez et al. 2018). The positive values of ($\Delta S°$) indicated the randomness at solid or solution interfaces during the adsorption of Cr(VI) and Pb(II) ions onto both PNS and FNS composites (Mohapatra & Anand, 2007; Chen & Shi, 2017). The positive values of ($\Delta H°$) showed the endothermic nature of the adsorption process which may also supported a slight increase in value of Pb(II) ions uptake of the adsorbents with the rise in temperature (Yarkandi 2014).

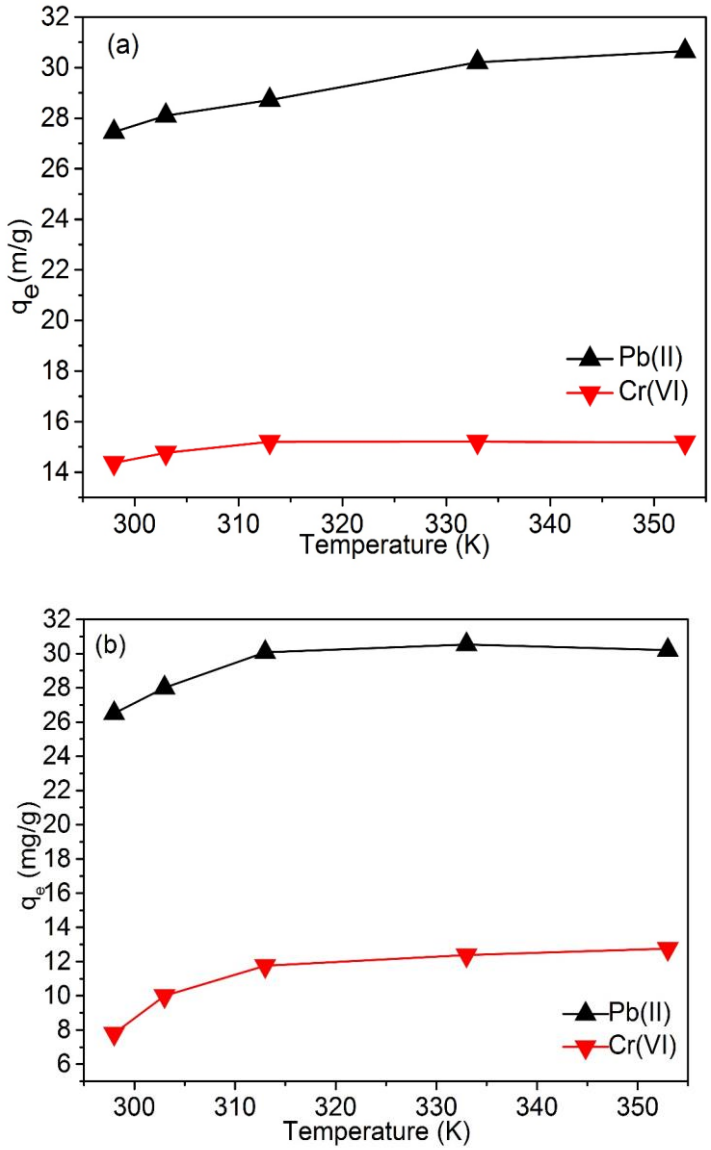

Figure 58: Temperature effect **(a)** PNS and **(b)** FNS composites of Pb(II) ions and Cr(VI) sorption. [Experimental conditions: volume of solution (40 mL), time (60 min), adsorbent dosage (0.1 g), concentration (100 ppm), agitation rate (200 rpm), pH of solutions during Pb(II) ions and Cr(VI) sorption (5)]

Table 21: Thermodynamic studies and their parameters

Parameter	FNS		PNS	
	Pb(II)	Cr(VI)	Pb(II)	Cr(VI)
ΔH^o (KJ mol^{-1})	$8x10^{-4}$	$7x10^{-4}$	$1x10^{-3}$	$1x10^{-3}$
ΔS^o (KJ $mol^{-1}K^{-1}$)	$3x10^{-3}$	$1x10^{-3}$	$3x10^{-3}$	$2x10^{-3}$

ΔG^o (KJ mol^{-1})				
298 K	-1.70	-4.66	-1.43	-1.19
303 K	-5.02	-4.76	-3.28	-1.26
313 K	-5.96	-4.92	-4.17	-1.36
333 K	-6.18	-5.78	-5.84	-1.67
353 K	-7.06	-5.07	-7.99	-1.44

8.7.2.6 Physicochemical studies of the adsorbents

The effect of pH can also be explained in terms of $pH_{(PZC)}$ of PNS and FNS composites. The point of zero charge is described as the point at which the surface basic or acidic functional groups no longer contribute to the pH value of the solution (Morifi et al. 2020). The point of zero charge $pH_{(PZC)}$ of PNS and FNS composites were 2.15 and 3.00 respectively. These results indicated that the surface of the PNS and FNS composites were acidic.

8.7.3 Comparative studies of Cr(VI) and Pb(II) ions

The modified *Nigella Sativa* adsorbents of PNS and FNS composite adsorption capacities for Cr(VI) and Pb(II) ions were compared with other affordable adsorbents materials reported in literature. The comparison studies as shown in Table 22 and 23 of both adsorbents showed higher performance than some of the reported adsorbents for Cr(VI) and Pb(II) ions adsorption. Therefore, PNS and FNS composites are promising low cost adsorbents for Cr(VI) and Pb(II) ions removal from aqueous solution.

Table 22: Maximum sorption capacities of previously reported various adsorbents for Pb(II) ions

Adsorbent	**Maximum capacity (mg/g)**	**Solution pH**	**Temperature (°C)**	**Reference**
Magnetic coffee waste	41.2	6	25	Edathil et al. 2018
Magnetic cane biochar	40.6	5	20	Mohan et al. 2015
Fe_3O_4@SiO_2-IP polymer	32.6	4.8	25	Guo et al. 2014
Fe^{3+}/Fe^{2+} black cumin seeds	39.67	5	25	This study
Poplar tree biomass	35.0	4	25	Demey et al. 2014
Plums biochar	28.8	6	25	Pap et al. 2018
Dolomite	19.7	6	45	Irani et al. 2011
Apple Pomace	16.4	4	25	Chand & Pakade, 2012
Apricot biochar	12.7	6	25	Pap et al. 2018
Wood biochar	7.9	5	25	Bardestani et al. 2019
Mushroom	3.9	6	25	Kariuki et al. 2017
Rice husk biochar	2.4	5	25	Liu & Zhang, 2009

Table 23: Maximum sorption capacities of previously reported various adsorbents for Cr(VI) ions

Adsorbent	Maximum capacity (mg/g)	Solution pH	Temperature (°C)	Reference
Iron oxide nanoparticles	45.0	1	25	Burks et al. 2014
Fe_3O_4 nanoparticles	26.5	2	25	Liang et al. 2019
Activated Iron bamboo biochar	25.7	2	25	He et al. 2019
Iron oxide dextrin	17.7	2	30	Mittal et al. 2017
Fe^{3+}/Fe^{2+} black cumin seeds	15.75	5	25	This study
Magnetite-pine composite	13.9	2	25	Pholosi et al. 2020
Banana waste	10.0	2	28	Sharma et al. 2016
Starch based iron oxide	9.0	2	25	Sing & Sinha, 2014
Activated carbon mango	7.80	2	35	Rai et al. 2016
Activated bamboo biochar	5.4	2	25	He et al. 2019

8.7.4 Conclusion

FNS and PNS composites were prepared and used as adsorbents to investigate the influence of surface modification and be used for the adsorption of Cr(VI) and Pb(II) ions. Sucrose and iron oxide were combined with *Nigella Sativa* seeds to prepare FNS composites. The composites were prepared by precipitation and characterized with XRD and FTIR. To investigate the adsorption efficiency of the prepared iron oxide composites for the removal of Cr(VI) and Pb(II) ions, batch adsorption studies were carried out under different parameters. The maximum adsorption capacities for Cr(VI) were 15.6 and 13.0 mg/g onto PNS and FNS composites respectively at pH 1. On the other hand maximum sorption of Pb(II) ions were 39.7

and 37.9 mg/g onto PNS and FNS composites at pH 5. Both PNS and FNS composites capacities increased with increasing initial concentration whereby Pb(II) ions adsorbed more than Cr(VI) ions. The adsorption of Cr(VI) ions was fast within 20 and 90 min for Pb(II) ions on both adsorbents. Sorption of Cr(VI) and Pb(II) ions on both adsorbents increased with increased temperature which displayed the endothermic nature of the processes (Tan et al. 2017). Freundlich isotherm was best fitted for both adsorbents for the sorption of Pb(II) ions and Langmiur for Cr(VI) ions. The rate of adsorption showed a good fit for pseudo first order kinetic model which suggested physisorption mechanism (Yildirim & Acaya, 2020) of Cr(VI) and Pb(II) ions was involved for both adsorbents. The negative free energy ($\Delta G°$) values indicated that the process feasible and spontaneous onto PNS and FNS composites (Edokpayi et al. 2019). The ($\Delta G°$) values decreased as temperature increased from 298 to 353 K which showed that adsorption process was favourable at higher temperature. The positive values of ($\Delta S°$) indicated the randomness of water molecules from the surface of both PNS and FNS composites. The positive values of ($\Delta H°$) showed the endothermic nature of the adsorption process (Nethaji et al. 2012). These results indicated that the easily available and affordable carbon source (sucrose) based *Nigella Sativa* seeds can be considered as adsorbent for removing Cr(VI) and Pb(II) ions from aqueous solution. The results showed that PNS composite had higher adsorption capacity of 39.7 mg/g for Pb(II) and 15.6 mg/g for Cr(VI) compared to FNS composite. Therefore PNS and FNS composites can used as low cost materials for the removal Pb(II) and Cr(VI) ions from aqueous solution. The *Nigella Sativa* seeds used in this study had high uptake for Pb(II) than Cr(VI) compared to the uptake of 10.07 mg/g for methylene blue reported by (Siddiqui & Chaudhry, 2018, 2019). Other adsorption studies on magnetized *Nigella Sativa* seeds for the removal of methylene blue dye had higher uptake compared to this study (Siddiqui et al. 2019a, 2019b).

8.7.5 Acknowledgement

We acknowledge the supports of National Research Fund-NRF (Grand number: 112983) for funding this work and the Department of Chemistry, Vaal University of Technology, Vanderbiljpark, South Africa.

References

ABDULLA, N.K., SIDDIQUI, S.I., TARA, N., HASHMI, A.A. & CHAUDHRY, S.A., 2019. Psidium guajava leave-based magnetic nanocomposite γ-Fe_2O_3@GL: A green technology for methylene blue removal from water. *Journal of Environmental Chemical Engineering,* 7, 103423.

AL JASSIR, M.S., SHAKER, A. & KHALIQ, M.A., 2005. Deposition of heavy metals on green leafy vegetables sold on roadsides of Riyadh City, Saudi Arabia. *Bulletin of Environmental Contamination and Toxicology,* 75, 1020-1027.

ACHARYA, R., NAIK, B. & PARIDA, K., 2018. Cr(VI) remediation from aqueous environment through modified-TiO_2-mediated photocatalytic reduction. *Beilstein Journal of Nanotechnology,* 9, 1448-1470.

ACHARYA, R., MARTHA, S. & PARIDA, K.M., 2017. Remediation of Cr(VI) using clay minerals, biomasses and industrial wastes as adsorbents. In advanced materials for waste water treatment. Islam S. Ed. John Wiley and Sons, Inc New York: 129-170.

AHMAD, R. & HASEEB, R.S., 2014. Black cumin seed (BCS): a non-conventional adsorbent for the removal of Cu (II) from aqueous solution. *Desalination Water Treatment*, 1-10.

AICHOUR, A. & ZAGHOUANE-BOUDIAF, H., 2019. Highly brilliant green removal from wastewater by mesoporous adsorbents: Kinetics, thermodynamics and equilibrium isotherm studies. *Microchemical Journal*, 146, 1255-1262.

AL JASSIR, M.S., SHAKER, A. & KHALIQ, M.A., 2005. Deposition of heavy metals on green leafy vegetables sold on roadsides of Riyadh City, Saudi Arabia. *Bulletin Environmental Contamination Toxicology*, 75, 1020-1027.

ALGUACIL, F.J., ALCARAZ, L., GARCIA-DIAZ, I., LOPEZ, F.A., 2018. Removal of Pb^{2+} in wastewater via adsorption onto an activated carbon produced from winemaking waste. *Metals*, 8(697), 1-15.

BAGBI, Y., SARSWAT, A., MOHAN, D., PANDEY, A. & SOLANKI, P.R., 2016. Lead (Pb^{2+}) adsorption by monodispersed magnetite nanoparticles: Surface analysis and effects of solution chemistry. *Journal of Environmental Chemical Engineering*, 4, 237-4247.

BARDESTANI, R., ROY, C. & KALIAGUINE S., 2019 The effect of biochar mild air oxidation on the optimization of lead(II) adsorption from wastewater. *Journal of Environmental Management*, 240, 404-420.

BEDIN, K.C., MARTINS, A.C., CAZETTA, A.L., PEZOTI, O. & ALMEIDA, V. C., 2016. KOH-activated carbon prepared from sucrose spherical carbon: Adsorption equilibrium,

kinetic and thermodynamic studies for methylene blue removal. *Chemical Engineering Journal*, 286, 476-484.

BEHJATI, M., BAGHDADI, M. & KARBASSI, A., 2018. Removal of mercury from contaminated saline wasters using dithiocarbamate functionalized-magnetic nanocomposite. *Journal of Environmental Management*, 213, 66 -78.

BHOWAL, A. & DATTA, S., 2001. Studies on transport mechanism of Cr(VI) extraction from an acidic solution using liquid surfactant membranes. *The Journal of Membrane Science*, 188, 1-8.

BURKS, T., AVILA, M., AKHTAR, F., GOTHELID, M., LANSAKER, P.C., TOPRAK, M.S., MUHAMMED, M. & UHEIDA. 2014. Studies on the adsorption of chromium(VI) onto 3-Mercaptopropionic acid coated superparamagnetic iron oxide nanoparticles. *Journal of Colloid and Interface Science*, 425, 36-43.

BYRNE, R. H., YAO, W., LUO, Y., MILLERO, F. J., 2010. Complexation of Pb(II) by chloride ions in aqueous solutions. *Aquatic Geochemistry,* 16, 325-335.

CHAND., P. & PAKADE, Y. B., 2013. Removal of Pb from water by adsorption on apple pomace: Equilibrium, kinetics, and thermodynamics studies. *Journal of Chemistry.*

CHEN, T., WANG, Q., LYU, J., BAI, P. & GUO, X., 2020. Boron removal and reclamation by magnetic magnetite (Fe_3O_4) nanoparticle: An adsorption and isotopic separation study. *Separation and Purification Technology,* 231, 115930.

DATTA, A.K., SAHA, A., BHATTACHARYA, A., MANDAL, A., 2012. Black Cumin (*Nigella Sativa* l.)-A review. *Journal Plant Development Sciences* 4(1), 1-43.

DEHBI, A., DEHMANI, Y., OMARI, H., LAMMINI, A., ELAZHARI, A. & ABDALLALOUI, A., 2020 Hematite iron oxide nanoparticles (α-Fe_2O_3): Synthesis and modelling adsorption of malachite green. *Journal of Environmental Chemical Engineering*, 8, 103394.

DEHGHANI, M. H., SANAEI, D., ALI, I. & BHATNAGAR, A., 2016. Removal of chromium(VI) from aqueous solution using treated waste newspaper as a low-cost adsorbent: Kinetic modeling and isotherm studies. *Journal of Molecular Liquids*, 215, 671-679.

DEMEY, H., MELKIOR, T., CHATROUX, A., ATTAR, K., THIERY, S., MILLER, H., GRATEAU, M., SASTRE, A.M., MARCHAND, M., 2019. Evaluation of torrefied poplar-biomass as a low-cost sorbent for lead and terbium removal from aqueous solutions and energy co-generation. *Chemical Engineering Journal*, 361, 839-852.

DHAL, B., THATOI, H.N., DAS, N.N. & PANDEY, B.D., 2013. Chemical and microbial remediation of hexavalent chromium from contaminated soil and mining/metallurgical solid waste: A review. *Journal of Hazardous Materials*, 250(251), 272-291.

DIAGBOYA, P.N. & DIKIO, D., 2018. Scavenging of aqueous toxic organic and inorganic cations using novel facile magneto-carbon black-clay composite adsorbent. *Journal Cleaner Production*, 180, 71-80.

DONG, Y., LU, B., ZANG, S., ZHAO, J., WANG, X. & CAI, Q., 2011. Removal of methylene blue from coloured effluents by adsorption onto SBA-15. *Journal of Chemistry Technology Biotechnology*, 86, 616-619.

DUBEY, R., BAJPAI, J. & BAJPAI, A., 2015. Green synthesis of graphene sand composite (GSC) as novel adsorbent for efficient removal of Cr (VI) ions from aqueous solution. *Journal of Water Process Engineering*, 5, 83-94.

EASLEY, R.A. & BYRNE, R.H., 2011 The ionic strength dependence of lead (II) carbonate complexation in perchlorate media. *Geochimica et Cosmochimica Acta*, 75, 5638-5647.

EDATHIL, A. A., SHITTU, I., ZAIN, J. H., BANAT, F. & HAIJA, M.A., 2018. Novel magnetic coffee waste nanocomposite as effective bioadsorbent for Pb(II) removal from aqueous solutions, *Journal of Environmental Chemical Engineering.*

EDOKPAYI, J.N, NDLOVU, S., S. & ODIYO, J.O., 2019. Characterization of pulverized Marula seed husk and its potential for the sequestration of methylene blue from aqueous solution. *BMC Chemistry*, 13(10).

ESMAEILI, E., NIASARI, M.S., MOHANDES, F., DAVAR, F. & SEYGHAKAR, H., 2011. Modifie single-phase hematite nanoparticles via a facile approach for large-scale synthesis. *Chemical Engineering Journal*, 170, 278-285.

FREUNDLICH, H.M.F., 1906. Over the adsorption in solution, *Journal of Physical Chemistry*, 57, 385-471.

GHERASIM, C.V., BOURCEANU, G., OLARIU, R.I. & ARSENE, C., 2011. A novel polymer inclusion membrane applied in chromium(VI) separation from aqueous solutions, *Journal of Hazardous Materials,* 197, 244-253.

GOSCIANSKA, J., MARCINIAK, M. & PIETRZAK, R., 2015. Ordered mesoporous carbons modified with cerium as effective adsorbents for azo dyes removal. *Separation and Purification Technology,* 154, 236-245.

GUEYE, M., RICHARDSON, Y., KAFACK, F.T. & BLIN, J., 2014. High efficiency activated carbons from African biomass residues for the removal of chromium(VI) from wastewater. *Journal of Environmental Chemical Engineering*, 2, 273-281.

GUO, B., DENG F., ZHAO, Y., LUO, X., LUO, S. & AU, C., 2014. Magnetic ion-imprinted and-SH functionalized polymer for selective removal of Pb(II) from aqueous samples. *Applied Surface Science*, 292, 438-446.

HE, R., YUAN, X., HUANG, Z., WANG, H., JIANG, L., HUANG, J., TAN, M. & LI, H., 2019. Activated biochar with iron-loading and its application in removing Cr (VI) from aqueous solution. *Colloids Surfaces* A, 579, 123642.

HO, Y. & MCKAY, G., 1999. Pseudo-second order model for sorption processes. *Process Biochemistry*, 34, 451-465.

HUSSEIEN M, AMER AA, EL-MAGHRABY A, HAMEDALLAH, N., 2009. A comprehensive characterization of corn stalk and study of carbonized corn stalk in dye and gas oil sorption. *Journal Analytical and Applied Pyrolysis*, 86, 360-363.

IRANI, M., AMJADI, M. & MOUSAVIAN, M.A., 2011. Comparative study of lead sorption onto natural perlite, dolomite and diatomite. *Chemical Engineering Journal*, 178, 317-323.

JORGE, M.J., NILSON, M.C., ARACELY HR, MARTINEZ, F., 2019. Data on the removal of metals (Cr^{3+}, Cr^{6+}, Cd^{2+}, Cu^{2+}, Ni^{2+}, Zn^{2+}) from aqueous solution by adsorption using magnetite particles from electrochemical synthesis. *Data in brief*, 24, 103956.

KARIUKI, Z., KIPTOO, J. & ONYANCH, D., 2017. Biosorption studies of lead and copper using rogers mushroom biomass 'Lepiota hystrix'. *South African Journal of Chemical Engineering*, 23, 62-70.

KUZNETSOV, V.O., PULIKKATHARA, M.X., LOBO, R.M.F., KHABASHEKUA, V.N. 2010. Solubilization of carbon nanoparticles, nanotubes, nano onions, and nanodiamonds through covalent functionalization with sucrose. *Russian Chemical Bulletin, International Edition*, 59(8), 2005-2008.

LANGMUIR, I., (1918) The constitution and fundamental properties of solids and liquids, *Journal of the American Chemical Society,* 40, 1361-1403.

LESAOANA, M., MLABA, R.P.V., MTUNZI, F.M., KLINK, P.E. & PAKADE, V.E., 2019. Influence of inorganic acid modification on Cr(VI) adsorption performance and the

physicochemical properties of activated carbon. *South African Journal Chemical Engineering*, 28, 8-18.

LI, J., FAN, M., LI, M. & LIU, X., 2020a. Cr(VI) removal from groundwater using double surfactant-modified nanoscale zero-valent iron (nZVI): Effects of materials in different status. *Science of the Total Environmental*, 717, 137112.

LI, Y., PAN, S., YU, Q., DING, X. & LIU, R., 2020b. Adsorption mechanism and electrochemical performance of methyl blue onto magnetic $Ni_{(1-x-y)}Co_yZn_xFe_2O_4$ nanoparticles prepared via the rapid combustion process. *Ceramic International*, 46, 3614-3622.

LIANG S, SHI S, ZHANG H, QIU, J., YU, W., LI, M., GAN, Q., YU, W., XIAO, K., LIU, B., HU, J., HOU, H. & YAMG, J., .2019, One-pot solvothermal synthesis of magnetic biochar from waste biomass: Formation mechanism and efficient adsorption of Cr(VI) in an aqueous solution. *Science of the Total Environment*, 695, 133886.

LIU, Y., 2009. Is the free energy change of adsorption correctly calculated? *Journal of Chemical Engineering Data*, 54, 1981-1985.

LIU, Z. & ZHANG, F.S., 2009. Removal of lead from water using biochars prepared from hydrothermal liquefaction of biomass. *Journal of Hazardous Materials*, 167, 933-939.

LUKANIN, O.A., RYZHENKO, B., N. & KUROVSKAYA, N.A., 2013. Zn and Pb solubility and speciation in aqueous chloride fluids at *T-P* parameters corresponding to granitoid magma degassing and crystallization. *Geochemistry International*, 51(10),802-830.

MALLAKPOUR, S. & BEHRANVAND, V., 2016. Chemical adsorption of D-sucrose on MWCNTs for compatibility improvement with alanine-based poly(amide-imide) matrix: morphology examination and thermal stability study. *Colloid Polymer Science*, 294, 239-246.

MANTILAKA, M.M.M.G.P.G., KARUNARATNE, D.G.G.P., RAJAPAKSE, R.M.G. & PITAWALA, H.M.T.H.A., 2013. Precipitated calcium carbonate/poly(methyl methacrylate) nanocomposite using dolomite: Synthesis, characterization and properties. *Powder Technology*, 235, 628-632.

MAREMENI, L.C., MODISE, S.J., MTUNZI, F.M., KLINK, M.J. & PAKADE V.E., 2018. Adsorptive removal of hexavalent chromium by diphenylcarbazide-grafted macadamia nutshell powder. *Bioinorganic Chemistry and Applications*, 2018.

MARKIEWICZ, B., KOMOROWICZ, I., SAJNOG, A., BELTER, M. & BARALKIEWICZ, D., 2015. Chromium and its speciation in water samples by HPLC/ICP-MS-technique establishing metrological traceability: A review since 2000. *Talanta*, 132, 814-828.

MATOS, T.T.S., SCHULTZ, J., KHAN, M.Y., ZANOELO, E.F., MANGRICH, A.S. & ARAUJO, B.R., 2017. Using magnetized (Fe_3O_4/biochar nanocomposites) and activated biochar as adsorbents to remove two neuro-active pesticides from waters. *Journal of the Brazilian Chemistry Society*, 28(10), 1975-1987.

MCNEILL, L.S., MCLEAN, J.E., PARKS, J.L. & EDWARDS, M.A., (2012) Hexavalent chromium review, part 2: Chemistry, occurrence, and treatment. *Journal-American Water Works Association,*104(7).

MEKONNEN, E., YITBAREK, M. & SORETA, T.R., 2015. Kinetic and thermodynamic studies of the adsorption of Cr(VI) onto some selected local adsorbents. *South African Journal of Chemistry,* 68, 45-52.

MITTAL, A., AHMAD R. & HASAN, I., 2016. Iron oxide-impregnated dextrin nanocomposite: synthesis and its application for the biosorption of Cr(VI) ions from aqueous solution. *Desalination and Water Treatment,* 57, 15133-15145.

MOHAN, D., SINGH, P., SARSWAT, A., STEELE, P.H. & PITTMAN Jr, C.U., 2015. Lead sorptive removal using magnetic and nonmagnetic fast pyrolysis energy cane biochars. *Journal of Colloid and Interface Science,* 448, 238-250.

MOHAPATRA, M. & ANAND, S., 2007. Studies on sorption of Cd(II) on Tata chromite mine overburden . *Journal of Hazardous Materials,* 148, 553-559.

MUBARAK, N, M., THINES, R. K., SAJUNI, N. R., ABDULLAH, E.C., SAHU, N.J., GANESAN, P. & JAYAKUMAR, N.S., 2014. Adsorption of chromium (VI) on functionalized and non-functionalized carbon nanotubes. *Korean Journal of Chemical Engineering,* 31(9), 1582-1591.

NETHAJI, S., SIVASAMY, A., & MANDAL, A.B., 2012. Adsorption isotherms, kinetics and mechanism for the adsorption of cationic and anionic dyes onto carbonaceous particles prepared from juglans regia shell biomass. *International Journal of Environmental Science and Technology,* 10, 231-242.

NIASARI, M.S., DAVAR, F. & MAZAHERI, M., 2009. Synthesis and characterization of ZnS nanoclusters via hydrothermal processing from [bis(salicylidene)zinc(II)]. *Journal Alloys and Compounds*, 470, 502-506.

NIKOLAYCHUK, P. A., 2018. The revised potential-pH diagram for Pb-H_2O system. *Ovidius University Annals of Chemistry,* 29(2), 55-67.

OLIVEIRA, R. N., MANCINI, M.C., OLIVEIRA, F.C.S.D., PASSOS, T.M., QUILTY, B., THIRE R.S. & McGUINNESS G.B., 2016. FTIR analysis and quantification of phenols and flavonoids of five commercially available plants extracts used in wound healing, *Revista Materia*, 21(3), 767-779.

ORBAK, A., Y. & ORBAK, I., 2019. Effective factor analysis for chromium(VI) removal from aqueous solutions and its application to tuncbilek lignite using design of experiments. *Journal of Chemistry,* 2019.

OUSSALAH A, BOUKERROUI A, AICHOUR A. & DJELLOULI, B., 2019. Cationic and anionic dyes removal by low-cost hybrid alginate/natural bentonite composite beads: Adsorption and reusability studies. *International Journal of Biological Macromolecules,* 124, 854-862.

PAKADE, V., NTULI, T. & OFOMAJA, A., 2017. Bisorption of hexavalent chromium from aqueous solutions by Macadamia nutshells powder. *Applied Water Science,* 7, 3015-3030.

PAKADE VE, NTULI TD & OFOMAJA, A.E., 2016. Biosorption of hexavalent chromium from aqueous solutions by Macadamia nutshell powder. *Applied Water Science*, 7, 3015-3030.

PAP S, BEZANOVIC V, RADONIC J, BABIC, A., SARIC, S., ADAMOVIC, D. SEKULIC, M.T., 2018. Synthesis of highly-efficient functionalized biochars from fruit industry waste biomass for the removal of chromium and lead. *Journal of Molecular Liquids*, 268, 315-325.

PHOLOSI, A., NAIDOO, E. B. & OFOMAJA, A.E., 2020. Intraparticle diffusion of Cr(VI) through biomass and magnetite coated biomass: A comparative kinetic and diffusion study. *South African Journal of Chemical Engineering*, 32, 39-55.

PUGAZHENDHI A, BOOVARAGAMOORTHY GM, RANGANATHAN K, NAUSHAD, M. & KALIANNAN, T., 2018. New insight into effective biosorption of lead from aqueous solution using Ralstonia solanacearum: characterization and mechanism studies. *Journal of Cleaner Production*, 174, 1234-1239.

PUZAS, J.E., CAMPBELL, J., KEEFE, R.J. & ROSIER, N., 2004. Lead toxicity in the skeleton and its role in osteoporosis. Nutrition and bone health. In: Holick M.F., Dawson-Hughes B. (eds) *Nutrition and Bone Health*. Nutrition and Bone Health. Humana Press, Totowa, NJ. 363-376.

RAI, M.K., SHAHI, G., MEENA, V., CHAKRABORTY, S., SINGH, R.S. & RAI, B.N., 2016. Removal of hexavalent chromium Cr (VI) using activated carbon prepared from mango kernel activated with H_3PO_4. *Resource-Efficient Technologies*, 2, S63-S70.

RODIGUEZ, M. H., YPERMAN, J., CARLEER, R., MAGGEN, J., DADI, D., GRYGLEWICZ, G., VAN DER BRUGGEN, B., HERNANDEZ, J. F. & CALVIS, A.O., 2018. Adsorption of Ni(II) on spent coffee and coffee husk based activated carbon. *Journal of Environmental Chemical Engineering,* 6, 1161-1170.

ROUIBAH, K., MENIAI, A.H., ROUIBAH, M.T. & DEFFOUS, L., 2009. Elimination of chromium(VI) and cadmium(II) from aqueous solutions by adsorption onto olive stones. *Open Chemical Engineering Journal,* 3, 41-48.

SAMPAIO CG, FROTA LS, MAGALHAES HS, DUTRA, L.M.U., QUEIROZ, D.C., ARAUJO, R. S., BECKER, H., DE SOUZA, J. R. R., RICARDO, M.P.S. & TREVISA, M.T.S., 2015. Chitosan/mangiferin particles for Cr(VI) reduction and removal. *International Journal of Biological Macromolecules,* 78, 273-279.

SANTHOSH, C., KOLLU, P., DOSHI, S., SHARMA, M., BAHADUR, D., VANCHINATHAN, M.T., SARAVANAN, P., KIM, B-S. & GRACE, A. N., 2014. Adsorption, photodegradation and antibacterial study of graphene-Fe_3O_4 nanocomposite for multipurpose water purification application. *RSC Advances,* 4, 28300-28308.

SHAHID, M., DUMAT, C., ASLAM, M. & PINELLI, E., 2012. Assessment of lead speciation by organic ligands using speciation models. *Chemical Speciation Bioavailability,* 24(4),248-252.

SHARMA, P.K., AYUBA, S. & TRIPATHI, C. N., 2016. Isotherms describing physical adsorption of Cr(VI) from aqueous solution using various agricultural wastes as adsorbents. *Cogent Engineering,* 3(1), 1186857.

SHOOTO, N.D., NAIDOO E., B. & MAUBANE M., 2019b. Sorption studies of toxic cations on ginger root adsorbent. *Journal Industrial and Engineering Chemistry*, 76, 133-140.

SHOOTO, N. D., THABEDE P. M., & NAIDOO, E. B., 2019a. Simultaneous adsorptive study of toxic metal ions in quaternary system from aqueous solution using low cost black cumin seeds (Nigella sativa) adsorbents. *South African Journal Chemical Engineering,* 30, 15-27.

SHUPACK, S. I., (1991) Chemistry of chromium and some resulting analytical problems. *Environmental Health Perspectives,* 92, 7-11.

SIDDIQUI, S. I. & CHAUDHRY, S. A., 2017. Iron oxide and its modified forms as an adsorbent for arsenic removal: a comprehensive recent advancement, *Process Safety and Environmental Protection*, 111, 592-626.

SIDDIQUI, S., I. & CHAUDHRY, S. A., 2018. Nigella Sativa plant-based nanocomposite-$MnFe_2O_4$/BC: An antibacterial material for water purification. *Journal of Cleaner Production,* 200, 996-1008.

SIDDIQUI, S., I. & CHAUDHRY, S. A., 2019. Nanohybrid composite Fe_2O_3-ZrO_2/BC for inhibiting the growth of bacteria and adsorptive removal of arsenic and dyes from water. *Journal of Cleaner Production,* 223, 849-868.

SIDDIQUI, S. I., CHAUDHRY, S. A. & ISLAM, S. U., 2017. Green adsorbents from plant sources for the removal of arsenic: an emerging wastewater treatment technology. In: Islam, S.U. (Ed.), Plant-based Natural Products: Derivatives and Applications. John Wiley Sons, Inc. 193-215.

SIDDIQUI, S. I., MANZOOR, O., MOHSIN, M. & CHAUDHRY, S. A., 2019b. *Nigella Sativa* seed-based nanocomposite-MnO_2/BC: An antibacterial material for photocatalytic degradation, and adsorptive removal of Methylene blue from water. *Environmental Research,* 171, 328-340.

SIDDIQUI, S. I., RATHI, G., & CHAUDHRY, S. A., 2018. Acid washed black cumin seed powder preparation for adsorption of methylene blue dye from aqueous solution: Thermodynamic, kinetic and isotherm studies. *Journal of Molecular Liquids,* 264, 275-284.

SIDDIQUI, S. I., ZOHRA, F. & CHAUDHRY, S. A., 2019a. Nigella Sativa seed based nanohybrid composite- Fe_2O_3-SnO_2/BC: A novel material for enhanced adsorptive removal of methylene blue from water. *Environmental Research,* 178, 108667.

SILWAMBA, M., ITO, M., HIROYOSHI, N., TABELIN, C.B., HASHIZUME, R., FUKUSHIMA, T., PARK, I., JEON, S., IGARASHI, T., SATO, T., CHIRWA, M., BANDA, K., NYAMBE, I., NAKATA, H., NAKAYAMA, S. & ISHIZUKA, M., 2020. Recovery of lead and zinc from zinc plant leach residues by concurrent dissolution-cementation using zero-valent aluminum in chloride medium. *Metals,* 10(531), 1-15.

SINGH, P. N., TIWARY, D. & SINHA, I., 2014. Improved removal of Cr(VI) by starch functionalized iron oxide nanoparticles. *Journal of Environmental Chemical Engineering*, 2, 2252-2258.

SIVADAS, D. L., VIJAYAN, S., RAJEEV, R., NINAN, K.N. & PRABHAKARAN, K., NINAN, 2016. Nitrogen-enriched microporous carbon derived from sucrose and urea with superior CO_2 capture performance. *Carbon*, 109, 7-18.

TAN, L., DONG, H., LIU, X., HE, J., XU, H. & XIE, J., 2017. Mechanism of palladium(II) biosorption by Providencia vermicola. *RSC Advances*, 7, 7060.

THABEDE, P. M., SHOOTO, N., D. & NAIDOO, E. B., 2020b. Removal of methylene blue dye and lead ions from aqueous solution using activated carbon from black cumin seeds, *South African Journal of Chemical Engineering*, 33, 39-50.

THABEDE, P. M., SHOOTO, N. D., XABA, T, NAIDOO, E. B., 2020a. Sulfuric activated carbon of black cumin (*Nigella sativa* L.) seeds for the removal of cadmium(II) and methylene blue dye. *Asian Journal of Chemistry*, 32(6), 1361-1369.

UNCETA, N., SEBY, F., MALHERBE, J. & DONARD, O. F. X., 2010. Chromium speciation in solid matrices and regulation: a review. *Analytical and Bioanalytical Chemistry*, 397, 1097-1111.

VADI, M. & NAJAFI, H., 2011. Adsorption isotherms of (+D) sucrose on multi-wall carbon nanotube. *Oriental Journal Chemistry*, 27(3), 1281-1284.

VERA, L.M., BERMEJO, D., UGUNA, M.F., GARCIA, N., FLORES, M. & GONZALEZ, E., 2019. Fixed bed column modeling of lead(II) and cadmium(II) ions biosorption on sugarcane bagasse. *Environmental Engineering Research,* 24(1), 31-37.

WANG, X., WANG, L., WANG, Y., TAN, R., KE, X., ZHOU, X., GENG, J., HOU, H. & ZHOU, M., 2017. Calcium sulfate hemihydrate whiskers obtained from flue gas desulfurization gypsum and used for the adsorption removal of lead. *Crystals,* 7, 270.

WEBER, J. W., MORRIS, J., C. & SANIT, J., 1963. Kinetics of adsorption carbon from solutions. *Journal of the Sanitary Engineering Division,* 89(2), 31-60.

YANG, L. & CHEN, J., 2008. Biosorption of hexavalent chromium onto raw and chemically modified Sargassum sp. *Bioresource Technology,* 99, 297-307.

YARKANDI, N. H., 2014. Removal of lead (II) from waste water by adsorption. *International Journal of Current Microbiology Applied Science,* 3(4), 207-228.

YILDIRIM, A. & ACAY, H., 2020. Biosorption studies of mushrooms for two typical dyes. *Journal of the Turkish Chemical Society,* 7(1), 295-306.

ZHANG, J., LIN, S., HAN, M., SU, Q., XIA, L. & HUI, Z., 2020. Adsorption properties of magnetic magnetite nanoparticle for coexistent Cr(VI) and Cu(II) in mixed solution. *Water,* 12(2), 446.

ZHANG, R., WANG, Z., ZHOU, Z., LI, D., WANG, T., SU, P. & YANG, Y., 2019 Highly effective removal of pharmaceutical compounds from aqueous solution by magnetic Zr-based MOFs composites. *Journal of Industrial Engineering Chemistry Research,* 58, 3876-3884.

ZHOU L, ZHANG G, WANG M, WANG, D., CAI, D. & WU, Z., 2017. Efficient removal of hexavalent chromium from water and soil using magnetic ceramsite coated by functionalized nano carbon spheres. *Chemical Engineering Journal*, 334, 400-409.

CHAPTER 9

Sorption of chromium(VI), cadmium(II) ions and methylene blue dye by pristine, defatted and carbonized *Nigella sativa* L. seeds from aqueous solution

This chapter is published as follows:

Patience Mapule Thabede, Ntaote David Shooto, Eliazer Bobby Naidoo. 2021. Sorption of chromium(VI), cadmium(II) ions and methylene blue dye by pristine, defatted and carbonized *Nigella sativa* L. seeds from aqueous solution**.** Asian Journal of Chemistry 33(2), 471-483.

This chapter is addressing objective (f) which reads as follows:

To modify black cumin seeds using different solvents such as acetone and N,N dimethylformamide (DMF) and carbonize the seeds at 600 °C for the sorption MB, Cd(II) and Cr(VI) while varying parameters such as temperature, concentration, time and pH.

Objective (i) is captured in each chapter for each set of results and it reads as follows

To conduct adsorption kinetics, isotherms and thermodynamics of Co(II), Ni(II), Cu(II), Cr(VI) and Pb(II) ions and methylene blue.

9.1 Abstract

The present study reports on the sorption study of chromium(VI), cadmium(II) ions and methylene blue (MB) dye by pristine, defatted and carbonized *Nigella Sativa L*. seeds from aqueous solution. The removal of oil from pristine *Nigella Sativa L*. (PNS) seeds was carried out by defatting the *Sativa* with acetone and N,N dimethylformamide and then labelled ANS and DNS respectively. Thereafter the defatted ANS and DNS adsorbents were carbonized at 600 °C for 2 hr under nitrogen and were labelled CANS and CDNS. The results of pristine, defatted and carbonized seeds were compared. The removal of Cr(VI), Cd(II) and MB dye from aqueous solutions was investigated by varying adsorbate concentration, solution pH, reaction contact time and temperature of the solution. The SEM images indicated that the surface morphology of PNS was irregular, whilst ANS and DNS had pores and cavities. CANS and CDNS was heterogeneous and had pores and cavities. FTIR spectroscopy showed that the adsorbents surfaces had bands that indicated oxygen containing groups. The solution pH had an influence on the removal uptake of Cr(VI), Cd(II) and MB. The sorption of Cr(VI) decreased when pH of the solution was increased due to different speciation of Cr(VI) ions whilst the removal of Cd(II) and MB increased when solution pH was increased. Pseudo First Order (PFO) kinetic model well described the adsorption of Cr(VI), Cd(II) and MB onto PNS. On the other hand, the kinetic data for ANS, CANS, DNS and CDNS was well described by Pseudo Second Order (PSO). Furthermore, the removal mechanism onto PNS and ANS was better described by Freundlich multilayer model. CANS, DNS and CDNS fitted Langmuir monolayer model. Thermodynamic parameters indicated that the sorption processes of Cr(VI), Cd(II) and MB was endothermic and effective at high temperatures for all adsorbents. (ΔS^o) and (ΔH^o) had positive values this confirmed that the sorption of Cr(VI), Cd(II) and MB onto all adsorbents was random and endothermic respectively. The values of (ΔG^o) confirmed that the sorption of Cr(VI), Cd(II) and MB on all adsorbents was spontaneous and predominated by physical

adsorption process. CANS had highest adsorption capacity of 99.82 mg/g for MB, 96.89 mg/g for Cd(II) and 87.44 mg/g for Cr(VI) followed by CDNS with 93.90, 73.91 and 65.38 mg/g for MB, Cd and Cr(VI) respectively. ANS capacities were 58.44, 45.28 and 48.96 mg/g whilst DNS capacities were 48.19, 32.69 and 34.65 mg/g for MB, Cd and Cr(VI) respectively. PNS had the lowest sorption capacities at 43.88, 36.01 and 19.84 mg/g for MB, Cd and Cr(VI) respectively. This implied that the untreated PNS adsorbs lower than the treated seeds.

Keywords: chromium, cadmium, methylene blue, defatted, carbonized

9.2 Introduction

Activated carbon (AC) is a material that is used in industrial processes for purification of liquid and product separation (Serrano-Gomez et al. 2015). AC is used as adsorbent for the removal of inorganic and organic pollutants in water, treatment of toxic compounds in medicine, as a material for storing hydrogen and many others (Thabede et al. 2020a). Chemical and physical activation together with heating process is often used to produce carbon-based materials in order to enhance porous structure, improves surface area, improving rate of adsorption (Goswami et al. 2016). However, these materials are not easy to generate because they require high cost precursors (Siddiqui & Chaudhry, 2017). Hence plant materials are used because they are abundant and sustainable resource that may provide oxygen containing groups which can easily interact with charged toxic pollutants from aqueous solution (Pugazhendhi et al. 2018). However, these materials need some modifications in order to get significant results for the removal of toxic ions and dyes (Siddiqui et al. 2017).

Sorption of dyes and toxic metals onto solid surface is one of the most increasing method for water treatment which is industrially favourable and environmentally friendly (Priyanka &

Saravanakumar, 2018). This method maybe be more effective, because the adsorbent could be prepared easily, and can be effective for wide range of pollutants which in turn will be effective for the removal of toxic metal ions (Santhosh et al. 2014). *Nigella Sativa* L. is an annual vegetal spice that belongs to the Ranunculacea family known as black cumin seed (Gali-Muhtasib et al. 2006; Abdallah & Shakak, 2019). It is used for remedial purposes in the Asia, India, Parkistan, Turkey, Sourthen Europe and Africa (Ardiana et al. 2020; Erdogan et al. 2020). Also, it has been traditionally used for the treatments related to respiratory health, intestinal health and stomach, liver and kidney function and immune system support. Other therapeutic effects include anti-inflammatory, anti-allergic, analgesic, anticancer, antioxidants and antiviral (Ahmad & Haseeba, 2014; Begum & Mannan, 2020; Thabede et al. 2020b). Black Cumin seeds contains appreciable amount of unsaturated especially polyunsaturated fatty acids which constitute the bulk of oil ranging from 48 to 70%, whilst monounsaturated (18-29%) and saturated fatty acids (12-25%) are in lesser amounts (Abdallah & Shakak, 2019). Fatty acids are reported to block the pores and in turn decreases the surface area of the biomaterials (Abdallah & Shakak, 2019). It is therefore important to extract the oil from the *Nigella Sativa L*. seeds before their application in waste water treatment (Garba et al. 2016). This process increases the cellulosic pore concentrations also, it increases the surface-active sites on the adsorbent material whereby functional groups such as -OH, -COO and -NH_2 can take part in the metal ion and dye binding (Al-Anbera et al. 2014; Chandra et al. 2015). Hence we investigated the sorption of chromium Cr(VI), cadmium Cd(II) and methylene blue (MB) dye using pristine, defatted and carbonized *Nigella Sativa* L. seeds.

Cr(VI) and Cd(II) ions are common toxins in wastewater resulting from industrial activities including paint manufacturing plants, textile manufacturing, petroleum refining, electroplating, paper, leather tanning, ceramic industries, and other metal finishing industries (Ali et al. 2019)

On the other hand, methylene blue dye (MB) is found in effluent released from manufactures such as finishers, textile producers and dyers (Al-Futaisi 2009; Narvekar et al. 2018). MB is a heterocyclic aromatic compound used for colouring products and it is one of the dyes mostly used in the above-mentioned industries (Anfar et al. 2017). There are several health and negative environmental effects of MB to human such as vomiting, chest pain, stomach pain, high fever, damages to central nervous systems cardiovascular and gastrointestinal (Cengiz & Cavas, 2008). Therefore, the removal of dyes from waste effluent becomes a global environmental concern because some of the dyes and their degradation products may be toxic also their treatment cannot depend on bio-degradation alone (Al-Futaisi et al. 2009; Anfar et al. 2017).

Cr(VI) is one of the pollutants which has caught attention in the research field due to its toxicity. There are two types of stable chromium in nature (Islam et al. 2019) trivalent Cr(III) and hexavalent Cr(VI). Cr(VI) has more toxic effects than Cr(III) to animals, humans and aquatic life due to its high solubility and mobility (Palanisamy et al. 2013; Alemu et al. 2018). It causes lung cancer, damage the kidneys, gastric and liver in humans (Gueye et al. 2014). Therefore, it is important to remove Cr(VI) in water before is discharged into the environment, also because Cr(VI) is non-biodegradable and can stay for a long time in the environment. Cadmium Cd(II) is one of the most toxic contaminants and it is a pollutant which is found in agricultural soil and aquatic environments (Zhou et al. 2019). Health hazards associates with Cd(II) is carcinogenic in nature and higher levels can cause hypertension, anaemia and damage to kidneys (Aghababaei et al. 2017).

The adsorption of toxic metal ions and dye from the aqueous solutions using different low-cost defatted adsorbents have been conducted by many researchers (Lu et al. 2009; Gilbert et al.

2011; Kowanga et al., 2016; Fontoura et al. 2017; Shooto et al. 2020). Gilbert et al. (2011) observed that the treatment of *C. papaya* seeds with hexane gave the sorption capacity of 1666.67 mg/g for Pb(II) and 1000.00 mg/g for Cd(II). Chandra et al. (2014) treated alga with n-hexane and compared the raw alga with the defatted alga for the removal of methylene blue dye. The results showed that the maximum adsorption capacity for raw *C. papaya* was 6.0 whilst the defatted alga was 7.73 mg/g and the specific surface area of raw, defatted was estimated to be 14.70, 18.94, m^2g^{-1} respectively. Kowanga et al. (2016) mentioned that the treatment of moringa powder with hexane made the moringa to be an efficient bio-sorbent for removal of Pb(II) and Cu(II) from aqueous solution. Fontoura et al. (2017) chemically treated microalgal biomass with a mixture of chloroform: methanol: water ratio for the removal of Acid Blue 161 dye. Their results showed that the maximum adsorbed amounts of AB-161 dye was 75.78 mg/g at 25 °C. Shooto et al. (2020) treated mucuna beans with acetone, methanol and dimethylformamide for the removal of Pb(II) ions and methylene blue dye from aqueous solution. Their findings revealed that the chemically treated adsorbents had higher adsorption capacity for methylene blue molecules than Pb(II) ions. The maximum capacities for Pb(II) with acetone, methanol and dimethylformamide were 18.94,16.15 and 17.60 mg/g respectively whereas the results for methylene blue were 22.78, 24.56 and 23.89 mg/g. Therefore, chemical treatment of biomass material will not only modify the chemical composition of the material but may also improve the adsorption capacity due to formation of new functional group (Lu et al., 2009). To the best of our knowledge, there is no study that has been conducted using defatted *Nigella Sativa* L. to remove chromium(VI), cadmium(II) ions and methylene blue dye in a system using pristine, defatted and carbonized *Nigella Sativa* L. seeds. The system parameters such as initial concentration, reaction contact time, temperature of the solution, and solution pH were varied.

9.3 Materials and preparation

Analytical grade chemicals acetone (C_2H_6CO)-99.5%, cadmium acetate $Cd(CH_3COO)_2$-99.99%, potassium dichromate ($K_2Cr_2O_7$), methylene blue dye ($C_{16}H_{18}ClN_3S$)-82%, and *N*,*N* dimethylformamide (C_3H_7NO) were purchased from Sigma Aldrich South Africa LTD and unprocessed *Nigella Sativa* L. seeds were procured at the health shop in Vanderbijlpark, South Africa.

9.3.1 Preparation of the pristine *Nigella Sativa* (PNS) seeds

Nigella Sativa seeds were washed with distilled water to remove dust and debris materials. The washing was carried out several times. Thereafter, the seeds were dried in an oven at 40 °C for 24 hr. The dried seeds were then stored in a desiccator for cooling. Thereafter, grounded using a blender with steel blades. The powder was sieved and then labelled pristine *Nigella Sativa* seeds (PNS).

9.3.2 Preparation of acetone *Nigella Sativa* (ANS) seeds

The method of preparing the adsorbents was adopted from Shooto et al. (2019a) with modifications. 10 g of the PNS seeds were added to 100 mL of acetone under stirring on a magnetic stove using the magnetic stirrer bar at room temperature. After 1 hr the resultant material was washed with distilled water to remove excess reagent and dried in the oven for 24 hrs at 50 °C. The seeds were designated acetone treated *Nigella Sativa* seeds (ANS).

9.3.3 Preparation of dimethylformamide *Nigella Sativa* (DNS) seeds

Pristine seeds (10 g) were mixed with 100 mL of dimethylformamide under stirring for 1 h. Then the material was isolated and rinsed in distilled water. The material was dried at 50 °C for 24 hrs in the oven. The seeds were designated dimethylformamide treated *Nigella Sativa* seeds (DNS).

9.3.4 Preparation of carbon-based acetone *Nigella Sativa* (CANS) and dimethylformamide *Nigella Sativa* (CDNS) seeds

Treated seeds (10 g) were carbonized at 600 °C for 2 hrs in a horizontal furnace under nitrogen thereafter, the furnace was allowed to cool off under nitrogen flow. The carbonized seeds were then designated carbonized acetone treated *Nigella Sativa* seeds (CANS) and carbonized dimethylformamide treated *Nigella Sativa* seeds (CDNS).

9.4 Adsorption experiments

The stock solutions of 100 mg/L for potassium dichromate ($K_2Cr_2O_7$), cadmium acetate $Cd(CH_3COO)_2$ and methylene dye ($C_{16}H_{18}ClN_3S$) were prepared by dissolving 0.1 g in 1 L of distilled water respectively. The solution pH effect was evaluated at pH 1, 3, 5, 7 and 9. The pH was adjusted by 0.1 M HCl for acidic medium and 0.1 M of NaOH for basic medium. A 20 mL of the adjusted solution was added to 0.1 g of the adsorbent and equilibrated for 60 min. Effect of initial concentration was studied using standard solutions of 20, 40, 60, 80 and 100 mg/L and agitated for 120 min at 200 rpm. Contact time effect was tested intervals of 1, 5, 10, 15, 20, 30, 60, 90 and 120 min. The effect of temperature was studied at 298, 303, 313, 333 and 353 K by agitation at 200 rpm for 120 min. After agitation the mixtures were centrifuged

at 5000 rpm for 5 min then decanted. The same procedure was followed for methylene blue dye. The determination of the point of zero charge (pHpzc) for all adsorbents was determined using 1M $NaNO_3$ concentration series of 100 mL. The solution pH 1 to 9 was adjusted by adding 0.1 M HCl for acidic medium and 0.1 M NaOH for basic medium. Then adjusted pH solutions were then added to 0.1 g of samples and agitated for 48 h at 200 rpm. After agitation the pH was measured. The final pH versus initial pH was plotted against pH values and the pHpzc was determined from the horizontal intersection point. The preparation method is shown in scheme 6.

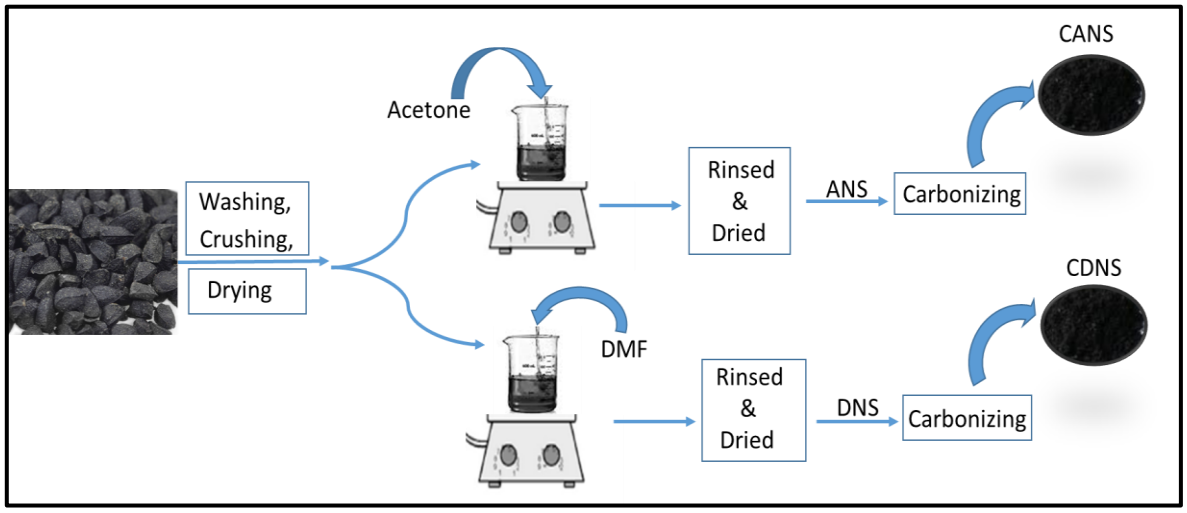

Scheme 6: Preparation of ANS, CANS, DNS and CDNS

9.5 Data Analysis

The amount of Cr(VI), Cd(II) ions and MB dye onto the adsorbents was calculated by using equation: $q_e=(C_o-C_e)v/m$; where (C_o) and (C_e) are the initial and final equilibrium concentrations (*mg/L*) of Cr(VI), Cd(II) and MB in the solution, (q_e) is the amount adsorbed on the surface (*mg/g*), *V* volume of the pollutants solution (*L*) and (*m*) is the mass of the adsorbent

(*g*). Equations (1) and (2) were used to determine the removal capacity and the adsorption percentage, R (%) of Cr(VI), Cd(II) ions and MB dye.

$$q_e = \frac{(C_o - C_e)\,V}{W} \qquad (1)$$

$$\%R = \frac{(C_o - C_e)}{C_o} \text{ x } 100 \qquad (2)$$

9.6 Adsorbents characterization

The biomaterials were characterized with scanning electron microscopy (SEM) taken on a Nova Nano SEM 200 from FEI operated at 10.0 kV in order to determine the surface morphology of the materials. Functional groups on the surface of the adsorbents were determined by Perkin Elmer Fourier transform infrared (FTIR) spectroscopy FTIR/FTNIR spectrometer, spectrum collected from 4000-400 cm^{-1}. The pH at point zero charge (pH_{PZC}) was determined by using the pH drift method where carbon adsorbents were added into 20 mL of 1 M $NaNO_3$ solutions with pH separately adjusted between 1 and 9. Adsorption capacity was determined using atomic adsorption spectroscopy (AAS) ASC 7000 from Shimadzu with auto sampler for determining the remaining Cr(VI) and Cd(II) in the solution. The MB dye analyses were determined using ultraviolet-visible (UV-Vis) spectrophotometer, Perkin Elmer Lambda 25 at 665 nm which collects spectra from 180 to 1100 nm UV and visible range with a slit of 1.0 and width of 0.1.

9.7 Result and discussion

9.7.1 Characterization of the bio-sorbents

9.7.1.1 SEM analysis

Figs.59a-e show the morphology of the bio-sorbent surfaces determined by scanning electron microscopy. The PNS images in Fig.59a showed that the surface of the adsorbent is composed of irregular morphology. Whilst, Figs.59b displayed improved sphere-like morphology which was porous and had cavities. Cavities might contribute to the bio-sorption of toxic ions and dyes (Asgher & Bhatti, 2012). The carbonized material for CANS in Fig.59c displayed dense textural structure and spherical morphology. Figs.59d-e the texture of the DNS and CDNS respectively showed that the surface was irregular. Defatting with DMF and carbonization showed different surface texture which could be attributed to the fact that extraction of oil from biomass through solvent extraction could lead to harsh effects of breaking the cell wall which may cause such surface topology (Fontoura et al. 2017). These characteristics are therefore, estimated to increase the adsorption processes of Cr(VI), Cd(II) and MB onto carbonized materials.

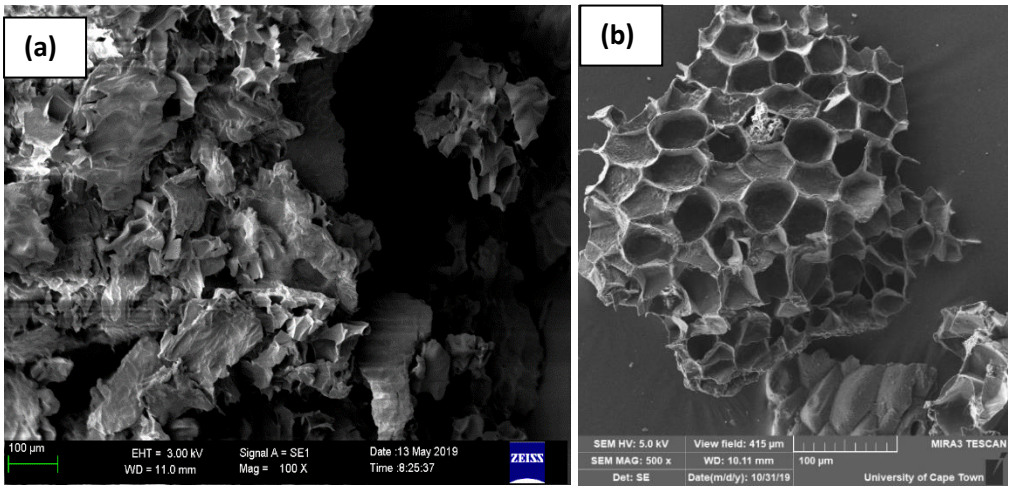

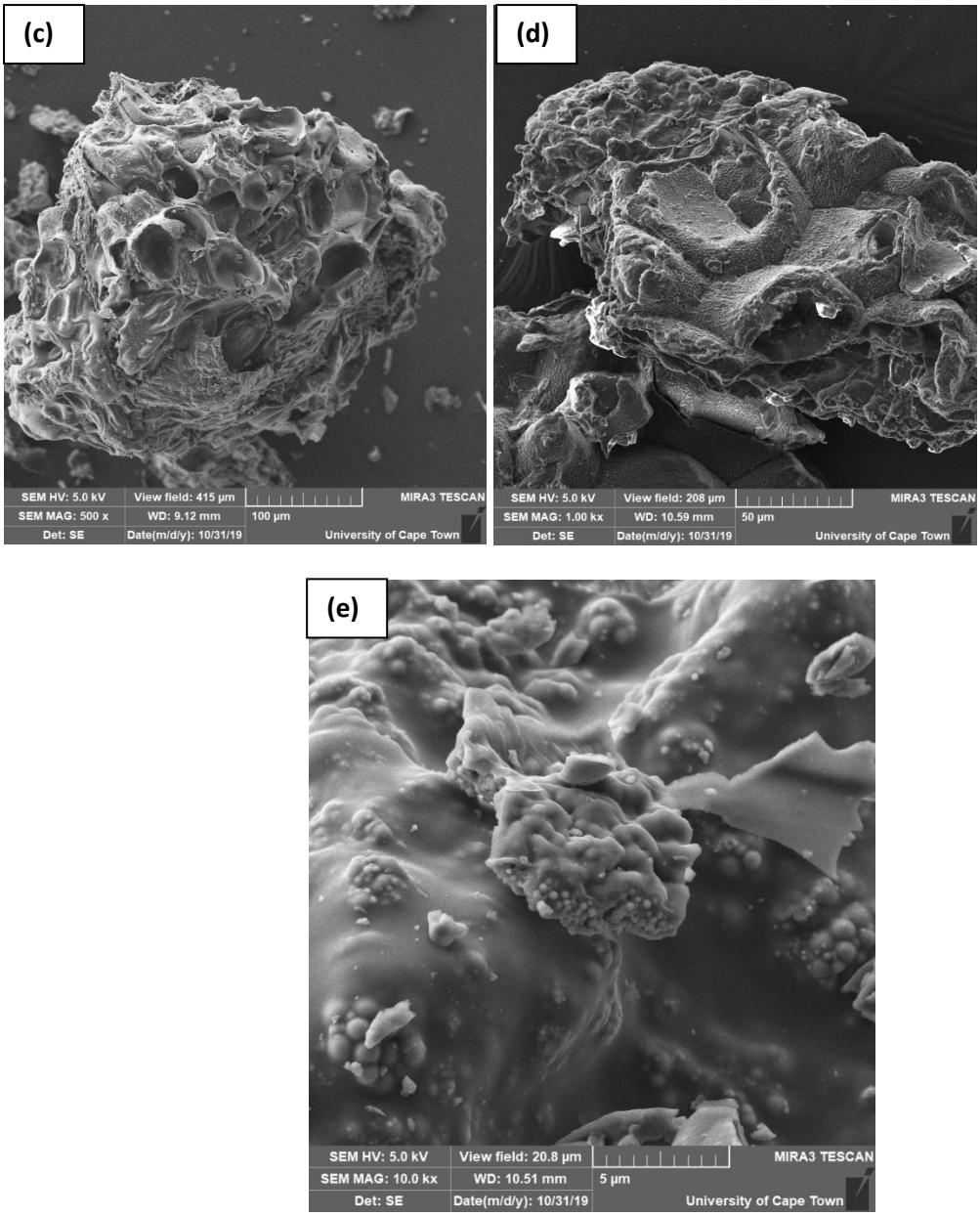

Figure 59: SEM images of (a) PNS, (b) ANS, (c) CANS, (d) DNS and (e) CDNS.

9.7.1.2 FTIR analysis

Fig. 60 represents the FTIR results of the adsorbents. Several peaks were identified which indicated the presence of various functional groups. A broad peak due to the free hydroxyl group (-OH) was observed at 3304, 3291, 3296 and 3298 cm^{-1} for PNS, ANS, DNS and CDNS respectively (Oliveira et al. 2016). CANS did not display any noticeable peaks except the small

peak at 1024 cm^{-1}. The small peak at 2999 cm^{-1} onto PNS was due to (-C-H) stretching in alkanes (Dahiru et al. 2018; Thabede et al. 2020a). This peak shifted 3007, 3012 and 3010 cm^{-1} on ANS, DNS and CDNS respectively. The two bands associated with methyl ($-CH_3$) and methylene ($-CH_2$) groups on PNS were observed at 2923 and 2848 cm^{-1} (Heidarinejad et al. 2018). These peaks shifted to 2919 and 2849 cm^{-1} for ANS, whilst the peaks on DNS shifted to 2923 and 2844 cm^{-1} and for CDNS they were observed at 2919 and 2852 cm^{-1}. The absorbance peak at 1757 cm^{-1} onto PNS was identified as the vibration of the carbonyl group stretching (-C=O) (Nagarjuna et al. 2018; Zhang et al. 2019a). This carbonyl peak on ANS shifted to 1744 cm^{-1}, whilst on DNS it shifted to 1740 cm^{-1} and 1749 cm^{-1} in CDNS. The absorption peaks on PNS at 1647 and 1549 cm^{-1} were assigned to (-OH) vibration (Danish et al. 2018) and ($-NH_2$) of the amide group respectively (Shooto et al. 2019b). However, on ANS the (-OH) peak shifted to 1649 and ($-NH_2$) peak shifted to 1540 cm^{-1}. On the other hand, the amide peaks on DNS were observed at 1638 cm^{-1} for the (-OH) group and 1545 cm^{-1} for the ($-NH_2$) group. Meanwhile on CDNS the peaks were observed at 1642 and 1540 cm^{-1} for (-OH) and ($-NH_2$) groups respectively. The carboxyl (-COOH) stretching band was assigned at 1464, 1450, 1452 and 1451 cm^{-1} on PNS, ANS, DNS and CDNS respectively (Abdel-Salam et al. 2018; Shooto et al. 2019b). The presence of CH_3 umbrella deformation vibrations were observed at 1376, 1368, 1365 and 1367 cm^{-1} on PNS, ANS, DNS and CDNS respectively (Tang et al. 2013; Yusuff & Arab, 2019). The bands at 1236, 1240, 1243 and 1248 cm^{-1} on PNS, ANS, DNS and CDNS were related to O-H bending vibration respectively (Oliveira et al. 2016). The peak associated with the (-C-O-C) stretching vibrations of cellulose and hemicellulose material (Ahmad & Haseeba, 2014; Shen et al. 2019) was observed at 1169 cm^{-1} on PNS. After defatting the seeds, this peak shifted to 1165, 1154 and 1158 cm^{-1} on ANS, DNS and CDNS respectively. The (-C-O) stretching vibration of carboxyl groups was observed at 1078, 1071, 1061 and 1068 cm^{-1} for PNS, ANS, DNS and CDNS respectively (Bai et al.

2010). The FTIR results showed that there were differences in the functional groups of the defatted and the pristine *Nigella Sativa* seeds and that the seeds had negatively charged groups on their surface. The four spectra (PNS, ANS, DNS and CDNS) were similar with slight shifts in characteristic absorbance peaks. For each adsorbent, the shifts in transmission frequency proposed that there was interaction of various chemical treatments to the PNS seeds (Danisha et al. 2018). This suggests that the hydroxyl, carbonyl, amides and carboxyl groups were available for bonding (Unuabonah et al. 2009).

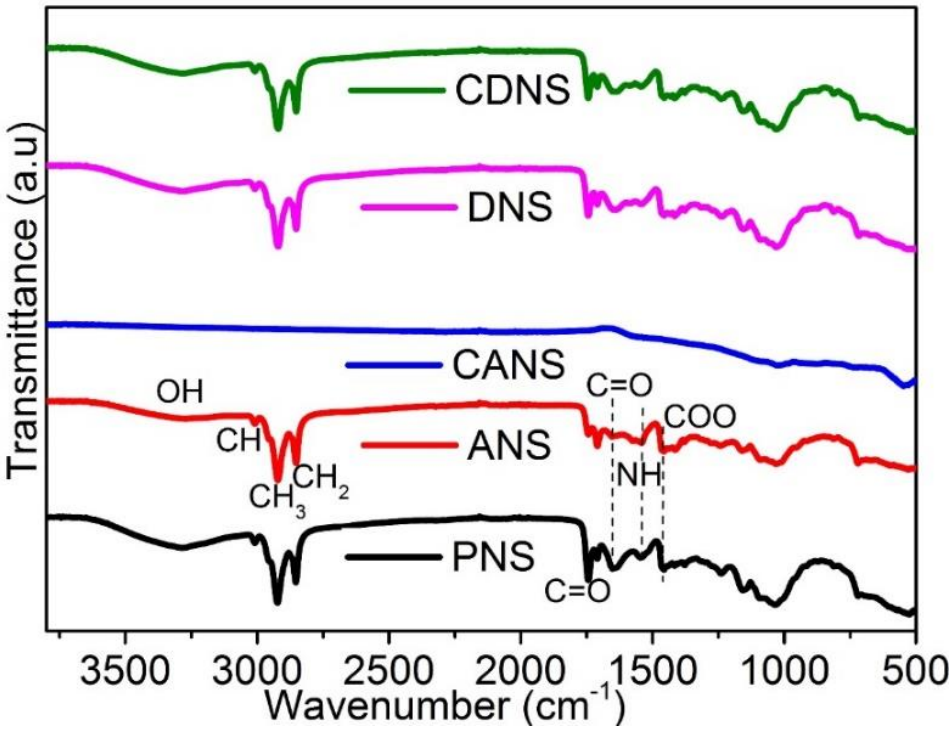

Figure 60: FTIR spectrum of PNS, ANS, CANS, DNS and CDNS

9.7.2 Adsorption studies

9.7.2.1 pH and point zero charge of the adsorbents

The zero-point charge (pHpzc) of any solid is the pH at which the charge on the surface of the adsorbent is zero (Chaudhry et al. 2017). The pHpzc values of PNS, ANS, ANS, DNS and CDNS are 5.81, 6.26, 5.65, 5.98 and 6.09, respectively. The pHpzc values of all adsorbents were acidic but closer to neutral. The results showed that all the adsorbents had a similar behaviour therefore it is expected that their pH pattern will be similar as well. The initial pH of adsorption is a very important parameter because it has an influence on the adsorption capacity (Aichour et al. 2018). It has the ability to change the ionization of the adsorbate, adsorbent surface load and the degree of the dissociation of the functional groups of adsorbate active sites (Nandi et al. 2009). The effect of pH was studied at 1, 3, 5, 7 and 9 as shown in Figs. 61a-e. The data showed that pH had an impact on adsorption performance for Cr(VI), Cd(II) and MB. Figs. 61a-e showed that removal of Cr(VI) decreased as the pH increased, this was because at acidic pH value Cr(VI) exists as H_2CrO_4, $HCrO_4^-$, $CrO_4^{2-}$and $Cr_2O_7^{2-}$ (Liu et al., 2018). At pH 2.0 the predominant species of Cr(VI) is $HCrO_4^-$ (Jia et al. 2018). The high adsorption capacity of Cr(VI) at low pH was due to the electrostatic attraction of the protonated surface of the adsorbents (Huang et al. 2020). The maximum adsorption capacity of Cr(VI) was obtained at pH 1 with maximum capacities ranging from highest of 74.4, 48.9, 42.6, 34.7 and 20.7 mg/g on CANS, ANS, CDNS, DNS and PNS respectively. Therefore, the adsorption capacity for Cr(VI) favoured acid conditions as compared basic conditions treatment. Meanwhile, the removal of Cd(II) and MB increased with the increased pH for all the adsorbents with low sorption at pH 1 and 3. This resulted in weak electrostatic interactions because at acidic pH conditions the functional groups on the adsorbents surface are protonated and acquired positive charge (Li et al. 2017; Thabede et al. 2020b). Therefore, few active sites were available to react with Cd(II) ions and MB (Thabede et al. 2020c). However, as the pH increases the surface of the adsorbents gradually became deprotonated and acquired negative charge. Hence, there was higher uptake. This was also observed by Thabede et al. (2020c). The

maximum adsorption capacities for Cd(II) were 87.9, 79.6, 42.1, 36.0 and 32.6 mg/g onto CANS, CDNS, ANS, PNS and DNS at pH 9 respectively. On the other hand, MB adsorption capacities were 95.7, 90.8, 58.4, 48.2 and 43.9 mg/g onto CANS, CDNS, ANS, DNS and PNS at pH 9 respectively. The results implied that percentage removal of Cd(II) and MB by *Nigella Sativa* seeds was lower in acidic medium which could due to the presence of positively charged hydrogen ions which competed and interfered with Cd(II) and MB for the available adsorption sites (Salman et al. 2016). It was observed that PNS, ANS, CANS, DNS and CDNS removed MB more than Cr(VI) and Cd(II) ions.

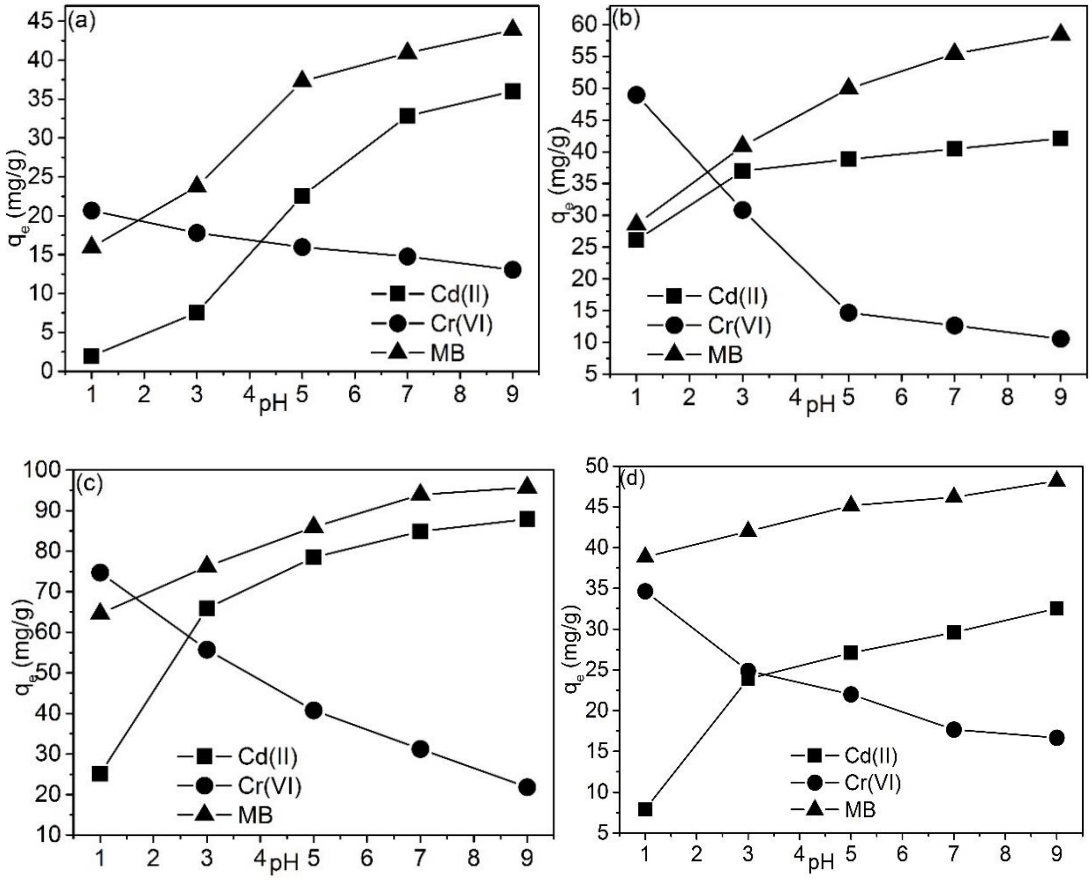

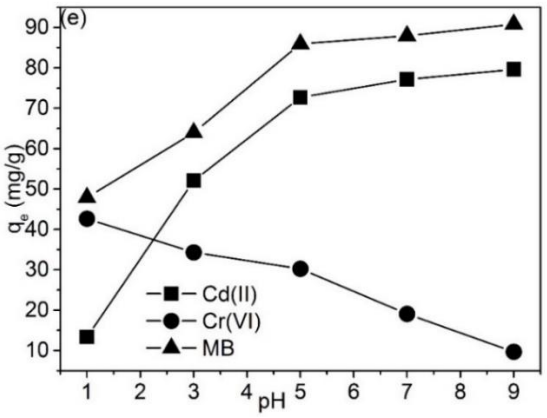

Figure 61: Effect of pH on (a) PNS, (b) ANS, (c) CANS, (d) DNS and (e) CDNS.

9.7.2.2 Contact Time effect and kinetic parameters determination

The equilibration time and kinetics of PNS, ANS, CANS, DNS and CDNS sorption was determined in batch method by studying contact time. The adsorption rate of Cr(VI), Cd(II) and MB onto PNS, ANS, CANS, DNS and CDNS versus time are shown in Fig. 62a-e. The trend of Cr(VI) onto all adsorbents in Fig. 62a-e showed that the adsorption rate was fast and happened in the first 10-15 min and thereafter, it became stable and reached equilibrium. The removal rate onto PNS, ANS, CANS, DNS and CDNS for Cd(II) was also quick in the beginning of the adsorption process within the first 20 min thereafter, the process slowed down and reached equilibrium. MB adsorption rate onto PNS, ANS, CANS and DNS in Fig 62a-d was observed between 15 and 20 min. On the other hand, the removal rate of MB onto CDNS took place in the beginning of the process within 1 min and thereafter, no significant changes were observed. The adsorption of MB was faster than Cr(VI) and Cd(II). The fast adsorption rate in the beginning of the process was due to abundant binding sites and availability of pores on adsorbents surfaces however, as time lapsed free binding sites and pores were consumed (Shooto et al. 2020). Thereafter, the rate slowed down because the binding sites and pores were exhausted and the adsorption was then controlled only by the rate at which Cr(VI), Cd(II) or MB molecules are transported from the external to the internal sites of the adsorbents. This

means that at initial stages, active sites were rapidly occupied by Cr(VI), Cd(II) and MB molecules through chemical interaction and as time elapsed there were no more vacant sites on the surfaces of the adsorbents, so no multilayer was formed hence equilibrium was attained (Kumar & Jiang, 2017).

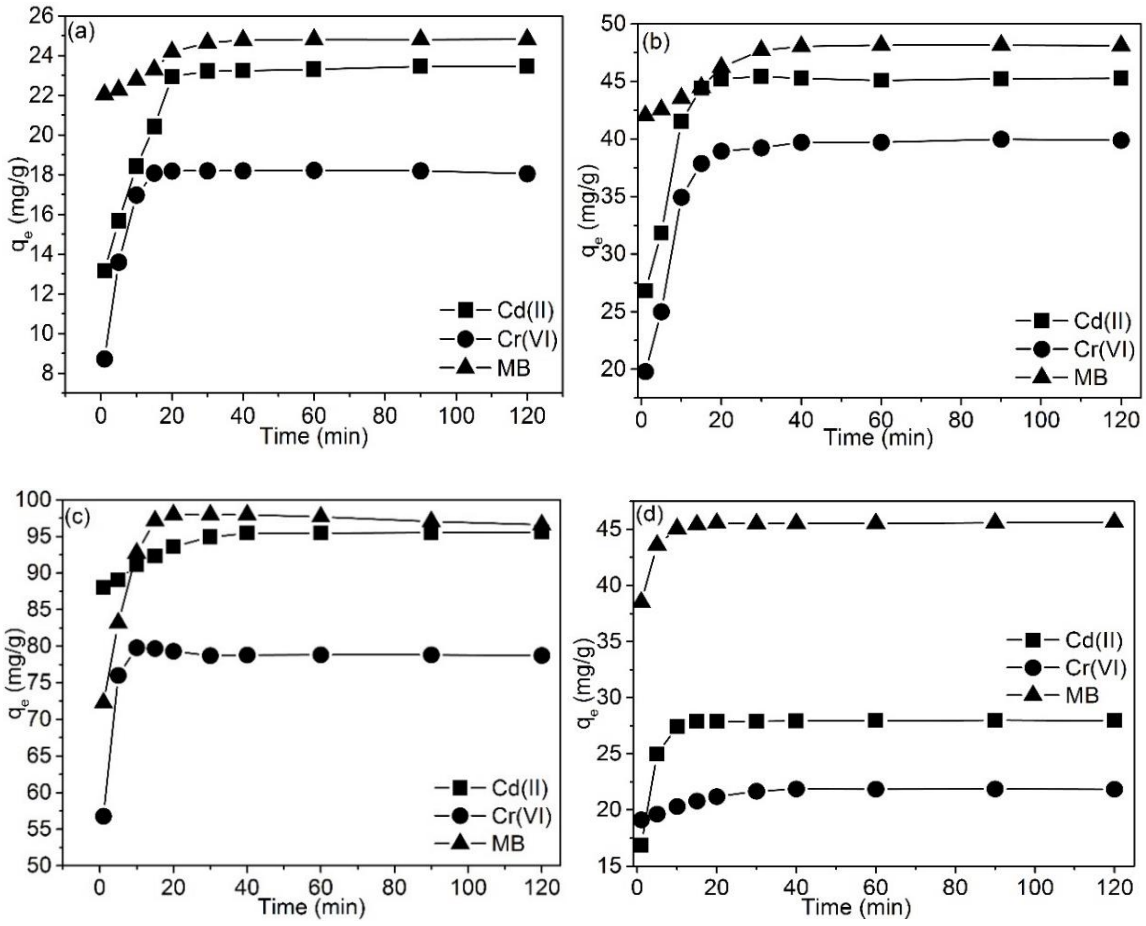

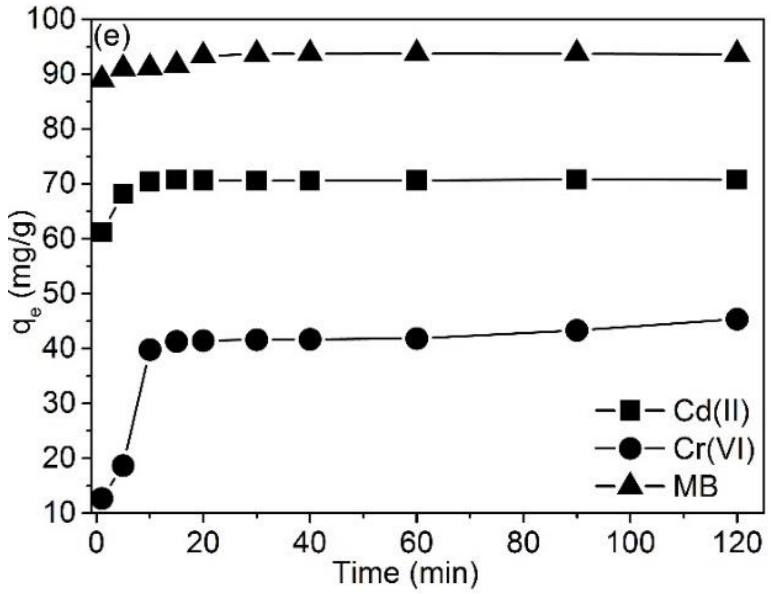

Figure 62: Effect of time on (a) PNS, (b) ANS, (c) CANS, (d) DNS and (e) CDNS for the adsorption of Cd(II), Cr(VI) and MB

The chemical and physical features of adsorbents and adsorbates influence the rate of adsorption (Siddiqui & Chaudhry, 2008). Hence, the results of Cr(VI),Cd(II) and MB adsorption from aqueous solution onto PNS, ANS, CANS, DNS and CDNS surfaces were fitted into kinetic models. Pseudo-first order (PFO), pseudo-second order (PSO) and intra-particle diffusion (IPD) non-linear equations as indicated in equation (3), (4) and (5) respectively were used to estimate the kinetic models. These equations were subjected to KyPlot software.

$$q_e = q_t(1 - e^{-k_1 t}) \quad (3)$$

$$q_e = \frac{1 + k_2 q_e t}{k_2 q_e^2 t} \quad (4)$$

$$q_t = k_i\left(t^{1/2}\right) + C \quad (5)$$

(q_e) and (q_t) are the amount of adsorbate removed (mg/g) at equilibrium and time interval (t) respectively, (K_1) measured in (min^{-1}), (K_2) measured in (g mg^{-1} min^{-1}) and (K_i) measured in (g g^{-1} $min^{1/2}$) are the rate constants of the PFO in (/min), PSO (g/mg/min) and IPD (g/g/$min^{-1/2}$) respectively and *C* (mg/g) is the adsorbate amount on the surface of the adsorbents. The pseudo-first order (PFO) kinetic model assumes that the sorption rate depends on the number of the unoccupied sites in solution whilst the pseudo-second order (PSO) kinetic model assumes that the sites on the adsorbent surface and adsorbate ions both determine the rate in the solution (Siddiqui & Chaudhry, 2008). The nature of the adsorption process was also calculated using intra-particle diffusion (IPD) kinetic model which determines whether adsorption takes place on the surface (ESA) or pores (EPA). The calculation of ESA and EPA is based on the assumption that concentration (*C*) is equal to the obtained experimental (q_e) value which means that the adsorption was due to surface (ESA) adsorption then ESA is equal to 100%. However, the remaining lower C value suggests that the adsorption was due to pore adsorption (EPA) (Shooto et al. 2020).

Table 24 show the kinetic models and the calculated parameters of all adsorbents. The kinetic models were used to predict the adsorption mechanism. The kinetic study of Cr(VI), Cd(II) and MB onto PNS had a correlation value closest to 1 at 0.998, 0.993 and 0.998 for PFO and the calculated adsorption capacities of 19.98, 20.98 and 21.31 mg/g respectively. The PFO results showed that they best fitted onto PNS than PSO. The calculated adsorption capacity for Cr(VI), Cd(II) and MB onto ANS were 30.63, 40.76 and 46.93 mg/g and was close to the experimental data with r^2 values of 0.996, 0.997 and 0.996 which fitted PSO respectively. Similarly, the calculated adsorption capacity of 81.44, 98.33 and 100.45 mg/g for Cr(VI), Cd(II) and MB onto CANS best fitted PSO with r^2 values of 0.999, 0.998 and 0.994 respectively. The data for DNS and CDNS fitted PSO for Cr(VI), Cd(II) and MB with r^2 values of 0.997, 0.995 and 0.995

onto DNS, whilst 0.998, 0.998 and 0.997 was observed onto CDNS. The calculated adsorption capacities of DNS were 22.99, 28.96 and 42.76 mg/g for Cr(VI), Cd(II) and MB respectively which was close to the experimental data. On the other hand, the experimental adsorption capacities of Cr(VI), Cd(II) and MB onto CDNS were close to the calculated adsorption data which was 49.55, 75.06 and 95.52 mg/g respectively. IPD results indicated pore adsorption (EPA) for Cr(VI) and Cd(II) ions onto PNS were 52.23 and 53.70 % respectively whilst, the removal MB was controlled by surface adsorption (ESA) with 85.78 %. IPD data showed that the removal of Cr(VI) was controlled by EPA with 55.54 % onto ANS. On the other hand, Cd(II) and MB adsorption onto ANS was due to ESA with 55.13 and 84.81 % respectively. The removal of Cr(VI), Cd(II) and MB onto CANS was dominated by ESA with 70.11, 90.96, 72.90 % respectively. Similarly, Cr(VI), Cd(II) and MB onto DNS was controlled by ESA with percentages of 72.38, 57.48 and 73.01 % respectively. The removals of Cr(VI) onto CDNS was controlled EPA with 77. % whilst Cd(II) and MB(II) removal was due to ESP with 79.14 and 90.20 % respectively. The low (K_2) values suggested that the adsorption rate decreased with the increase of the phase contact time and the adsorption rate were proportional to the number of unoccupied sites (Kolodynska et al. 2017).

Table 24: Kinetic models and their parameters onto PNS, ANS, CANS, DNS and CDNS

Isotherms	PNS			ANS			CANS			DNS			CDNS		
	Cr(VI)	Cd(II)	MB	Cr(VI)	Cd(II)	MB	Cr(VI)	Cd(II)	MB	Cr(VI)	Cd(II)	MB	Cr(VI)	Cd(II)	MB
PFO q_e (mgg^{-1})	19.98	20.98	21.31	12.51	16.76	15.62	17.45	16.96	18.71	37.85	12.96	30.76	25.87	41.54	65.54
K_1 (min^{-1})	0.17	0.17	0.18	0.10	0.14	0.13	0.13	0.14	0.16	0.32	0.11	0.26	0.22	0.34	0.55
r^2	0.9982	0.993	0.998	0.8663	0.894	0.898	0.7815	0.888	0.789	0.799	0.869	0.896	0.755	0.968	0.896
PSO q_e (mgg^{-1})	11.27	11.98	10.89	30.63	40.76	46.93	81.44	98.33	100.45	22.85	28.96	42.76	49.55	75.06	95.52
K_2 ($mg^{(1-n)}$ L^n g^{-1})	0.094	0.099	0.091	0.26	0.34	0.39	0.68	0.82	0.84	0.19	0.24	0.36	0.41	0.63	0.80
r^2	0.859	0.907	0.98	0.996	0.997	0.996	0.999	0.998	0.994	0.997	0.995	0.995	0.998	0.998	0.997
IPD C (mgg^{-1})	8.70	10.82	21.29	17.77	25.50	20.85	55.96	86.98	71.44	15.83	16.09	33.32	11.18	56.04	84.56
K_i ($g\ g^{-1}\ min^{0.5}$)	0.073	0.090	0.18	0.15	0.21	0.17	0.47	0.72	0.60	0.13	0.13	0.28	0.093	0.47	0.70
r^2	0.86	0.88	0.92	0.72	0.96	0.89	0.97	0.89	0.91	0.86	0.90	0.95	0.89	0.79	0.98
EPA[a] %	52.23	53.70	14.22	55.54	44.86	15.19	29.89	9.04	27.10	27.62	42.52	26.99	77.35	20.86	9.80
ESA[a] %	47.77	46.30	85.78	44.65	55.14	84.81	70.11	90.96	72.90	72.38	57.48	73.01	24.65	79.14	90.20

Experimental (mgg^{-1})	18.22	23.46	24.82	39.38	45.44	48.17	79.81	95.62	97.99	21.87	27.99	45.64	45.36	70.81	93.75

9.7.2.3 Concentration effect and equilibrium isotherms determination

The effect of Cr(VI), Cd(II) and MB initial concentration onto PNS, ANS, CANS, DNS and CDNS was studied from 20, 40, 60, 80 and 100 mg/L and are represented in Figs. 63a-e. The adsorption capacity of Cd(II) and MB onto PNS (Fig. 63a) increased with increasing initial concentration whilst the sorption of Cr(VI) showed a decreased between 80 to 100 mg/L. The maximum sorption capacities was found to be 17.77, 23.77 and 24.40 mg/g for Cr(VI), Cd(II) ions and MB respectively. The adsorption onto ANS and CANS (Figs. 63b-c) showed a similar pattern. The sorption of Cr(VI), Cd(II) and MB had maximum adsorption capacities of 40.02, 48.41, and 49.02 mg/g onto ANS respectively. Whereas the maximum sorption onto CANS were 77.81, 95.15 and 99.82 m/g for Cr(VI), Cd(II) and MB respectively. The increased in initial concentration was due to higher concentration gradient which acted as a driving force to overcome resistances to mass transfer of ions between the aqueous phase and the solid phase (Akpomie et al. 2015). In Figs. 63d-e it was observed that as the initial concentration of Cr(VI) increased from 20 to 80 mg/L so did the adsorption capacity however a further increase of initial concentration between 80 and 100 mg/L gradually reduced to reach equilibrium. The adsorption of Cd(II) in Figs. 63d-e shows that the adsorption capacity increased between 20 and 40 mg/L thereafter, equilibrium was attained with a slight decrease. A similar observation was obtained for the removal of MB in Figs. 63d-e where there was an increase in the initial concentration between 20 and 60 mg/L a further increase attained equilibrium. A decrease might be due to that the adsorbents had a certain number of active sites and at higher concentrations the active sites become saturated (Huang et al. 2012; Olabemiwo et al. 2017).

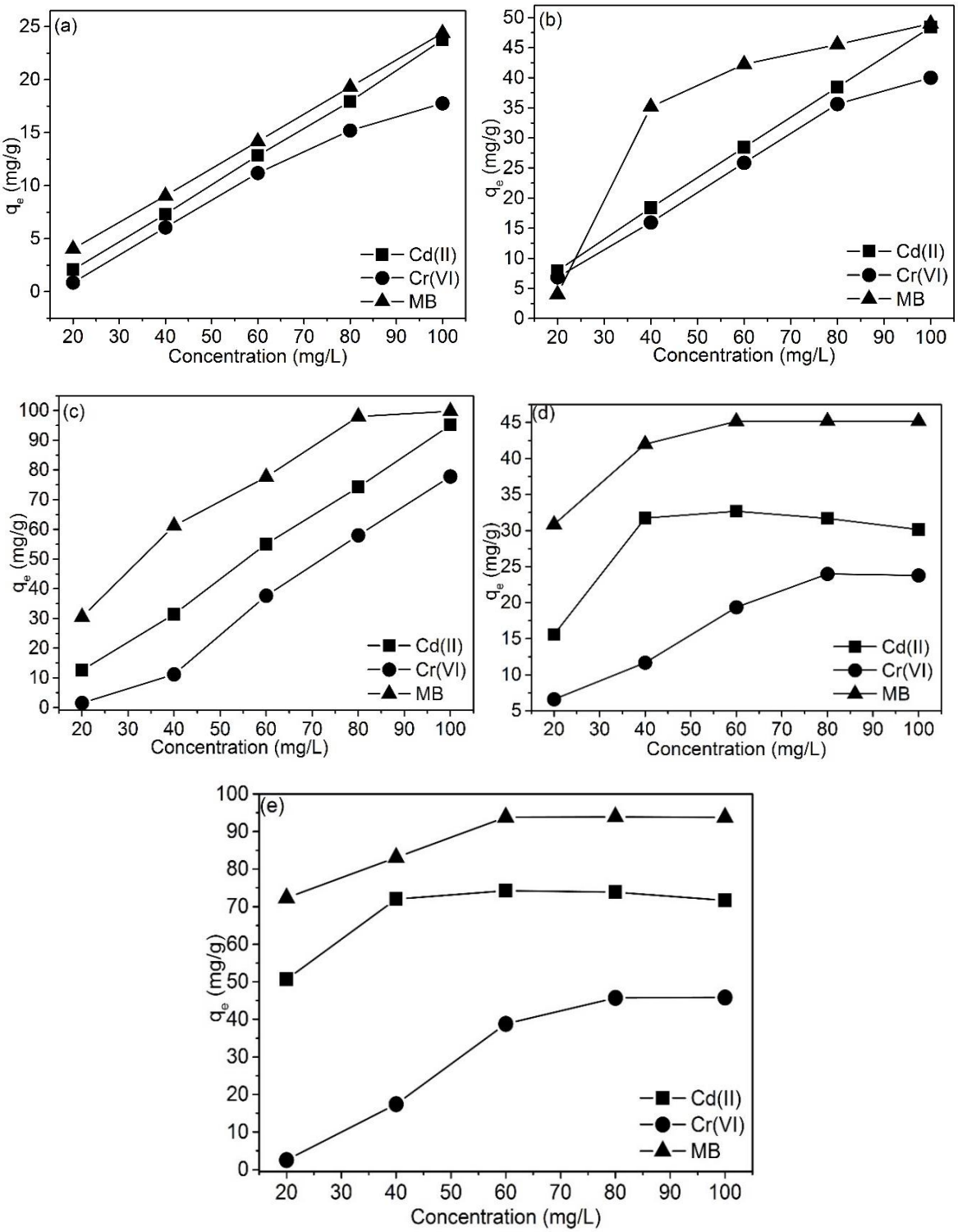

Figure 63: Effects of concentration on (a) PNS, (b) ANS, (c) CANS, (d) DNS and (e) CDNS for the adsorption of Cd(II), Cr(VI) and MB

.

The nonlinear adsorption isotherm models (Langmuir and Freundlich) were used to estimate the equilibrium data by using equations (6) and (7) respectively. Maximum adsorption capacity Q_o (mg/g), of Cr(VI), Cd(II) and MB. Langmuir interaction energy constant represented by b (Lmg^{-1}), k_f ($mg^{(1-n)}$ L^n g^{-1}) and n are the Freundlich model capacity factor and Freundlich linearity constant, respectively. Langmuir model proposes that the adsorption take place through chemisorption using monolayer adsorption of the sorbate on the adsorbent and is homogeneous in nature (Aloma et al. 2012; Basu et al. 2017). The model further calculates a saturation value of the sorbent, as it suggests that the adsorbent has definite number of binding sites and each site is responsible for binding only one metal ion with almost zero interaction amongst the adsorbed ions (Shokrollahi et al. 2017). On the contrary the Freundlich model indicates multilayer sorption and is heterogeneous in nature (Saeed et al. 2009).

$$q_e = \frac{Q_o b C_e}{1 + bC_e} \quad (6)$$

$$q_e = k_f C_e^{1/n} \quad (7)$$

Table 25 show adsorption models for Langmuir and Freundlich results for PNS, ANS, CANS, DNS and CDNS calculated at 298 K. The data showed coefficients for Cr(VI), Cd(II) and MB with 0.9971, 0.993 and 0.998 respectively onto PNS which best fitted Freundlich model. Similarly, correlation coefficient onto ANS also fitted Freundlich model with r^2 of 0.996, 0.995 and 0.994 for Cr(VI), Cd(II) and MB respectively. This suggested that Cr(VI), Cd(II) and MB onto PNS and ANS surface formed multilayer and was heterogeneous in nature (Aichour et al., 2018). The SEM images of PNS and ANS in Fig.57b showed that the surfaces had rough structure development which was not homogenous. A similar observation was discovered by Chaudhry et al. (2016). The values (r^2) for CANS showed that they also fitted Freundlich model

than Langmuir model and the correlation values for Cr(VI), Cd(II) and MB were 0.993, 0.994 and 0.996 respectively. The equilibrium data indicated that the sorption results for Cr(VI), Cd(II) and MB onto DNS fitted Freundlich model with high r^2 of 0.995, 0.996 and 0.991. Similarly, the coefficient of determination values (r^2) for Cr(VI), Cd(II) and MB fitted Freundlich model onto CDNS.

Table 25: Adsorption isotherm models onto PNS, ANS, CANS, DNS and CDNS

Isotherms	**PNS**			**ANS**			**CANS**			**DNS**			**CDNS**		
	Cr(VI)	**Cd(II)**	**MB**	**Cr(VI)**	**Cd(II)**	**MB**	**Cr(VI)**	**Cd(II)**	**MB**	**Cr(VI)**	**Cd(II)**	**MB**	**Cr(VI)**	**Cd(II)**	**MB**
Langmuir Q_o(mgg^{-1})	25.64	38.54	18.79	24.52	10.65	25.54	47.75	67.18	34.89	14.57	18.86	29.86	12.87	69.06	86.61
B (Lmg^{-1})	0.21	0.32	0.16	0.20	0.089	0.21	0.39	0.56	0.29	0.12	0.16	0.25	0.11	0.56	0.72
r^2	0.883	0.874	0.819	0.864	0.913	0.886	0.895	0.969	0.955	0.906	0.896	0.881	0.855	0.886	0.896
Freundlich 1/n (mgg^{-1})	19.27	21.74	27.51	43.63	43.12	42..63	90.35	72.06	94.55	23.31	31.06	48.06	41.85	73.26	97.72
k_f ($mg^{(1-n)}$ L^n g^{-1})	0.16	0.18	0.23	0.36	0.36	0.36	0.75	0.60	0.79	0.19	0.26	0.40	0.35	0.61	0.81
r^2	0.997	0.993	0.998	0.996	0.995	0.994	0.993	0.994	0.996	0.995	0.996	0.991	0.997	0.992	0.995
Experimental (mgg^{-1})	17.77	23.77	24.40	40.02	48.41	49.02	95.15	77.82	99.82	23.99	32.69	45.19	45.81	74.26	93.90

9.7.2.4 Temperature effect and thermodynamic parameters determination

The sorption of Cr(VI), Cd(II) and MB onto PNS, ANS, CANS, DNS and CDNS are shown in Figs. 64a-e. The trend in Figs. 64a-e shows that removal of Cd(II) and MB increased as the temperature increased from 298 to 303 K thereafter equilibrium was reached on all adsorbents. The maximum sorption capacities of Cd(II) onto PNS, ANS, CANS, DNS and CDNS were 23.46, 48.11, 96.89, 31.37 and 73.91 mg/g respectively whilst MB capacities were 24.44, 48.60, 97.97, 45.92 and 92.60 mg/g respectively. This increase in temperature was important because it showed that high temperature was required so that the ions in the solution had enough kinetic energy (Igberase et al. 2017). The data in Figs. 64a-e showed that the sorption of Cr(VI) onto PNS, ANS, CANS, DNS and CDNS increased as temperature increased from 298 to 353 K. This showed the endothermic nature of the sorption processes (Thabede et al. 2020b), with maximum sorption capacities of 19.84, 42.48, 87.44, 29.99 and 65.38 mg/g respectively onto PNS, ANS, CANS, DNS and CDNS. The gradually increased adsorption at higher temperatures indicated that adsorbate-adsorbent interaction was feasible at higher temperatures, suggesting that higher temperatures were more favourable to the adsorption process (Kumar & Jiang, 2017).

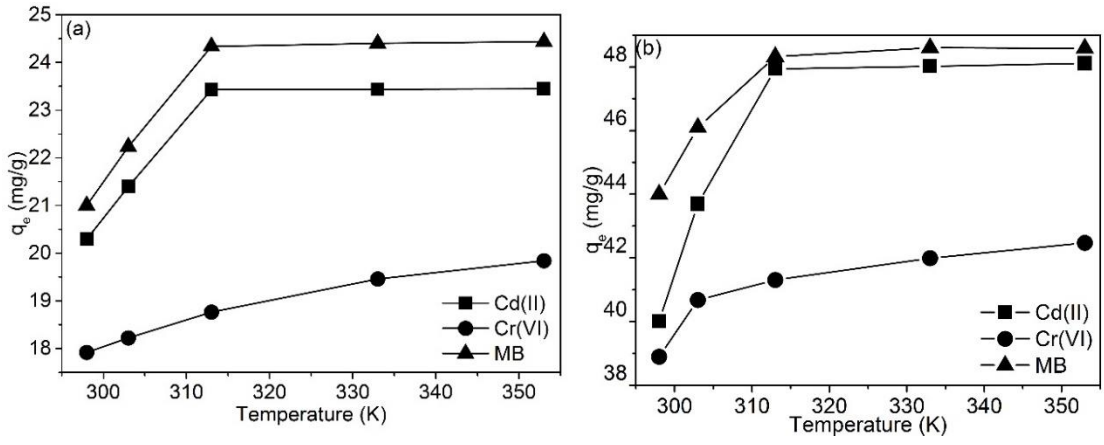

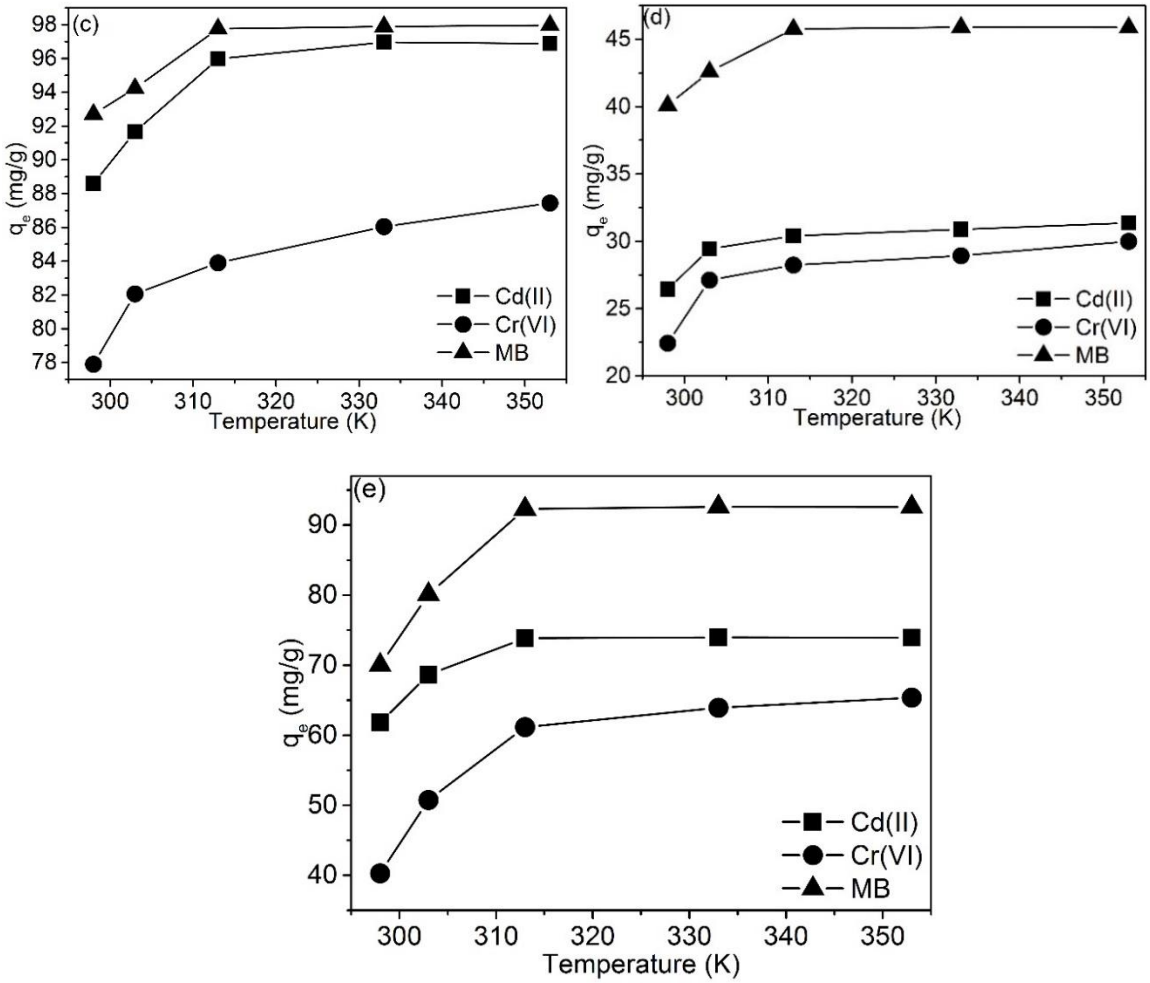

Figure 64: Effects of temperature on (a) PNS, (b) ANS, (c) CANS, (d) DNS and (e) CDNS for the adsorption of Cd(II), Cr(VI) and MB.

Thermodynamic parameters are significant tools to check the feasibility and spontaneity of the adsorption process (Chaudhry et al. 2016). Thermodynamic entropy change (ΔS^o) and enthalpy change (ΔH^o) and Gibbs free energy change (ΔG^o) were assessed using equations (8) and (9). ΔH^o and ΔS^o were attained from the slope and intercept of the van't Hoff plot of ln K against 1/T. K_c is the equilibrium constant of thermodynamic function which was calculated by equation (10) where q_e is the amount of Cr(VI), Cd(II) and MB adsorbed per unit mass of samples (mg/g) onto PNS, ANS, CANS, DNS and CDNS. C_e is the equilibrium concentration (mg/L); R is the gas constant (8.314 $J.mol^{-1}$ K^{-1}); and T is the temperature (K).

$$In\ K_c = -\frac{\Delta H^o}{RT} - \frac{\Delta S^o}{R} \quad (8)$$

$$\Delta G^o = -RT\ In\ K_c \quad (9)$$

$$K_c = \frac{q_e}{C_e} \quad (10)$$

Thermodynamic parameters (ΔS^o, ΔH^o and ΔG^o) for Cr(VI), Cd(II) and MB are shown in Table 26 for PNS, ANS, CANS, DNS and CDNS calculated at 298, 303, 313, 333 and 353 K. The sorption processes of Cr(VI), Cd(II) and MB indicated positive values for (ΔS^o and ΔH^o) on all adsorbents. The positive values for (ΔS^o) suggested the increased randomness of the ions in the solution as the adsorption processes approached equilibrium (Aichour & Zaghouane-Boudiaf, 2019) meanwhile the positive (ΔH^o) indicated that the reaction was endothermic. An endothermic reaction increased the removal uptake of Cr(VI), Cd(II) and MB as temperature of the system was increased, this was in agreement with temperature effect results (Thabede 2020b). The calculated (ΔG^o) values were negative for PNS, ANS, CANS, DNS and CDNS in all the investigated temperatures and became more negative with an increase in temperature. The negative values indicated that the removal Cr(VI), Cd(II) and MB on all the adsorbents were spontaneous and feasible (Shifera et al. 2016). Physical adsorption of Gibb's free energy change (ΔG^o) ranges between -20 and 0 kJ/mol whilst the chemical adsorption is between -80 to -400 kJ/mol (Ali et al, 20190). Therefore, the data in Table 4 showed that the adsorption process was predominated by physical adsorption process. This indicated that higher adsorption occurred at higher temperatures and that at higher temperature and ions were readily desolvated and their adsorption becomes more favourable (Awual et al. 2014).

Table 26: Thermodynamic parameters PNS, ANS, CANS, DNS and CDNS

Parameter	PNS			ANS			CANS			DNS			CDNS		
	Cr(VI)	Cd(II)	MB	Cr(VI)	Cd(II)	MB	Cr(VI)	Cd(II)	MB	Cr(VI)	Cd(II)	MB	Cr(VI)	Cd(II)	MB
ΔH^o (KJ mol^{-1})	$4x10^{-4}$	$4.x10^{-3}$	$8.x10^{-4}$	$1x10^{-4}$	$1x10^{-3}$	$9x10^{-4}$	$9x10^{-4}$	$8x10^{-4}$	$5x10^{-4}$	$7x10^{-4}$	$1x10^{-3}$	$2x10^{-3}$	$4x10^{-4}$	$2x10^{-3}$	$5x10^{-3}$
ΔS^o (KJ $mol^{-1}K^{-1}$)	$2x10^{-4}$	$8x10^{-3}$	$5x10^{-3}$	$4x10^{-4}$	$6x10^{-3}$	$5x10^{-4}$	$4x10^{-3}$	$6x10^{-3}$	$4x10^{-4}$	$3x10^{-3}$	$2x10^{-3}$	$7x10^{-3}$	$3x10^{-4}$	$5x10^{-3}$	$1.x10^{-3}$
ΔG^o (KJ mol^{-1})															
288 K	-7.70	-3.04	-4.44	-1.91	-6.11	-5.63	-3.21	-7.62	-7.69	-2.23	-9.43	-3.78	-9.49	-2.19	-6.06
298 K	-7.65	-3.26	-5.20	-1.75	-6.37	-5.89	-3.83	-8.48	-8.96	-1.32	-8.41	-4.15	-8.82	-2.34	-6.19
308 K	-7.40	-3.42	-5.78	-1.32	-6.93	-6.13	-4.29	-9.03	-9.03	-1.12	- 6.60	-4.40	-7.49	-2.70	-6.47
318 K	-7.20	-2.82	-6.42	-1.28	-7.33	-6.65	-4.81	-9.59	-9.25	-1.06	-5.89	-4.78	-6.69	-2.89	-7.00
328 K	-7.11	-3.99	-7.06	-1.21	-7.23	-7.56	-5.19	-9.81	-9.51	-1.01	-5.05	-5.05	-4.70	-3.06	-7.42

9.7.3 Comparative studies of Cr(VI) and Cd(II) ions and MB dye

A comparative study of sorption capacities of different adsorbents are presented in Table 27, 28 and 29. The defatted and carbonized *Nigella Sativa* adsorbents of ANS, CANS, DNS and CDNS adsorption capacities for Cr(VI), Cd(II) and MB were compared with other adsorbents from literature. The comparison studies showed that ANS, CANS, DNS and CDNS had higher adsorption capacities than some of the reported adsorbents. Therefore, the defatted *Nigella Sativa* L. seeds can be used as low cost adsorbents for the removal of Cr(VI), Cd(II) and MB in aqueous solution.

Table 27: Literature reports of activated carbon materials for the removal of Cr(VI) ions

Adsorbent	**Maximum capacity (mg/g)**	**Reference**
Peanut shell	106.4	Gueye et al. 2014
Defatted *Nigella Sativa* L.	87.44	This study
Carbon microsphere	65.5	Han et al. 2018
Peganum harmala seed	53.5	Khosravi et al. 2018

Pinewood sawdust	42.7	Yang et al. 2017
Macadamia	40.9	Lesaoana et al. 2019
Bamboo bark	18.9	Zhang et al. 2015
Carbon nanotubes	14.3	Bayazit & Kerkez, 2014

Table 28: Literature reports of activated carbon materials for the removal of Cd(II) ions

Adsorbent	**Maximum capacity (mg/g)**	**Reference**
Glebionis coronaria L.	106.9	Tounsadia et al. 2016
Defatted AC *Nigella Sativa* L.	96.89	This study
Rice straw	74.6	Zhang et al. 2019
Trapa natans husks	50.2	Yin et al. 2019
Phragmites australis	40.6	Guo et al., 2017
Buffalo weed	11.6	Yakkala et al. 2014
Chicken feather	7.8	Chen et al. 2019
Oxidized granular AC	5.7	Huang et al. 2007

Table 29: Literature reports of activated carbon materials for the removal of MB

Adsorbent	**Maximum capacity (mg/g)**	**Reference**
Magnolia Grandiflora L.	101.3	Wang et al. 2019
Defatted *Nigella Sativa* L.	99.82	This study
Licorice root waste	82.9	Ghaedi et al. 2014
Reed	77.4	Wang et al. 2018

Coconut bunch waste	70.9	Hameed et al. 2008
Ficus carica bast	49.9	Pathania et al. 2017
Activated lignin-chitosan	36.2	Albadarin et al. 2017
Feldspar clay	19.9	Diagboya & Dikio, 2018

9.7.4 Reusability studies

The reusability of adsorbents is an important factor for its practical application. In order to make the adsorption process inexpensive it is vital that the adsorbent display significant properties such as the ability to regenerate, high adsorption capacity, and be able to be reusable in the adsorption process (Aichour et al. 2018). The reusability of PNS, ANS, CANS, DNS and CDNS were investigated using 0.01 M hydrochloric acid as an eluting agent and distilled water. The adsorption/desorption results of the adsorbents for Cr(VI), Cd(II) and MB are shown in Figs. 65a-e. The data showed that originally PNS, ANS, CANS, DNS and CDNS displayed high removal uptake. After four cycles of adsorption-desorption the removal percentages decreased for all adsorbents. This might be due to inability of the adsorbents to desorb metal ions and dye from the adsorbents surface and cavities during the regeneration processes (Shooto 2020) and the mass loss of the adsorbents during desorption (Akpomie et al. 2015) hence the lower uptake. These findings indicated that PNS, ANS, CANS, DNS and CDNS adsorbents may be reusable in aqueous solution for treatment.

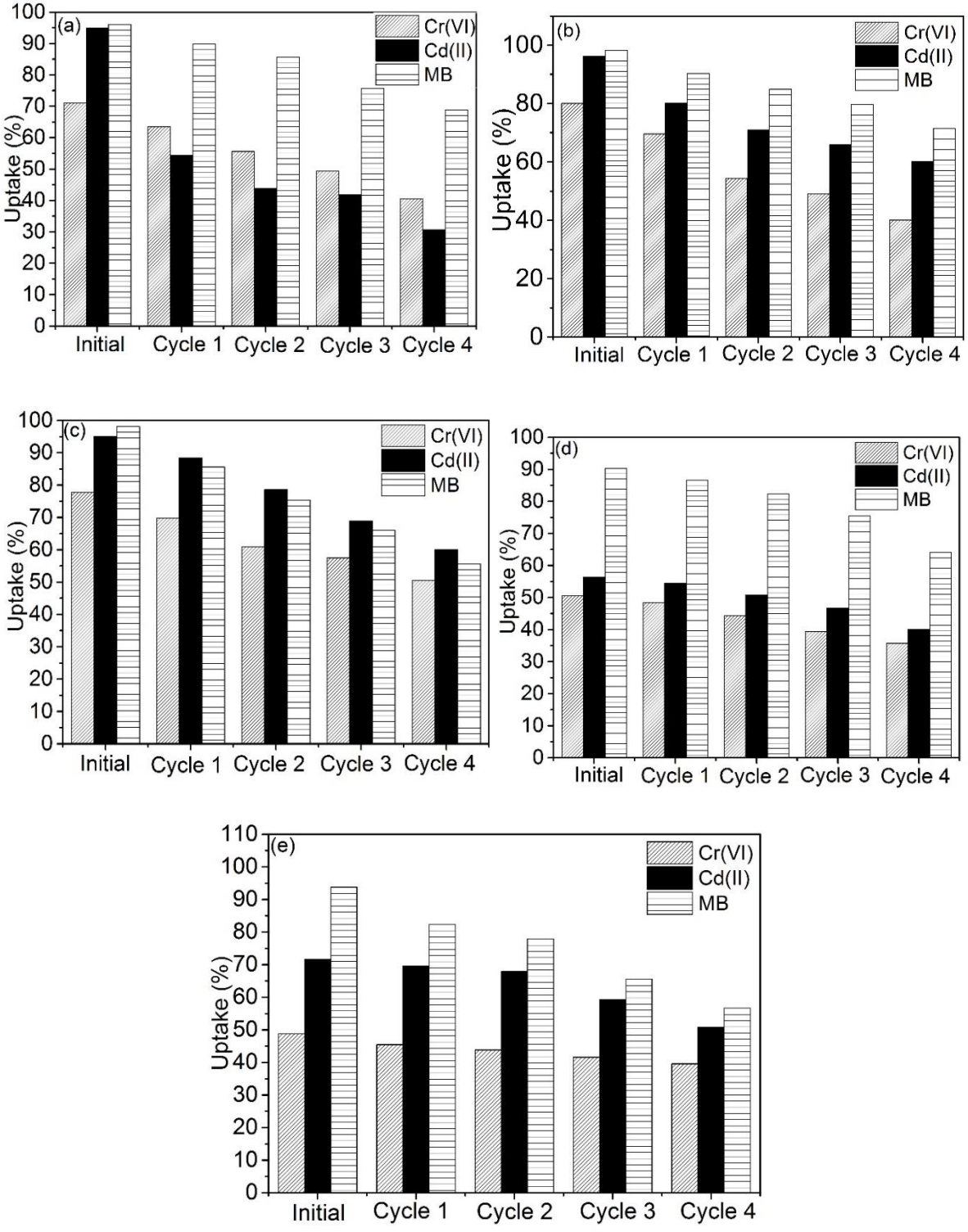

Figure 65: Regeneration studies on (a) PNS, (b) ANS, (c) CANS, (d) DNS and (e) CDNS.

9.7.5 Conclusion

The effectiveness of the defatted and carbonized *Nigella Sativa L*. seeds was studied in batch experiments for the removal of Cr(VI), Cd(II) and MB in aqueous solution. *Nigella Sativa L*. seeds were defatted using different solvents such as acetone and DMF thereafter carbonized at 600 °C. The defatted and the carbon defatted seeds were compared with the pristine *Nigella Sativa L.* (PNS) seeds. A series of adsorption tests were conducted using different parameters namely; contact time, initial concentration, temperature and pH. The adsorption of Cr(VI), Cd(II) and MB was influenced by the solution pH. The high Cr(VI) removal was observed at pH 1 on all adsorbents whilst the maximum adsorption capacities for Cd(II) and MB were at pH 9. SEM images showed different surface morphological properties with distinct cavities and pore structures resulting from the chemically treated *Nigella Sativa* seeds. The FTIR spectra of PNS, ANS, DNS and CDNS showed shifts in transmission frequencies which suggested that there was interaction of adsorbents with the adsorbates. The functional groups which played a key role in the adsorption of Cr(VI), Cd(II) and MB were amides, carbonyl, and carboxyl. The adsorption of Cr(VI), Cd(II) and MB was fast ranging from 1 and 20 min thereafter, the rate slowed down due to exhaustion of the pores and binding sites. The kinetic models predicted the adsorption mechanism of Cr(VI), Cd(II) and MB onto PNS as PFO which suggested that the rate of adsorption depended on the unoccupied sites. On the other hand, the adsorption mechanism onto ANS, CANS, DNS and CDNS showed a good fit for PSO which indicated that the sites on the adsorbents surface and the adsorbate ions and the dye played a key role in the adsorption rate. The effect of concentration showed that the adsorption capacity increased with increasing initial concentration. The high coefficient of determination r^2 showed that PNS and ANS best fitted Freundlich model which proposed multilayer formation of adsorbate and heterogeneous in nature. However the adsorption of Cr(VI), Cd(II) and MB onto CANS, DNS and CDNS fitted to Langmuir isotherm which assumed that the adsorption took

place through monolayer and was a homogenous process. The adsorption capacities of all adsorbents increased with temperatures showing that the process was feasible at higher temperatures and that high temperatures were favourable for the adsorption process. The values of (ΔS^o and ΔH^o) were positive for the sorption of Cr(VI), Cd(II) and MB on all adsorbents which suggested the increased freedom of ions in the solution and that the reaction was endothermic respectively. The (ΔG^o) values were negative for PNS, ANS, CANS, DNS and CDNS for all temperatures and were more negative with an increase in temperature. This indicated that the removal Cr(VI), Cd(II) and MB on all the adsorbents were spontaneous and feasible. The results showed that CANS had highest adsorption capacity of 99.82 mg/g for MB, 96.89 m/g for Cd(II) and 87.44 mg/g for Cr(VI) compared to CDNS, ANS, DNS and PNS. The capacity trend was CANS>CDNS>ANS>DNS >PNS. The reusability results showed the black cumin seeds adsorbents can be recycled for the adsorption of Cr(VI), Cd(II) and MB from aqueous solution. This presents potential advantages such easy generation of the adsorbents and their ability to be reused more than three times. These results showed the prepared adsorbents were effective for the sorption of the Cr(VI), Cd(II) and MB in batch analyses.

9.7.6 Acknowledgement

We would like to acknowledge National Research Fund (NRF) which is the sponsor of this research and the Vaal University of Technology is greatly appreciated.

References

ABDALLAH M. & SHAKAK, M.A.S., 2019. Effect of black cumin seeds Oil (*Nigella sativa* L.) on the stability of crude peanut oil during frying process. *GCNU Journal ISSN*, 1858.

ABDEL-SALAM, O. E., SHOEI, M.A. AND ELKILANY, H.A., 2018. Characterization of the hard-anodizing layers formed on 2014-T3 Al alloy, in sulphuric acid electrolyte containing sodium lignin sulphonate. *Egyptian Journal of Petroleum*, 27(4), 497-504.

AGHABABAEI, A., NCIBI M.C. & SILLANPAA, M., 2017. Optimized removal of oxytetracycline and cadmium from contaminated waters using chemically-activated and pyrolyzed biochars from forest and wood-processing residues. *Bioresource Technology*, 239, 28-36.

AHMAD, R. & HASEEBA, S., 2014. Black cumin seed (BCS): a non-conventional adsorbent for the removal of Cu (II) from aqueous solution *Desalination Water Treatment*, 56(9), 2512-2521.

AICHOUR, A. & ZAGHOUANE-BOUDIAF, H. 2019. Highly brilliant green removal from wastewater by mesoporous adsorbents: Kinetics, thermodynamics and equilibrium isotherm studies. *Microchemical Journal*, 146, 1255-1262.

AICHOUR, A., ZAGHOUANE-BOUDIAF, H., IBOR, C.V. & POLO, M.S., 2018. Bioadsorbent beads prepared from activated biomass/alginate for enhanced removal of cationic dye from water medium: Kinetics, equilibrium and thermodynamic studies. *Journal of Molecular Liquids*, 256, 533-540.

AKPOMIE, K.G., DAWODU F.A. & ADEBOWALE, K.O., 2015. Mechanism on the sorption of heavy metals from binary-solution by a low-cost montmorillonite and its desorption potential. *Alexandria Engineering Journal*, 54(3), 757-767.

AL-ANBERA, M.A., AL-ANBERB, Z.A., AL-MOMANIC, I., AL-MOMANID F. & ABU-SALEM, Q., 2014. The performance of Defatted Jojoba Seeds for the removal of toxic high concentration of the aqueous ferric ion. *Desalination Water Treatment*, 52(1-3), 293-304.

ALBADARIN, A.B., COLLINS, M.N., NAUSHAD, M., SHIRAZIAN, S., WALKER G. & MANGWANDI, C., 2017. Activated lignin-chitosan extruded blends for efficient adsorption of methylene blue. *Chemical Engineering Journal*, 307, 264-272.

ALEMU, A., LEMMA, B., GABBIYE, N., ALULA, M.T. & DESTA, M.T., 2018. Removal of chromium (VI) from aqueous solution using vesicular basalt: A potential low-cost wastewater treatment system. *Desta Heliyon*, 4(7), e00682.

AL-FUTAISI, A., JAMRAH, A. & AL-HANAI, R., 2009. Aspects of cationic dye molecule adsorption to palygorskite. *Desalination.*, 214(1-3), 327-342.

ALI, I. H., AL MESFER, M.K., KHAN, M. I., DANISH, M AND ALGHAMDI, M.M., 2019. Exploring adsorption process of lead (II) and chromium (VI) ions from aqueous solutions on acid activated carbon prepared from *Juniperus procera* leaves. *Processes*, 7(4), 217.

ALOMA, I., MARTIN-LARA, M.A., RODRIGUEZ, I.L., BLAZQUEZ, G. & CALERO, M., 2012. Removal of nickel (II) ions from aqueous solutions by biosorption on sugarcane bagasse. Journal of Taiwan Institute of Chemical Engineers, 43(2), 275-281.

ANFAR, Z., HAOUTI, R.E., LHANAFI, S., BENAFQIR, M., AZOUGARH Y. & ALEM, N.E., 2014. Treated digested residue during anaerobic co-digestion of Agri-food organic waste: Methylene blue adsorption, mechanism and CCD-RSM design. *Journal of Environmental Chemical Engineering*, 5(6), 5857-5867.

ARDIANA, M., PIKIR, B.S., SANTOSO, A., HERMAWAN, H.O. & AL-FARABI M.J., 2020. Effect of *Nigella sativa* supplementation on oxidative stress and antioxidant parameters: A meta-analysis of randomized controlled trials. *The Scientific World Journal*, 2020, 1-7.

ASGHER, M. & BHATTI, H.N., 2012. Evaluation of thermodynamics and effect of chemical treatments on sorption potential of *Citrus* waste biomass for removal of anionic dyes from aqueous solutions. *Ecological Engineering*, 38(1), 79-85.

AWUAL, M. R., RAHMAN, I.M.M., YAITA, T., KHALEQUE M.A. & FERDOWS, M. 2014. pH dependent Cu(II) and Pd(II) ions detection and removal from aqueous media by an efficient mesoporous adsorbent. *Chemical Engineering Journal*, 236, 100-109.

BAI, J., YAO, H., FAN, F., LIN, M., ZHANG, L., DING, H., LEI, F., WU, X., LI, X., GUO J., AND QIN, J. 2010. Biosorption of uranium by chemically modified *Rhodotorula glutinis, Environmental of Radioactivity*, 101(11), 969-973.

BASU, M., GUHAB, A. K. & RAYA, L., 2017. Adsorption Behavior of Cadmium on Husk of Lentil. *Process Safety and Environmental Protection*, 106, 11-22.

BAYAZIT, S.S. & KERKEZ, O. 2014. Hexavalent chromium adsorption on superparamagnetic multi-wall carbon nanotubes and activated carbon composites**.** *Chemical Engineering Research and Design*, 92, 2725-2733.

BEGUM, S. & MANNAN, A., 2020. Review on Nigella sativa: A Marvel Herb. *Journal of Drug Delivery Therapeutics*, 10(2), 213-219.

CENGIZ, S. & CAVAS, L., 2008. Removal of methylene blue by invasive marine seaweed: *Caulerpa racemosa* var. *cylindracea. Bioresource Technology*, 99(7), 2357-2363.

CHANDRA, T.S., MUDLIAR, S.N., VIDYASHANKAR, S., MUKHERJI, S., SARADA, R., KRISHNAMURTHI, K. & CHAUHAN, V.S., 2015. Defatted algal biomass as a non-conventional low-cost adsorbent: Surface characterization and methylene blue adsorption characteristics. *Bioresource Technology*, 184, 395-405.

CHAUDHRY, S. A., ZAIDI, Z. AND SIDDIQUI, S. I., 2017. Isotherm, kinetic and thermodynamics of arsenic adsorption onto Iron-Zirconium Binary Oxide-Coated Sand (IZBOCS): Modelling and process optimization. *Journal of Molecular Liquids*, 229, 230-240.

CHAUDHRY, S.A., KHAN T.A. & ALI, I., 2016. Adsorptive removal of Pb(II) and Zn(II) from water onto manganese oxide-coated sand: Isotherm, thermodynamic and kinetic studies. 2016. *Egyptian Journal of Basic and Applied Sciences*, 3(3), 287-300.

CHEN, H., LI, W., WANG, J., XU, H., LIU, Y., ZHANG, Z., LI, Y., & ZHANG, Y., 2019. Adsorption of cadmium and lead ions by phosphoric acid-modified biochar generated from chicken feather: Selective adsorption and influence of dissolved organic matter. *Bioresource Technology*, 292, 121948.

DAHIRU, M., ZANGO, Z.U. & HARUNA, M.A., 2018. Cationic dyes removal using low-cost banana peel biosorbent**.** *American Journal of Materials Science*, 8(2), 32-38.

DANISHA, M., AHMAD, T., HASHIM, R., SAID, N., AKHTARD, M.N., MOHAMAD-SALEHE J. & SULAIMAN, O. 2018. Comparison of surface properties of wood biomass activated carbons and their application against rhodamine B and methylene blue dye. *Surfaces Interfaces*, 11, 1-13.

DIAGBOYA, P.N. & DIKIO, E.D., 2018. Scavenging of aqueous toxic organic and inorganic cations using novel facile magneto-carbon black-clay composite adsorbent. *Journal of Cleaner Production*, 180, 71-80.

ERDOGAN, U., YILMAZER, M. & ERBAS, S., 2020. Hydrodistillation of Nigella Sativa Seed and Analysis of Thymoquinone with HPLC and GC-MS. *Bilge International Journal Science and Technology*, 4(1), 27-30.

FONTOURA, J.T., ROLIM, G.S., MELLA, B., FARENZENA M. & GUTTERRES, M., 2017. Defatted microalgal biomass as biosorbent for the removal of Acid Blue 161 dye from tannery effluent. *Journal of Environmental Chemical Engineering*, 5(5), 5076-2084.

GALI-MUHTASIB, H., EL-NAJJAR, N. & SCHNEIDER-STOCK, R., 2006. The medicinal potential of black seed (*Nigella sativa*) and its components. Advances *in Phytomedicine*, 2, 133-153.

GARBA, Z.N., BELLO, I., GALADIMA A. & LAWAL, A.Y., 2016. Optimization of adsorption conditions using central composite design for the removal of copper (II) and lead (II) by defatted papaya seed. *Karbala Internal Journal of Modern Science*, 2(1), 20-28.

GHAEDI, M., GHAZANFARKHANI, M.D., KHODADOUST, S., SOHRABI N. & OFTADE, M., 2014. Acceleration of methylene blue adsorption onto activated carbon prepared from dross licorice by ultrasonic: Equilibrium, kinetic and thermodynamic studies. *Journal of Industrial and Engineering Chemistry*, 20(4), 2548-2560.

GILBERT, U.A., EMMANUEL, I.U., ADEBANJO, A.A. & OLALERE, G.A., 2011. Biosorptive removal of $Pb^{2+}$and Cd^{2+} onto novel biosorbent: Defatted *Carica papaya* seed. *Biomass Bioenergy*, 35(7), 2517-2525.

GOSWAMI, R., SHIM, J., DEKA, S., KUMARI, D., KATAKI, R. & KUMAR, M., 2016. Characterization of cadmium removal from aqueous solution by biochar produced from *Ipomoea fistulosa* at different pyrolytic temperatures. *Ecological Engineering*, 97, 444-451.

GUEYE, M., RICHARDSON, Y., KAFACK F.T.& BLIN, J., 2014. High efficiency activated carbons from African biomass residues for the removal of chromium(VI) from wastewater. *Journal Environmental Chemical Engineering*, 2, 273-281.

GUO, Z., ZHANG, X., KANG, Y. & ZHANG, J., 2017. Biomass-derived carbon sorbents for Cd(II) removal: activation and adsorption mechanism. *ACS Sustainable Chemistry and Engineering*, 5(5), 4103-4109.

HAMEED, B.H., MAHMOUD D.K. & AHMAD, A.L., 2008. Equilibrium modeling and kinetic studies on the adsorption of basic dye by a low-cost adsorbent: Coconut (*Cocos nucifera*) bunch waste. *Journal of Hazardous Materials*, 158(1), 65-72.

HAN, J., ZHANG, G., ZHOU, L., ZHAN, F., CAI, D. & WU., Z. 2018. Waste carton-derived nanocomposites for efficient removal of hexavalent chromium. *Langmuir*, 34(21), 5955-5963.

HEIDARINEJAD, Z., RAHMANIAN, O., FAZLZADEH M. & HEIDARI, M., 2018. Enhancement of methylene blue adsorption onto activated carbon prepared from Date Press Cake by low frequency ultrasound. *Journal of Molecular Liquids*, 264, 591-599.

HUANG, H., WANG, Y., ZHANG, Y., NIU, Z., LI, X., 2020. Amino-functionalized graphene oxide for Cr(VI), Cu(II), Pb(II) and Cd(II) removal from industrial wastewater. *Open Chemistry*, 18(1), 97-107.

HUANG, J., YE, M., QU, Y., CHU, L., CHEN, R., HE Q. & XU, D., 2012. Pb (II) removal from aqueous media by EDTA-modified mesoporous silica SBA-15. *Journal of Colloid Interface Science*, 385(1), 137-146.

HUANG, X., GAO, N.Y. & ZHANG, Q.L., 2007. Thermodynamics and kinetics of cadmium adsorption onto oxidized granular activated carbon. *Journal of Environmental Sciences*, 19(11), 1287-1292.

IGBERASE, E., OSIFO P. & OFOMAJA, A., 2017. The Adsorption of Pb, Zn, Cu, Ni, and Cd by Modified Ligand in a Single Component Aqueous Solution: Equilibrium, Kinetic, Thermodynamic, and Desorption Studies. *International Journal of Analytical Chemistry*.

ISLAM, M.M., KHAN, M.N., MALLIK, A.K. & RAHMAN, M.M., 2019. Preparation of bio-inspired trimethoxysilyl group terminated poly(1-vinylimidazole)-modified-chitosan composite for adsorption of chromium (VI) ions. *Journal of Hazardous Materials*, 379, 120792.

JI, B., WANG, J., SONG, H. & CHEN, W., 2019. Removal of methylene blue from aqueous solutions using biochar derived from a fallen leaf by slow pyrolysis: Behavior and mechanism. *Journal of Environmental Chemical Engineering*, 7(3), 103036.

JIA, Z., SHU, Y., HUANG, R., LIU, J. AND LIU, L., 2018. Enhanced reactivity of nZVI embedded into supermacroporous cryogels for highly efficient Cr(VI) and total Cr removal from aqueous solution. *Chemosphere*, 199, 232-242.

KHOSRAVI, R., MOUSSAVI, G., GHANEIAN, M.T., EHRAMPOUSH, M.H., BARIKBIN, B., EBRAHIMI, A.A. & SHARIFZADEH, G., 2018. Chromium adsorption from aqueous solution using novel green nanocomposite: Adsorbent characterization, isotherm, kinetic and thermodynamic investigation. *Journal of Molecular Liquids*, 256, 163-174.

KOLODYNSKA, D., KRUKOWSKA, J. & THOMAS, P., 2017. Comparison of sorption and desorption studies of heavy metal ions from biochar and commercial active carbon. *Chemical Engineering Journal*, 307, 353-363.

KOWANGA, K.D., GATEBE, E., MAUTI, G.O. & MAUTI, E.M., 2016. Kinetic, sorption isotherms, pseudo-first-order model and pseudo-second-order model studies of Cu(II) and Pb(II) using defatted Moringa oleifera seed powder. *Journal of Phytopharmacology*, 5(2), 71-78.

KUMAR, A.S.K. & JIANG, S-J., 2017. Synthesis of magnetically separable and recyclable magnetic nanoparticles decorated with β-cyclodextrin functionalized graphene oxide an excellent adsorption of As(V)/(III). *Journal of Molecular Liquids*, 237, 307-408.

LESAOANA, M., MLABA, R.P.V., MTUNZI, F.M., KLINK, M.J., EJIDIKE P. & PAKADE, V.E., 2019. Influence of inorganic acid modification on Cr(VI) adsorption performance and the physicochemical properties of activated carbon. *South African Journal of Chemical Engineering*, 28(1), 8-18.

LI, X., WANG, S.F., LIU, Y.G., JIANG, L.H., SONG, B.A., LI, M.F., ZENG, G., TAN, X., CAI X. & DING, Y., 2017. Adsorption of Cu(II), Pb(II), and Cd(II) ions from acidic aqueous solutions by diethylenetriaminepentaacetic acid-modified magnetic graphene oxide**.** *Journal of Chemical Engineering Data*. 62(1), 407-416.

LIU, Q., LIU, Q., LIU, B., HU, T., LIU, W. YAO, J. 2018. Green synthesis of tannin-hexamethylendiamine based adsorbents for efficient removal of Cr(VI). *Journal of Hazardous Materials,* 352, 27-35.

LU, D., CAO, Q., LI, X., CAO, X., LUO, F. & SHAO, W., 2009. Kinetics and equilibrium of Cu(II) adsorption onto chemically modified orange peel cellulose biosorbents. *Hydrometallurgy,* 95,145-152.

NAGARJUNA, R., SAIFULLAH, M.S.M. & GANESAN, R. 2018. Oxygen insensitive thiol-ene photo-click chemistry for direct imprint lithography of oxides**.** *RSC Advances*, **8**, 11403-

NANDI, B.K., GOSWAMI A. & PURKAIT M.K., 2009. Adsorption characteristics of brilliant green dye on kaolin. *Journal of Hazardous Materials,* 161, 387-395.

NARVEKAR, A.A., FERNANDES, J.B. & TILVE, S.G., 2018. Adsorption behavior of methylene blue on glycerol-based carbon materials. *Journal Environmental Chemical Engineering*, 6(2), 1714-1725.

OLABEMIWO, F.A., TAWABINI, B.S., PATEL, F., OYEHAN, T.A., KHALED M. & LAOUI, T., 2017. Cadmium removal from contaminated water using polyelectrolyte-coated industrial waste fly ash. *Bioinorganic Chemical and Application*.

OLIVEIRA, R.N., MANCINI, M.C., OLIVEIRA, F.C.S., PASSOS, T.M., QUILTY, B., THIRE, R.M. & MCGUINNESS, G.B., 2016. FTIR analysis and quantification of phenols and flavonoids of five commercially available plants extracts used in wound healing. *Revista Materia,* 21, 767-779.

PALANISAMY, K. L., DEVABHARATHI, V. & SUNDARAM, N. M., 2013. The utility of magnetic iron oxide nanoparticles stabilized by carrier oils in removal of heavy metals from waste water. *International Journal of Research in Applied, Natural and Social Sciences*, 1(4), 15-22.

PATHANIA, D., SHARMA S. & SINGH, P., 2017. Removal of methylene blue by adsorption onto activated carbon developed from *Ficus carica* bast. *Arabian Journal of Chemistry,* 10, S1445-S1451.

PRIYANKA, M., & SARAVANAKUMAR, M.P., 2018. Ultrahigh adsorption capacity of starch derived zinc-based carbon foam for adsorption of toxic dyes and its preliminary investigation on oil-water separation. *Journal of Cleaner Production,* 197, 511-521.

PUGAZHENDHI, A., BOOVARAGAMOORTHY, G.M., RANGANATHAN, K., NAUSHAD M. & KALIANNAN, T., 2018. New insight into effective biosorption of lead from aqueous solution using Ralstonia solanacearum: Characterization and mechanism studies. *Journal of Cleaner Production*, 174, 1234-1239.

SAEED, A., IQBAL, M., & HOLL, W.H., 2009. Kinetics, equilibrium and mechanism of Cd^{2+} removal from aqueous solution by mungbean husk. *Journal of Hazardous Materials*, 168(2-3), 1467-1475.

SALMAN, T. F., N., TEMEL, TURAN, G. AND ARDALI, Y., 2016. Removal of lead (II) from aqueous solution by batch adsorption on various inexpensive adsorbents using experimental design. *Desalination and Water treatment,* 56, 1566-1565.

SANTHOSH, C., KOLLU, P., DOSHI, S., SHARMA, M., BAHADUR, D., VANCHINATHAN M., SARAVANAN, P., KIMEAND, B-S. & GARCE, A.N., 2014. Adsorption, photodegradation and antibacterial study of graphene-Fe_3O_4 nanocomposite for multipurpose water purification application, *RSC Advances Journal*, 4, 28300-28308.

SERRANO-GOMEZ, J., LOPEZ-GONZALEZ, H., OLGUIN M.T. & BULBULIAN, S., 2015. Carbonaceous material obtained from exhausted coffee by an aqueous solution combustion process and used for cobalt (II) and cadmium (II) sorption. 2015. *Journal of Environmental Management*, 156, 121-127.

SHEN, Z., ZHANG, J., HOU, D., TSANG, D.C.W., OK Y.S. AND ALESSI, D.S. 2019. Synthesis of MgO-coated corncob biochar and its application in lead stabilization in a soil washing residue. E*nvironment International*, 122, 357-362.

SHIFERA, L., SIRAJ K. & YIFRU, A., 2016. Adsorption of lead (II) and chromium (VI) onto activated carbon prepared from pineapple peel: Kinetics and thermodynamic study. *Indian Journal Chemical Technology*, 24, 145-152.

SHOKROLLAHI, A., ALIZADEH, A., MALEKHOSSEINI, Z. & RANJBAR, M., 2011. Removal of bromocresol green from aqueous solution via adsorption on *Ziziphus nummularia* as a new, natural, and low-cost adsorbent: Kinetic and thermodynamic study of removal process. *Journal Chemical Engineering Data*, 56, 3738-3746.

SHOOTO, N. D., THABEDE, P. M. & NAIDOO, E. B., 2019b. Simultaneous adsorptive study of toxic metal ions in quaternary system from aqueous solution using low cost black cumin seeds (Nigella sativa) adsorbents. *South African Journal of Chemical Engineering*, 30, 15.

SHOOTO, N.D., 2020. Removal of lead(II) and chromium(VI) ions from synthetic wastewater by the roots of *harpagophytum procumbens* plant. *Journal of Environmental Chemical Engineering*, 8(6), 104541.

SHOOTO, N.D., NKUTHA, C.S., GUILANDE, N.R. & NAIDOO, E.B. 2020. Pristine and modified mucuna beans adsorptive studies of toxic lead ions and methylene blue dye from aqueous solution. *South African Journal of Chemical Engineering,* 31(1), 33-43.

SHOOTO, N.D., THABEDE, P.M., BHILA, B., MOLOTO H. & NAIDOO, E. B., 2019a. Lead ions and methylene blue dye removal from aqueous solution by mucuna beans (velvet beans) adsorbents. *Journal of Environmental Chemical Engineering,* 8(2), 103557.

SIDDIQUI S.I. & CHAUDHRY, S.A., 2017. Arsenic removal from water using nanocomposites: A Review. *Current Environmental Engineering*, 4(2), 81-102.

SIDDIQUI, S.I. & CHAUDHRY, S.A., 2008. Nigella sativa plant-based nanocomposite-$MnFe_2O_4$/BC: An antibacterial material for water purification. *Journal of Cleaner Production*, 200, 996-1008.

SIDDIQUI, S.I., CHAUDHRY, S.A. & ISLAM, S.U. & ISLAM, S.U. 2017. Green Adsorbents from Plant Sources for the Removal of Arsenic: An Emerging Wastewater Treatment

Technology. Plant-based Natural Products: Derivatives and Applications. (Ed.), John Wiley & Sons, Inc., 193.

TANG, Y., CHEN, L., WEI, X., YAO Q. AND LI, T., 2013. Removal of lead ions from aqueous solution by the dried aquatic plant, *Lemna perpusilla* Torr. *Journal of Hazardous Materials*, 244-245, 603-612.

THABEDE, P.M., SHOOTO, N.D. & NAIDOO, E.B., 2020b. Removal of methylene blue dye and lead ions from aqueous solution using activated carbon from black cumin seeds. *South African Journal of Chemical Engineering*, 33, 39-50.

THABEDE, P.M., SHOOTO, N.D. XABA T. & E.B. NAIDOO, 2020c. Adsorption studies of toxic cadmium(II) and chromium(VI) ions from aqueous solution by activated black cumin (*Nigella sativa*) seeds. *Journal of Environmental Chemical Engineering*, 8(4), 104045.

THABEDE, P.M., SHOOTO, N.D., XABA, T. & NAIDOO, E.B., 2020a. Sulfuric activated carbon of black cumin (*Nigella sativa* L.) seeds for the removal of cadmium(II) and methylene blue dye. *Asian Journal of Chemistry*, 32, 1361-1369.

TOUNSADIA, H., KHALIDI, A., FARNANE, M., ABDENNOURI M. & BARKA, N., 2016. Experimental design for the optimization of preparation conditions of highly efficient activated carbon from Glebionis coronaria L. and heavy metals removal ability. *Process Safety and Environmental Protection*, 102, 710-723.

UNUABONAH, E.I., ADIE, G.U., ONAH, L.O. & ADEYEMI, O.G., 2009. Multistage optimization of the adsorption of methylene blue dye onto defatted Carica papaya seeds. *Chemical Engineering Journal*, 155(3), 567-579.

WANG, Y., ZHANG, Y., LI, S., ZHONG, W. & WEI, W. 2018. Enhanced methylene blue adsorption onto activated reed-derived biochar by tannic acid. *Journal of Molecular Liquids*, 268, 658-666.

YAKKALA, K., YU, M-R., ROH, H., YANG, J-K. & CHANG, Y-Y. 2014. Buffalo weed (*Ambrosia trifida L. var. trifida*) biochar for cadmium (II) and lead (II) adsorption in single and mixed system. *Desalination and Water Treatment*, 51(40-42), 7732-7745.

YANG, P., GUO, D., CHEN, Z., CUI, B., XIAO, B., LIU S. & M. HU., 2017. Removal of Cr (VI) from aqueous solution using magnetic biochar synthesized by a single step method. *Journal of Dispersion Science and Technology*, 38(11), 1665-1674.

YIN, W., ZHAO, C., XU, J., ZHANG, J., GUO, Z. & SHAO, Y., 2019. Removal of Cd(II) and Ni(II) from aqueous solutions using activated carbon developed from powder-hydrolyzed-feathers and *Trapa natans husks. Colloids Surfaces A Physicochemical and Engineering Aspects*, 560, 426-433.

YUSUFF, A.S., 2019. Adsorption of hexavalent chromium from aqueous solution by *Leucaena leucocephala* seed pod activated carbon: equilibrium, kinetic and thermodynamic studies. *Araba Journal of Basic Applied Sciences*, 26(1), 89.

ZHANG, H., ZHOU, J., MUHAMMAD, Y., TANG, R., LIU, K., ZHU, Y. AND TONG, Z., 2019a. *Colloidal Materials and Interfaces*, 6.

ZHANG, Y-J., OU, J-L., DUAN, Z-K., XING, Z-J. & WANG, Y., 2015. Adsorption of Cr(VI) on bamboo bark-based activated carbon in the absence and presence of humic acid. Colloids *Surfaces A Physicochemical and Engineering Aspects*, 481, 108-116.

ZHANG, Z., YUE, X., XU, W., ZHANG H. & LI, F., 2019. Amino modification of rice straw-derived biochar for enhancing its cadmium (II) ions adsorption from water. *Journal of Hazardous Materials*, 379, 120783.

ZHOU, N., WANG, Y., YAO, D., LI, S., TANG, J., SHEN, D., ZHU, X., HUANG, L., ZHONG, M., ZHI Z. & ZHOU, Z., 2019. Novel wet pyrolysis providing simultaneous conversion and activation to produce surface-functionalized biochars for cadmium remediation. *Journal of Cleaner Production*, 221, 63-72.

CHAPTER 10

10.1 Conclusion

The main aim of the study was to produce adsorbents from black cumin (*Nigella Sativa* L.) seeds and to demonstrate that the seeds can be used for the adsorption of pollutants (Co, Ni, Cu, Cr, Pb ions and molecules of methylene blue dye) in aqueous solution. The black cumin seeds were chemically treated using NaOH, HCl, $KMnO_4$, H_3PO_4, H_2SO_4 and modified using sucrose and nanoparticles. The AT-BCS and BT-BCS were effectively utilized for quaternary adsorption study of Cu(II), Co(II), Pb(II) and Ni(II) ions from aqueous solution. The maximum capacity trend was BT-BCS>AT-BCS>UT-BCS. The best fitted isotherm model was found to be Langmuir. Kinetic studies tested shown that PFO had a good fit which suggested that there was electrostatic attraction and Van der Waal forces.

The development of activated bioadsorbents for the sorption of Cd(II) and Cr(VI) using KMBS H_3BS showed that the highest adsorption capacities were at pH 1 and 9 for Cr(VI) and Cd(II) ions respectively. The maximum adsorption capacity for Cr(VI) ions was 16.12, 15.98 and 10.15 mg/g onto KMBS, H_3BS and PBS respectively. Meanwhile, for Cd(II) ions it was 19.15, 19.09 and 16.80 mg/g for KMBS, H_3BS and PBS respectively. Contact time effect revealed that the sorption rate of Cr(VI) ions onto PBS increased from 5 until 60 min. However, the sorption rates for KMBS and H_3BS was more rapid from 5 to 30 min. The sorption rates of Cd(II) ions were also rapid from 5 min until 60, 30 and 20 min for PBS, KMBS and H_3BS respectively.

The carbonization and activation using 10 and 20 % H_2SO_4 at 200 ℃ for the adsorption of MB dye and Cd(II) ions showed that the adsorption of MB on all adsorbents best fitted PFO whilst Cd(II) data fitted PSO model. The carbonization at different pyrolysis had an influence on the adsorption process. The entropy, ($\Delta S°$) was positive for MB and Cd(II) ions whilst ($\Delta G°$) had negative values. Freundlich isotherm model was best described for Cd(II) whilst Langmuir model fitted for MB dye. The activation (10 and 20 % H_2SO_4) at 300 ℃ of BCS the removal of Pb(II) ions and (MB) dye showed that the adsorption capacity increased with increasing initial concentration of the solutions. The temperature results showed that the sorption of Pb(II) ions and MB dye on all adsorbents increased with increasing temperature.

FNS and PNS composites investigated for the uptake of Cr(VI) and Pb(II) ions. Sorption of Cr(VI) and Pb(II) ions on both adsorbents displayed the endothermic nature of the adsorption processes. The maximum adsorption capacities for Cr(VI) were 15.6 and 13.0 mg/g onto PNS and FNS composites at pH 1 respectively. On the other hand, maximum sorption for Pb(II) ions were 39.7 and 37.9 mg/g onto PNS and FNS composites at pH 5. The defatting with acetone, DMF and carbonization at 600 ℃ of *Nigella Sativa L*. seeds for the sorption of Cr(VI), Cd(II) ions and MB dye indicated that SEM images had different surface morphological properties with distinct cavities and pore structures consequential from the defatted *Nigella Sativa* seeds. The FTIR spectra of PNS, ANS, DNS and CDNS suggested that there was interaction of adsorbents with the adsorbates with functional groups such as amides, carbonyl, and carboxyl. The reusability results showed that the adsorbents can be recycled for the adsorption of Cr(VI), Cd(II) and MB from aqueous solution. The adsorption capacities of all adsorbents showed that the process was feasible at higher temperatures and favourable.

The present study displayed that black cumin seeds are efficient and effective for the uptake of Co(II), Ni(II), Cu(II), Cr(VI), Pb(II), Cd(II) and MB dye. The study showed that the highest adsorption capacity was obtained using CANS with values of 99.82 mg/g for MB, 96.89 m/g for Cd(II) and 87.44 mg/g for Cr(VI).This also indicated potential benefits of easy generation of the adsorbents and ability of being reusable more than three times.

10.2 Contribution of this research work

The literature on the study of the black cumin seeds as adsorptive material was found to be very few.

(a) Prior to this research work, no document was found that reported on treatment of black cumin seeds by HCl and NaOH. The research work, established that the treated black cumin seeds had improved physicochemical properties such as surface area and porosity. Therefore, this positively affected the adsorption capacity of the biomaterials for quaternary uptake of Pb(II), Cu(II), Co(II) and Ni(II) cations from aqueous solution. Also, this work was the first to use black cumin seeds in quaternary adsorption studies.

(b) The research work also exploited the effect of different activating agents. Strong and mild oxidizing agents, $KMnO_4$ and H_3PO_4 respective were reacted with black cumin seeds. The characterization revealed that the substances imparted oxygen containing functional groups to the surface. This enhanced the adsorptive power of black cumin seeds towards Cd(II) and Cr(VI) ions. Upon exhaustive search no research work was found that reported on similar work for black cumin seeds.

(c) The research work furthermore investigated the effect of H_2SO_4 at different concentrations (10 % and 20 %) on biochar from black cumin seeds at 200 and 300 ^oC

for the removal of Cd(II), Pb(II) ions and MB dye. The obtained results showed that H_2SO_4 hydrolysed some of the lignocellulose materials from biochar. Also, H_2SO_4 functionalized the surface of biochar obtained at 300 ^oC with bisulphate groups. This significantly improved the surface of materials. The treatment increased the uptake of Cd(II), Pb(II) ions and MB. To the best knowledge of the authors, it is the first time that such study was reported for black cumin seeds.

(d) Black cumin seeds have high content of fatty acids and this hinders their reactivity by blocking the active sites such as pores on the surface and the functional groups. Therefore, in this work we tested the effectiveness of different organic solvents to extract fatty acids from black cumin seeds. The results revealed that acetone extracted more fatty acids from the surface of black cumin seeds than DMF. Subsequently, it was found that acetone treated seeds had more pores on the surface and removed Cr(VI), Cd(II) ions and MB dye more than DMF treated seeds. This was attributed to the surface texture and porosity of the material. Prior to this work, no similar study was reported for black cumin seeds. The results from this study will add new knowledge to the application of black cumin seeds in wastewater treatment.

10.3 Recommendations

Based on the results, it is recommended that further adsorption study for black cumin seeds be conducted for estimation of adsorption in wastewater treatment.

- Further testing should be carried out to determine the adsorption of toxic metal ion contaminants at higher concentrations.

- Further study is essential to evaluate the feasibility of black cumin seeds for the removal of toxic metals ions from the real environment.
- Also, a study should be conducted for the removal of anions such as nitrates and sulphates in water environment.
- A further study of the effectiveness of the seeds using additional regenerating solutions such as HNO_3, $NaNO_3$, $CaCl_2$ and NH_4Cl can be investigated at various solution concentrations and temperatures.

APPENDIX

South African Journal of Chemical Engineering 30 (2019) 15–27

Contents lists available at ScienceDirect

South African Journal of Chemical Engineering

journal homepage: www.elsevier.com/locate/sajce

Simultaneous adsorptive study of toxic metal ions in quaternary system from aqueous solution using low cost black cumin seeds (Nigella sativa) adsorbents

Ntaote David Shooto*, Patience Mapule Thabede, Eliazer Bobby Naidoo

Applied Chemistry and Nano-Science Laboratory, Department of Chemistry, Vaal University of Technology, P.O. Box X021, Vanderbijlpark, 1900, South Africa

ARTICLE INFO

Keywords:
Adsorption
Isotherms
Kinetic
Thermodynamic
Black cumin seeds

ABSTRACT

A new adsorbent obtained from alkaline treatment of black cumin seeds (BCS) has been developed for the adsorption of cation pollutants cobalt [Co(II), lead Pb(II), copper Cu(II) and nickel Ni(II)] from aqueous solutions. The alkaline treated black cumin seeds were labeled; base treated black cumin seeds (BT-BCS), acid treated black cumin seeds (AT-BCS) and untreated black cumin seeds (UT-BCS). The absorbents were analyzed by scanning electron microscope (SEM), fourier-transform infrared spectroscopy (FTIR) and X-ray diffraction spectroscopy (XRD). The SEM images showed that UT-BCS is composed of spherical shaped particles. AT-BCS and BT-BCS images showed irregular surface morphology. AT-BCS and BT-BCS –IR spectra observed new bands. Pseudo First Order kinetic (PFO) model gave consistent fit in describing the adsorption of all the cations. The PFO good fit suggest that the adsorption mechanism involved, Van der Waal forces. The estimated pore adsorption (EPA) was more dominant than estimated surface adsorption (ESA). Equilibrium data had a good fit for Langmuir isotherm model for all cations this indicates that adsorption took place on active sites having equal affinity for these ions and further suggests that monolayer adsorption occurred on adsorbents surface at the end of adsorption process. BT-BCS was the best performing adsorbent with capacity of 190.7 mg/g for Cu(II), AT-BCS and UT-BCS with capacities of 180.1 and 135 mg/g respectively for Pb(II). Adsorption trend is BT-BCS > AT-BCS > UT-BCS. Reusability data suggests that (BCS) adsorbents retained ≥ 90% of their initial cations adsorption, these adsorbents may be reusable in wastewater treatment.

1. Introduction

An accelerated urbanization and industrialization growth in the last century has caused the discharge of wastewater into fresh water bodies without proper pretreatment. This poses a serious threat to the environment, human health and natural aquatic system (Myers et al., 2013). The scope of wastewater pollutants is too large and includes; toxic metal ions, pesticides, organic pollutants, dyes, etc (Shooto et al., 2016; Munze et al., 2017; Nagpal and Kakkar, 2018; Tran et al., 2019). Many of these pollutants are toxic to human and the ecosystem. They accumulate in human body and are non-biodegradable (Atique et al., 2017). For the sake of the current study we focused on four toxic metals that are being characterized as the priority pollutants from the various health organizations; Co(II), Pb(II), Cu(II) and Ni(II) ions (Veli and Alyuz, 2007).

Copper is needed only in small quantities by human body to support some biological processes. It is a commonly used metal by many municipalities and industries. Upon long term exposure even at lower concentrations, Cu(II) contaminated water has toxic effects on vital organs such as the brain, heart and liver (Jaishankar et al., 2014). It is also reported to cause vomiting, stomach cramps and kidney failure (Potera, 2004). Pb(II) is a slow, pernicious, but most malignant poison. Via any route or level of exposure it replaces calcium on the bones and accumulates in the skeletal system (Puzas et al., 2004). It further causes neurodevelopmental effects, brain damage (Wani et al., 2015), kidney, liver disorders as well as reproduction and development (Savic et al., 2014; Luo et al., 2012; Adham, 1997). Exposure to higher concentrations of Co(II) causes neurological problems such as changes in brain structure, cognitive function impairment and depression (Clark et al., 2014). Co(II) toxicity also affect all major organ systems and causes respiratory problems and fatigue (Pelclova et al., 2012). Long term Ni (II) exposure is associated with headaches, dyspnea, carcinogenic, cytotoxicity and genotoxicity (Kasprzak et al., 2003).

Therefore, it is necessary to remove such toxic metal ions from the

* Corresponding author.
E-mail address: ntaotes@vut.ac.za (N.D. Shooto).

https://doi.org/10.1016/j.sajce.2019.07.002
Received 12 April 2019; Received in revised form 11 June 2019; Accepted 23 July 2019

South African Journal of Chemical Engineering 33 (2020) 39–50

Contents lists available at ScienceDirect

South African Journal of Chemical Engineering

journal homepage: www.elsevier.com/locate/sajce

Removal of methylene blue dye and lead ions from aqueous solution using activated carbon from black cumin seeds

Patience Mapule Thabede*, Ntaote David Shooto, Eliazer Bobby Naidoo

Applied Chemistry and Nano-Science Laboratory, Department of Chemistry, Vaal University of Technology, P.O. Box X021, Vanderbijlpark 1900, South Africa

ARTICLE INFO

Keywords:
Black cumin activated carbon
Adsorption
Kinetics
Isotherms
Thermodynamic

ABSTRACT

This work reports the preparation of carbon from black cumin seeds (BCC) and then activated with 10 and 20 % sulfuric acid (H_2SO_4) to obtain new adsorbents designated black cumin activated carbon (BCAC-10) and (BCAC-20) respectively for the adsorption of lead (Pb(II)) ions and methylene blue (MB) dye from aqueous solution. The adsorbents were characterized by scanning electron microscopy (SEM), Fourier transformed infrared (FIR), thermogravimetric analyzer (TGA), X-ray diffractometer (XRD) and Brunauer, Emmett and Teller (BET) analysis. The SEM images show that both activated carbon adsorbents (BCAC-10 and BCAC-20) have rough irregular surfaces with cavities. FTIR results show the ($-COO^-$), ($-NH_2$), ($-HSO_4^-$), (-C=O) functional groups were involved in the adsorption processes of Pb(II) ions and methylene blue (MB) dye . Nitrogen adsorption studies show that there is an increase in surface area and pore size for both BCAC-10 and BCAC-20 in comparison with BCC. The operational parameters (concentration, contact time, temperature and pH) of Pb(II) ions and MB dyes adsorption were assessed in batch mode. It was observed that the trends for Pb(II) ions and MB dye adsorption increased with increasing initial concentration of the solution, (i.e.) greater uptake was observed in solutions with higher initial concentration. Therefore the adsorption of Pb(II) ions with initial concentration of 100 mg/L was 17.19, 17.71 and 17.98 mg/g onto BCC, BCAC-10 and BCAC-20 respectively. Whilst for MB dye it was 11.63, 12.71 and 16.85 mg/g onto BCC, BCAC-10 and BCAC-20 respectively. The equilibrium data for Pb(II) ions and MB dye fitted Freundlich isotherm model onto BCC, BCAC-10 and BCAC-20. This suggested that the process involve multi-layer adsorption with interactions between the adsorbate and the adsorbents. The results show that the adsorption processes of Pb(II) ions and MB dye were rapid in the first 20 min. It was observed that the maximum adsorption trend of Pb(II) ions and MB dye was obtained at pH 9 which made the surface of black cumin seeds to be negatively charged and therefore making it easier to be attracted to positively charged Pb (II) ions and MB dye. Kinetic studies showed that the adsorption of Pb(II) ions and MB dye onto BCC best fitted; pseudo-first order model whilst BCAC-10 and BCAC-20 data fits; pseudo-second order. The estimated pore adsorption for Pb(II) ions onto BCC, BCAC-10 and BCAC-20 was 65.85, 94.28 and 78.43 % respectively whilst MB dye was 73.37, 70.82 and 95.74 % respectively. Temperature and thermodynamics data indicated that the adsorption capacity of adsorbents increase with increasing temperature and the enthalpy (ΔH°) values indicated that the adsorption of Pb(II) ions and MB dye on the adsorbents was endothermic reaction. The entropy (ΔS°) gave positive values which indicated the randomness and degree of freedom for Pb(II) ions and MB dye in aqueous solution. The free energy (ΔG°) values for the adsorption of Pb(II) ions onto BCC, BCAC-10 and BCAC-20 show an increase in negative values as the temperature increases.

1. Introduction

Water pollution is an environmental problem facing the world today due to various industries such mining and smelting, fertilizers and pesticide, metallurgy, iron and steel, electrolysis, energy and fuel production, etc discharging waste that contain toxic metals (Wang et al., 2009). The disposal of toxic metals from industrial effluent without treatment is a matter of great concern (Dargahi et al., 2016). Toxic metals are one of the dangerous materials found in water. They are pathogenic and has the ability to accumulate in living organisms over a long period of time. There are many toxic metals, this study will focus on Pb(II) ions and MB dye.

Dyes are intensely colored, and consume dissolved oxygen (Zhang et al., 2011). Some dyes can penetrate light and destroy aquatic

* Corresponding authors.
E-mail addresses: mapulepseabelo@gmail.com (P.M. Thabede), ntaotes@vut.ac.za (N.D. Shooto).

https://doi.org/10.1016/j.sajce.2020.04.002
Received 24 October 2019; Received in revised form 5 March 2020; Accepted 4 April 2020

Journal of Environmental Chemical Engineering 8 (2020) 104045

Contents lists available at ScienceDirect

Journal of Environmental Chemical Engineering

journal homepage: www.elsevier.com/locate/jece

Adsorption studies of toxic cadmium(II) and chromium(VI) ions from aqueous solution by activated black cumin (*Nigella sativa*) seeds

Patience Mapule Thabede*, Ntaote David Shooto, Thokozani Xaba, Eliazer Bobby Naidoo

Applied Chemistry and Nano Science Laboratory, Department of Chemistry, Vaal University of Technology, P.O. Box X021, Vanderbijlpark 1900, South Africa

ARTICLE INFO

Editor:Yunho Lee

Keywords:
Modified black seeds
Hexavalent chromium
Divalent cadmium
Adsorption

ABSTRACT

Few studies that reported on black cumin seeds (BS) showed that the material has good adsorption capacity towards metal ions. Therefore, it is fair to conduct further studies on the material. However, literature survey shows that no previous study on black cumin seeds has reported on the effect of phosphoric acid (H_3PO_4) and potassium permanganate ($KMnO_4$) activating agents on the removal of toxic cadmium Cd(II) and chromium Cr (VI) ions from aqueous solution. Pristine black seeds were designated (PBS), the H_3PO_4 and $KMnO_4$ activated seeds (H_3BS) and (KMBS) respectively. The seeds were characterized by SEM, BET, XRD and FTIR. SEM micrographs revealed that H_3BS and KMBS were more porous than PBS. The BET surface area of H_3BS and KMBS increased to 10.3 and 9.30 m^2/g respectively. FTIR spectra confirmed the presence of −OH, −COOH, −C═O and $-NH_2$ functional groups attached to the surface of all adsorbents. Adsorption batch studies revealed that the adsorption capacities of all adsorbents increased with increase in the concentration of Cd(II) and Cr(VI) in solutions. The isotherm data revealed that Cd(II) and Cr(VI) ions removal uptake onto all adsorbents found good fit for Langmiur. This implies that the uptake processes occurred on active sites having equal affinity and further suggest monolayer adsorption. It was observed that all adsorbents had higher uptake for Cd(II) than Cr(VI) ions. It was found that the maximum adsorption capacity for Cr(VI) ions was 17.70 mg/g at pH 1 and temperature 353 K whilst for Cd(II) ions it was 19.79 mg/g onto KMBS at pH 9 and temperature 298 K. The sorption rate of Cr (VI) ions onto PBS increased sharply from 5 to 60 min and thereafter attained equilibrium. The same rapid sorption rates were observed for KMBS and H_3BS from 5 min and the processes were much faster and stabilized in 30 min. The sorption rates of Cd(II) ions were rapid from 5 min and remained significant until 60, 30 and 20 min mark for PBS, KMBS and H_3BS adsorbents respectively. Thereafter, little to no sorption was recorded for either adsorbents. Temperature increase had a positive effect on the uptake of Cd(II) and Cr(VI) ions onto all adsorbents. This was indicative of the endothermic nature. All the sorption processes of metal ions gave values that were positive for (ΔH^o) also suggesting that reactions were endothermic, and this was in agreement with temperature effect studies. It was observed that the uptake removal of Cd(II) and Cr(VI) ions found a good fit for PSO kinetic model. All metal ions sorption processes had positive (ΔS^o) values which indicates the increased randomness of the metal ions in the solution as the uptake processes approached equilibrium. Reusability test results showed that the pristine and modified adsorbents can be reused multiple times, showing the economic benefit of the adsorbents.

1. Introduction

Pollution of water by metal ions of Cd(II) and Cr(VI) is a serious challenge worldwide. These water contaminants mainly originate from accelerated industrialization. The challenge with metal ions of Cd(II) and Cr(VI) in particular within water bodies is that they are toxic, non-biodegradable and persistent. Cd(II) and Cr(VI) ions enter water through careless disposal of compounds containing cadmium and chromium by mines, paint, electroplating, plastic and cadmium-nickel battery manufacturing factories [1,2].

Cd(II) and Cr(VI) ions are harmful to the living organisms and the environment [3]. They are highly toxic even at low concentration and detrimental to human health and well-being [4]. Drinking cadmium (Cd (II)) ions contaminated water is highly carcinogenic and causes irreparable multiple organ damage such as skeletal, kidneys, reproductive, cardiovascular, central and peripheral nervous system and lungs [5–7]. Drinking chromium Cr(VI) ion contaminated water is likewise toxic, it is reported to cause physical health problems that are irreversible such

* Corresponding author.
E-mail addresses: mapulepseabelo@gmail.com (P.M. Thabede), ntaotes@vut.ac.za (N.D. Shooto).

https://doi.org/10.1016/j.jece.2020.104045
Received 24 February 2020; Received in revised form 27 April 2020; Accepted 12 May 2020
Available online 18 May 2020

Hindawi
Adsorption Science & Technology
Volume 2021, Article ID 6655227, 15 pages
https://doi.org/10.1155/2021/6655227

Research Article

Magnetite Functionalized *Nigella Sativa* Seeds for the Uptake of Chromium(VI) and Lead(II) Ions from Synthetic Wastewater

Patience Mapule Thabede, Ntaote David Shooto, Thokozani Xaba, and Eliazer Bobby Naidoo

Applied Chemistry and Nano-Science Laboratory, Department of Chemistry, Vaal University of Technology, P.O. Box X021, Vanderbijlpark 1900, South Africa

Correspondence should be addressed to Patience Mapule Thabede; mapulepseabelo@gmail.com

Received 25 July 2020; Accepted 14 December 2020; Published 12 January 2021

Academic Editor: Danina Krajišnik

The aim of the present study was to utilise pristine and magnetite-sucrose functionalized *Nigella Sativa* seeds as the adsorbents for the uptake of chromium(VI) and lead(II) ions from synthetic wastewater. Prestine *Nigella Sativa* seeds were labelled (PNS) and magnetite-sucrose functionalized *Nigella Sativa* seeds (FNS). The PNS and FNS composites were characterized by Fourier-transform infrared spectroscopy (FTIR) and X-ray powder diffraction (XRD). The FTIR analysis of both adsorbents revealed the presence of vibrations assigned to 1749 and 1739 cm^{-1} (-C=O) for ketonic group for both adsorbents. The amide (-NH) peak was observed at 1533 and 1527 cm^{-1} on FNS and PNS composites, respectively, whilst the carboxyl group (-COOH) were observed at 1408 cm^{-1} on both adsorbents. The XRD results of FNS and PNS composites showed a combination of spinel structure and y-Fe_2O_3 phase confirming the formation of iron oxide. The influence of operational conditions such as initial concentration, temperature, pH, and contact time was determined in batch adsorption system. The kinetic data of Cr(VI) and Pb(II) ions on both adsorbents was described by pseudo-first-order (PFO) model which suggested physisorption process. The sorption rate of Cr(VI) ions was quicker, it attained equilibrium in 20 min, and the rate of Pb(II) ions was slow in 90 min. Freundlich isotherm described the mechanism of Pb(II) ions adsorption on PNS and FNS composites. Langmuir best fitted the uptake of Cr(VI) ions on PNS and FNS. The results for both adsorbents showed that the removal uptake of Pb(II) ions increased when the initial concentration was increased; however, Cr(VI) uptake decreased when the initial concentration increased. The adsorption of Cr(VI) and Pb(II) ions on both adsorbents increased with temperature.

1. Introduction

Chromium compounds find their way into the natural water stream as a consequence of the industrialization and improper disposal of wastes which is usually from leather tanning, metal finishing, electroplating, and pigments industries [1]. Hexavalent chromium is one of the most contaminant that has attracted extensive attention among researchers due to its toxicity. Shupack [2] indicated that hexavalent chromium Cr(VI) species may occur in different ionic forms, namely chromate (CrO_4^{2-}), dichromate ($Cr_2O_7^{2-}$), or hydrogen chromate ($HCrO_4^-$) in aqueous solution; meanwhile, Cr(III) tends to form hydrated species such as hydrated trivalent chromium $[Cr(H_2O)_6]^{3+}$, chromium hydroxide complexes $[Cr(OH)(H_2O)_5]^{2+}$, or $Cr(OH)_2(H_2O)$. According to ([3] : 671), Cr(III) species are fairly less toxic as compared to Cr(VI) which is extremely toxic. The World Health Organisation (WHO) has restricted the limit of Cr(VI) to 0.05 mg/L in drinking water [4]. On the other hand, [5] : 1 reported that industries release effluent from batteries, automobile manufacturing units, and paint which contain lead Pb(II) ions. Pb(II) is one of the most toxic ions found in industrial wastewater [6]. The presence of lead Pb(II) ions in water is another major concerned because it affects human health, aquatic animals, peripheral nervous system, anaemia, loss of appetite, vomiting, severe abdominal

Asian Journal of Chemistry; Vol. 32, No. 6 (2020), 1361-1369

ASIAN JOURNAL OF CHEMISTRY

https://doi.org/10.14233/ajchem.2020.22597

Sulfuric Activated Carbon of Black Cumin (*Nigella sativa* L.) Seeds for the Removal of Cadmium(II) and Methylene Blue Dye

PATIENCE MAPULE THABEDE*, NTAOTE DAVID SHOOTO*, THOKOZANI XABA and ELIAZER BOBBY NAIDOO

Applied Chemistry and Nano-Science Laboratory, Department of Chemistry, Vaal University of Technology, P.O. Box X021, Vanderbijlpark 1900, South Africa

*Corresponding authors: E-mail: mapulepseabelo@gmail.com, ntaotes@vut.ac.za

Received: 18 December 2019; *Accepted*: 27 January 2020; *Published online*: 30 May 2020; AJC-19882

Carbon from black cumin seeds was modified with 10 and 20% sulfuric acid to obtain the activated adsorbents. Pristine carbon from black cumin seeds, 10 and 20% H_2SO_4 activated carbon from black cumin seeds were labelled CBC, ACBC-10 and ACBC-20, respectively. The adsorbents were characterized by SEM, XRD, FTIR, TGA and BET. The adsorbents maximum trend for Cd(II) was ACBC-10 > ACBC-20 > CBC. The maximum capacity trend for methylene blue dye was ACBC-20 > ACBC-10 > CBC. The kinetic model best fitted pseudo second order for Cd(II) which gave r^2 values of 0.991-0.998. The methylene blue fitted pseudo first order model with r^2 values ranging from 0.993-0.997. Pseudo first order suggested that the adsorption mechanism for methylene blue onto adsorbents involved van der Waal forces of attraction. The equilibrium data fitted Langmuir isotherm model for CBC, ACBC-10 and ACBC-20 with r^2 of 0.994 to 0.998 for the removal of methylene blue whilst the removal of Cd(II) followed Freundlich with r^2 ranging from 0.992 to 0.997. This suggested that the different adsorption processes were involved between the adsorbate and the adsorbents. Gibb′s free energy (ΔG^o) for Cd(II) and methylene blue onto CBC, ACBC-10 and ACBC-20 suggested that the reaction was spontaneous. The adsorption of Cd(II) and methylene blue was endothermic, positive values (ΔH^o). This suggested that the enthalpy (ΔH^o) had a weak interactive force process whose low energy is associated with electrostatic attraction.

Keywords: Activated carbon, Black cumin seeds, Methylene blue, Cadmium(II), Adsorption, sulfuric acid.

INTRODUCTION

The presence of organic dyes in streams and rivers create environmental problem [1]. Hence its elimination is very important due to its toxicity and carcinogenicity. About 15% of dyes are found in industrial effluents during operations and manufacturing processes [2]. Many synthetic dyes have been discovered and usually used in pharmaceutical, chemical, leather, food, paper and textile industries and cannot easily be degraded [3]. Excess of dyes leads to the change of aquatic life properties like chemical oxygen demand (COD), biological oxygen demand (BOD), dissolved oxygen (DO), taste, pH, colour and odour, which ultimately can damage aquatic life [4]. Methylene blue, a cationic dye is not only carcinogenic but also pollutes water environment. Methylene blue can cause abdominal disorders, respiratory disease and blindness [5].

Cadmium is found in fruits, seafood, vegetables, rice and meats. Hence, it is important to control it to minimum especially in aqueous water [6]. The use of cadmium in industries and discarding of waste containing Cd(II) have led to an increase in the residual concentration of cadmium in water, soil, air and food and its exposure is associated with many health effects of acute exposure and chronic conditions [7]. Cadmium(II) is one of the most toxic metals, which has an extensive range of sources including, chemical, nuclear, electroplating and electronic industries [8]. Intake of water containing cadmium is harmful and has the risk of causing chronic diseases, such as gastro-intestinal cancer, kidney damage and liver disease also causes Itai-itai disease, hypertension and bone degradation [9,10]. Due to toxic effects of metal ions and dyes on human health, the removal of these pollutants is compulsory before it adds in the environment and passes into the human food chain.

Reverse osmosis [11,12], chemical precipitation [13], electro-dialysis [14], ion-exchange [15] and many others are conven-tional methods employed for the removal of dyes and metal ions from aqueous solutions. Disadvantages of these

Asian Journal of Chemistry; Vol. 33, No. 2 (2021), 471-483

ASIAN JOURNAL OF CHEMISTRY

https://doi.org/10.14233/ajchem.2021.23021

Sorption of Chromium(VI), Cadmium(II) Ions and Methylene Blue Dye by Pristine, Defatted and Carbonized *Nigella sativa* L. Seeds from Aqueous Solution

PATIENCE MAPULE THABEDE*, NTAOTE DAVID SHOOTO* and ELIAZER BOBBY NAIDOO

Applied Chemistry and Nano Science Laboratory, Department of Chemistry, Vaal University of Technology P.O. Box X021, Vanderbjlpark 1900, South Africa

*Corresponding authors: E-mail: mapulepseabelo@gmail.com; ntaotes@vut.ac.za

Received: 12 October 2020; *Accepted*: 4 December 2020; *Published online*: 15 January 2021; AJC-20237

Present study reports on the sorption study of chromium(VI), cadmium(II) ions and methylene blue dye by pristine, defatted and carbonized *Nigella sativa* L. seeds from aqueous solution. The removal of oil from pristine *Nigella sativa* L. (PNS) seeds was carried out by defatting the *Nigella sativa* with acetone and *N,N*-dimethylformamide and then labelled ANS and DNS, respectively. Thereafter the defatted ANS and DNS adsorbents were carbonized at 600 ºC for 2 h under nitrogen and labelled as CANS and CDNS. The results of pristine, defatted and carbonized seeds were compared. The removal of Cr(VI), Cd(II) and methylene blue dye from aqueous solutions was investigated by varying adsorbate concentration, solution pH, reaction contact time and temperature of the solution. The SEM images indicated that the surface morphology of PNS was irregular, whilst ANS and DNS had pores and cavities. CANS and CDNS was heterogeneous and had pores and cavities. FTIR spectroscopy showed that the adsorbents surfaces had bands that indicated a lot of oxygen containing groups. The pH of the solution had an influence on the removal uptake of Cr(VI), Cd(II) and methylene blue. The sorption of Cr(VI) decreased when pH of the solution was increased due to different speciation of Cr(VI) ions whilst the removal of Cd(II) and methylene blue increased when solution pH was increased. Pseudo first order kinetic model well described the adsorption of Cr(VI), Cd(II) and methylene blue onto PNS. On the other hand, the kinetic data for ANS, CANS, DNS and CDNS was well described by pseudo second order. Furthermore, the removal mechanism onto PNS and ANS was better described by Freundlich multilayer model. The CANS, DNS and CDNS fitted Langmuir monolayer model. Thermodynamic parameters indicated that the sorption processes of Cr(VI), Cd(II) and methylene blue was endothermic and effective at high temperatures for all adsorbents. The ΔS° and ΔH° had positive values this confirmed that the sorption of Cr(VI), Cd(II) and methylene blue onto all adsorbents was random and endothermic, respectively. The values of ΔG° confirmed that the sorption of Cr(VI), Cd(II) and methylene blue on all adsorbents was spontaneous and predominated by physical adsorption process. The CANS had highest adsorption capacity of 99.82 mg/g for methylene blue, 96.89 mg/g for Cd(II) and 87.44 mg/g for Cr(VI) followed by CDNS with 93.90, 73.91 and 65.38 mg/g for methylene blue, Cd(II) and Cr(VI), respectively. The ANS capacities were 58.44, 45.28 and 48.96 mg/g whilst DNS capacities were 48.19, 32.69 and 34.65 mg/g for methylene blue, Cd(II) and Cr(VI), respectively. PNS had the lowest sorption capacities at 43.88, 36.01 and 19.84 mg/g for methylene blue, Cd(II) and Cr(VI), respectively.

Keywords: Chromium, Cadmium, Methylene blue, *Nigella sativa*, Pristine, Defatted, Adsorption.

INTRODUCTION

Activated carbon (AC) is a material that used in the industrial processes for purification of liquid and product separation [1]. Activated carbon is used as adsorbent for the removal of inorganic and organic pollutants in water, treatment of toxic compounds in medicine, as a material for storing hydrogen and many others [2]. Chemical and physical activation together with heating process is often used to produce carbon-based materials in order to enhance porous structure, improves surface area, improving rate of adsorption [3]. However, these materials are not easy to generate because they require high cost precursors [4]. Hence plant materials are used because they are abundant and sustainable resource that may provide oxygen containing groups which can easily interact with charged toxic pollutants from aqueous solution [5]. However, these materials need some modifications in order to get significant results for the removal of toxic ions and dyes [6].